



**HAL**  
open science

## Séchage par atomisation : propriétés de collage des particules en relation avec l'agglomération

Alessandro Gianfrancesco

► **To cite this version:**

Alessandro Gianfrancesco. Séchage par atomisation : propriétés de collage des particules en relation avec l'agglomération. Sciences du Vivant [q-bio]. AgroParisTech, 2009. Français. NNT : 2009AGPT0029 . pastel-00005602

**HAL Id: pastel-00005602**

**<https://pastel.hal.science/pastel-00005602v1>**

Submitted on 11 Jan 2010

**HAL** is a multi-disciplinary open access archive for the deposit and dissemination of scientific research documents, whether they are published or not. The documents may come from teaching and research institutions in France or abroad, or from public or private research centers.

L'archive ouverte pluridisciplinaire **HAL**, est destinée au dépôt et à la diffusion de documents scientifiques de niveau recherche, publiés ou non, émanant des établissements d'enseignement et de recherche français ou étrangers, des laboratoires publics ou privés.

# THESE

pour obtenir le grade de

**Docteur**

de

**l'Institut des Sciences et Industries du Vivant et de  
l'Environnement  
(AgroParisTech)**

Spécialité : Génie des Procédés Alimentaires

*présentée et soutenue publiquement par*

**Alessandro GIANFRANCESCO**

**le 19 Juin 2009**

**SPRAY DRYING ENGINEERING: PARTICLE STICKINESS  
IN RELATION WITH AGGLOMERATION**

SECHAGE PAR ATOMISATION :  
PROPRIETES DE COLLAGE DES PARTICULES  
EN RELATION AVEC L'AGGLOMERATION

**Travail réalisé à AgroParisTech, UMR GénIAI 1145, 1 av. des Olympiades, F-91300  
Massy**

## **JURY**

Prof. John DODDS, Professeur Emérite

Dr. Jean-Dominique DAUDIN, INRA Theix

Prof. Arsène ISAMBERT, Ecole Centrale Paris

Prof. Elisabeth DUMOULIN, Agroparistech Massy

Dr. Christelle TURCHIULI, Université Paris XI, IUT Orsay

Dr. Stefan PALZER, Nestlé NRC Lausanne

Rapporteur

Rapporteur

Examineur

Examineur

Examineur

Examineur



A María, senza di chi questa Tesi non sarebbe mai neanche cominciata



## Acknowledgements

My biggest thanks goes to María, for her invaluable day by day moral support and advice. This work is the first half of our common project, which was born several years ago in Toulouse. Without her, this work would never have been written.

I wish to express my deepest thanks to my supervisor Prof. Elisabeth Dumoulin, for her guidance and support all along this work. I am also very grateful to Dr. Christelle Turchiuli, which codirected this thesis with competence and patience.

I am grateful to Prof. John Dodds and Dr. Jean-Dominique Daudin for accepting to examine this thesis.

I would like to thank Dr. Stefan Palzer, for accepting to examine this work and for giving me the opportunity to carry out part of my thesis in Nestlé PTC of Singen.

This work was done in the framework of the Marie-Curie Biopowders Research Training Network RTN 512247. I thank all the members of the network and in particular the coordinator Prof. John Fitzpatrick. I am grateful to the European Union Commission for financing this work.

I wish to express my gratitude to Prof. Denis Flick, for his precious help in numerical simulation and for the interesting and human discussions.

Special thanks to Dr. Alain Sommier, for his invaluable assistance in particular for instrumentation. I am also very grateful to Jean-Sébastien Vimont and Christophe Chipeaux for their help especially for implementing the Labview program for data acquisition.

I also thank Prof. Fabrice Ducept, for his help in the interpretation of residence time distribution data.

I am very grateful to Amandine Berthomé and Iris Schmitz, for their contribution to my work during their student projects. They gave me precious support both for scientific and human issues.

I would like to thank all the members of the GIA/SPAB department at Agroparistech Massy for the technical support and the good working atmosphere. I would like to especially mention for their help Aurélien Neveu, Robert Sawka, Monique Belgome, Pablo Granda.

I would like to express my gratitude also to all the PhD students of the GIA/SPAB departement, which contributed to the good daily atmosphere in these three years: Camille, Emilie, Gilles, Houssein, Imen, Juan, Marjorie, Mohammed, Nawel, Régis, Reza, Richard, Samir, Souad, Teresa, Thibaud.

I would like to thank all the people in Nestlé PTC of Singen, and in particular Dr. Helge Hulmer for supervising my work there. Special thanks to Michael Hirt and Pierre Taymans for their technical support.

I would like to express my gratitude to all my friends, my parents and my family that constantly supported me even at distance.



## RESUME DE THESE

Le séchage par pulvérisation est une technique très utilisée dans l'industrie chimique et alimentaire pour la production de poudres. Une solution liquide est pulvérisée en fines gouttelettes (10-50 $\mu$ m), qui sont rapidement séchées par de l'air chaud à l'intérieur d'une chambre de séchage. Chaque goutte conduit à un grain de poudre, de taille proche de la taille de la goutte initiale.

Pour améliorer certaines propriétés du produit final – telles que l'écoulement et les propriétés de dissolution – une étape ultérieure d'agglomération est souvent nécessaire, pour créer des structures plus larges et poreuses. Cette agglomération peut avoir lieu en forçant des collisions entre particules soit à l'intérieur de la chambre de séchage, en recyclant les particules sèches les plus petites (les « fines »), soit dans un lit fluidisé externe ou intégré. Dans tous les cas, pour que l'agglomération puisse avoir lieu, il est nécessaire que les collisions soient suivies par l'adhésion entre les particules, dont au moins une doit avoir une surface « collante », puis par le séchage pour consolider la structure ainsi établie.

La caractérisation de l'état collant des gouttes au cours du séchage en fonction des paramètres opératoires et de leur position dans la chambre doit permettre une optimisation de l'étape d'agglomération.

L'étude bibliographique met en évidence que l'état collant de la surface de particules peut être relié au phénomène de la transition vitreuse. Le séchage par pulvérisation étant un procédé rapide, la substance à sécher passe de l'état liquide à celui de solide amorphe en passant par un état caoutchouteux collant pour des températures supérieures et proches de la température de transition vitreuse. Celles-ci dépendent fortement de la composition du matériau considéré et de sa teneur en eau. Elles sont notamment fonction de l'activité de l'eau de la particule qui évolue au cours du séchage. Pour prévoir les propriétés de collage des gouttes qui sèchent, il est donc nécessaire de connaître l'évolution de leur température et de leur teneur en eau dans la chambre de séchage. Une mesure directe est très difficile, à cause des difficultés d'échantillonnage à l'intérieur du séchoir. Mais du fait des échanges de chaleur et de matière entre les gouttes et l'air de séchage, l'évolution des propriétés de l'air (température et humidité relative) au cours du séchage est aussi représentative de l'évolution du produit ; l'air est refroidi et humidifié avec une vitesse dépendant de la vitesse d'évaporation de l'eau des gouttes.

Cette étude a été réalisée dans un séchoir pilote co-courant (Niro Minor) équipé d'une turbine. L'objectif de la partie expérimentale était d'obtenir une meilleure compréhension de l'évolution des propriétés des gouttes tout au long du séchage par pulvérisation, en les reliant à l'évolution des propriétés de l'air de séchage.

Des solutions aqueuses de maltodextrine DE12 et DE21 ont été choisies comme produits modèles à sécher (sucres) pouvant présenter un comportement collant lors du séchage.

La chambre de séchage a été équipée de 12 thermocouples pour mesurer la température de l'air et d'un hygromètre capacitif pour mesurer son humidité relative. A partir de ces deux mesures, la teneur en eau de l'air à différentes positions dans la chambre a pu être calculée, ainsi qu'un bilan massique sur l'eau dans l'air, entre l'entrée du séchoir et ces différentes positions. Avec l'hypothèse que les particules sont entraînées par l'air en suivant la même trajectoire, il a été possible de déduire la variation de la teneur en eau des particules en train de sécher dans la chambre.

Des expériences avec pulvérisation d'eau pure ont permis de tester le système de mesure et de caractériser les pertes thermiques due à l'échange de chaleur entre les parois du séchoir et l'air ambiant.





L'effet de différents paramètres opératoires (température de l'air d'entrée, débit d'air, débit de liquide, vitesse de rotation de la turbine) sur le comportement au séchage a été testé. Pour toutes les conditions testées, la plupart du séchage (>90% d'eau évaporée) a lieu très rapidement près de l'atomiseur, à cause des fortes différences initiales de température et de tension de vapeur d'eau entre l'air et les gouttes.

Il faut noter que le capteur d'humidité utilisé était résistant aux hautes températures, mais il ne garantissait pas une précision suffisante pour les faibles valeurs d'humidité relative. Pour une température élevée de l'air d'entrée (200°C) et un faible débit liquide (1.8 kg.h<sup>-1</sup>), cela se traduit par une erreur importante sur la détermination de la teneur en eau de l'air, et donc sur le bilan massique sur l'eau évaporée. Mais dans ces conditions opératoires, le séchage peut de toute façon être considéré comme terminé dans la partie haute de la chambre près de l'atomiseur. Les faibles variations de température de l'air relevées entre le haut et le bas de la chambre sont dues aux pertes thermiques par les parois.

Pour les autres conditions opératoires (faible température de l'air en entrée (144°C), forts débits de liquide), le séchage se déroule tout au long de la chambre conduisant à une augmentation de la teneur en eau de l'air avec une diminution de sa température. L'humidité relative de l'air à la sortie de la chambre est un « indicateur limite » de la teneur en eau et de l'activité de l'eau de la poudre finale, même si l'équilibre entre l'air et le produit n'est jamais atteint.

Le séchage des solutions de maltodextrines a été comparé au séchage de l'eau, pris comme référence. Pour une même quantité d'eau à évaporer dans les mêmes conditions opératoires, les températures de l'air étaient plus faibles et l'humidité relative plus élevée pendant le séchage d'eau pure. Ceci est en accord avec le fait que l'évaporation d'eau pure est plus facile que l'évaporation de l'eau liée en solution. Pour les deux maltodextrines séchées, les différences dans les propriétés de l'air montrent que le comportement au séchage de la MD21 était plus proche de celui de l'eau par rapport à la MD12. Cela semble être dû à la plus faible viscosité des solutions de MD21, qui facilite la diffusion de l'eau du cœur vers la surface de la goutte. De plus, une viscosité inférieure peut provoquer la formation d'un plus grand nombre de gouttes de taille plus faible lors de l'atomisation, conduisant à une surface d'échange totale des gouttes plus grande et donc à un séchage initial plus rapide. La faible variation de taille n'a pas pu être observée lors des essais.

La teneur en eau moyenne de la poudre dans la chambre calculée à partir des bilans massiques sur l'eau dans l'air a été combinée avec les températures de transition vitreuse  $T_g$  et les isothermes de sorption pour le produit considéré. De cette manière, des conditions opératoires et des positions dans la chambre pour lesquelles les particules pourraient être collantes ont été déterminées.

Des études précédentes ont montré que les particules de maltodextrine sont considérées comme collantes quand leur température de surface est comprise entre  $T_g$  et une température  $T_s$  de 20 à 30°C supérieure. Dans ce domaine, le matériau atteint des valeurs de viscosités favorables à la formation de ponts (liquides et solides) avec d'autres particules. En dessous de la transition vitreuse, les particules sont considérées comme sèches, et au dessus de la  $T_s$  comme liquides non collantes.

Dans toutes les conditions testées, la maltodextrine DE12 a été rapidement séchée jusqu'à atteindre des valeurs de teneur en eau et d'activité de l'eau en-dessous de la transition vitreuse. Le comportement collant est dans ce cas envisageable seulement tout près de l'atomiseur. La maltodextrine DE21 présentant des températures de transition vitreuse plus faibles à cause de son poids moléculaire inférieur, conduit à des propriétés collantes plus longtemps au cours du séchage dans la chambre.



La simulation numérique du procédé de séchage a aussi été utilisée dans le but de prévoir le comportement collant des gouttes. L'étude bibliographique a montré que des modèles de dynamique des fluides numérique (CFD) sont nécessaires pour obtenir une simulation complète du procédé. Un modèle simplifié de CFD a été appliqué pour obtenir des informations complémentaires sur les trajectoires de l'air et des particules dans la chambre, en mettant en évidence des zones de recirculation de l'air. L'évolution des caractéristiques des particules a aussi pu être calculée.

Par rapport aux modèles classiques, la diffusion de l'eau dans la matrice solide n'a pas été directement calculée. La plus faible vitesse d'évaporation de l'eau liée en solution par rapport à l'eau pure a été prise en compte en considérant une pression de vapeur d'eau réduite pour la goutte de solution. Un coefficient de réduction ( $<1$ ) a été identifié à partir des mesures expérimentales de la température et de l'humidité de l'air pendant le séchage d'eau libre et d'eau liée en solution. Ce coefficient est différent pour les deux maltodextrines DE12 et DE21. L'évolution de la teneur en eau des particules calculée est en accord avec les résultats expérimentaux.

L'avantage principal de cette approche est qu'elle peut être appliquée directement à d'autres produits, car la composition du liquide à sécher et la diffusion de l'eau dans la matrice ne sont pas considérées directement. Cependant, les différences entre le cœur et la surface ne sont pas prises en compte, et les propriétés de surface ne sont pas parfaitement décrites. En particulier, la température de la particule est surestimée dans le calcul.

Des zones où les particules de MD12 et MD21 pourraient être collantes dans la chambre ont été identifiées avec le modèle, et se sont avérées en accord avec les résultats expérimentaux. La simulation CFD représente un outil efficace pour une prévision qualitative de l'effet des paramètres du procédé sur le comportement collant des particules.

Les régions collantes ainsi localisées dans la chambre de séchage ont été exploitées pour effectuer des tests d'agglomération par introduction de poudre. Un système d'insertion de poudre a été spécifiquement développé pour pouvoir reinsérer une partie de la poudre produite à différentes positions dans la chambre. Les collisions entre la poudre insérée et les particules collantes en train de sécher (diamètres moyens  $< 30 \mu\text{m}$ ) ont provoqué la formation d'une fraction de particules ayant un diamètre supérieur à  $100 \mu\text{m}$ , avec des propriétés de mouillabilité et d'écoulement améliorées.

Cette augmentation de taille a permis de valider la prévision du comportement collant dans une grande partie de la chambre pour la MD21, tandis qu'aucune agglomération n'a eu lieu pour MD12, comme prévu.

Pour la maltodextrine MD21, il a été possible de mettre en évidence le fait qu'une plus grande fraction de poudre agglomérée a été obtenue en introduisant la poudre non pas immédiatement près de l'atomiseur, pratique usuelle dans l'industrie, mais plus loin dans la chambre. Les fines sont généralement introduites près de l'atomiseur à cause de la forte densité de gouttes dans cette zone, avec une plus grande probabilité de collisions. Mais les gouttes étant liquides, des collisions avec des particules de poudre à cet endroit provoquent plutôt l'enrobage ou la coalescence, avec une faible augmentation de taille. Les particules doivent recirculer plusieurs fois si un grossissement est demandé, avec des conséquences négatives possibles sur la qualité du produit final.

L'insertion de poudre dans le haut de la chambre « loin » (10cm) de l'atomiseur et au milieu de la chambre a permis d'obtenir jusqu'à 16% de poudre avec un diamètre supérieur à  $100\mu\text{m}$ . L'estimation du comportement collant des particules à partir de mesures sur l'air et des propriétés des matériaux pourrait donc permettre d'optimiser le choix de la position d'insertion de la poudre en fonction des propriétés recherchées pour le produit final.

Le dispositif expérimental d'insertion de poudre devrait être amélioré pour permettre une insertion symétrique et sélective des fines particules, après séparation de la fraction déjà



agglomérée. De plus, l'insertion d'une poudre différente de celle produite pourrait être envisagée.

La démarche expérimentale développée dans cette thèse a finalement été appliquée à un séchoir semi-industriel équipé d'une buse bifluide de pulvérisation, d'un retour de fines et d'un lit fluidisé interne. Les mesures sur l'air dans la chambre ont permis de mieux comprendre l'évolution du séchage d'un hydrolysate de protéines, et les propriétés de ce matériau (isotherme de sorption, température de transition vitreuse) ont été déterminées pour aider à l'interprétation des résultats.

L'étude a confirmé que l'insertion des fines sèches près de l'atomiseur (gouttes liquides) avait comme fonction principale d'améliorer le séchage en diminuant la teneur en eau initiale des gouttes pulvérisées. L'augmentation de taille (agglomération) a plutôt lieu à l'intérieur du lit fluidisé intégré, les particules pouvant arriver à l'équilibre avec l'air à cause du temps de séjour élevé. En contrôlant les températures dans la chambre à différentes positions il est possible de prévoir les propriétés de la poudre, et notamment de provoquer un état collant favorable à l'agglomération

Cette application a mis aussi en évidence des limites qui doivent être prises en compte. En premier lieu, la détermination exacte des débits d'air entrants est fondamentale pour la résolution correcte des bilans massiques et thermiques. Dans notre cas seul le débit d'air de séchage en entrée était mesuré. Il faudrait tenir compte des débits d'air secondaires tels que l'air comprimé (froid) de retour des fines, l'air du lit fluidisé et de la buse de pulvérisation conduisant à un débit total en sortie (non mesuré) différent du débit d'entrée.

De plus, en fonction de la géométrie du séchoir, des recirculations d'air peuvent avoir lieu dans la chambre. La connaissance des écoulements de l'air est en particulier importante pour choisir les positions des capteurs (T, RH) dans la chambre, et pour l'interprétation des résultats. Des mesures de vitesse d'air à différentes positions et la simulation numérique CFD proposée pourraient être utilisées pour calculer et prédire les trajectoires de l'air, pour une meilleure maîtrise du séchage dans un équipement donné.

Ce travail de thèse a été réalisé sur le site de Massy de Agroparistech, financé par le 6<sup>ème</sup> programme cadre de l'Union Européenne dans le cadre du projet *Biopowders* du réseau « Marie Curie Research training network ». Les essais industriels ont été réalisés au PTC de Nestlé à Singen (Allemagne).



# TABLE OF CONTENTS

<b>INTRODUCTION</b>	<b>1</b>
<b>PART I – BIBLIOGRAPHY</b>	<b>5</b>
<b>1. The spray drying process: from liquid to powder</b>	
1.1. Bases of spray drying	
1.2. Which characteristics for powders ?	
1.2.1. Powder water content and water activity	
1.2.2. Density	
1.2.3. Flowability and instant properties	
<b>2. Drying of liquid drops</b>	
2.1. Atomization of liquid feed in drops	
2.1.1. Rotary atomizer	
2.1.2. Pressure nozzle	
2.1.3. Pneumatic nozzle	
2.1.4. Sonic nozzle	
2.2. Drying of drops in air	
2.2.1. Evolution of air properties along drying (Mollier diagram)	
2.2.2. Drying rate: heat and mass transfer equations	
2.2.3. Evolution of drops properties along drying	
2.2.4. Configuration for air/drops contact	
<b>3. Particle sticky behaviour along spray drying</b>	
3.1. The glass transition phenomenon in drying	
3.2. Characterization of stickiness of powders	
3.2.1. Methods using powder “in bulk”	
3.2.2. Methods using drying drops or fluidized particles	
<b>4. Agglomeration and spray drying process</b>	
4.1. Agglomerates: structure and formation	
4.2. Equipments for spray drying and agglomeration	
4.2.1. Multistage spray drying	
4.2.2. Fines return	
<b>5. Process control for spray drying</b>	
5.1. Energetic considerations in spray drying	
5.2. Measurements on air and product	
5.3. Control	
<b>6. Modeling of spray drying and agglomeration</b>	
6.1. Principle	
6.2. CFD models of spray drying	
6.2.1. Simulation of turbulence	
6.2.2. Simulation of drop transport	
6.2.3. Drying kinetics of drops	
6.3. Simulation of agglomeration	
6.3.1. Collisions between particles	
6.3.2. Collision result	
6.4. Conclusion on CFD simulation of spray drying and agglomeration	
Conclusion	





**1. Products**

- 1.1. Maltodextrin solutions
- 1.2. Protein hydrolysate aqueous solution

**2. Equipments and instrumentation**

- 2.1. Niro Minor spray dryer
- 2.2. Niro FSD 4.0 spray dryer

**3. Measurements on liquid feed, air and products**

- 3.1. Measurements on liquid feed solutions
- 3.2. Measurements on air
  - 3.2.1. Air flow rate
  - 3.2.2. Air temperature
  - 3.2.3. Air relative humidity
- 3.3. Measurements on powders
  - 3.3.1. Water content
  - 3.3.2. Water activity
  - 3.3.3. Powder size distribution
  - 3.3.4. Sorption isotherms and glass transition
  - 3.3.5. Wettability
  - 3.3.6. Bulk and tapped density
  - 3.3.7 SEM microscopy
  - 3.3.8. Conductivity of solutions for DTS measurements
  - 3.3.9. Colour

**4. Conditions of spray drying trials**

- 4.1. Trials in Niro Minor
- 4.2. Trials in Niro FSD 4.0.
- 4.3. Residence time distribution measurements in Niro Minor

**PART III – Results and discussion****1. Definition of process operating conditions****85**

- 1.1. Measurements on air without liquid atomization
  - 1.1.1. Heating of the chamber
  - 1.1.2. Determination of heat losses
- 1.2. Water spray drying
  - 1.2.1. Time to reach steady state inside the chamber
  - 1.2.2. Positions for air properties measurements
  - 1.2.3. Choice of operating parameters
  - 1.2.4. Mass and heat balances on drying air
  - 1.2.5. Estimation of possible secondary ambient air flow rate
- 1.3. Operating conditions for maltodextrin solutions drying
  - 1.3.1. Choice of maltodextrin solution flow rates
  - 1.3.2. Residence time distribution inside Niro Minor

Conclusion

**2. Drying behaviour and stickiness development for maltodextrin solutions****102**

- 2.1. Drying of maltodextrin DE12 solutions and comparison with water
  - 2.1.1. Considerations on drying behavior of water and maltodextrin solutions
  - 2.1.2. Effect of process parameters on spray drying behavior of liquid solutions
- 2.2. Comparison between MD21, MD12 and water drying behavior
- 2.3. Stickiness of maltodextrin DE12 and DE21 particles along spray drying



Conclusion

**3. Spray drying CFD simulation** **119**

- 3.1. The model
  - 3.1.1. Equations for continuous phase: air
  - 3.1.2. Equations for the discrete phase: drops/particles
  - 3.1.3. Definition of the dryer geometry
  - 3.1.4. Boundary conditions
  - 3.1.5. Numerical solution
- 3.2. Determination of simulation parameters
  - 3.2.1. Validation of the global heat transfer coefficient  $h$  and  $T_{IN}$ , with water drying
  - 3.2.2. Sensibility to inlet air turbulence intensity and grid size effect
  - 3.2.3. Sensibility to initial drop diameter
  - 3.2.4. Effect of drop vapour pressure  $P_v$
- 3.3. Application of simulation
  - 3.3.1. Model validation
  - 3.3.2. Continuous phase at steady state: air
  - 3.3.3. Discrete phase at steady state: drying particles
- 3.4. Determination of powder stickiness inside the chamber
  - 3.4.1. Effect of liquid feed flow rate on particle stickiness for MD12, and MD21
  - 3.4.2. Effect of inlet air temperature

Conclusion

**4. Powder insertion inside Niro Minor to perform agglomeration** **149**

- 4.1. Theoretical considerations: factors affecting agglomeration inside spray dryer
  - 4.1.1. Stickiness of colliding particles
  - 4.1.2. Collision probability between drying particles and inserted particles
  - 4.1.3. Force of the impact between particles
- 4.2. Powder insertion system
  - 4.2.1. Design of powder insertion device
  - 4.2.2. Choice of insertion positions and powder jet shape
  - 4.2.3. Choice of operating conditions
- 4.3. Results of powder insertion trials
  - 4.3.1. Discussion on obtained agglomeration

Conclusion

**5. Industrial application: spray drying of protein hydrolysate** **151**

- 5.1. General conditions of trials
- 5.2. Water trials without fluid bed: drying behavior and measurements feasibility
- 5.3. Protein hydrolysate solution drying trials feasibility
  - 5.3.1. Drying trials for  $T_{IN}$  180°C
  - 5.3.2. Effect of inlet air temperature (160°C and 200°C)
- 5.4. Discussion about the drying behavior, the role of fines return and fluid bed during protein hydrolysate solution spray drying
  - 5.4.1. Spray drying behavior: air properties evolution inside the chamber
  - 5.4.2. Position of fines return (top and bottom)
  - 5.4.2. Role of the fluid bed (with top fines return)

**CONCLUSION** **178**

**LIST OF SYMBOLS** **185**

**REFERENCES** **187**

- ANNEX I Modeling of residence time distribution function in Niro Minor
- ANNEX II Properties of air and water for CFD simulation
- ANNEX III Articles, congresses, industrial visits



## Introduction

Powders exist in a wide variety of industries as chemicals, pharmaceuticals, cosmetics, agriculture and food, like plastics beads, ceramic materials, detergents, fertilizers or medicines.

In food industry powders represent stable dried products, ingredients, with a reduced weight and volume for transport, able to be designed for easy dosage and dissolution, while retaining nutritional and functional properties. Food powders may be added directly to a dish in a small quantity (salt, pepper, spices, sugar, aromas), or may be consumed or processed with other constituents in a solvent (water, milk, oil). Examples of powders include milk and derivatives, flour, cocoa, sugar, coffee, soup, vegetables, meat, fish, sauce mix, vending machine powders and ingredients (colourings, enzymes, yeasts).

Depending on the desired end-use, specific properties of individual particles are required with or without interaction with other particles (e.g. for powders mixing), or with solvent (e.g. instant dissolution); and the whole powder should behave as a “fluid” for easy transport and dosage. In some cases specific shape and surface of particles could be requested for improving the aspect (coating) and the attractiveness of a commercial product.

Several processes are used for production of powders like crystallisation, precipitation, freeze drying, extrusion, milling, roller or spray drying. They differ mainly by the material to transform, by the operating conditions and the energy to use (heating, cooling, mechanical forces), and by the characteristics of the final product (size, shape, crystallized or amorphous structure, solubility, stability...). A final drying step is often required to control the required powder properties. For powder utilisation, one important step will be (very often) to be disintegrated again in a solvent either in a preliminary mixture or directly as a food substance.

Whatever the user, an industrial or a consumer, one of the main properties will be the ability of powder to be dosed and to dissolve. Besides adapted composition, that means a good flowability without interaction between particles (no sticking, smooth surface) and a structure favourable to the penetration of solvent. Individual particles aggregated in solid agglomerates have shown such properties and the spray drying process coupled with fluidised bed was adapted to produce such agglomeration.

Spray drying is a continuous process which transforms a concentrated liquid in a powder, limiting the possible modifications of composition during the process. The industrial equipments are usually high towers more or less sophisticated, with high powder flow rates and consumption of air and energy. Some are dedicated, others are flexible and used for different products.

The principle is to atomize the liquid feed (solution, suspension or emulsion) in small drops (10-20  $\mu\text{m}$ ) to increase the surface of exchange with the drying agent, usually (constituted by) hot air. Each drop is quickly dried (by air), until obtaining a solid dry particle, with size close to the initial liquid drop size.

The composition of the powder depends on the initial liquid composition, which may be modified along drying. The particles obtained from a simple spray drying step are small, with a wide size distribution. The presence of very fine particles (called “fines”) is generally unwanted as it may represent risks for the environment (dust formation, explosions), it can lead to product losses and could have a negative effect on physical properties like solubility in water. These fines are usually reused either by return inside the drying chamber to collide with the drying drops, or in a fluidised bed internal or external to the dryer, to improve the drying process, and sometimes for further



agglomeration. That step will lead to final particles with shape, size and properties modified according to the process used.

Finally the powder will be transported, stored in bags, in packages, avoiding if possible any modification of properties of the dry product. Hygroscopic components should be maintained in an atmosphere avoiding caking and variation of water content; and mechanical resistance will be good enough to resist shocks able to destroy the structure, producing again fines.

This study on spray drying process has for objectives to understand the evolution of drop drying with hot air inside a pilot equipment, by linking the evolution of drops properties (temperature, water content) to the evolution of drying air properties (temperature, relative humidity) along the process.

The final goal should be to be able to determine process conditions that could lead to a controlled agglomeration inside the chamber, avoiding or minimizing the production of fines and their recirculation, leading inside the process itself to particles with desired properties, especially size and solubility.





**PART I**  
**BIBLIOGRAPHIC STUDY**



## 1.1. Bases of spray drying

The spray drying process transforms a pumpable liquid into a powder, i.e. individual dry solid particles. The liquid feed is made of a solvent, usually water, and constituents which are soluble (solution) and/or insoluble (emulsion, suspension). Soluble components correspond to short or long chain polymers (polysaccharides, proteins,...) and to small molecules as salts. The dry particles will be made of these dry constituents with still some traces of water (or solvent). So, to get a powder state it is necessary to remove, to extract, to evaporate water which is more or less strongly linked, adsorbed onto constituents, in pores, which means using special drying conditions (Bimbenet and Dumoulin, 1999).

In spray drying, a gas, usually hot air, is used to bring to the liquid the energy for evaporation of water and to transport the water vapour. The liquid flow (thickness) is first reduced by forming a thin film that is then broken in small drops to increase the exchange surface and to improve the heat and mass transfers with hot air. The transfer coefficients are also enhanced by creating a turbulent air flow around the liquid drops.

These conditions lead to some important parameters to take into consideration:

- The **time** necessary to effectively realize the drying till obtaining a dry particle must be minimized. That means an optimized air/drop contact and a limited (reduced) quantity of water to extract: the liquid must be previously concentrated.
- The formation of a film of liquid then its breakage in drops (**atomization**) with a regular size and shape to control the drying process must be facilitated: choice of the atomization device, physical properties of the liquid feed (viscosity, surface tension). Anyway, the size of drops must be small for easy drying but not too small to obtain powder easy to handle and to use afterwards.
- The **temperature of drying air** must be high compared to the liquid one to accelerate the initial transfer of water from drop to air; but maintaining the product at a reasonable temperature during a short time to avoid deterioration: the spray drying process must be a fast drying process.

Therefore, the spray drying process is a continuous process with three main operations:

- The **atomization** of a well formulated liquid feed, to produce a continuous spray of drops (some microns), with a great surface of exchange with drying .
- The **drying** of liquid drops due to an efficient contact between drops and moving hot air. The liquid solvent (water) is evaporated from the drop surface till obtaining a dry particle. The circulation of air and the transport of particles need a space and distance/time provided by the geometry of the drying chamber.
- The **separation** of the final dry powder from cooled and humidified air, and its recovery with possible further processing to modify powder properties.

A possible spray drying installation is shown on Figure 1.1. (Pisecky, 1997) with the drying chamber (1), the hot air inlet (2), the atomizer (3) connected to liquid feed, and the powder recovery system (4), with possible cyclone separation (5) of small light particles (fines) carried away by exhausted air. In industry recovered fines are usually returned to the drying chamber or to a fluid bed to help to achieve drying or to form agglomerates, and to reduce product losses.

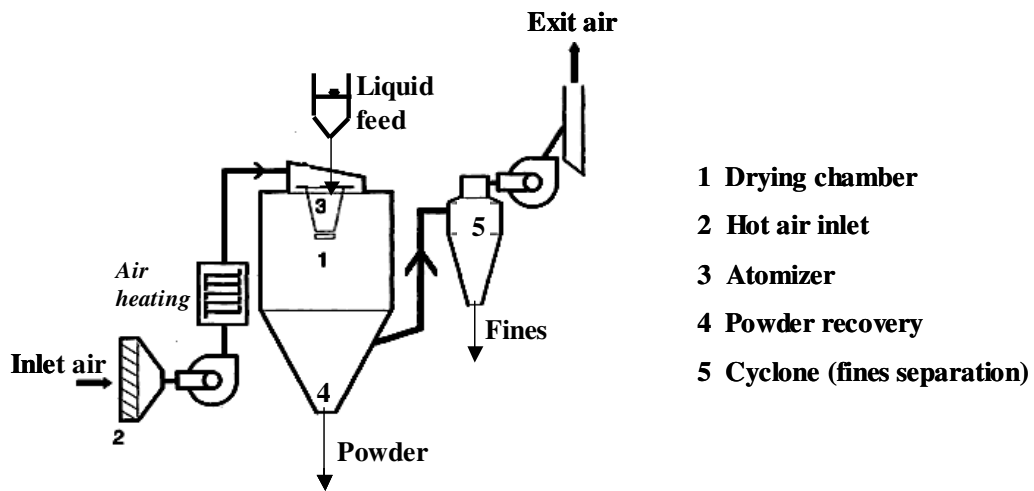


Figure 1.1. Flowsheet of a typical spray drying installation (adapted from Pisecky, 1997).

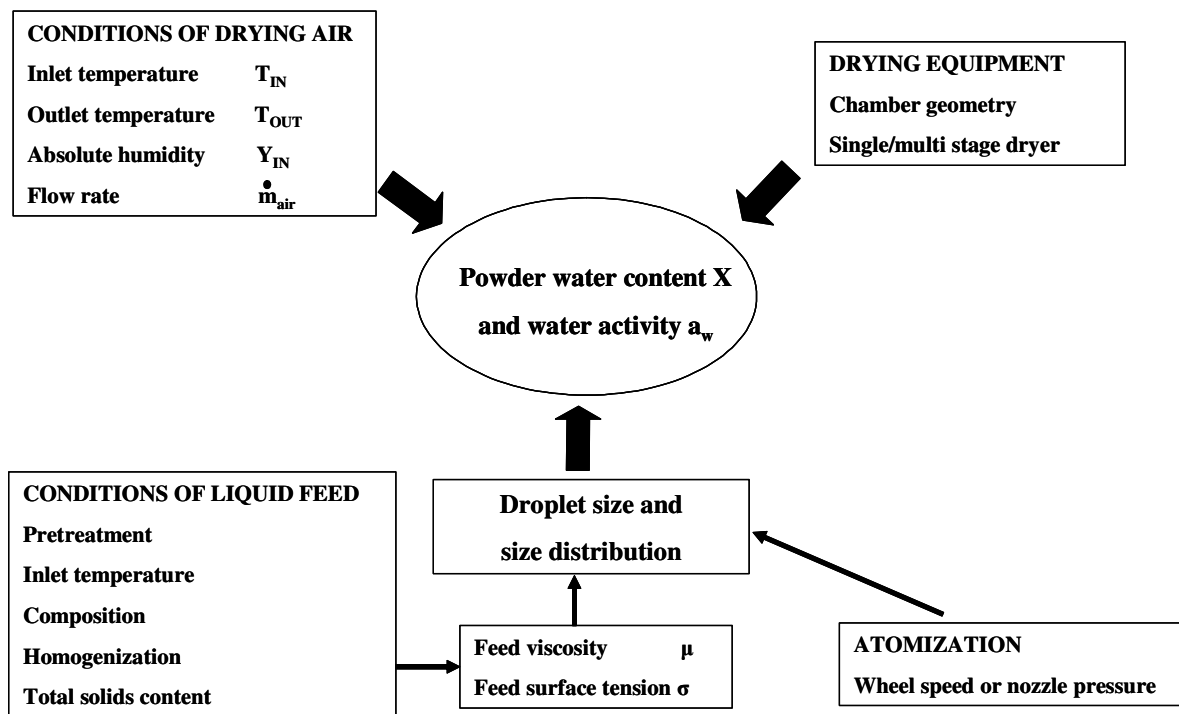


Figure 1.2. Factors affecting final moisture content of spray dried powders.

## 1.2. Which characteristics for powders?

The main characteristics of final spray dried powders are related to end-use properties: water content and water activity for stability, size and size distribution for powder mixing and handling, bulk density and flowability for transportation, and wettability and dispersibility for instant properties (Huntington, 2004; Melcion et al., 2003; Aguilera, 2008).

The initial composition of the liquid feed has an influence on both drying and powder rehydration, and also on the final repartition of components into particles or on the surface (i.e. fat for flowability). Therefore the initial liquid composition is closely in relation with the powder properties (Shrestha et al., 2008; Adhikari et al., 2004; Goula et al., 2008).

### 1.2.1. Powder water content and water activity

Water content  $X$  is generally expressed on dry basis ( $\text{kg water} \cdot \text{kg}^{-1}$  total solids), total solids (dry matter) being constant during drying process (if no losses). But, it may also be expressed on wet basis  $X_{\text{wet}}$  as a function of total weight (evolving during drying).

Water content of a commercial product is often the most important specification for industrial powders. It is often fixed by the maximal value allowed by the law (e.g. 3% or inferior to 3%), to avoid reduction of shelf life due to biochemical reactions and development of bacterial activity. From an economic point of view, it is convenient to operate close to the allowed limit, because each percent of humidity to remove could represent an important energy cost on year basis. Spray dried powders water content is affected by several factors including properties of liquid feed (concentration, temperature, viscosity, surface tension), type of atomizer (nozzle or rotary), type of spray dryer and drying air characteristics (flow rate, inlet and exit temperature, relative humidity) (Fig. 1.2).

The water contained in a substance is more or less interacting with the constituents (solutes, hydrates...). The level of interaction of water with dry matter is expressed by the water activity  $a_w$ , defined as the ratio between the water vapour pressure of the humid product and the saturated vapour pressure of pure water at the considered temperature.

$$a_w = \frac{P_v(T)}{P_w^{\text{sat}}(T)} \quad \text{eq. 1.1}$$

A low water activity value will be associated with water strongly bound with dry matter (last traces of water) or in pores, corresponding to a low water vapour pressure  $P_v(T)$ . If a product is in equilibrium with a gas atmosphere (air) in a close vessel, product and air temperatures are the same and product  $a_w$  is equal to air relative humidity. This equilibrium is characterized by the sorption isotherms, which represent  $a_w$  variation as a function of water content  $X$  of the product for a given temperature (each point representing an equilibrium state) (Labuza, 1968; Mathlouthi and Rogé, 2003). Sorption isotherms depend on temperature, but slightly for the range of temperature (20 – 40°C) and for the polysaccharides used in this study. Usually they are established by water sorption on the dry product and hysteresis exists between absorption and desorption (Fig. 1.3). To notice that the drying process is a water desorption process, and the equilibrium between air and product represents a limit.

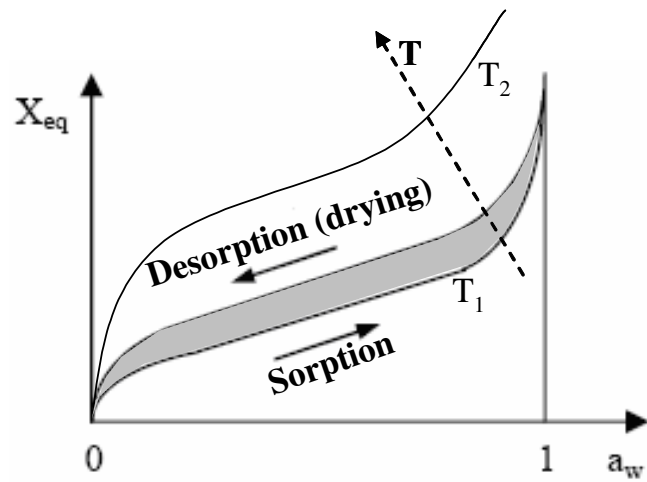


**Figure 1.3.** Sorption and desorption isotherms.

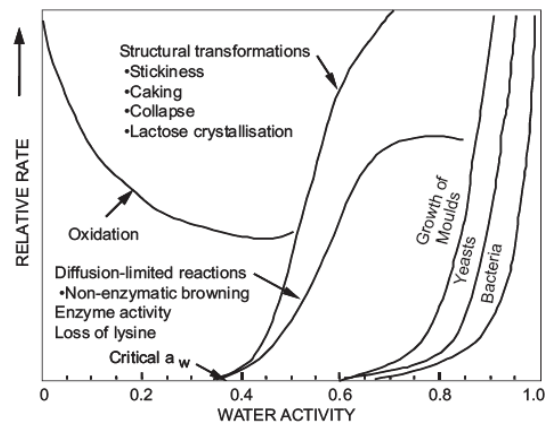


**Figure 1.4.** Bacterial growth and undesired reactions rate in food powders as a function of product water activity (from Bhandari and Hartel, 2005).

Sorption isotherm can be modelled with the Guggenheim-Anderson-de Boer (GAB) or the Brunauer-Emmet-Teller (BET) equations (Bimbenet et al., 2002):

$$X = \frac{x_m \cdot C_{GAB} \cdot a_w}{(1-a_w) \cdot (1+(C_{GAB}-1) \cdot a_w)} \quad \text{GAB equation} \quad \text{eq. 1.2}$$

$$\frac{X}{D} = \frac{C \cdot a_w}{(1-a_w) \cdot (1+(C-1) \cdot a_w)} \quad \text{BET equation} \quad \text{eq. 1.3}$$

C, D,  $x_m$  and  $C_{GAB}$  are empirical regression parameters

One of the goals of drying is to lower  $a_w$  below a critical value to obtain a stable powder, avoiding growth of micro-organisms and development of unwanted reactions (Fig. 1.4). But water activity is also in relation with glass transition phenomena and sticky properties of products. Stickiness during drying and/or caking during storage can occur for some powders made of potentially sticky components (e.g. sugars), for specific conditions of temperature and humidity (Shrestha et al., 2007a,b,c).

### 1.2.2. Density

Powder density is generally described by the bulk density  $\rho_{\text{bulk}}$  ( $\text{kg}\cdot\text{m}^{-3}$ ), defined as the ratio between the mass of many particles of the material and the total (bulk) volume they occupy. The total volume includes individual particles volume, inter-particle voids volume and internal pores volume. It represents an important property for powder handling, for marketing and economics, even if the different needs can be in contrast between them. As an example, a high bulk density is required for reducing transportation costs that depend on total volume. But a low bulk density may correspond to a more attractive product with improved instant properties (Pisecky, 1997).

Bulk density is not an intrinsic property of a material; it can change depending on how the material is handled. For this reason, the bulk density of powders is usually reported both as "freely settled" and "tapped" density. The tapped density refers to the bulk density of the powder after a specified compaction process, usually involving controlled vibration of the container (in relation with transportation, shocks of packages).

Bulk density depends on the density  $\rho_s$  of the solid composing the powder, on air volume inside the particles (occluded and in open pores) and on the shape of the particles that influences the amount of interstitial air between the particles. A regular spherical particle shape minimizes the amount of interstitial air. Controlling the amount of occluded air could lead to a higher or lower bulk density. For example, stirring of the liquid feed solution may result in the creation of air bubbles inside the liquid, then in the drops and in final powder particles.

A lower bulk density is usually obtained with particles agglomeration. By assembling several small particles with solid bridges, a porous structure is formed (agglomerate) with voids between particles, increasing the mean size, decreasing the fines proportion, and leading to specific instant properties.

### 1.2.3. Flowability and instant properties

Flowability is defined as the ability of a powder to exhibit a free-flow behaviour. Good flowability of final powders is required for easy transportation in pipes (i.e. to fill packages) and for various uses like in vending machines. Several factors affect powder flowability, like size, shape and composition of the surface of the particles (Teunou et al., 1999; Fitzpatrick et al., 2004). Large mean particle size, narrow particle size distribution, spherical shape and smooth surfaces with no sticky or fat components contribute to a better flowability.



**Table 1.1.** Total spray exchange surface depending on drops diameter for a fixed sprayed liquid volume of 1 m<sup>3</sup> (Mujumdar, 1995).

Total Volume (m <sup>3</sup> )	Droplet diameter (m)	Number of droplets	Droplet surface A <sub>drop</sub> (m <sup>2</sup> )	Total spray surface A <sub>tot</sub> (m <sup>2</sup> )
1	1.234	1	3.14	3.14
1	1 x 10 <sup>-2</sup> (1cm)	1.986 x 10 <sup>6</sup>	3.14 x 10 <sup>-4</sup>	623.6
1	1 x 10 <sup>-3</sup> (1mm)	1.986 x 10 <sup>9</sup>	3.14 x 10 <sup>-6</sup>	6236
1	1 x 10 <sup>-4</sup> (100µm)	1.986 x 10 <sup>12</sup>	3.14 x 10 <sup>-8</sup>	62360
1	1 x 10 <sup>-5</sup> (10µm)	1.986 x 10 <sup>15</sup>	3.14 x 10 <sup>-10</sup>	623600

Food powders are often reconstituted as liquid solutions (emulsions, suspensions) by adding water (or a liquid, e.g. milk). If the result is an homogeneous liquid obtained rapidly without unsolved lumps, the powder has a good instant behaviour. The particles size, porosity, composition and the presence of some components (hydrophobe) on the surface will play an important role in the behaviour of the powder during reconstitution.

The instant properties are described as sinkability, wettability, dispersibility and solubility (Schubert, 1993; Fang et al., 2008). The sinkability expresses how particles penetrate the liquid surface. The wettability determines the time necessary for liquid penetration in the porous structure of powder, thanks to capillarity; it is often the rate determining step. Wettability is measured as the wetting time of a fixed amount of powder in contact with a water surface, till the last particles of powder penetrate the water surface. A quick wetting is enhanced by a good porosity of powder.

Particle size is another parameter: for example, for milk powders particles diameter should be between 200 and 300  $\mu\text{m}$ , with fines ( $d < 100 \mu\text{m}$ ) fraction lower than 20%. Too small particles are difficult to wet due to high surface tension of liquid compared to particles weight (Pisecky, 1997).

Dispersibility is the aptitude for the powder to be re-distributed as single particles in the reconstituting liquid. Solubility refers to the rate and extent to which the components of the powder particles dissolve in the liquid.

Dispersibility and solubility determine if the powder is completely dissolved or not, by evaluation of powder residuals observed in the liquid solution after filtration. The percent of dissolved powder compared to the total solids concentration give a dispersibility index (Pisecky, 1997).

To improve instant properties of spray dried powders, an agglomeration step is often performed (Buffo et al., 2002).

## **2. Drying of liquid drops**

The atomization of liquid into drops is the first step of the spray drying process. It determines the size and drying behavior of drops, influencing the final powder properties (Hecht and King, 2000; Horvat et al., 2002; Wu and Liu, 2002; Walton and Mumford, 1999; Xiao et al., 2008). The liquid feed is a solution (or emulsion, suspension), usually concentrated by evaporation before spray drying to eliminate most of the water easily removable by an economical operation.

The complex formulation of the liquid feed solution is studied as a function of the aptitude of components to dry to obtain the desired composition of the final powder. The dry matter content is limited by the possibility of pumping the solution to the atomizer (viscosity, temperature).

### **2.1. Atomization of liquid feed in drops**

The principle of atomization consists in giving energy to the liquid to form a thin liquid film and to break it in a large number of drops to increase the exchange surface available for heat and mass transfers with drying air. By decreasing the drop size from 1 mm to 10  $\mu\text{m}$ , the total spray surface is multiplied by 100 (Table 1.1).

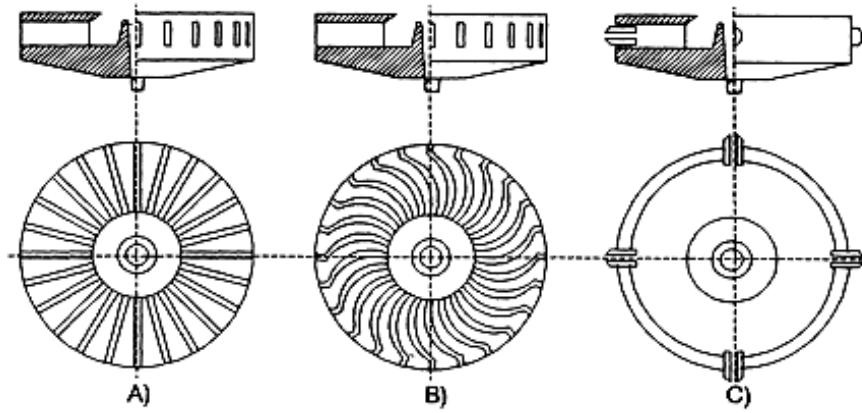


**Figure 1.5.** Rotary atomizer with (a) straight radial vanes, with (b) curved vanes and with (c) bushings (adapted from Pisecky, 1997).

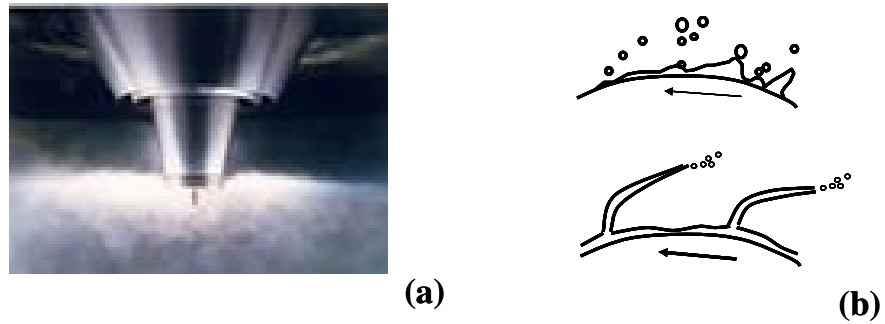


**Figure 1.6.** Spray from a rotary atomizer (a) and mechanisms of drop formation (b) (www.niro.com; Masters, 1985).

The minimal energy  $P_K$  needed to form the new exchange surface  $A_{tot}$  can be expressed as  $P_K = A_{tot} \cdot \sigma$  (with  $\sigma$  surface tension of liquid ( $N \cdot m^{-1}$ )) (Masters, 1985). Due to the energy losses, this minimal energy is only a part of the total energy used by the atomizer.

The type of energy transferred to the liquid to break it in drops is used to classify the atomizers: *rotary atomizer* with centrifugal energy, *pressure nozzle* with pressure energy, and *pneumatic nozzle* with kinetic energy.

### 2.1.1. Rotary atomizer

A rotary (or wheel) atomizer consists of two circular plates (top and bottom) with radial vanes (straight or curved) or bushings between them (Fig. 1.5). The liquid feed enters in the centre, accelerates across the vanes forming a thin film of liquid that is ejected at the wheel peripheral speed and readily disintegrates into droplets forming a wide jet with an “umbrella” shape; initial trajectory is almost horizontal (Fig. 1.6). Typical peripheral speed for rotary atomizers varies from 100 to 200  $m \cdot s^{-1}$ . The rotary atomizer can be moved by compressed air (pilot equipments) or by an electrical engine.

The characteristics of the liquid spray depend on the peripheral speed and geometry of the rotary atomizer, on the flow rate and physical properties of liquid (King et al., 1984).

Size and size distribution of final powder depend on the initial droplets size distribution. The Sauter mean diameter  $d_{3,2}$ , defined as the ratio of the total droplets volume to the total droplets surface, is often used to characterize particle and drop average size. For rotary atomizers, the following empirical correlations are proposed (Masters, 1985; Mujumdar, 1995):

$$\frac{d_{3,2}}{r} = 0.4 \left( \frac{\dot{m}_l}{N_v \cdot b \cdot \rho \cdot N \cdot r^2} \right)^{0.6} \cdot \left( \frac{N_v \cdot \mu \cdot b}{\dot{m}_l} \right)^{0.2} \cdot \left( \frac{\sigma \cdot b^3 \cdot \rho \cdot N_v^3}{\dot{m}_l^2} \right)^{0.1} \quad \text{eq. 1.4}$$

$$d_{3,2} = 0.241 \cdot \left( \frac{1}{N} \right)^{0.6} \left( \frac{1}{\rho} \right)^{0.3} \left( \frac{\mu \dot{m}_l}{2r\rho} \right) \cdot \left( \frac{\sigma}{Nvb} \right)^{0.1} \quad \text{eq. 1.5}$$

$$d_{3,2} = 1.62 \cdot 10^{-3} \cdot N^{-0.53} \cdot \dot{m}_l^{0.21} \cdot (2r)^{-0.39} \quad \text{eq. 1.6}$$

$d_{3,2}$  mean Sauter diameter of drops (m) = (droplets volume)/(droplets surface),  $\dot{m}_l$  liquid flow rate ( $kg \cdot s^{-1}$ ),  $N$  rotary speed of disk (rpm),  $r$  diameter of disk (m),  $b$  height of vanes (m),  $N_v$  number of vanes,  $\rho$  density of liquid ( $kg \cdot m^{-3}$ ),  $\sigma$  surface tension of liquid ( $N \cdot m^{-1}$ ) and  $\mu$  viscosity of liquid (Pa.s)

The last equation can be used when the physical properties of the liquid are not known. And to apply these correlations to non-newtonian fluids, the dynamic viscosity must be substituted by the apparent viscosity of the fluid.

These empirical correlations can be applied to all types of rotary atomizer to estimate the drop size with a precision of  $\pm 30\%$ . To determine the drop size and size distribution for a given atomizer - requested for example for a numerical simulation of the process – a specific correlation may be developed or a direct measuring technique should be used.

Non-intrusive laser techniques like PDA (*Phase Doppler Anemometry*) could allow direct measurement of the drop size distribution and velocity at the exit of atomizer assuming that the droplets are spherical (Albrecht, 2003). However, use of PDA is difficult for rotary atomizers due to the wide shape of the liquid spray. Other mechanical, electrical and optical measuring methods are listed by Dodge (1987).

**Table 1.2.** Typical droplet size, maximum liquid feed flow rate and energy consumption of several kinds of atomizers (Mujumdar, 1995).

Atomizer	Range of drop size ( $\mu\text{m}$ )	Liquid flow rate ( $\text{kg.h}^{-1}$ )	Energy consumption ( $\text{kJ for } 1000 \text{ kg.h}^{-1}$ )
Rotary wheel	1-600	< 2000	25.0
Pressure nozzle	10-800	< 100	2.5 (3-5 MPa)
Pneumatic nozzle	5-300	< 1000	40.0 (air 0.3 MPa; $0.5\text{-}0.6 \text{ m}^3.\text{kg}^{-1}$ )
Sonic nozzle	5-1000	-	-

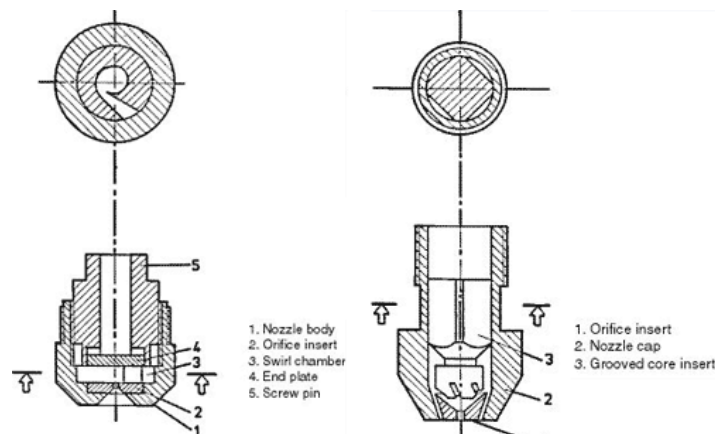


**Figure 1.7.** Pressure nozzle (adapted from Pisecky, 1997).

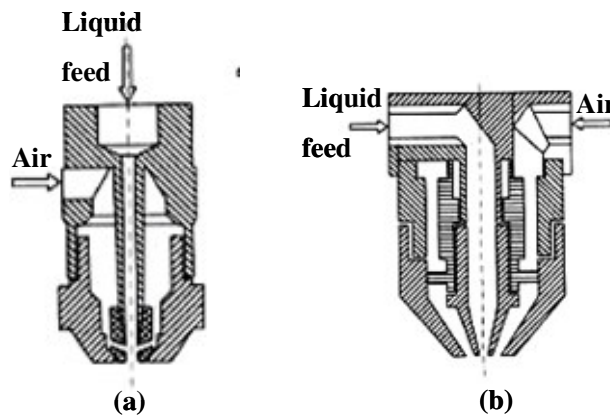


**Figure 1.8.** Two-fluid nozzle with (a) internal air/liquid mixing and (b) external mixing (adapted from Pisecky, 1997).

By controlling the wheel velocity, it is possible to change the drops size distribution. In comparison with other atomizing devices, the wheel atomizer is more flexible because it can operate with different liquid flow rates without big modifications in droplets size and it is able to operate with higher feed viscosity (or concentration) and with liquid feed containing possibly abrasive solids. Finally, high capacities (Table 1.2) can be handled by a single rotary atomizer.

As a disadvantage, the energetic cost is higher than for pressure nozzles. Furthermore, the drying chamber must have a large diameter to avoid collisions between the radially ejected drops and the walls of the chamber.

Another possible problem may appear due to the aspiration of air by the rotating wheel (like a fan). This air can be incorporated into the droplets, and modify final properties of the powder like density. If this effect is unwanted, it is better to use the configuration with curved vanes, which reduces the air aspiration effect.

### 2.1.2. Pressure nozzle

With a pressure nozzle (Fig. 1.7) the spray is created by the conversion of the pressure energy applied to the liquid into kinetic energy giving, at the same time, a rotary motion to the thin liquid film.

The liquid is forced through an orifice by a high pressure pump (5-7 MPa). It enters tangentially in the nozzle and exits from the orifice (diameter = 0.4 to 4 mm) forming a cone having an angle in the range of 40°-140°.

The pressure nozzle leads to the formation of a spray more homogeneous in terms of drop size distribution than the one produced by a rotary atomizer. The applied pressure influences the angle of the cone and the drops size, which can be estimated with empirical correlations like the following (Mujumdar, 1995):

$$d_{3,2} = 286[(2.54 \cdot 10^{-2})d_{or} + 0.17] \exp\left[\frac{39}{v_{ax}} - (3.13 \cdot 10^{-3})v_1\right] \quad \text{eq.1.7}$$

$d_{3,2}$  mean Sauter diameter of drops (m),  $d$  diameter of the orifice,  $v_1$  inlet air velocity (m.s<sup>-1</sup>),  $v_{ax}$  axial air velocity (m.s<sup>-1</sup>).

Other correlations are proposed by Masters (1985), Lefebvre (1989) and Kim and Marshall (1971). A single pressure nozzle can atomize a liquid flow rate up to 100 kg.h<sup>-1</sup>. For this reason several nozzles are normally used inside industrial spray drying towers. In that case the collisions between the drops of the different sprays formed by each nozzle can lead to coalescence or agglomeration, with an influence on the final powder properties.

The main differences between pressure nozzle and rotary atomizers consist in the formation of air-free droplets, in the possibility of directing the spray of different nozzles in order to obtain or to avoid collisions between drops and in the smaller diameter of the chamber due to the more compact shape of the spray. Furthermore, the nozzle has a lower investment cost and the maintenance is easier due to the absence of moving parts.

As disadvantage for nozzles, varying the liquid flow rate modifies the characteristics of the spray: a higher flow rate leads to higher velocity with formation of smaller drops. If the viscosity of the fluid is high, the orifice can be blocked; fluid containing abrasive particles can damage the orifice.

### 2.1.3. Pneumatic nozzle

The pneumatic (or two-fluid) nozzle uses compressed air (or steam) to atomize the liquid. Mixing between liquid feed and atomizing air can be internal or external (Fig. 1.8). In some spray drying towers, the two-fluid nozzle is installed in the bottom of the chamber (Fig. 1.9)

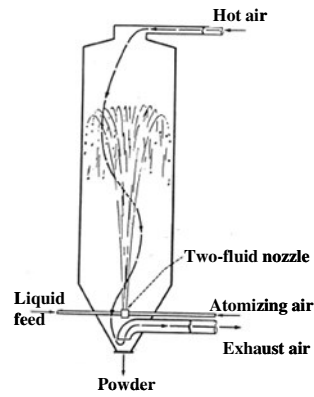


**Figure 1.9.** Spray drying chamber with fountain two-fluid nozzle (adapted from Mujumdar, 1995).

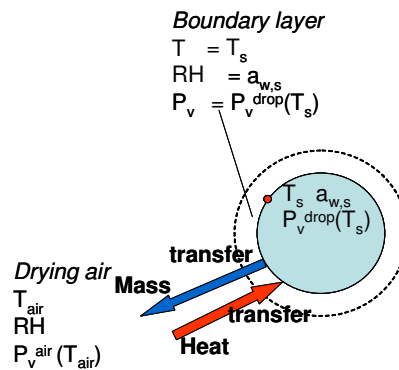


**Figure 1.10.** Convective drying of a liquid drop; heat and mass transfers between drying air and drop surface through the boundary layer.

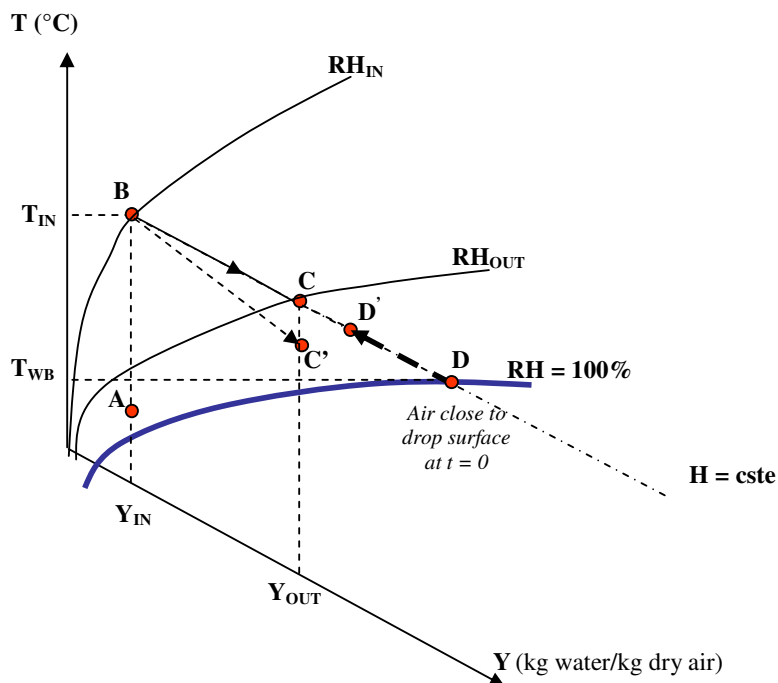


**Figure 1.11.** Mollier diagram - Air temperature and relative humidity evolution during spray drying.

and depending on the atomizing air pressure the liquid can be sprayed at different heights inside the chamber (“fountain” nozzle).

Pneumatic nozzles are used to produce sprays in which the drops diameter can be changed by varying the air/liquid ratio. With two-fluid nozzles it is possible to maintain the same drop size distribution when changing the liquid flow rate, by adjusting the compressed air flow rate.

The main disadvantage of this kind of atomizer is the cost of compressed air (or steam). Due to the compact shape of the spray from nozzles compared to the rotary atomizer spray, it is easier to measure directly the drops size by laser diffraction by performing some spray experiments outside the dryer chamber (Jimenez, 2007).

#### 2.1.4. Sonic nozzle

Some liquid feed as non-newtonian liquids or highly viscous materials can not be atomized with rotary wheel or pressure nozzles. For this reason attention has been paid to the development of a different atomization technique using sonic energy (Sears and Ray, 1980; Upadhyaya, 1982). The break-up of liquid occurs in the field of high-frequency sound created by a sonic resonance cup placed in front of the nozzle.

**In conclusion**, the choice of atomizer depends on the physical properties of the liquid feed and on the wanted properties of the final powder in terms of size, size distribution, density, agglomeration. It determines the required energy to form the spray of drops (Table 1.2), their size and size distribution, their trajectory and their speed at the entrance in the chamber. A narrow drop size distribution is required for a better control of the drying process (same behavior for all the drops) and of the final powder properties.

In industry, there is no general rule, the choice depending mainly on the product, on the know-how and equipments.

## 2.2. Drying of drops in air for co-current spray dryer

Spray drying is a convective drying process in which hot air provides energy for evaporation of solvent (usually water) from liquid drops, inside the limited volume of a chamber. In co-current dryer, just after drop formation by atomization, drops are in contact with inlet air. Drops and air move together and exchange heat and water. The water vapor is transferred from drop surface to surrounding air through the air boundary layer surrounding each particle (Fig. 1.10). As a consequence, drops/particles are drying and air is cooled and humidified while crossing the chamber.

### 2.2.1. Evolution of air properties along drying (Mollier diagram)

The evolution of air properties (T, RH, Y) during the spray drying can be followed on a Mollier diagram (Fig. 1.11). Drying air is taken from ambient and heated up to the desired inlet temperature  $T_{IN}$ , without variation in its water content  $Y_{IN}$  (A→B on Fig. 1.11). Then during drying, air temperature decreases, while relative humidity and water content increase (B→C on Fig. 1.11). The total amount of water evaporated from drying drops that goes into air, can be calculated with a global mass balance of water applied either to air or to the product between the entrance and the exit of the dryer (Bimbenet et al., 2002). Or balance equations may be also written between entrance and any point in the dryer if we are able to know the properties of air (Y) and particles (X) at this point.

Assuming that dry air flow rate  $\dot{m}_{air}$  and total solids flow rate  $\dot{m}_s$  are constant, the total evaporated water flow rate  $\dot{m}_{ew}$  is:





$$\dot{m}_{ew} = \dot{m}_{air} (Y_{OUT} - Y_{IN}) = \dot{m}_s (X_{IN} - X_{OUT}) \quad \text{eq. 1.8}$$

The conditions of exit air ( $T_{OUT}$ ,  $Y_{OUT}$ ,  $RH_{OUT}$ ) depend on the amount of evaporated water and on the inlet air temperature and flow rate. In particular, for a fixed inlet air flow rate  $\dot{m}_{air}$  and temperature  $T_{IN}$ , the exit air temperature  $T_{OUT}$  will depend on the liquid feed flow rate. For this reason, the exit air temperature is often the parameter used for control of liquid feed flow rate (I.5).

In practice drying is not isenthalpic due to some heat losses. As a consequence, for the same amount of evaporated water, outlet air temperature  $T_{OUT}$  will be lower than for isenthalpic drying and  $RH_{OUT}$  will be higher ( $B \rightarrow C'$ ).

To simplify, in the following descriptions we will assume an isenthalpic drying.

### 2.2.2. Drying rate: heat and mass transfer equations

The drying rate will depend on the heat and mass transfers between air and drops.

At any moment we can assume that the drop surface is in equilibrium with the air boundary layer. In this layer air temperature is equal to the drop surface temperature  $T_s$ , and air relative humidity is equal to the drop surface water activity  $a_{w,s}$ . At a given temperature, from water activity definition, the water vapour pressure at the surface of the drop can be written as:

$$P_v^{drop}(T_s) = a_{w,s} \cdot P_w^{sat}(T_s) \quad \text{eq. 1.9}$$

We assume that all the drops of the spray have the same small diameter, neglecting shrinkage during drying (constant drop diameter) and an homogeneous temperature (surface and core,  $T_{drop} = T_s$ ). For isenthalpic drying (no heat losses), the heat exchanged between air and drops is used to evaporate water, with the general equation for one drop:

$$h_c \cdot A_{drop} \cdot (T_{air} - T_s) = \Delta H_v \cdot \frac{dm}{dt} \quad \text{eq.1.10}$$

If we consider all the drops  $N_{drops}$  in air at the same distance from atomizer (axial symmetry), the general mass transfer (water) from drops surface to air can be expressed as:

$$\begin{aligned} \frac{dm}{dt} \cdot N_{drops} &= k_c N_{drops} A_{drop} (P_v^{drop}(T_s) - P_v^{air}(T_{air})) \\ &= k_c A (a_w \cdot P_w^{sat}(T_s) - RH \cdot P_w^{sat}(T_{air})) \end{aligned} \quad \text{eq.1.11}$$

$h_c$  convective heat transfer coefficient between air and drops ( $W \cdot m^{-2} \cdot K^{-1}$ );  $N_{drops}$  number of drops;  $A_{drop}$  one drop surface ( $m^2$ );  $A$  total drops exchange surface ( $N_{drops} \cdot A_{drop}$ ) ( $m^2$ );  $T_{air}$ ,  $T_s$  air and drop surface temperature ( $^{\circ}C$ );  $\Delta H_v$  water specific heat of vaporization ( $J \cdot kg^{-1}$ );  $\frac{dm}{dt}$  evaporated water mass flow rate ( $kg \cdot s^{-1}$ );  $k_c$  mass transfer coefficient between air and drops ( $s \cdot m^{-1}$ );  $P_{v,drop}$ ,  $P_{v,air}$  water vapour pressure at drop surface and in air (Pa);  $P_{w,sat}$  saturated water vapour pressure (Pa);  $a_w$  water activity;  $RH$  air relative humidity.

Convective heat transfer coefficient  $h_c$  and mass transfer coefficient  $k_c$  can be calculated from correlations of Ranz-Marshall for drops and analogy between heat and mass transfer (Bimbenet et al., 2002):

$$\begin{aligned} Nu &= h_c \cdot d_p / k_{\infty} = 2 + 0.6 Re^{1/2} \cdot Pr^{1/3} \quad \text{for } 1 < Re < 450, Pr < 250 \\ Sh &= k_c \cdot d_p / D_w = 2 + 0.6 Re^{1/2} \cdot Sc^{1/3} \quad \text{for } 1 < Re < 450, Sc < 250 \end{aligned}$$

$Nu$  Nusselt number;  $k_{\infty}$  thermal conductivity of continuous phase ( $W \cdot m^{-1} \cdot K^{-1}$ );  $Sh$  Sherwood number;  $D_w$  water vapour diffusion coefficient in air ( $m^2 \cdot s^{-1}$ );  $Pr$  Prandtl number ( $c_p \cdot \mu_{air} / k_{\infty}$ );  $Sc$  Schmidt number ( $\mu_{air} / (D_w \cdot \rho_{air})$ )

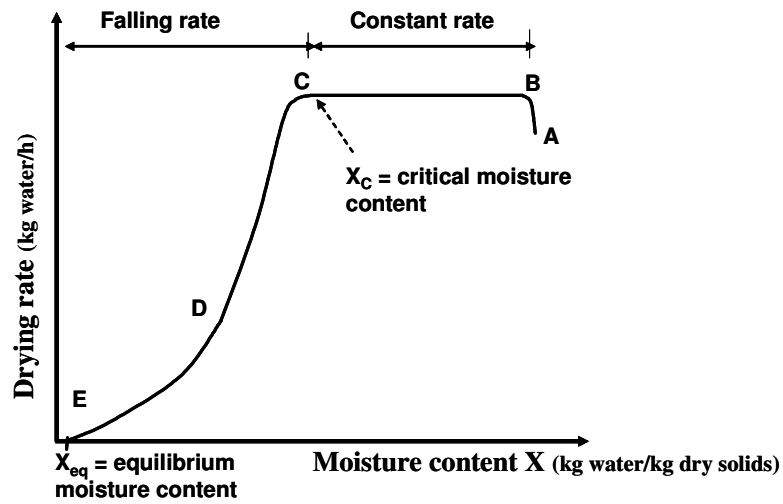


**Figure 1.12.** Evolution of drying rate of liquid drops.

**Table 1.3.** Time for complete evaporation of a water drop in still air as a function of initial diameter (average temperature difference between drying air and drop 65 °C;  $\lambda$  (65°C) = 0.027 W.m<sup>-1</sup>.K<sup>-1</sup>;  $\Delta H_v$  = 2390 kJ.kg<sup>-1</sup>)

$d_{drop}$ ( $\mu\text{m}$ )	Time for complete evaporation (s)
10	0.02
30	0.15
50	0.42
100	1.7

These equations show that the drying rate will depend on different parameters more or less linked and evolving along drying:

- the initial liquid flow rate and the surface of one drop (temperature and diameter almost constant)
- the heat and mass transfer coefficients
- the water activity of particle which is decreasing along the process
- the air relative humidity (increasing) and the air temperature (decreasing).

### 2.2.3. Evolution of drops properties along drying

At the beginning of drying, atomized solution drops (water + dry matter) are liquid and their surface water activity may be considered equal to 1 (free water). Close to drop surface, the layer of air immediately in contact has a relative humidity  $RH = 100\%$  (Fig. 1.11 D) and the temperature is the wet bulb temperature ( $T_s = T_{wb}$ ; e.g.  $T_{IN} = 200^\circ\text{C} \rightarrow T_{wb} \sim 50^\circ\text{C}$ ). Drops are almost instantly heated up to this temperature (AB, Fig. 1.12), and then drying occurs at constant rate (BC, Fig 1.12).

The drying particle will then reach a critical value of moisture content for which the surface is no longer saturated and  $a_{w,s}$  will decrease progressively while drying occurs. Drying becomes limited by the internal water mass transfer (diffusion from the still humid core to the surface), which is described by the diffusion coefficient  $D_v$  (Raederer, 2001). In this phase, drop surface temperature could increase if heat provided by drying air is bigger than the heat needed for evaporation (Fig. 1.11 D $\rightarrow$ D').

As a consequence there will be a reduction of gradients of temperature and gradients of water vapor pressure gradients between drop surface and surrounding air, resulting in a decrease of the evaporation rate (falling rate drying period, CD in Fig. 1.12).

Just after atomization, liquid drops are in contact with hot air (usually 120 to 300°C) with low relative humidity. Due to the large exchange surface of the small drops and to the high air temperature, air flow rate and air turbulence around the drops, heat and mass exchanges are very quick so that most of drying could be completed in some seconds depending on the chosen operating conditions.

Considering a spherical water drop (surface water activity remains equal to 1 until complete evaporation) with a relative air/particle velocity close to 0, time necessary for drying (evaporation) in still air ( $v = 0 \text{ m}\cdot\text{s}^{-1}$ ) can be calculated as (Masters, 1985):

$$t = \frac{\Delta H_v \cdot \rho}{8 \cdot \lambda \cdot \Delta T} \cdot (d_{in}^2 - d_{fin}^2) \quad \text{eq. 1.12}$$

$d_{in}$  droplet initial diameter;  $d_{fin}$  droplet final diameter (= 0 if complete evaporation);  $\Delta T$  average temperature difference between drying air and drop;  $\lambda$  average thermal conductivity of gaseous film surrounding the evaporating droplet ( $\text{W}\cdot\text{m}^{-1}\cdot\text{K}^{-1}$ );  $\Delta H_v$  specific heat of vaporization of water ( $\text{kJ}\cdot\text{kg}^{-1}$ ).

For an average drying air temperature of 65°C, drying time for complete evaporation should be lower than 2 seconds for droplets diameter between 10 and 100  $\mu\text{m}$  (Table 1.3). But in the case of a solution, time necessary for drying will be increased due to water interaction with solutes.

Ideally the final powder particle should be in equilibrium (temperature and water activity) with exit air (D $\rightarrow$ E in Fig. 1.12, D $\rightarrow$ D' in Fig. 1.11) but as the process is very fast, equilibrium between air and product is usually not reached inside the spray dryer chamber. The particles being small ( $\sim 20 \mu\text{m}$ ), the temperature is homogeneous but the core is probably more humid than the surface.

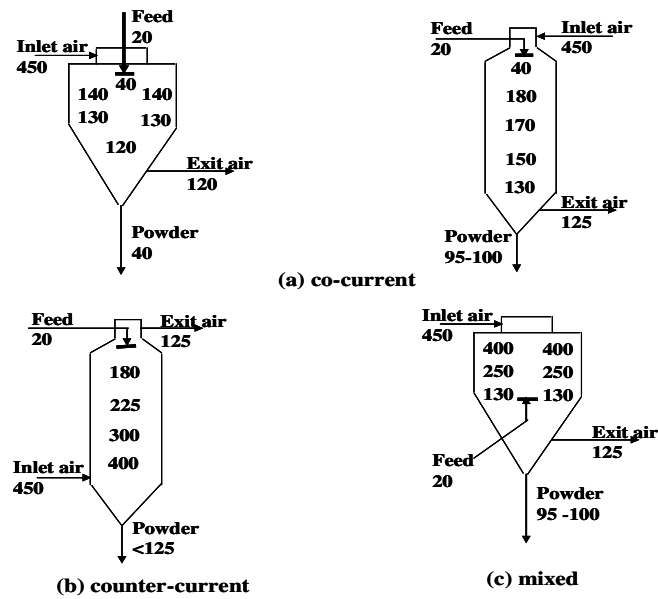


**Figure 1.13.** Air/drops contact inside the spray dryer chamber with typical air temperature values: (a) co-current, (b) counter-current and (c) mixed (Mujumdar, 1995).

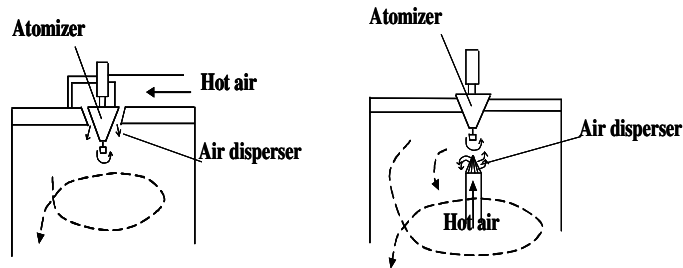


**Figure 1.14.** Air swirling flow due to air disperser in co-current spray dryers (Masters, 1985).

Removal of water may result in shrinkage of the drying material: normally, the volume occupied by dry matter and water is decreased by an amount equal to that of evaporated water with no porosity (Alamilla-Beltran et al., 2005). But formation of very small internal voids could replace the volume of evaporated water, and according to the composition and fast drying the final particle size can be similar to the initial droplet size (Raederer, 2001; Chen, 2002).

#### **2.2.4. Configurations for air/drops contact**

The mode of contact between the air stream and the liquid drops strongly affects the drying process and the final powders properties. Three configurations of the air/drops contact are proposed (Fig.1.13):

- 1. Co-current contact** (Fig. 1.13a), in which the drops have the same direction as air (usually from top to the bottom of the chamber). It is the most used system for drying of heat sensitive products. Due to the high temperature difference between air and drops at the entrance of the chamber, water evaporation is quick. An advantage is that the dried particles in the bottom of the chamber are in contact with an air at low temperature whilst particles in contact with the hot entering air are at the wet bulb temperature ( $a_w = 1$ ). In the example in Fig.1.13 air enters at 450°C, and dry powder leaving the chamber is in contact with an air at 120°C.
- 2. Counter-current contact** (Fig. 1.13b), in which hot air enters by the bottom of the chamber where it is in contact with almost dried drops that fall down. Air exits from the top of the chamber. This kind of contact allows a better thermal efficiency of the process, but it is not suitable for heat sensitive products (like many food products) because the final dry powder in the bottom of the chamber is directly in contact with the inlet hot air (450°C in example in Fig.1.13). This configuration is used with nozzles.
- 3. Mixed contact** (Fig. 1.13c), used to reduce the dimension of the chamber. If product is not heat sensitive, it is the cheapest configuration.

In each configuration, air flow inlet direction inside the chamber can be controlled by dispersion devices that may cause a swirling flow and turbulence to enhance heat and mass transfers (Fig.1.14).

The main consequences of the choice of the air/drops contact configuration are on:

- The trajectories and residence time of particle inside the chamber
- The maximal temperature reached by the powder
- The deposition on walls (product losses)
- The size and the geometry of the chamber.

**In our study we focused on co-current spray dryers, usual in food industry.**

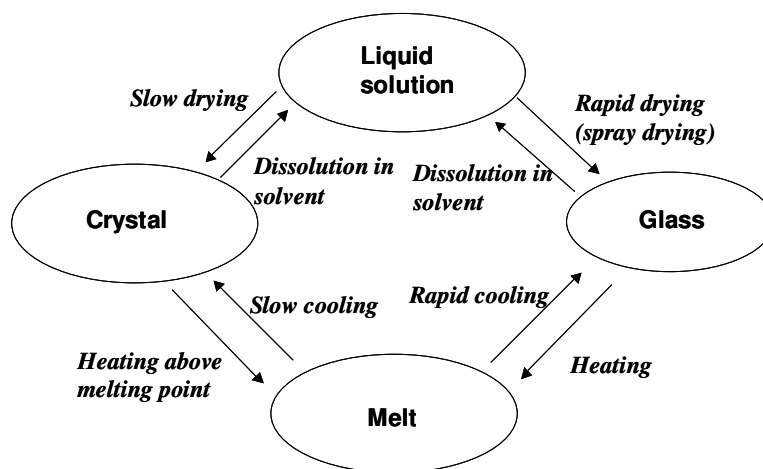


**Figure 1.15.** Schematic diagram indicating possible phase transitions of a material (adapted from Bhandari and Hartel, 2005).

**Table 1.4.** Glass transition temperature of several dry food materials (Adhikari et al., 2003).

Materials	Molecular weight (g.mol <sup>-1</sup> )	T <sub>g</sub> (°C)
Fructose	180	5
Glucose	180	31
Galactose	180	32
Sucrose	342	62
Maltose	342	87
Lactose	342	101
<i>Maltodextrins</i>		
DE36	500	100
DE25	720	121
DE20	900	141
DE10	1800	160
DE5	3600	188
Water	18	-135

### 3. Particles sticky behaviour along spray drying

#### 3.1. The glass transition phenomenon in drying

Drying of solutions with soluble components like salt (NaCl) will lead to crystallization. When solutes may show an amorphous phase, the final state of dried product will depend on the components and on the drying rate (fast or slow), with intermediate states to consider. The slow drying of a substance like lactose solution leads normally to the formation of a crystalline solid, when the solubility limit is reached. The corresponding values of concentration and melting temperature  $T_m$  can be read on a state diagram of the considered substance (Roos and Karel, 1991a; Vuataz, 2002; Schuck, 2002). The crystalline state is energetically stable: molecules are strongly bound and form a well organized structure. But if drying is fast enough to prevent the formation of crystals, the material reaches the solid state keeping the liquid random structure; this configuration of “fixed liquid” is called amorphous or glassy state, in which the high viscosity does not allow the molecules to rearrange in an organized structure (Fig. 1.15). The passage from the liquid to the glassy state is called glass transition, with a glass transition temperature  $T_g$  (or domain of temperature) associated to this transition (Bhandari and Hartel, 2005). The glass transition corresponds to the modification of several properties of the substance.

When the product is dried below  $T_g$  (Downton et al., 1982; Roos, 1995):

- The viscosity increases till about  $10^{12}$  Pa.s (for  $T_g$ )
- The thermal capacity  $C_p$  decreases
- The dielectric coefficient and thermal expansion coefficient decrease
- The free volume of molecules decreases

The increase of viscosity will correspond, for a critical value, to an intermediate rubbery state for which the substance becomes “sticky” before glass transition. The viscosity value of a substance close to the glass transition as a function of its temperature can be calculated with the Williams-Landel-Ferry (WLF) (1955) equation, which is valid in the range  $T_g - (T_g+100^\circ\text{C})$ .

$$\log\left(\frac{\mu}{\mu_g}\right) = \frac{C(T-T_g)}{B+(T-T_g)} \quad \text{eq.1.13}$$

$T_g$  glass transition temperature ( $^\circ\text{C}$ );  $\mu_g$  viscosity at  $T_g$  ( $10^{12}$  Pa.s); C and B empirical coefficients. The values of constant parameters B and C used by Williams-Landel-Ferry (C = -17.4; B = 51.6) are valid for most of the polymers.

The rubbery state is obtained for values of viscosity between  $10^{12}$  Pa.s (at  $T_g$ ) and  $10^7$  Pa.s, corresponding to a sticky temperature ( $T_{\text{sticky}}$ ), in a domain 10 to  $30^\circ\text{C}$  higher than  $T_g$  depending on the considered material (Adhikari et al., 2007).

$T_g$  is a specific property of each dry pure substance, strongly dependent on its molecular weight. Polymers as sucrose having a low molecular weight have a low  $T_g$ . For similar products (maltodextrins) the smaller the molecule, the lower the  $T_g$  of the substance. Glass transition temperatures of some food substances are reported in Table 1.4.

The knowledge of the  $T_g$  of pure substances allows predicting the  $T_g$  of mixtures (water and other components). The  $T_g$  of a mix is a non-linear function of  $T_g$  of each component. It could be calculated with the Gordon-Taylor (eq. 1.14) and the Couchmann-Karasz equations for 2 components (eq. 1.15):



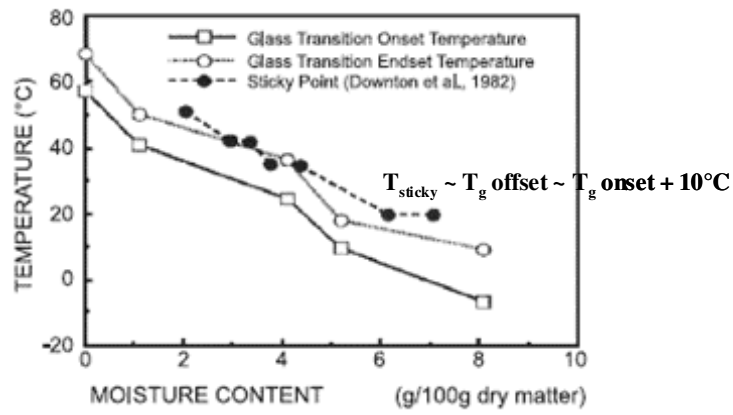


**Figure 1.16.** Relation between onset  $T_g$ , offset  $T_g$  and sticky temperature  $T_{\text{sticky}}$  (from Roos and Karel, 1991c).

$$T_g = \frac{w_1 \cdot T_{g1} + K \cdot w_2 \cdot T_{g2}}{w_1 + K \cdot w_2} \quad \text{eq. 1.14}$$

$$\ln T_g = \frac{w_1 \cdot \ln T_{g1} + \frac{\Delta C_{p2}}{\Delta C_{p1}} \cdot w_2 \cdot \ln T_{g2}}{w_1 + \frac{\Delta C_{p2}}{\Delta C_{p1}} \cdot w_2} \quad \text{eq. 1.15}$$

$w_1$  ,  $w_2$  mass fraction of component 1, 2;  $T_{g1}$ ,  $T_{g2}$  glass transition temperature of pure component 1, 2; K empirical regression coefficient;  $C_{p1}$  ,  $C_{p2}$  specific heat of component 1, 2

These equations can be extended to mixtures having more than two components.

$T_g$  of a product depends strongly on its water content. Actually, water has a very low glass transition temperature of -135 °C, so that the presence of even small amounts of water strongly decreases the  $T_g$  of foodstuffs. Water behaves as the major plasticizer for food substances. As water content of particles evolves very quickly during spray drying, surface  $T_g$  of the particle will vary strongly during the process.

Combining GAB equation for sorption isotherms (eq. 1.2) with Gordon-Taylor equation (eq. 1.14) for glass transition temperature, a direct relationship between glass transition temperature and water activity could be obtained (Palzer, 2005a).

$$T_g(a_w) = \frac{(1 - a_w) \cdot (1 + (C - 1) \cdot a_w) \cdot T_g + K \cdot B \cdot C \cdot a_w \cdot T_{gw}}{(1 - a_w) \cdot (1 + (C - 1) \cdot a_w) + K \cdot B \cdot C \cdot a_w} \quad \text{eq. 1.16}$$

(K, B, C parameters)

This relationship is useful for food substances mixtures, in which water activity at the equilibrium is the same for all the constituents even if they have different water contents (Roos, 2002; Schuck et al., 2005).

The techniques to evaluate the glass transition temperature  $T_g$  of a product are based on the measurement of the modification of the physical properties of the substance (Shrestha et al., 2007a; Boonyai et al., 2007):

-DSC (Differential Scanning Calorimetry) to measure the variation of Cp or of enthalpy associated to glass transition;

-NMR (Nuclear Magnetic Resonance) to measure the mobility of molecules (Ruan et al., 1999),

-DMTA (Dynamic Mechanical Thermo Analysis), to evaluate changes in mechanical properties.

A small amount of powder (11-15 mg) is necessary for measurements (Adhikari et al., 2001). The phase change from amorphous to rubbery state does not occur at a fixed temperature, but in a range of temperatures (second order thermodynamic transition). It is possible to consider as  $T_g$  of the substance either the temperature at which properties modifications begin (onset  $T_g$ ), or the end of properties modifications (offset  $T_g$ ) or the middle temperature (midset  $T_g$ ).

The existence of a correlation between glass transition temperature – used in polymer science – and sticky temperature  $T_{sticky}$  has been proposed for food powders by Roos and Karel (1991a,b,c). Several studies show that the sticky domain is situated 10-30°C higher than onset  $T_g$ , and close to the offset  $T_g$  (Fig. 1.16). But the appearance of stickiness depends also on the time during which the product is exposed to a temperature

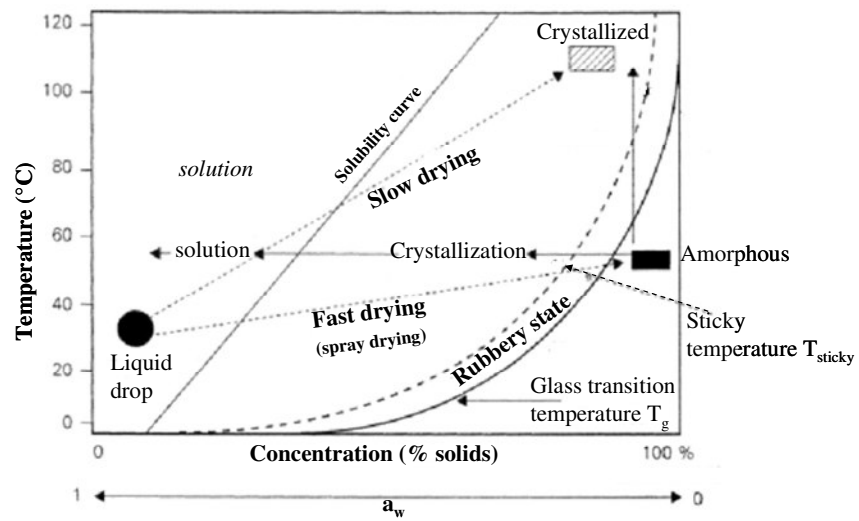


**Figure 1.17.** Drying of lactose on a state diagram (adapted from Senoussi, 1994).

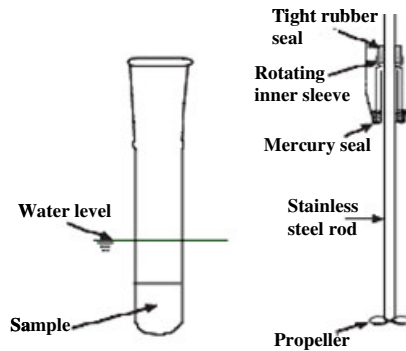


**Figure 1.18.** Scheme of the stirrer stickiness test for powders (from Adhikari et al., 2001).

higher than  $T_g$  (Roos and Karel, 1991c; Karel et al., 1994; Lloyd et al., 1996; Ozmen and Langrish, 2002; Palzer, 2005b).

In spray drying, particles have to be dried in a way to cross rapidly the domain of stickiness ( $a_w, T$ ) to get a final amorphous non-sticky powder (Bhandari and Howes, 1999; Truong et al., 2005a,b). Drop drying could be represented on a state diagram where the glass transition temperature evolution as a function of water content is shown (Fig. 1.17 for lactose).

The amorphous glassy state ( $T < T_g$ ) is a non stable state and an amorphous powder can evolve to the rubbery sticky state with a velocity that depends on the variation of its water content and temperature. If the powder is exposed to temperature and/or relative humidity conditions above its glass transition, the molecular mobility leads to the rubbery state with possible caking/sintering. Knowledge of glass transition temperature is important in order to choose the best storage conditions for a given powder ( $a_w$  known). These concepts can represent limit values.

Stickiness of particles in spray drying may be considered as having a negative effect on the process (e.g. powder deposition on the walls of the drying chamber) and on the final properties of powders (e.g. caking) (Bhandari, 2008; Woo et al., 2008). But on the other side, the sticky state of drying particles surface may be used to perform agglomeration inside the dryer chamber or in a fluid bed favouring collisions between sticky particles. Creation of stable solid bridges between two colliding particles to obtain agglomerates requires that at least one of the particles should be sticky (cf § 4).

## 3.2. Characterization of stickiness of powders

In addition to glass transition temperature determination, several techniques have been developed to characterize powder sticky behaviour (Boonyai et al., 2004). The sticky temperature ( $T_{\text{sticky}}$ ) is obtained by measuring the effect of modifications of powder properties like resistance to stirring or optical surface properties. Techniques can be divided into two main categories:

- Methods using powder “in bulk”
- Methods using drying drops or fluidized particles

### 3.2.1. Methods using powder “in bulk”

The **stirrer technique** (Lazar et al., 1956; Hennigs et al., 2001; Ozkan et al., 2002; Kudra, 2002) consists in placing a sample of powder with a known water content, inside an ampoule containing a stirrer (Fig. 1.18). The ampoule is placed in a controlled heating bath, which allows increasing slowly the temperature. Surface of particles during heating becomes viscous and sticky, leading to aggregation between particles; when resistance to stirring increases dramatically, the value of temperature is considered being the sticky temperature  $T_{\text{sticky}}$ .

This test has been used for several food powders like tomato, onion, fruit juice, milk and dairy products and mixtures of maltodextrin/sucrose/fructose. When using a manual stirring, the reproducibility of the measurement was difficult. Further developments allowed an automatic stirring.

Problems associated with this technique are the formation of a hollow channel inside the sample due to stirring, the non homogeneity of temperature inside the sample and the loss of water during the test due to evaporation at high temperature. The powder sample size varies between 5g (Chuy and Labuza, 1994) and 50-75g (Hennigs et al., 2001; Ozkan et al., 2002).

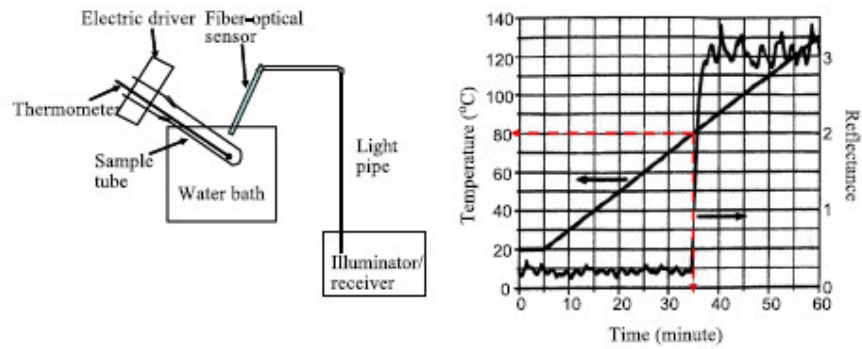


**Figure 1.19.** Powder stickiness test by reflectance measurements (Adhikari et al., 2001).

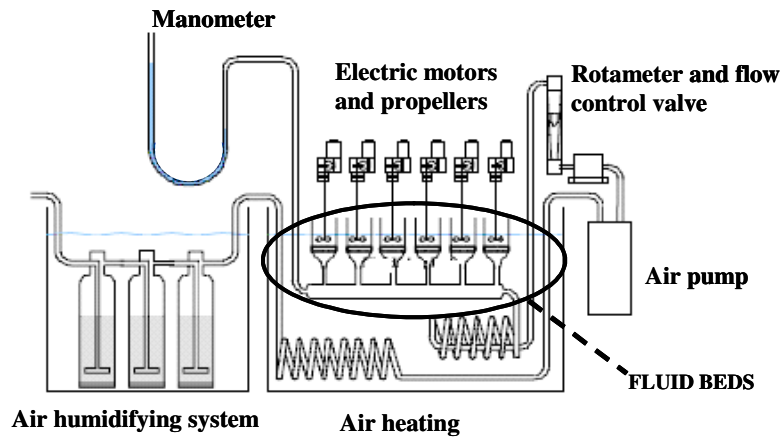


**Figure 1.20.** Fluidization stickiness test (Dixon and Bloore, 1999, from Boonyai et al., 2004).

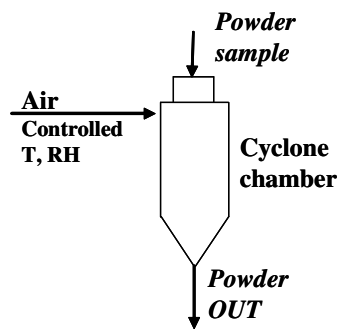


**Figure 1.21.** Cyclone stickiness test (adapted from Boonyai et al., 2004).

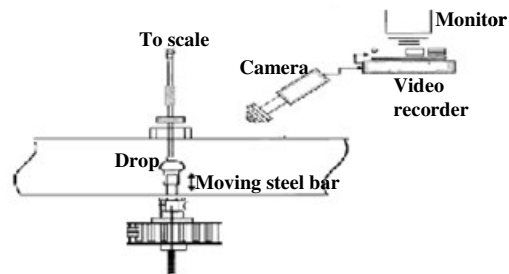


**Figure 1.22.** In-situ drop drying stickiness test (Adhikari and al., 2003).

**The ampoule technique** uses samples (1g) of powder with known water content in a closed ampoule, placed in a heating bath. Temperature is progressively increased until caking of powder (“collapse”) is observed ( $T_{\text{sticky}}$ ). Examples of use of this technique include freeze dried polysaccharides (Tsourouflis et al., 1976), infant dairy products (Chuy and Labuza, 1994) and maltodextrin DE 21 (Palzer, 2005b). Experimental conditions can affect the results. A variation of the heating rate (e.g.  $5^{\circ}\text{C}\cdot\text{min}^{-1}$  or  $10^{\circ}\text{C}\cdot\text{min}^{-1}$ ) can modify the result of the test, and the definition of “collapse” is not clear enough to have a good accuracy and reproducibility of measurements. It is also possible to evaluate adhesion against walls of the ampoule, by returning the ampoule and observing if sticking against walls occurs. An evolution of the ampoule technique has been proposed by Lockemann (1999). It consists in measuring the variation of powder reflectance during heating thanks to an optical fiber probe (Fig. 1.19); this technique cannot be applied to transparent materials.

Stickiness measured on dried powders in bulk is not representative of the behaviour of the material during the drying process. During spray drying, the dynamic of drying (contact between air and drop and possible impact with other drop or particle) strongly affects product properties evolution, and characterization of stickiness should be better represented by tests made in a dynamic situation closer to the reality of the considered process.

### 3.2.2. Methods using drying drops or fluidized particles

Dixon and Bloore in 1999 (from Boonayi et al., 2004) developed a **fluidization test** to study sticking between particles in fluid bed exposed to different air humidities and temperatures (Fig. 1.20).

The air conditioned in temperature and relative humidity, passes through several fluid beds in which equilibrium between fluidized powder and air is reached and the behaviour of the fluidized powder is observed. Relative humidity of air is slowly increased while temperature is kept constant and the sticky point is reached when fluidization becomes difficult. Repeating the test for different temperatures it is possible to obtain a sticky curve giving  $T_{\text{sticky}}$  as a function of air relative humidity (equal to the powder water activity at equilibrium).

In the **cyclone test** (Boonayi et al., 2006), like in the fluidization test, air relative humidity and temperature are controlled. This air passes through a cyclone, in which 1g of powder is introduced from the top and it is observed if there is adhesion on the walls or between the particles (Fig. 1.21). Powder particles can be considered as individual particles surrounded by a hot swirling air flow that moves them through the cyclone. Air humidity is increased for each tested temperature until reaching a sticky state, and this allows obtaining a sticky curve ( $T_{\text{sticky}}$  versus product water activity (equal to the air relative humidity at equilibrium)).

Adhikari et al. (2003, 2004, 2005, 2007) developed an in-situ drop drying test to measure the sticky behavior of a drop surface during drying (Fig. 1.22). This device is an improvement of the tack test of Green (1941) to verify the adhesion of ink to a surface.

The drop (diameter ~5 mm) – a solution of fructose and maltodextrin – is placed on a support connected to a scale and immersed in a hot air flow. The drop drying is filmed with a video camera. From weight variation, it is possible to calculate the amount of water evaporated and so the average water content of the drop during drying.

To measure stickiness, the support of the drop is mechanically moved up until having a contact between the drop surface and a stainless steel probe attached to a microbalance. The contact lasts 2-4 s, and then the drop support is moved down. Stickiness is evaluated by the tensile strength needed to separate the drop from the surface. A microthermocouple may be inserted in the centre of the drop.

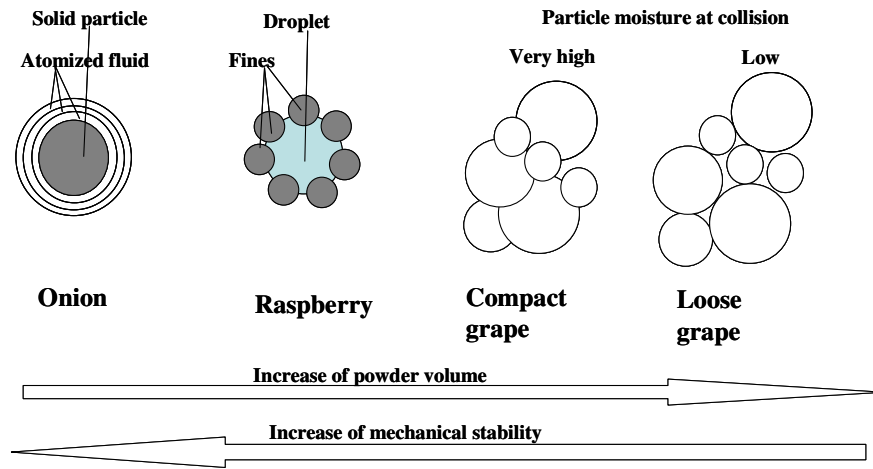


**Figure 1.23.** Different structures of agglomerates (adapted from Pisecky, 1997).

This technique simulates adhesion of a drop during drying to a wall with low speed. Inside the spray dryer chamber the drops will probably move with the air at a higher speed.

None of these sticky tests is really representative of spray drying; either the techniques consider development of stickiness on an already dry powder, or they consider a liquid drop in drying conditions different from those in spray drying. But they can help to determine a domain of temperature and relative humidity for which the powder should be sticky.

## **4. Agglomeration and spray drying process**

In this part, the use of particle stickiness is studied to create “agglomeration” during the spray drying process.

Particles in powder produced by simple spray drying have an average diameter smaller than 50 $\mu\text{m}$ , leading to bad flowability, bad instant properties and high density. To obtain better handling and to modify final powder properties, the drying particles may be associated with other particles at some stage of the drying process, in order to modify final powder structure and porosity and/or to increase particle size (Knight, 2001; Pietsch, 1991; Xiao et al., 2008). This is often realized by adding at different positions in the chamber, the dry fines collected from cyclones.

Such “agglomeration” contributes to the drying process and results in:

- A decrease of the amount of fines ( $d < 50 \mu\text{m}$ ), responsible of explosion problems.
- A modification of the bulk density of the final powder.
- An improvement of flowability and instant properties (wettability, dispersibility, solubility) of the final powder.

### **4.1. Agglomerates: structure and formation**

To create agglomeration, it is necessary to have collisions between particles followed by adhesion/fusion of the particle surfaces at the contact point to form stable bridges or coalescence. The way of performing the agglomeration process influences the structure of the agglomerates, their mechanical stability and their instant properties (Pietsch, 1991; Turchiuli et al., 2005).

Different structures may be produced (Pisecky, 1997; Graham, 1997) (Fig. 1.23):

- Agglomerates corresponding to the “fusion” of two particles in one, without the possibility to identify initial particles, and with a low change in particle size.
- “Onion” agglomerates, with good mechanical stability but hard to dissolve. They are created by contact of a dry particle (e.g. fine particle or different component added) with liquid drops, so that the dry particle is covered by successive layers of liquid.
- “Raspberry” agglomerates, created by contact of still humid big particles with a large amount of fine particles. They may have a poor dispersibility.

These last two structures rather correspond to coating mechanism.

- “Grape” agglomerates, when the different initial particles may be identified with space in between. They give the best instant properties. Depending on the agglomeration process conditions a compact grape or a loose grape structure can be obtained, with a big difference on bulk density of the powder due to the different amount of interstitial air. A too stable powder may have a low dispersibility, while a dispersible one may be too brittle (problems in transport and storage).

For instant powders, structures between the compact and loose grape structure will be preferred, to have at the same time mechanical stability and dispersibility.



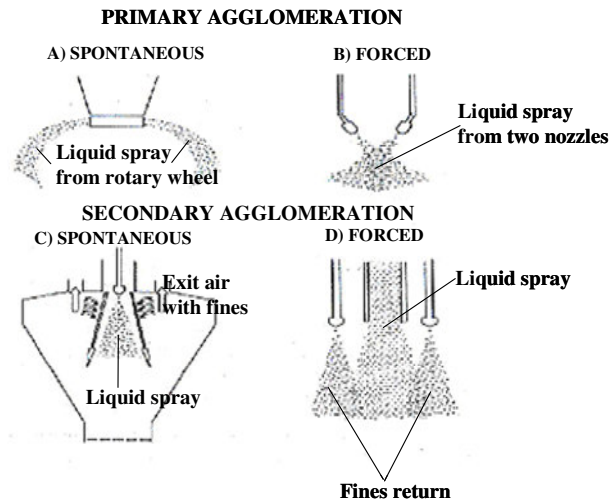


**Figure 1.24.** Different types of possible agglomeration inside the spray drying chamber (adapted from Pisecky, 1997).

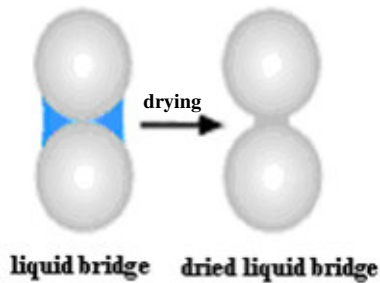


**Figure 1.25.** Liquid and solid bridges between particles leading to grape agglomerate.

Agglomeration of spray dried powders can be obtained either outside the chamber (in a fluidised bed) or inside the chamber. In this work we are interested in agglomeration inside the spray dryer chamber. Collisions between particles of similar diameter, could be spontaneous (due to drop/particle trajectories inside the chamber) or forced (thanks to the orientation of nozzles or to fines return/powder addition) (Fig. 1.24).

Several kinds of collisions are possible inside the chamber:

1. between **two liquid drops**, leading to a coalescence.
2. between **a liquid drop and an added dry particle** with formation of an *onion* structure, in which the solid dry particle will be more or less covered by the liquid. If it is realized in the external fluid bed, with liquid pulverization, the agglomerates may have a *grape* structure.
3. between **two dry particles**, leading to rebound without adhesion.
4. between a **dry particle and a sticky (on surface) particle**. For example, dry fine particles are returned inside the chamber where they may collide with particles that are drying. If these particles surface are in the sticky/rubbery state, the collision results in the formation of semi-liquid bridges that are further dried leading to stable solid bridges (Fig. 1.25). Agglomerates with a grape structure might be obtained, having good instant properties. The force of the collision (direction, intensity) could also influence the structure of the formed agglomerates (more or less compact) and the stability of the bridges. It depends on particles relative speed and mass (pressure at collision).

## 4.2. Equipments for spray drying and agglomeration

### 4.2.1. Multistage spray drying

Simple spray drying is not often used in food industry due to the small resulting particle size and the difficulty to reach desired powder properties, especially instant properties.

A multistage drying layout is preferred, in which after the first stage the spray dried powder has a water content higher than the desired value for the final product. The last percents of water are dried in an internal or external fluid bed, in which an additional air flow rate enters through a perforated plate, fluidizes and dries the powder. Due to higher residence time in the fluid bed, low air temperature can be used for this second drying step (typically lower than 150°C). The multistage layout allows then working with lower air temperature for the first spray drying step, by this improving thermal efficiency of the process.

The fluid bed may help to develop collisions between particles with still humid surfaces, leading to agglomeration. To improve it, water or a water-based solution (additional component) can be sprayed on the surface of the powder in the fluid bed.

At the beginning, fluid beds were always external to the spray dryer chamber (Fig 1.26), but from 1980, fluid beds were also integrated inside the drying tower (Fig. 1.27). In this configuration the powder falls in the bed after a first drying in the tower. Depending on the height of the fluid bed, some fluidized particles can also be reinserted inside the chamber where contact with drying drops could lead to agglomeration. The presence of fluid bed in the bottom of the tower also limits the possibility of contact between humid particles and bottom walls, avoiding sticking problems on walls. In industry spray dryers with integrated fluid beds can be of Compact Drying (CD) type or of Multi-Stage Drying type (MSD). The figure 1.27 illustrates both configurations; the fluid bed has (a) an annular shape for Compact Drying and (b) a ring shape for MSD.

For three stages drying, a further external fluid bed can be added to improve the drying process and/or for further agglomeration and/or coating (Mounir and Allaf, 2008).

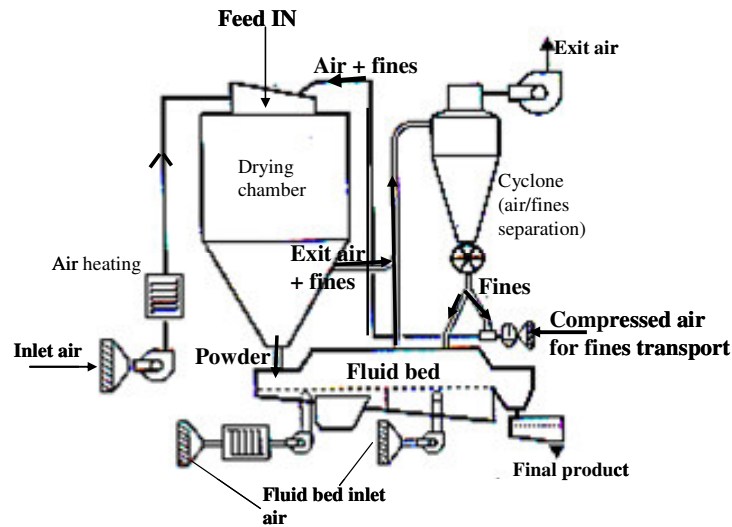


Figure 1.26. Two stage spray dryer with external fluid bed (adapted from Pisecky, 1997).

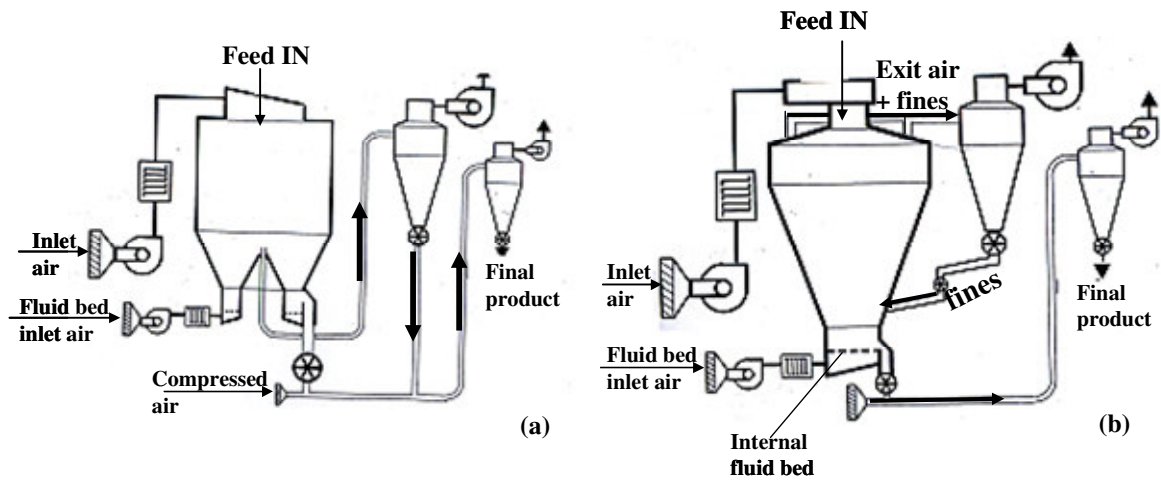


Figure 1.27. Two stage spray dryer with internal fluid bed: (a) compact dryer CD with annular fluid bed and (b) Multi Stage Dryer MSD with circular fluid bed (adapted from Pisecky, 1997).

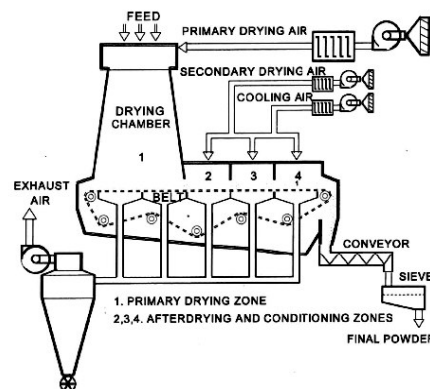


Figure 1.28. NIRO Filtermat spray dryer with integrated conveyor belt (Pisecky, 1997).

A special multi stage spray dryer equipped with an integrated belt dryer (Filtermat) (Fig. 1.28) was developed by Niro Company (Pisecky, 1997; www.niro.com). The primary dryer chamber is cylindrical without conical part, by this avoiding contact between still humid particles and chamber walls. Humid powder falls on a horizontal conveyor belt where it could be dried at low temperatures by secondary air coming downwards (section 2, 3 and 4 in Fig. 1.28). The moist powder layer acts like a filter, so that a limited amount of fines is recovered from the exhaust air. At the end of the belt, the powder layer brakes and final product is collected. This dryer is suitable for gentle drying of sticky, hygroscopic and thermoplastic products. It produces non-dusty, agglomerated, easy-to-use powders.

#### **4.2.2. Fines return**

Agglomeration inside the chamber can occur spontaneously by collisions between drops and particles due to air turbulence, and/or it can be forced. When using nozzles for atomization, collisions between spray drops can be achieved by directing clouds of two or more nozzles towards each other. That results mainly in coalescence between liquid drops.

Another way to perform agglomeration is the reintroduction of the smallest powder particles, called fines. Lighter fines particles are transported by air and separated in a cyclone (or bag filter). Then, they are reinserted inside the spray dryer (or in the fluid bed), where collisions with drying drops or sticky particles could lead to adhesion. Fines can be transported by gravity, pneumatic conveying systems, vibrating conveyors. Particles are continuously returned to the chamber until when they reach a critical size and weight for which they are no more transported by exit air and they are collected in the final powder. Fines return is used in all the multistage drying configurations, except the Filtermat in which no or very low amount of fines is produced.

The important factors to obtain a controlled agglomeration are the amount of recycled fines (usually unknown and/or not controlled in industrial practice) and the place of introduction inside the chamber (forced secondary agglomeration). The amount of returned fines is not known precisely: it corresponds to a stable state for the drying process, leading to a final powder respecting the specifications for the used drying parameters (flow rates and temperatures for air and product).

Fines are usually returned next to the atomization cloud, where the drop density is the highest, to have a high collision probability. Attention has to be paid to the fact that close to the atomizer fines can be in contact with hot drying air (co-current drying), with risks of thermal degradation of the product (e.g. Maillard reactions) and of fire explosions. For this reason, cold air is often used in fines transport lines.

Insertion techniques depend on the kind of spray dryer and atomizer. Often, industrials found easier to return fines close to nozzle atomizers, due to the more compact shape of the liquid spray compared to rotary atomizer (industrial contacts Sofivo, Bionov, Techniprocess).

With a rotary atomizer, the fines can be introduced below (Fig. 1.29a) or above (Fig. 1.29b) the spray cloud. NIRO has developed a system allowing fines introduction above the rotary wheel thanks to an air disperser, in which cold air circulates to protect fines from the hot air (FRAD Fines Return Air Disperser, Fig. 1.30). Fines enter by four pipes equipped with an adjustable deflector at the exit, so that insertion position can be changed. Distance between rotary wheel and fines insertion could affect the shape and kind of agglomerates formed. A previous model of the FRAD (Pisecky and Hansen, 1990) also allowed varying the vertical insertion position thanks to telescopic fines insertion pipes.

Petersen and Gude (1973) proposed a spray dryer with rotary atomizer equipped with a cyclone inside the dryer chamber (Fig. 1.31). Cold humid air containing fines in the bottom of the chamber is sucked into the cyclone through some rotating blades. Fines are separated and exit from the cyclone close to the atomizer wheel, while air is sucked by a fan and released to

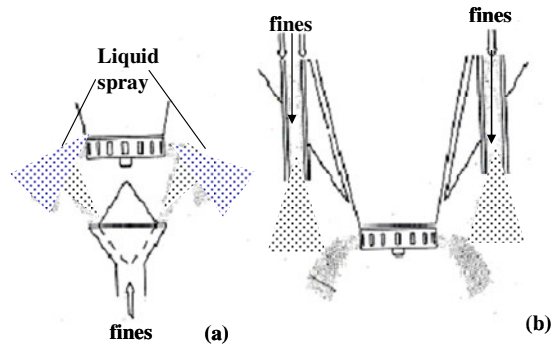


**Figure 1.29.** Fines return to rotary atomizer; (a) below spray (b) above spray (Pisecky, 1997).

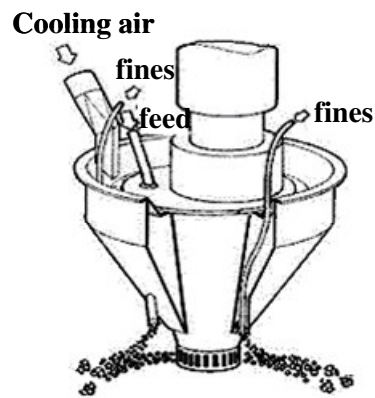


**Figure 1.30.** FRAD fines return system to rotary atomizer (www.niro.com, 2008).

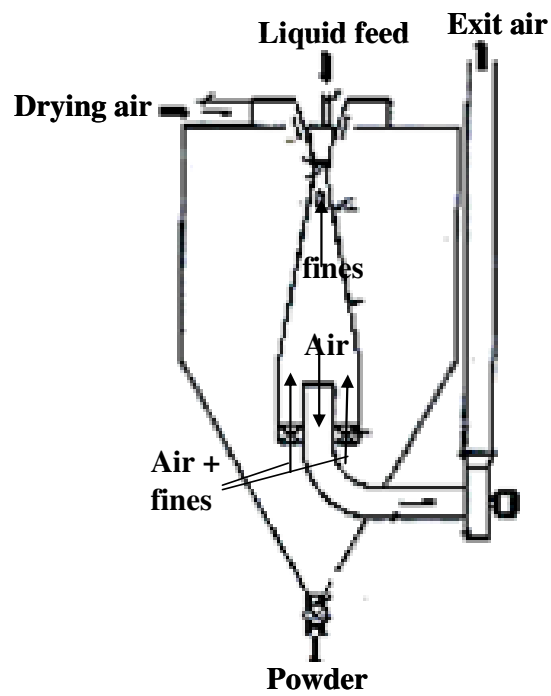


**Figure 1.31.** Spray dryer with internal cyclone (adapted from Petersen and Gude, 1973).

*Part I – Bibliographic study*

the atmosphere. A further pipe allows introduction of compressed air or steam. This configuration led to formation of “onion-type” agglomerates.

In spray dryers equipped with nozzles, fines can be inserted around one nozzle (Fig. 1.32a), in between two or more nozzles (Fig. 1.32b) or in a swirl air flow between several nozzles (Fig. 1.32c).

Normally the inserted fines are dry and not sticky, but they also can be heated up and humified to be in a sticky state when returning inside the chamber. In the process proposed by Schulz (1966) (Fig. 1.33), fines are returned close to the atomizer (a wheel or a nozzle) and put in contact with a steam jet. Direction of the steam allows changing fines contact point with the liquid spray.

In some spray dryers fines return is performed in an integrated fluid bed in the bottom of the tower. The fluidization air brings the small particles inside the chamber where they can collide with particles that are still drying. The size of returned particles and the height of introduction can be varied controlling the pressure drop inside the fluid bed.

In conclusion, various systems are used to reinsert fine particles in spray dryers. This is done mainly in order to regulate the drying process, avoiding in the same time the loss of product in industrial practice. It is not easy to know the percent of recycled powder, but it seems to be very high, maybe superior to 50%.

On the point of view of product quality, these small particles will circulate a longer time inside the chamber (not controlled). This may be source of degradation. A better understanding of this process could be useful to imagine some other possibility to improve drying and /or to induce agglomeration inside the chamber, with or without fines return.

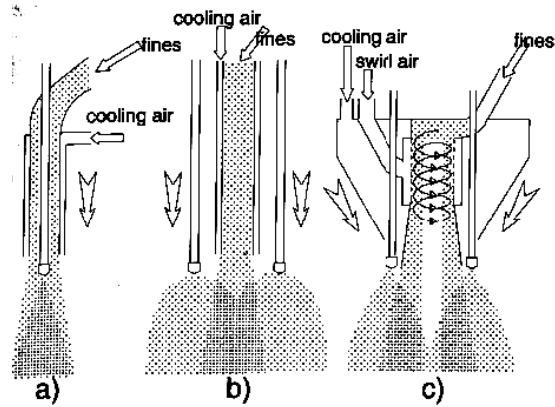


**Figure 1.32.** Fines return to nozzle atomizer (adapted from Pisecky, 1997).

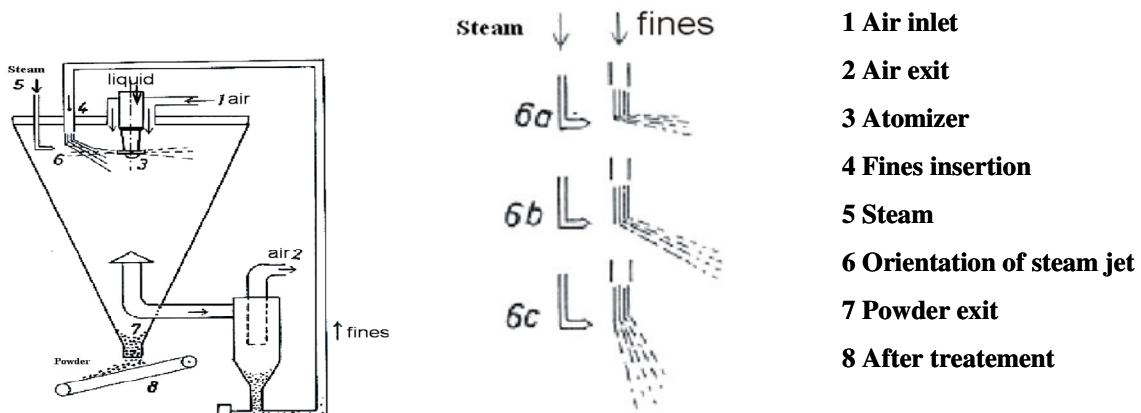
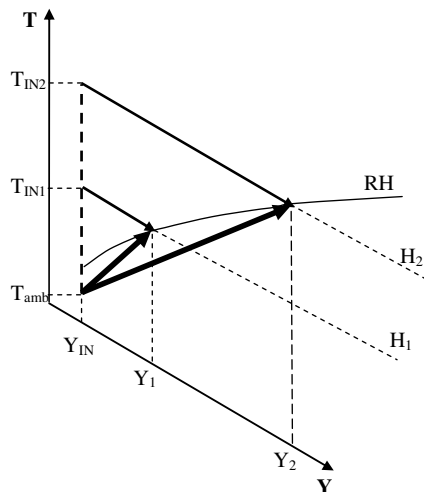


**Figure 1.33.** Spray dryer with fines return close to atomizer and steam (general flow sheet and different orientations of fines insertion position with steam jet) (adapted from Schulz, 1966).



$$T_{IN2} > T_{IN1}$$

$$MEC_2 = \frac{H_2 - H_{amb}}{Y_2 - Y_{IN}} < MEC_1 = \frac{H_1 - H_{amb}}{Y_1 - Y_{IN}}$$

**Figure 1.34.** Evaluation from Mollier diagram of mass heat energetic consumption MEC for isenthalpic drying at two different inlet air temperatures.

## 5. Process control for spray drying

### 5.1. Energetic considerations in spray drying

Spray drying allows continuous production of high tonnage of powders, with typical evaporative capacities varying from 500 to 4000 kg water.h<sup>-1</sup>. Heat consumption is high, up to 6000 kJ per kg of evaporated water (Schuck et al., 1998). This is mainly due to the need to remove rapidly the last water molecules adsorbed on particles (bound water). The main part of free water is normally removed before spray drying by classical evaporation process, to increase the liquid feed concentration. A higher feed concentration allows increasing the liquid feed flow rate and leads to reduced heat consumption, keeping the feed viscosity in a range compatible with pumping (Table 1.5).

Energetic consumption is mainly related to the cost of air heating. The Mass Energetic Consumption MEC can be expressed as:

$$\text{MEC} = \frac{\text{kJ for air heating}}{\text{kg evaporated water}} = \frac{\dot{m}_{\text{air}} \cdot (H_{\text{IN}} - H_{\text{amb}})}{\dot{m}_{\text{air}} \cdot (Y_{\text{OUT}} - Y_{\text{IN}})} = \frac{(H_{\text{IN}} - H_{\text{amb}})}{(Y_{\text{OUT}} - Y_{\text{IN}})} \quad \text{eq. 1.17}$$

On a Mollier diagram it could be seen that for reaching the same final air relative humidity (→ same final product water activity and water content if equilibrium is approached) it would be energetically more efficient to perform spray drying with an higher inlet air temperature  $T_{\text{IN}}$  (Fig. 1.34). Considering two different temperatures  $T_{\text{IN}2} > T_{\text{IN}1}$  we have:

$$\text{MEC}_2 = \frac{H_2 - H_{\text{amb}}}{Y_2 - Y_{\text{IN}}} < \text{MEC}_1 = \frac{H_1 - H_{\text{amb}}}{Y_1 - Y_{\text{IN}}} \quad \text{eq. 1.18}$$

Increasing the differences between inlet and outlet air temperature also increases the thermal efficiency of the spray drying operation, which can be expressed as (Mujumdar, 1995):

$$\eta_{\text{thermal}} = \frac{T_{\text{IN}} - T_{\text{OUT}}}{T_{\text{IN}} - T_{\text{amb}}}$$

Multistage drying with fines return improves thermal efficiency of the process (Schuck et al., 1998; Pisecky, 1997). However the air inlet and outlet temperatures are limited by the temperature that can be afforded by the drying particles without degradation, and by the wanted final powder water content. For the same inlet air temperature  $T_{\text{IN}}$ , lower exit air temperature  $T_{\text{OUT}}$  (with higher relative humidity) can be reached at the exit of the spray dryer chamber. In that case the product leaving the spray dryer still contains quite high moisture content (> 6%), and the last percent of water are removed in the external or integrated fluid bed.

### 5.2. Measurements on air and product

In spray dryers measurements are usually performed mainly at the entrance and at the exit (Nath and Satpathy, 1998; Woo et al., 2007). Usually air flow rate and temperature are measured at the entrance and/or at the exit of the chamber. But these measurements are not sufficient to determine product properties evolution during drying that could affect final



**Table 1.5.** Heat consumption for various liquid feed concentrations for production of 1 kg of powder (Mujumdar, 1995).

<i>Feed concentration (%)</i>	<i>Approximate heat consumption (kJ.kg<sup>-1</sup> powder)</i>
10	23.65 x 10 <sup>3</sup>
20	10.46 x 10 <sup>3</sup>
30	6.17 x 10 <sup>3</sup>
40	3.97 x 10 <sup>3</sup>
50	2.68 x 10 <sup>3</sup>

powder quality. Schuck et al. (2005a, 2008) put in evidence the interest of measuring also air relative humidity at the exit of the chamber to optimize the process while achieving desired powder properties. They found that exit air relative humidity is a good indicator of the final product water content. Actually, for different spray drying conditions, the same exit air relative humidity led to powders having the same water content.

To characterize product evolution during drying, direct powder sampling inside the chamber was performed. Zbicinski et al. (2002) used a sampler with the shape of a rectangular plate in a co-current spray dryer (nozzle atomizer, cylindrical chamber 6 m height, 0.5 m diameter). The sampler was inserted inside the chamber at different heights through holes in glass control windows. This enabled measurement of average moisture content of the material at specified distances from the atomizer. Roustapour et al. (2006) performed the same kind of measurements at different heights and longitudinal distances in a co-current spray dryer (height 1.85 m; diameter 1.25 m) equipped with a rotary atomizer. The results showed a very fast decrease in moisture content (more than 80% of water evaporated 25 cm below chamber roof).

However several questions are associated to this measurement technique. First the sampler should remain inside the chamber for several minutes to collect enough powder to analyze, so that properties of the collected powder may be modified during sampling time. Furthermore liquid and/or sticky particle will stick on the sampler and, when extracting the sampler, particles coming from other positions (with different properties) may also be collected. Finally the technique is invasive and not easy to apply to different spray dryers.

We have seen (chapter 1.2) that the evolution of air properties (T, RH) was linked to product properties evolution along drying (water evaporation), so that measurement of air temperature and relative humidity in the chamber may give useful information about drying (drying rate, average moisture content) of drops/particles.

Temperatures inside spray dryers were measured by several authors (Zbicinski et al., 2002; Bandhari, 1992; Frydman, 1998). A big decrease in air temperature was observed close to atomization, indicating that most of drying occurred in the first part of the chamber, where the temperature gradient between air and drops is the biggest. King et al. (1984) observed that in small-scale spray dryers the atomization zone could take up the whole chamber with uniform temperatures inside the chamber.

But a very little number of studies are reported until now with measurements of air relative humidity (Kieviet and Kerkhof, 1996; Kieviet et al., 1997) inside the chamber, probably because of the difficult feasibility and representativity of the measurements. Such a measurement coupled with air temperature could allow determining the air water content, then the amount of water evaporated at several positions inside the chamber, and thus estimating product average water content evolution.

Another important parameter to determine on spray drying process is the particle residence time distribution. This provides information about the product flow pattern inside the equipment according to the operating conditions (Villermaux, 1993). It is a statistical representation of the residence time of the product in the spray dryer and it is a key characteristic since it determines the time during which particles stay in contact with drying air (Kieviet and Kerkhof, 1995) thus affecting final powder properties. However, few studies exist on determination of particle residence time in spray dryers.

It is often assumed that the residence time distribution of the particle is the same as that of the drying air (Masters, 1985). Zbicinski et al. (2002) used Laser Doppler Anemometry to measure particles velocity at several heights inside a simple co-current spray dryer chamber (nozzle atomizer, 6 m height, 0.5 m diameter). Average air residence time varied from 4 to 6s, and calculated particle residence time was of the same order of magnitude.

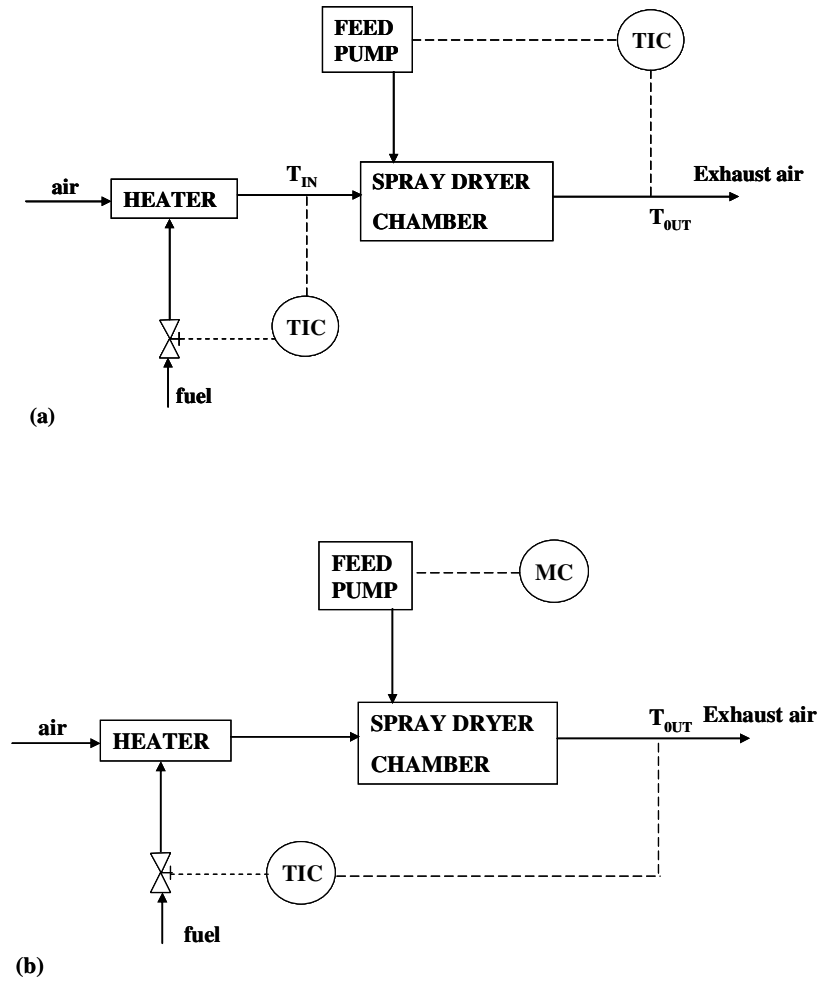


**Figure 1.35.** Basic automatic control systems in spray dryers.  
(a) outlet temperature control by regulation of feed rate and inlet temperature control by regulation of air heating system; (b) outlet temperature control by regulation of air heating and manual regulation of feed rate (adapted from Masters, 1985).

Residence time distribution is usually determined by adding a tracer in the feed and by measuring the response in product stream. Kieviet and Kerkhof (1995) injected Rhodamine as a tracer in the form of a short pulse (1s) during spray drying of an aqueous solution of maltodextrin in a co-current pilot spray dryer equipped with a rotary atomizer (height 2m; diameter 2.2 m). Concentration of Rhodamine in dried powder was then determined by dissolving the powder in water and measuring the absorbance of the solution (related to Rhodamine concentration). Average particle residence time inside the tower was of about 2 minutes, while air average residence time was approximately 30s. According to the authors, longer particle residence time compared to air may be due to the inertia of particles that cannot follow the air, and/or to the fact that some particles could hit the chamber walls and remain stuck for some time.

Jeantet et al. (2008) used NaCl as a tracer during spray drying of a skim milk solution in a three stage spray dryer tower (nozzle atomizer, 3.9 m height, 2.1 m diameter) equipped with an internal fluid bed and a fines return system. Particles average residence time varied from 9.5 to 12 minutes. In this case, fines return and internal fluid bed are probably responsible for the higher particle residence time compared to simple spray dryer, as particles can recirculate several times before being collected.

### **5.3. Control**

The aim of spray dryer control system is to maintain the production of powder with desired quality, especially water content, taking into account the possible variations of process parameters.

Spray dryers can be controlled either manually (MCS – Manual Control System) or automatically (ACS – Automatic Control System). Manual control is used only for laboratory or small pilot plants.

The outlet air temperature is the parameter that is normally controlled since it represents the quality of final powder. For a given air flow rate and air inlet temperature, it corresponds to an air relative humidity in close relation with the powder water content and temperature.

Furthermore safety requirements due to explosion risks often limit the maximum outlet air temperature (co-current configurations).

Two basic types of control systems are commonly employed (Fig. 1.35) (Masters, 1985). The first system (a) is composed by two circuits, one controlling the outlet air temperature by feed rate regulation and a second one controlling the inlet air temperature by air heaters regulation. Air temperature in the exhaust pipe is assigned, measured and transmitted to a temperature indicating controller (TIC). Deviations from the desired set point are counteracted by varying the feed rate without affecting inlet air temperature. If a failure in the feed system occurs (e.g. pump damage, atomizer blockage), a safety system can shut down air heating if exit air temperature rises above a security level. In these cases also a fire prevention system can start, stopping liquid feed and spraying cold water inside the chamber.

In the second system (b) exit air temperature is controlled by regulation of inlet air heating. In this case the liquid feed rate is kept constant, so that no modification in production rate occurs. This system is mainly used with nozzle dryers, in which feed rate should be constant not to modify initial droplet size distribution. From a practical point of view, this second system has an operational disadvantage due to the long response time of the heater control circuit when deviation in exit air temperature is detected.



## 6. Modeling of spray drying and agglomeration

### 6.1. Principle

Due to the high industrial diffusion of the spray drying process and to its complexity, a lot of studies have been made on spray drying simulation (Birchal et al., 2006). Several aspects of the physics of the process must be considered (Oakley, 2004):

- **Atomization.** The droplets size and size distribution (kind of atomizer, composition, viscosity) affect the drying rate and the residence time of particles inside the chamber and so the final product characteristics (size and size distribution of particles, water content, shape...). Simplified theoretical models are available for drops size distribution from atomization under ideal conditions, but currently the method of prediction for real spray dryers is the use of empirical correlations relating mean drop size to the operating parameters of the atomizer and properties of the feed (section 2.1). The low precision of these correlations can affect the result of simulation.
- **Gas flow and particle motion.** The liquid drops will move through the chamber under the influence of the turbulent gas flow. Thus simulation of gas motion is important to determine total residence time of particles inside the chamber and to simulate their trajectories. Calculation of humidity and temperature of the gas allows correctly simulating heat and mass transfer between the two phases (gas/particle). A complexity factor is the fact that the air flow is turbulent inside the chamber.
- **Drying behavior.** At the beginning of drying – when the droplet still has a liquid surface – drying rate will be governed by mass (water) transfer through the boundary layer between the drop surface and the drying air. But as drying continues the drop surface becomes more viscous, its temperature increases and drying rate will be determined by moisture transport through the particle itself. Moisture transport through a solid particle is highly material dependent, and modeling requires experimental data to provide model parameters. Furthermore, changes in particle morphology during drying should also be taken into account in a complete spray drying model.

The proposed spray drying models can be classified in three categories (3 levels) depending on their complexity (Kemp and Oakley, 2002).

First level models are based on heat and mass balances, with short calculation time. They require knowledge of the product sorption isotherm (solid-vapor equilibrium). They allow estimating exit air properties and final product water content assuming that equilibrium between air and particles is reached. They can be used for a preliminary spray dryer design.

Second level models take into account the drying kinetics and the particle residence time inside the chamber. These models are used to predict the effect of the modification of operating parameters on final powder (without modeling flow patterns inside the chamber). Particle residence time can be considered as equal to the average gas residence time or it can be experimentally determined for the considered dryer.

To design a new spray dryer or to study problems of sticking on walls or of agglomeration during spray drying a full simulation of gas and particle flow patterns is required: third level models. From the end of 80's, the introduction of Computational Fluid Dynamics (CFD) allowed obtaining a numerical solution of the fluid transport equations and so calculating gas and particle motion inside the chamber. In 1994, Oakley showed the increasing industrial interest for CFD simulation for process scale-up. The main applications in food industry should be the study of aroma losses and thermal degradation of the product, the minimization of product losses due to sticking on walls and the study of agglomeration.

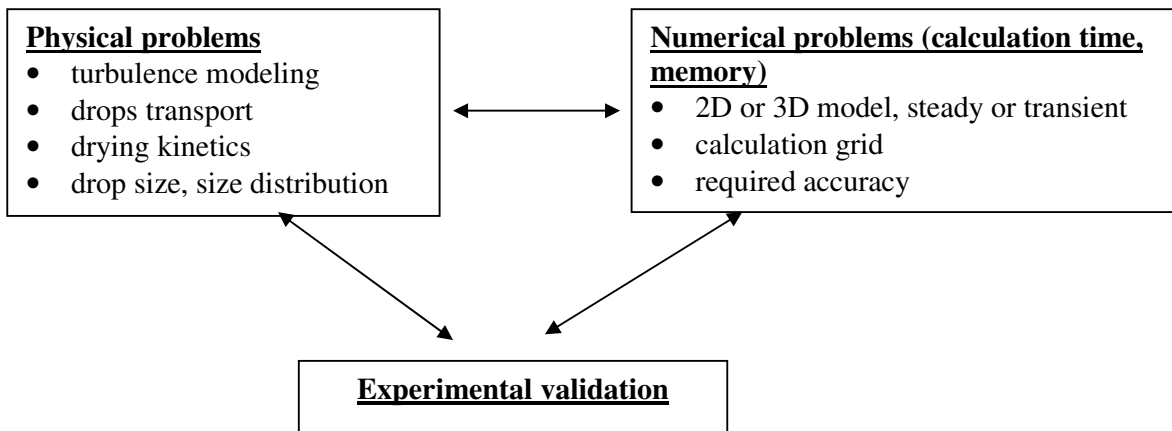


**Figure 1.36.** Factors to consider in spray drying CFD simulation.

As our goal is to understand sticking and agglomeration during spray drying, we will look more in detail at these models.

## **6.2. CFD models of spray drying**

CFD models of spray drying use a mixed Eulerian-Lagrangian approach for respectively the continuous (gas) phase and the discrete phase (drops/particles). CFD operates with the discrete volumes method where the studied global volume is divided in a large number of small volumes. The gas flow pattern inside the chamber is calculated solving the Navier-Stokes equations of mass and momentum conservation. The Gauss theorem is applied to transform the conservation differential equations in algebraic equations with the hypothesis that, for example, air pressure, velocity and temperature are uniform in each discrete volume. Calculation starts from defined initial and boundary conditions and it is iterated until convergence is reached. Once the gas flow pattern is simulated, particle motion is calculated considering drag and gravity forces acting on the particle. The common approach is the “Particle in Source Model”, used for the first time by Crowe (Langrish and Fletcher, 2001), in which a discrete number of liquid drops is chosen as being representative of the size distribution of the atomized liquid. The sum of the flow rates of drops of each size class is equal to the total liquid flow rate. It is also possible to consider coupling between gas and liquid phase, taking into account the effect of particle motion on gas flow pattern.

This kind of simulation is possible by using commercial softwares like CFX, PHOENICS, FIDAP, STAR-CD or FLUENT with high computer calculation power. However, a 3D non-steady simulation of an industrial spray dryer may require very long calculation times (more than one week. For this reason some simplifications are usually adopted looking for the best balance between calculation time and desired result accuracy depending on the considered application. The complexity of modeling is also due to the non-linearity of the process (Kerkhof, 1994). Some examples of this non-linearity are the saturated vapor pressure variation as a function of temperature, the sorption isotherms and the evolution of transport properties as the water diffusion coefficient during drying. The main complexity factors that affect a spray drying CFD simulation are summarized in Figure 1.36.

The simulation results are reliable if they do not depend on the chosen computational grid and on the number of particles used as representative of the discrete phase. If independence is verified, it is then possible to adopt a coarser grid resulting in reduced calculation time. Choice between a transient or a steady state simulation depends on the considered application. For a new problem a transient model should be chosen, but for simulating normal operating conditions a steady state simulation can be performed resulting in a simplification of the model (Truong et al., 2005a,b).

### **6.2.1. Simulation of turbulence**

The air flow inside the chamber is usually turbulent, and a good simulation of turbulence is important for a correct flow pattern calculation. The k-epsilon turbulence model is the most used model due to its robustness, even if more accurate results can be obtained with other models like RSM (Reynolds Stress Model). The principle of k-epsilon model consists in introducing inside the averaged Navier-Stokes equations (also called Reynolds equations) a turbulent viscosity to model Reynolds stress and a turbulent diffusivity to represent mass and heat turbulent fluxes. This viscosity is calculated with the turbulent energy per mass unit  $k$  and the dissipation per mass unit (epsilon). These two parameters are obtained solving a transport equation for each one. Huang et al. (2004) compared the results of four different turbulence models in a steady 3D simulation of a spray dryer equipped with a rotary atomizer. They found that k-epsilon model modified with a different definition of turbulent viscosity





gave the best agreement between calculated results and experimental measurement. A major limit for a complete validation of turbulence simulation is the lack of experimental data on gas flow patterns inside the chamber.

The kind of atomizer used also affects the air behavior. Most of simulation studies considered spray dryers equipped with nozzles; use of a rotary wheel results in the creation of a sucking effect that modifies the air flow pattern introducing a further instability source (Huang et al., 2006). Due to the local nature of these instabilities, a 3D simulation would be better than a 2D geometry simplification because simulation results show that the gas flow pattern is often asymmetric inside the chamber.

### **6.2.2. Simulation of drop transport**

Calculation of drop trajectories can cause numerical problems if a transient state simulation is required. In the steady state simulation, only the droplet source term in the continuity equations need to be stored. However, in the transient state, for each time step some new drops are injected at the entrance and the position and state (temperature, velocity, moisture content...) of each particle at each time step must be stored. Furthermore in transient state a large time is necessary before the first dry particles exit from the chamber, and so the calculation time must be long enough to reach a semi-steady state.

The drop behavior is also an important aspect to consider for scale-up problems from a pilot to an industrial spray dryer. Most of the studies simulate pilot equipments, and to extrapolate the results to bigger spray dryers a complete dynamic similitude must be obtained (Oakley, 1994). If the geometry of the spray dryers and the air inlet conditions are the same, the air flow pattern will be similar; but the similitude between drops trajectories is more difficult to obtain. This will depend on the drops Reynolds number. To have the same Reynolds value in two different spray dryers the same inlet drop velocity and size distribution should be obtained by atomization: a so high accuracy in atomization control is not available.

### **6.2.3. Drying kinetics of drops**

From a physical point of view the most difficult part of a CFD model of spray drying is the modeling of the drying kinetics of drops. The goal is to calculate temperature and water content of drops during drying. The knowledge of their evolution inside the chamber is fundamental to predict adhesion phenomena of particle (between them or on the walls). As in these phenomena the surface properties of the drop/particle are involved, this means that a complete model should be able to predict spatial variation of temperature and especially of moisture content inside the particle. Interactions between water and dry matter make more difficult the use of a universal model, because water diffusion depends on the nature of the considered material and on the water content inside the particle.

In the first step of drying, the drop can be considered as liquid and the drying rate is calculated from heat and mass balances between the liquid surface and the surrounding air: the two phases are in equilibrium at wet bulb temperature ( $a_w = 1$ ). When the surface begins to dry ( $a_w < 1$ ), the evaporation velocity decreases more or less depending on the substance. The drying kinetics modeling approaches in literature can be divided in two main classes: simplified models (characteristic drying curve) and models that simulate diffusion.

In the simplified approaches only the average particle moisture content is considered. In the Characteristic Drying Curve Model (CDC), the drying rate  $\dot{m}_{ew,l}$  ( $\text{kg}\cdot\text{s}^{-1}$ ) of a liquid drop (water solution containing dissolved solids) is related to the drying rate of a pure water drop  $\dot{m}_{ew}$  by the definition of a relative drying velocity  $f = \dot{m}_{ew,l} / \dot{m}_{ew}$ . For a given substance,  $f$  is a function of only one parameter, the characteristic moisture content  $\Phi$  defined as (Langrish and Kockel, 2001):



$$\Phi = \frac{X - X_{eq}}{X_c - X_{eq}} \quad \text{eq. 1.19}$$

X average particle moisture content,  $X_{eq}$  moisture content at equilibrium,  $X_c$  critical moisture content, for which the particle surface is no more completely liquid ( $a_w < 1$ ) and drying rate decreases (Figure 1.12).

When  $\Phi \geq 1$  the drying rate is equal to the liquid drop drying rate at the wet bulb temperature, and so  $f = 1$ . For  $\Phi < 1$  ( $X_{eq} < X < X_{cr}$ ) the drying rate is reduced  $\dot{m}_{ew,l} = f \cdot \dot{m}_{ew}$ .

The curve  $f$  as a function of  $\Phi$  is unique for each material and independent from temperature, humidity and velocity of the drying gas. The shape of this curve is determined experimentally by studying the drying kinetics of one drop of the considered material. Langrish and Kockel (2001) have analysed several studies reported in literature, and they found that for many materials the correlation between  $f$  and  $\Phi$  can be considered as linear.

It must be noticed that the experimental trials for drying kinetics are performed with drops having a diameter of some millimetres in order to have measurable weight losses during drying. In the spray drying process drying drops are smaller (about  $100\mu\text{m}$ ) and their drying kinetics might be different.

The simplified CDC models have the big advantage that they can be implemented in a CFD simulation. On the other side these models are based on an average particle moisture content and do not allow to calculate the surface characteristics. Langrish and Kockel (2001) noticed that due to the small drops diameters in spray drying moisture content gradients inside the particles will probably be very small. Adhikari et al. (2005) showed that the mass Biot number (which depends on water diffusion coefficient and is an index of the importance of internal diffusive forces) shows variations inside the drop due to moisture content gradients for sticky products.

Diffusive models consider that water evaporation from the surface is at one moment governed by water diffusion from the particle humid core to the surface. These models take into account water content gradient inside the drop while, due to the small diameter, temperature is assumed as uniform.

In these models a diffusion equation is added to the mass and heat transfer equations between gas and surface (Straatsma et al., 1999a,b). To solve it, experimental data must be obtained to calculate the diffusion coefficient  $D_w$  of water inside the particle (Raederer et al., 2002; Frias et al., 2001). Adhikari et al. (2005) used an effective diffusivity calculated from the drying kinetics of a maltodextrin/sucrose solution.

Verdurmen et al. (2004) determined the drying kinetics of a single drop using an acoustic levitator described by Yarin et al. (1999). A diffusive model allows simulating surface properties of particles during drying, which may be used to determine their sticky behaviour. In any case the determination of the diffusion coefficient, the implementation of these models in a CFD code and their validation are complex, especially for 3D transient simulations. A further problem is the possible particle shape modification along drying. Numerical models are normally based on ideal shrinkage behaviour during water evaporation, considering that the particle remains spherical. All the authors agree that a lot of work must still be done to correctly calculate spatial variation of moisture content inside particle during drying.

### 6.3. Simulation of agglomeration

Agglomeration during spray drying can occur due to spontaneous collisions between particles caused by air turbulence or it can be forced for example by fines return inside the chamber. This results in a modification of the size distribution of the final powder compared to the



initial liquid drops size distribution. The aim of agglomeration modeling is to predict this final distribution depending on the process operating parameters.

The spray dryer can be considered as a disperse system, in which the drops/particles number density inside the chamber is in the range of  $10^{11}$  particles.m<sup>-3</sup>. Due to the complexity of the different physical mechanisms, few studies about agglomeration in disperse systems have been performed.

The classical approach to agglomeration modelling consists in making population balances to evaluate evolution of size and size distribution of particles during the process (Hogg, 1992; Heinrich et al., 2002). This method can be used with an Eulerian approach, in which the studied system is considered as a mix of two continuous coupled phases. It was already observed that for spray drying simulation a Lagrangian approach is used for the liquid phase, considered as a discrete phase, in order to follow the particles trajectories and to calculate the spatial variation of temperature and moisture content inside the drop. Nijdam et al. (2004) compared two models of coalescence between liquid drops inside a spray and they found that the Lagrangian approach to the liquid phase was easier to implement in a CFD spray drying model. The effect of air turbulence and the evolution of particle properties was better taken into account.

In Lagrangian models particle sample is tracked using a stochastic (Monte-Carlo) method. Particles can be simultaneously followed – as in the DSMC (Direct Simulation Monte Carlo) approach – or tracked in sequence one by one (Sommerfeld, 2001). In the first case, all the particles are simulated at the same time in the computational field to determine intersections between trajectories where collisions can occur. In the sequential approach just one particle is tracked and the collision probability is calculated from a local particle distribution.

Each agglomeration model considers two steps: collisions between particles and result of collision (sticking, coalescence, rebound...) (Guo et al., 2004).

### 6.3.1. Collisions between particles

In comparison with a concentrated system, as a fluid bed in which the probability of contact is high, the determining step of agglomeration inside the drying chamber is the probability of collision between particles.

In a stochastic model, a collision probability must be defined. The collision calculation is performed by couples of particle “packs”, without possible collisions inside each pack. The pack having the lower particle number  $N_1$  is called “collector”, and the pack with more particles  $N_2$  is called “contributor”. The collision frequency  $\nu$  between one drop of collector and the drops of contributor is proportional to the drops relative speed, to the number density and to the inverse of considered volume, which is often a cell of the computational grid. In a time step  $\Delta t$  the expected collision number is  $\lambda = \nu \cdot \Delta t$ . The probability to have  $m$  collisions is given by the Poisson distribution:

$$p(m) = \frac{1}{m!} \lambda^m e^{-\lambda} \quad \text{eq. 1.20}$$

So the probability to have at least one collision is complementary to the probability to have zero collision ( $m = 0$ ). This gives an expression for calculating the collision probability  $p_{\text{coll}}$ :

$$p_{\text{coll}} = 1 - e^{-\lambda} \quad \text{eq. 1.21}$$

If the collision probability is higher than a fixed critical value, the model evaluates the collision result.

### 6.3.2. Collision result

The evaluation of the result of collisions between particles is the most complex part of an agglomeration model, because several factors like the product nature, the surface properties of



drops and the force of the impact must be considered. The model proposed by Guo et al. (2004) and Nidjam et al. (2004) do not consider the nature of the substance and simulate coalescence between two liquid drops. A contact angle  $\phi$  is defined, and coalescence occurs if  $\phi$  value is higher than a critical value. This value is related to the relative speed and the distance between particles; the new particle size is calculated from the volume conservation  $d^3 = d_1^3 + d_2^3$ .

A more complete model should include the effect of material properties on the particle behaviour. Agglomeration can occur only if the surface of at least one particle is sticky. The main properties affecting the sticky state of the particle are the surface tension and the dynamic viscosity of the surface. The dynamic viscosity is strongly modified during drying, and based on this property the particles can be classified in three categories (Verdurmen et al., 2004):

- Surface tension dominated particles (STD): liquid drops in the first part of drying
- Viscous forces dominated (VD) particles: particles during further steps of drying
- Dry particles

The glass transition concept is used to distinguish between viscous particles (sticky) and dry particles (Adhikari et al., 2003). If the surface temperature of the particle is lower than the sticky temperature  $T_{\text{sticky}}$ , the particle is considered as dry (this approach is valid for amorphous constituents). Based on this particle classification, four kinds of collisions can be identified:

- Collisions between liquid drops (STD particles)
- Collisions between a STD drop and a viscous or dry particle
- Collisions between two viscous particles
- Collisions between two dry particles

Each type of collision is calculated with a sub-model. Collisions between liquid drops can give coalescence, and collisions between dry particles do not modify particle size. The simulation of collisions where at least one particle is viscous is based on a force balance, in which the more viscous particle penetrates the less viscous particle; if penetration is higher than 50% of the particle diameter, the result of collision is seen as coalescence, if not as agglomeration. The validation of an agglomeration model is usually performed by comparison of measured and simulated average final particles diameter and/or size distribution.

#### **6.4. Conclusion on CFD simulation of spray drying and agglomeration**

CFD is a potential tool to simulate spray drying process and to better understand phenomena difficult to study with other modelling techniques, like sticking on walls and agglomeration. The main advantages of CFD consist in the prediction of flow pattern inside the drying chamber and of the evolution of product properties during drying, without limitation in the dryer geometry.

But the complexity of the process and the numerical calculation limit the validity of obtained results. Especially the transient state simulation still requires too high calculation time and memory. For this reason, most of published studies are based on steady state simulation. That may be used to study the behaviour of a spray dryer in normal operating conditions, but it is not sufficient for new plants design purpose. The simulation approach for the discrete phase (liquid drops) is normally Lagrangian, and this allows calculating particles trajectories and simulating temperature and moisture content evolution during drying. Due to turbulent fluctuations a 3D simulation seems to be necessary to correctly follow particles motion inside the chamber. To characterize with a good accuracy the evolution of temperature and water content of the particle during drying, the drying model should include water diffusion





equation. The main difficulty is to collect experimental data to estimate the internal diffusion coefficient.

Concerning agglomeration modelling, most of existing models are based on population balance solutions, which cannot be easily used with a Lagrangian approach for discrete phase (CFD). Stochastic models that can be integrated in a CFD spray drying simulation have been developed to simulate agglomeration in dispersed systems; but most of the studies just consider possible coalescence between liquid drops. Further work must be done to write and to validate agglomeration models taking into account the different possible collisions inside the drying chamber. To do this, a better comprehension of mechanisms that lead to cohesion/adhesion is necessary. To extend CFD use to industrial scale, experimental data must be obtained for validation.

## **Conclusion**

In spray drying, liquid drops are quickly dried into solid dry particles. In the case of polymers solutions evolving from an initial liquid state to a final amorphous solid state, particles could pass through an intermediate sticky/rubbery state, depending on their composition, temperature and water content.

The bibliographic study put in evidence how the knowledge of conditions for which particle surface is in a sticky/rubbery state is important on one hand to avoid unwanted product deposition on chamber walls, and on the other hand to perform agglomeration promoting collisions between sticky particles.

Agglomeration is often required in industrial practice to reduce dust formation, to improve flowability and instant properties of the final powder, by increasing particle size and by creating new structures.

To have controlled agglomeration inside the drying chamber, collisions between two or more particles should occur to form a new particle with a shape depending on the state of the colliding particles surface (liquid, sticky, dry solid) and on the force of the impact. Adhesion to form solid bridges between particles is possible only if the surface of at least one of the particles is in the “sticky” state at the moment of collision. If the surface is too liquid, coalescence or covering of the particle will occur; if the surface is too dry, collisions will result in rebound.

Almost all the industrial spray dryers configurations involve the reinsertion of the smallest particles (fines) inside the chamber, to improve drying and/or to perform agglomeration. Fines are usually inserted close to the atomizer where liquid drops density is maximal, but in this position drops are more likely to be still liquid. A better comprehension of drops drying behaviour could lead to determination of positions where the drying drops surface is in the sticky state, more favourable for size enlargement.

Several techniques have been developed to characterize stickiness of particles, but most of them are based on measurements performed on already dry powder or during drying of single liquid drops in conditions not totally representative of the fast spray drying process. Stickiness of the particle surface can be associated to the glass transition temperature of the considered material. During drying, the viscosity of the drop increases until reaching a critical value for which the particle surface can be considered as sticky. This critical value occurs for a domain of temperatures between the glass transition temperature and the sticky temperature some



## *Part I – Bibliographic study*

degrees higher than glass transition. The glass transition temperature depends strongly on the water activity/water content, which varies all along drying. The knowledge of particle water content evolution becomes necessary to estimate particle stickiness, but a direct measurement is difficult to perform.

Some authors tried to perform powder sampling inside pilot spray dryer chambers to analyze evolution of particle properties during drying; however sampling techniques are invasive and difficult to apply in bigger spray dryers.

The evolution of air properties (temperature, relative humidity) could be considered as representative of the drying process: the water evaporated from product goes into air lowering its temperature and increasing its water content and relative humidity. Measurements of air temperature and relative humidity inside the chamber could allow estimating air water content and thus the amount of evaporated water at different positions by mass balances. In that way the evaporation rate and average particle water content could be calculated, as a function of process parameters.

The simulation of the spray drying process should be a useful tool to optimize process operation, evaluating the effect of operating parameters on final product properties, on energy consumption. Furthermore a validated simulation should allow calculating the evolution of product properties along drying, to predict stickiness inside the drying chamber, useful to avoid product losses due to sticking on walls, and to perform controlled agglomeration.

This study of the spray drying process was conducted on a pilot equipment with a rotary atomizer. Model materials were selected as able to exhibit stickiness behaviour during drying: two different maltodextrins were chosen.

The air properties (temperature, relative humidity) were determined in different chosen positions in the dryer. They will be used to calculate and follow the transformation of drops into dry particles (temperature, water content, water activity). From knowledge of drying material (sorption isotherms, glass transition temperature), it will be possible to determine operating conditions and positions in the dryer for which the particles may be sticky. Application of CFD modelling will give another approach.

To verify the sticky conditions, experiments will be done with defined local powder insertion during spray drying and the resulting powder analyzed (size and shape).

Semi-industrial drying trials will be performed and interpreted by using this methodology.



**PART II**  
**MATERIALS AND METHODS**







**Table 2.1.** Properties of maltodextrins used for preparation of aqueous solutions (data Roquette)

	<b>Glucidex 12</b>	<b>Glucidex 21</b>
DE	11-14	20-23
Glucose (%)	1	3
Maltose (%)	2	7
Oligo and Polysaccharides (%)	97	90
T <sub>g</sub> dry powder (°C)	180	140

## 1. Products

### 1.1. Maltodextrin solutions

Maltodextrins are mixtures of poly and oligosaccharides, generated from starch syrup by enzymatic or acid hydrolysis (Zapsalis and Beck, 1985). The more advanced the hydrolysis, the higher the dextrose equivalent (DE) number, representing reducing sugars in relation to glucose ( $DE_{\text{glucose}} = 100$ ). The average molecular weight of maltodextrin is inversely proportional to the DE number.

Two maltodextrin powders DE12 and DE21 (Glucidex, Roquette, Fr) were used in our study. The maltodextrin DE12 has a higher molecular weight and a longer glucose chain, corresponding to higher glass transition temperatures (Table 2.1).

Initial maltodextrin powder, with a water content of ~ 5%, was dried during at least 24 h in oven at 100°C before preparation of aqueous solutions for spray drying.

Aqueous solutions (40% w/w dry matter) were prepared the day before the trial, by dissolving progressively the maltodextrin powder in desionised water at ambient temperature, under mechanical stirring. Preparation time was of about 1 hour. The solution protected with a plastic film was kept one night at ambient temperature to get a solution where maltodextrin was completely dissolved. Density of aqueous solutions was of about 1200 kg.m<sup>-3</sup>.

For residence time distribution trials, two 40% dry matter w/w aqueous solutions were prepared, one containing 50% maltodextrin DE12 and 50% NaCl, and the other one containing only maltodextrin DE12 colored with some drops of eosine.

### 1.2. Protein hydrolysate aqueous solution

Spray drying of an aqueous solution of a protein hydrolysate produced by a fermentation process was performed in Nestlé PTC of Singen (Germany). Due to biological reactions during production, the composition of the raw liquid solution could slightly vary from one batch to another. For this reason, all the trials were performed with the same liquid batch (stored at ambient temperature in a closed vessel – 2 months – *stability was not verified*).

The average water content of the liquid solution was  $63.50 \pm 0.46\%$  w/w corresponding to 36.5% dry matter w/w, with 50% of the dry matter composed by salt (Nestlé data).

## 2. Equipments and instrumentation

Spray drying trials were performed in two pilot plants. A NIRO *Minor* was used in Agroparistech Massy (France) for testing maltodextrin solutions behavior during drying and the feasibility of measurements of air properties. A NIRO FSD 4.0 was used for protein hydrolysate solution drying (Nestlé PTC, Singen, Germany) to apply the methodology to a different equipment.

### 2.1. NIRO Minor spray dryer

The NIRO Minor pilot spray dryer (NIRO, Copenhagen, Dk) is a one-stage co-current spray dryer, equipped with a rotary atomizer. The water evaporative capacity is of 1 to 4 kg.h<sup>-1</sup> according to operating conditions (Fig. 2.1).



## Part II – Materials and methods

The drying chamber ( $V \sim 0.5 \text{ m}^3$ ) is a cylinder with a conical base ( $d = 0.8 \text{ m}$ ,  $h = 1.2 \text{ m}$ , cone angle  $\sim 60^\circ$ ). A vibrating automatic hammer is used to periodically remove powder stuck on chamber walls.

The liquid feed (water or maltodextrin aqueous solutions) was pumped at ambient temperature (peristaltic pump Masterflex 77201, Fr; 5 to 280  $\text{mL}\cdot\text{min}^{-1}$ ). The solution tank was placed on a scale (IB12 Sartorius, Ge; accuracy  $\pm 0.1\text{g}$ ) to measure the feed mass flow rate.

Liquid was atomized by a rotary wheel atomizer ( $d_{\text{wheel}} = 5 \text{ cm}$ , with 24 rectangular holes (6 mm height x 3.5 mm wide). The speed was controlled by compressed air pressure (4 to 6 bar, corresponding to 22500 to 30000 rpm).

Drying air was sucked from ambient by a fan placed after the cyclone at the exit, so that pressure inside the chamber was inferior to atmospheric pressure. Air flow rate could be varied by changing the fan rotation frequency (25 to 45 Hz).

Before entering the dryer chamber, air was heated by three electrical resistances (0.7 – 1.5 – 2 kW; temperature  $< 350^\circ\text{C}$ ). A temperature probe placed just after the resistances was linked to a PID regulator. The air entered into the drying chamber close to the atomizer (co-current drying) with a swirl imposed by an air disperser (Fig. 2.1b). A thermocouple (K-type;  $d 1.5 \text{ mm}$ ;  $\pm 1.5^\circ\text{C}$ ) placed inside the air disperser gave the air temperature at the entrance of the chamber ( $T_{\text{IN}}$ ).

Humid air and dry powder exit from the bottom of the chamber, where a platinum probe measured air temperature  $T_{\text{OUT}}$ . The humid air flow rate was measured after the fan with an Annubar probe (Pitot tube) connected to a water column ( $\Delta P$ ). Air flow rate was calculated with the following formula:

$$\dot{m}_{\text{HumidAir}} = 0.0125 \cdot S_f \cdot d_{\text{pipe}}^2 \cdot \rho_{\text{air}}^{0.5} \cdot (\Delta P)^{0.5} \quad \text{eq. 2.1}$$

$\dot{m}_{\text{HumidAir}}$  air flow rate ( $\text{kg}\cdot\text{h}^{-1}$ );  $S_f$  flowrate coefficient (0.638 for 35 mm pipe diameter);  $d_{\text{pipe}}$  pipe internal diameter (35 mm);  $\rho_{\text{air}}$  air density ( $= f(T)$ ) ( $\text{kg}\cdot\text{m}^{-3}$ );  $\Delta P$  height difference of water column (mm of water)

Air temperature and wet bulb temperature were also measured after the Annubar probe to estimate the air water content, so that the dry air flow rate could be calculated as:

$$\dot{m}_{\text{air}} = \frac{\dot{m}_{\text{HumidAir}}}{1 + Y_{\text{exit}}} \quad \text{eq. 2.2}$$

$\dot{m}_{\text{air}}$  dry air flow rate ( $\text{kg}\cdot\text{h}^{-1}$ );  $Y_{\text{exit}}$  exit air water content ( $\text{kg water}\cdot\text{kg}^{-1}$  dry air)

Humid air and powder were transported in pipes ( $d 0.05 \text{ m}$ ,  $l 2 \text{ m}$ ) then separated in a cyclone ( $V \sim 0.009 \text{ m}^3$ ). After the fan the air was released to the atmosphere. The powder was regularly collected in glass jars at the bottom of the cyclone (changed every 5 to 10 minutes). Powder temperature was measured with a thermometer when changing jar.

## 2.2. NIRO FSD 4.0 spray dryer

The NIRO-FSD 4.0 (NIRO, Copenhagen, Dk) pilot spray dryer is a two-stage co-current spray dryer, equipped with bi-fluid nozzle atomizer, internal fluid bed and fines return (Fig. 2.2). Its water evaporative capacity is between 15 and 20  $\text{kg}\cdot\text{h}^{-1}$ .

The drying chamber is composed by a cylinder with a conical base ( $d = 1.2 \text{ m}$ ,  $h = 2 \text{ m}$ , cone angle  $40^\circ$ ). It is equipped with two automatic hammers to remove powder from the walls.

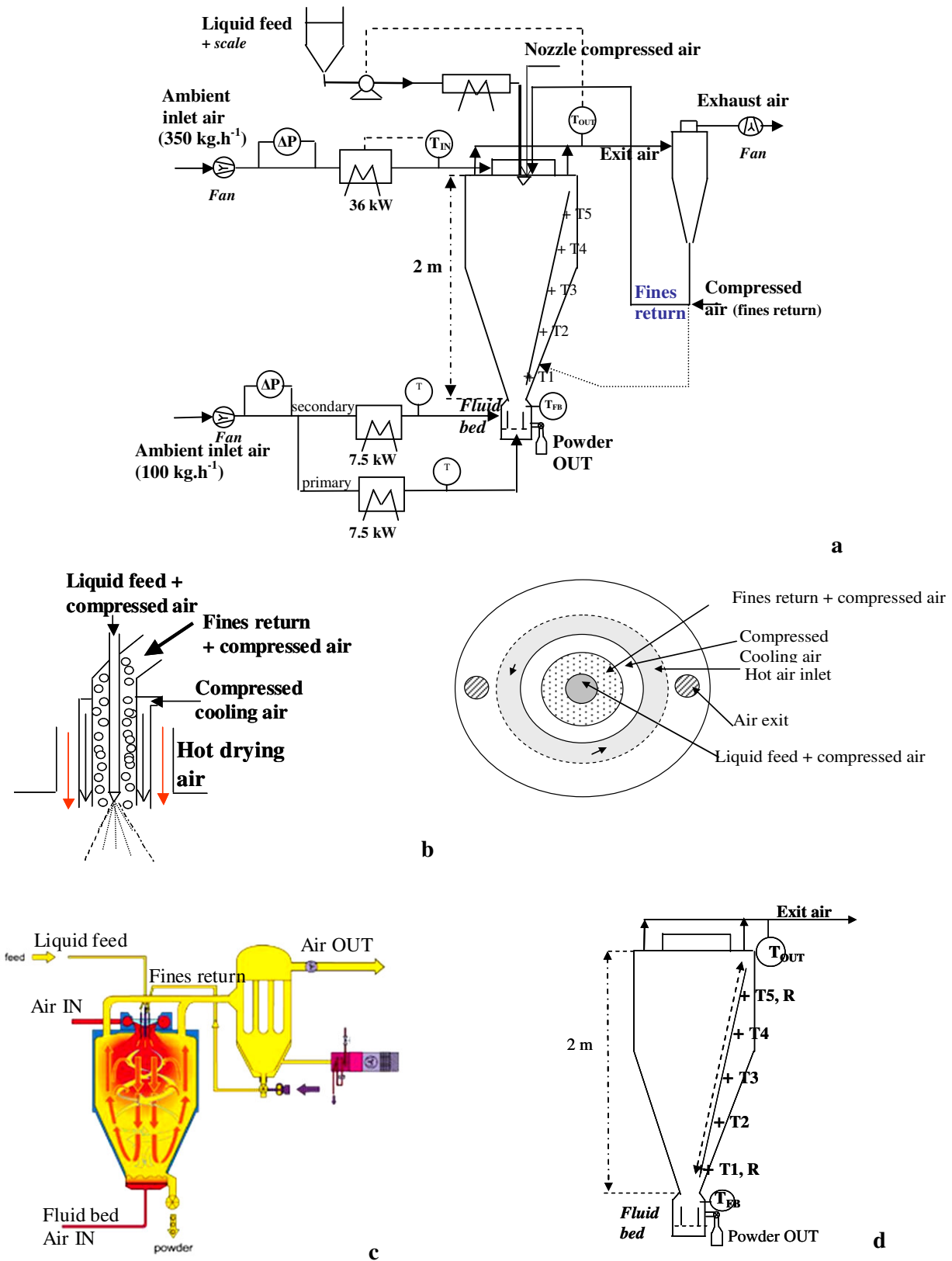


**Figure 2.2.** (a) Flowsheet of the pilot spray dryer NIRO-FSD 4.0; (b) bifluid nozzle with fines return and scheme of the top of the spray drying chamber; (c) air circulation scheme inside the chamber; (d) position of probes for measurements of air properties (+: thermocouples, R: hygrometer).

## *Part II – Materials and methods*

Drying air is sucked from ambient by a fan placed at the exit, so that pressure in the chamber was inferior to atmospheric pressure.

The liquid feed at ambient temperature was pumped (pump ViscoTec 2RB10-KF) from a tank to the atomizer (minimum flow rate  $12 \text{ kg}\cdot\text{h}^{-1}$ ). It could be heated up to  $80^\circ\text{C}$  by electrical resistances. The tank was installed on a scale to measure mass flow rate. The liquid feed flow rate was controlled as a function of the exit air temperature  $T_{\text{OUT}}$ .

The atomization device is a two-fluid nozzle, in which liquid feed is mixed with compressed air (Fig. 2.2b). Compressed air pressure could be varied between 0.5 and 6 bars. Additional compressed air is used for nozzle cooling.

Inlet air for drying tower was taken from ambient, filtered and heated by a 36 kW electrical resistance that allowed setting air inlet temperature up to  $300^\circ\text{C}$ . For safety reasons heating is limited to  $230^\circ\text{C}$ . Inlet air flow rate was measured at the entrance with a Venturi flow meter ( $\Delta P$ ) and inlet temperature  $T_{\text{IN}}$  was measured with an on-line thermocouple. At the top of the chamber, the air passed through an air disperser providing a swirled air flow inlet around the nozzle so that the drying was co-current.

In the bottom of the chamber an integrated fluid bed, with additional hot air, allowed further treatment (drying, agglomeration) of the powder. The installation was adapted to perform trials with or without the fluid bed. Additional air for fluid bed, when used, was supplied by a fan and split in two different streams. Primary fluidization air entered through the bottom of the fluid bed, while secondary air entered on the side. An equal flow rate was assumed for both streams. Each stream may be heated by a 7.5 kW electrical resistance up to  $140^\circ\text{C}$ . Total additional air flow rate may be varied between 50 and  $150 \text{ kg}\cdot\text{h}^{-1}$ . Usual flow rate was  $100 \text{ kg}\cdot\text{h}^{-1}$ . Air temperature inside the fluid bed was measured in the upper part of the fluid bed (position not well defined).

Air exited from the drying chamber by two holes in the top of the chamber (Fig. 2.2b). Exit air temperature  $T_{\text{OUT}}$  was measured by an on-line thermocouple. Fine particles dragged by exit air were separated in a cyclone and totally reinserted in the chamber with pneumatic system (uncontrolled compressed air flow rate). The pneumatic fines return system allowed insertion either near the nozzle or in the cone in the bottom part of the chamber (dashed line Fig.2.2a). Exhaust air was further cleaned by a water scrubber and then released to atmosphere.

Powder was recovered at the bottom of fluid bed in a closed tank. The tank capacity was sufficient to collect powder produced during the whole trial ( $\sim 1 \text{ h}$ ) without opening.

The exit air flow rate resulted from the different air inlets: drying air, fluidized bed air, compressed air for fines return, bi-fluid nozzle air and nozzle cooling air (the last three flow rates were not evaluated) with possible mixing of these different air streams in the chamber (Fig. 2.2c).

The two equipments used in this study are co-current spray dryers. They differ by the size (factor 2), the kind of atomizer (rotary and bi-fluid) and the configuration. The NIRO FSD 4.0 has a more complex configuration with fines return and possible fluid bed, a higher evaporative capacity (x 5).

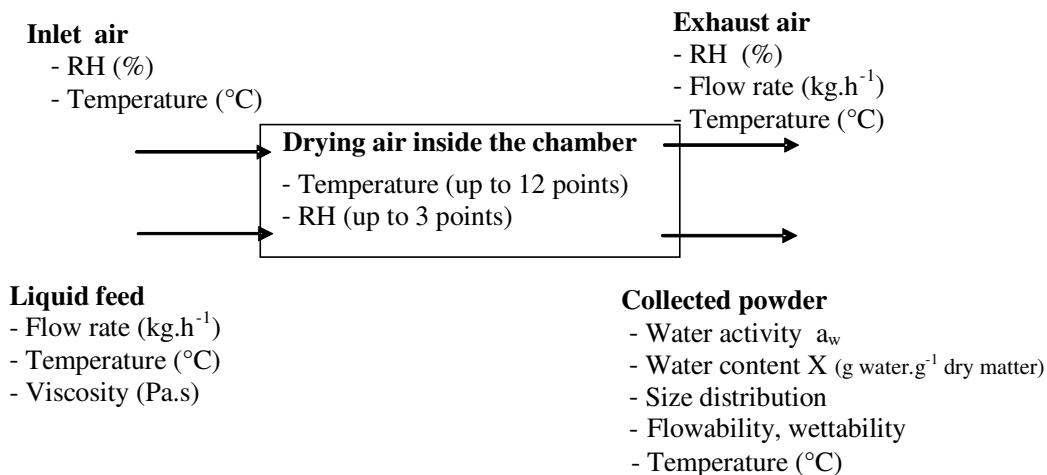


**Figure 2.3.** Measurements performed on liquid feed, air and powders in NIRO Minor.

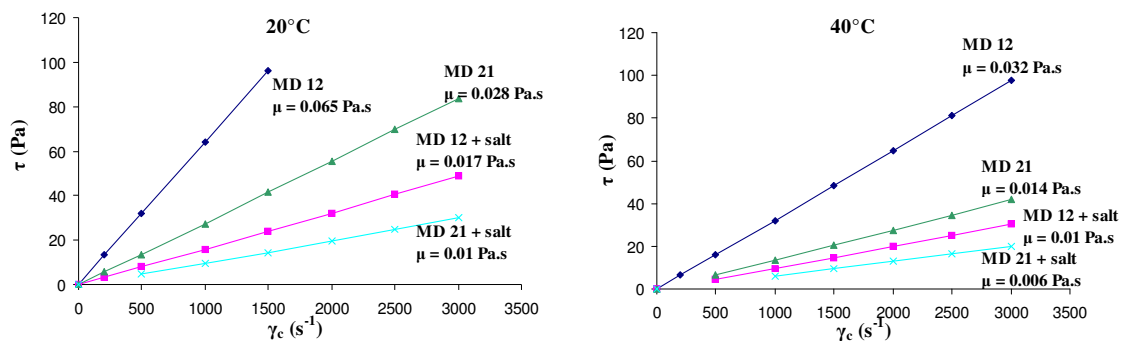


**Figure 2.4.** Viscosity of aqueous solution (40% w/w) of maltodextrin DE12 and DE 21 with and without NaCl (50% of total solids) at 20°C and 40°C.

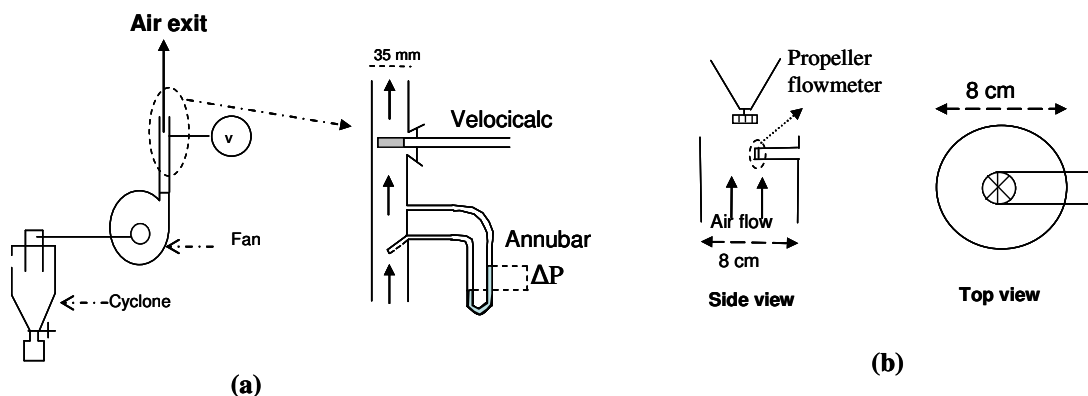


**Figure 2.5.** Measurements of air flow rate in NIRO Minor. (a) at the exit of the plant (b) at the air entrance inside the chamber.

### 3. Measurements on liquid feed, air and products

The measurements performed on liquid feed, air and products in Niro *Minor* are summarized in Fig. 2.3.

#### 3.1. Measurements on liquid feed solutions

The viscosity  $\mu$  (Pa.s) of maltodextrin aqueous solutions was measured at 20 and 40°C with a rotational viscometer (Rheomat R180, Lamy, France). The liquid sample was put in the gap between two coaxial cylinders ( $R1/R2 = 0.95$ ). The external cylinder was fixed (stator) while the internal rotated (rotor) at the set velocity. The cylinders with the liquid sample were placed in a thermostatic bath and liquid temperature was measured with a thermocouple.

Relationship between shear stress  $\tau$  (Pa) and shear velocity gradient  $\gamma_c$  ( $s^{-1}$ ) was obtained directly by imposing different shear velocity gradient (from 1 to 3000  $s^{-1}$ ) to the liquid sample and measuring the corresponding shear stress.

All the maltodextrin solutions tested showed a newtonian behavior (Fig. 2.4): viscosity  $\mu$  was independent from shear velocity gradient and a linear relationship exists between shear stress and shear velocity gradient  $\tau = \mu \cdot \gamma_c$

#### 3.2. Measurements on air

##### 3.2.1. Air flow rate

As air was sucked from the exit, the spray dryer chambers were under depression. Pressure inside the chamber of NIRO *Minor* was measured with a water column.  $\Delta P$  was equal to  $\sim -340$  Pa ( $35 \pm 1$  mm H<sub>2</sub>O) for a fan frequency of 45 Hz, and to  $\sim -230$  Pa ( $23.5 \pm 1$  mm H<sub>2</sub>O) for a fan frequency of 35 Hz.

To check total air flow rate obtained with the Annubar probe at the exit of the chamber after the fan, air flow rate in NIRO *Minor* was also measured with two velocimeters with hot wire (Velocicalc, TSI, USA) and with propeller (Hontzsch Instruments, Ge). Measurements were made at two positions, the active sensor component being placed perpendicular to the air flow:

a) On inlet air, at the end of the inlet air pipe ( $d = 0.08$  m) inside the chamber (without the air disperser) (Fig. 2.5b). But no reliable results could be obtained from these measurements because in this position air flow was not stable (transition zone from pipe to the chamber) and measurements were not possible.

b) On exit air, in the straight exhaust air pipe ( $d = 0.035$  m), 80 cm after the fan just after the Annubar probe (Fig. 2.5a.; only Velocicalc). From measured air velocity  $v_{air}$  ( $m \cdot s^{-1}$ ) it was possible to calculate the air mass flow rate  $\dot{m}_{HumidAir}$  ( $kg \cdot h^{-1}$ ) with the following equation:

$$\dot{m}_{HumidAir} = v_{air} \cdot A_{pipe} \cdot \rho_{air} = \dot{V}_{air} \cdot \rho_{air} \quad \text{eq. 2.3}$$

$A_{pipe}$  pipe section ( $m^2$ );  $\rho_{air}$  air density ( $kg \cdot m^{-3}$ ), depending on air temperature ( $1.29 \text{ kg} \cdot m^{-3}$  at  $0^\circ C$ )  
 $(\rho_{air} = 1.29 \cdot (273/(273+T)))$

Measurements were done without liquid atomization, for the fan frequencies (35 and 45 Hz) and the inlet air temperatures used in spray drying trials ( $T_{IN}$  144 and  $200^\circ C$ ).



**Table 2.3.** Air flow rate at the exit of pilot spray dryer calculated from measurements with the Annubar probe and Velocicalc velocimeter ( $T_{IN}$ : 14 – 144 – 200°C;  $f_{fan}$  : 35 – 45 Hz )

$f_{fan}$ (Hz)	$T_{IN}$ (°C)	$T_{exit}$ (°C)	Annubar			Velocicalc		
			$\Delta P$ (mm H <sub>2</sub> O)	$\dot{m}_{air}$ (kg.h <sup>-1</sup> )	$\dot{V}_{air}$ (m <sup>3</sup> .h <sup>-1</sup> )	$v_{air}$ (m.s <sup>-1</sup> )	$\dot{m}_{air}$ (kg.h <sup>-1</sup> )	$\dot{V}_{air}$ (m <sup>3</sup> .h <sup>-1</sup> )
45	14	16.5	118±2	117±1	96±1	30.3±0.3	123±4	105±1
45	144	50.0	115±2	<b>110±1</b>	101±1	30.0±0.3	<b>113±4</b>	104±1
45	200	65.0	109±2	105±1	101±1	27.7±0.3	107±4	103±1
35	14	16.5	60±2	<b>81±1</b>	66±1	18.7±0.3	<b>78±3</b>	65±1

**Table 2.4.** Methods used for air relative humidity measurements.

<i>Method</i>	<i>Measured Variable</i>	<i>Position</i>	<i>Provider</i>	<i>Specifications</i>
<b>Psychrometry</b>	$T_{wb}, T_{air}$	Ambient air	Jules Richard	
		Exit air (Niro Minor)	thermometers	
<b>Capacitive hygrometer</b>	$T_{air}, RH$	Inside chamber	Hygroclip Rotronic	Range: 1-100% RH ±1%; -50°C to 200°C ±1°C
		Ambient air (Minor)	RS 1367 Radiospares	Range: 1-100% RH ±3%; -20° to 70°C ±1%
<b>Dew point hygrometer</b>	$T_{dp}, T_{air}$	Inside chamber (Niro Minor)	SIM-12H, General Eastern	Range: -10°C – 75°C ±0.2°C

The calculated air mass flow rates were in agreement between the two probes (Table 2.3). For a given fan frequency, the total volumetric air flow rate was the same whatever the inlet air temperature tested, while mass flow rate decreased slightly when increasing temperature. It was however about  $110 \text{ kg}\cdot\text{h}^{-1}$  for a fan frequency of 45 Hz and hot inlet air, and  $80 \text{ kg}\cdot\text{h}^{-1}$  for fan frequency of 35 Hz.

### **3.2.2. Air temperature**

Thermometers were used to measure ambient air temperature and exit air temperature. For air temperature measurements inside the chambers 5 to 12 thermocouples (K-type,  $d = 1\text{mm}$ ,  $\pm 1.5^\circ\text{C}$ ) were implemented. They were calibrated at  $0^\circ\text{C}$  (ice bath) and  $100^\circ\text{C}$  (boiling water) and installed inside the chamber. In the upper cylindrical part of the chamber, two thermocouples were placed on the same radius to measure possible radial differences.

In NIRO Minor (Fig. 2.1c) they were fixed on an iron support at different positions (accuracy  $\pm 2 \text{ cm}$ ). Thermocouples connection wires were connected (through plexiglass window) to a computer for data acquisition and temperatures were recorded through a Labview program (National Instruments, USA).

To avoid powder sticking on thermocouples head when drying liquid solutions, a protecting hat has been used with some of the thermocouples. Measured temperatures were the same with and without the protection, so that further trials were performed without protection.

In NIRO FSD 4.0. 5 thermocouples were fixed to a long inox bar that entered from the cleaning-in-place hole in the chamber top. Temperatures values were read on a transducer (not recorded) (Fig. 2.2d).

### **3.2.3. Air relative humidity**

Methods used for air relative humidity measurements are summarized in Table 2.4.

The **psychrometry** method was used to measure humidity of ambient air and exit air in the case of NIRO Minor. For ambient air, a psychrometer Jules Richard was used. It is composed by two thermometers, one for the “dry” temperature  $T_{\text{air}}$ , the other one covered by a humid gaze (RH 100%) for the “wet bulb” temperature  $T_{\text{wb}}$ . A small fan forces ambient air to flow on the two thermometers. Those two temperatures allow reading on a Mollier diagram the air relative humidity (RH) and absolute humidity  $Y$  (Fig 2.6).

For exit air humidity measurement, two thermometers (“dry temperature” and “wet bulb temperature”) were placed in the air exit pipe after the fan, inside the exit air flow. One of the thermometers was covered by a gaze humidified just before measurement.

A **capacitive thermohygrometer** (Hygroflex, Rotronic, Switzerland) was used to measure air humidity inside the dryer chambers. It is equipped with a probe Hygroclip (range: 1-100% RH;  $-50 + 200^\circ\text{C}$ ; accuracy  $\pm 1\%$  RH;  $\pm 0.2^\circ\text{C}$  at  $23^\circ\text{C}$ ) protected from powder with a metallic filter. The sensitive element is an hygroscopic polymer absorbing water from surrounding air until equilibrium is reached. The dielectric constant and thus the capacity of the condenser are modified depending on air relative humidity at the measured temperature. The thermohygrometer equipment indicated the air temperature and relative humidity.

The capacitive hygrometer was calibrated in a RH controlled atmosphere with saturated salt solution at two temperatures ( $\text{NaNO}_3$ : 75% RH at  $20^\circ\text{C}$ ; 63% RH at  $80^\circ\text{C}$ ) (Table 2.5). The sensor placed inside the spray dryer chamber during a water atomization trial once the steady state was reached, gave a stabilized value after 10 min.

**Table 2.5.** Temperature and relative humidity measured by the Rotronic thermohygrometer in controlled atmospheres (20 and 80°C with 63 and 75% of relative humidity).

Air temperature imposed (°C)	Air temperature measured (°C)	RH saturated salt solution NaNO <sub>3</sub> (%)	RH measured (%)
80.0	78.3	63 %	64.5 %
20.0	21.2	75 %	73 %

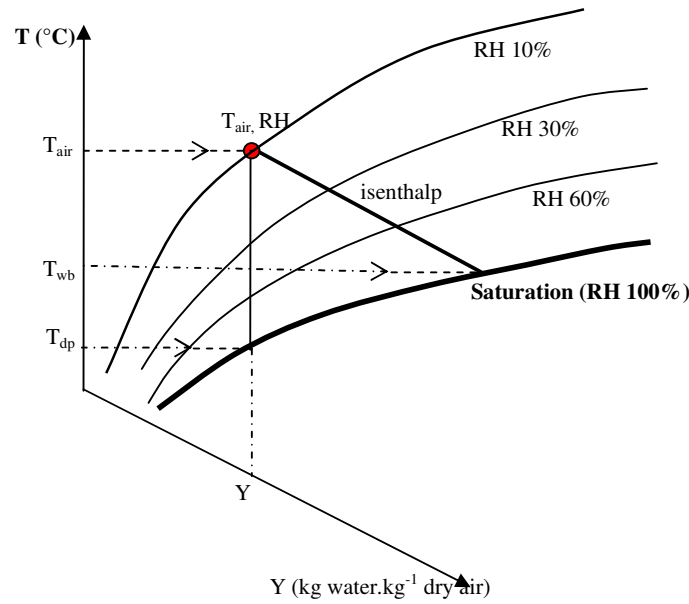


**Figure 2.6.** Mollier diagram with different approaches to measure air relative humidity RH and water content  $Y$  ( $T_{wb}$ : wet bulb temperature;  $T_{dp}$ : dew point temperature).

In NIRO Minor, air relative humidity was measured inside the chamber at steady state at two different positions A (top) and B (bottom) (Fig. 2.1c) by moving the hygrometer from position A to B once the steady state was reached. Values were recorded on a PC using a Labview program. A second thermohygrometer (RS 1367, Radiospare, France) was used to check RH values measured by psychrometry on ambient and exit air.

In NIRO FSD the Rotronic thermohygrometer was fixed on a stainless steel bar that could be moved from bottom to top of the chamber (Fig.2.2).

A **dew point hygrometer** (SIM-12, General Eastern, USA) was used in some trials in NIRO Minor to measure and check air relative humidity in the upper part of the chamber. The air to analyze was sucked from the chamber with a vacuum pump and flow above a mirror cooled by Peltier effect. Equilibrium between air and mirror surface occurred. Temperature of the mirror was progressively lowered, till the formation of the first condensation drop, detected by an optoelectronic system. The temperature for which this condensation occurred was the air dew point temperature  $T_{dp}$ . From this temperature and temperature of air inside the chamber (measured by a thermocouple fixed on the hygrometer air sampling pipe) air properties were determined (Fig. 2.6). To avoid condensation before detection on the mirror, the sampling pipe was heated up to 60°C. These off-line measurements were in agreement with those given in-situ by capacitive hygrometer.

### 3.3. Measurements on powders

#### 3.3.1. Water content

Water content  $X$  (g water.g<sup>-1</sup> dry matter) was measured on powders by oven drying. A powder sample (2-3 g) was weighted ( $m_i$ ) and oven dried (at 105°C for maltodextrin powders and at 70°C under vacuum for protein hydrolysate) until constant weight (checked every 24 h). Constant weight was usually obtained after 48 h drying; it corresponded to the dry matter weight  $m_s$ . Water content was calculated as  $X = (m_i - m_s) / m_s$

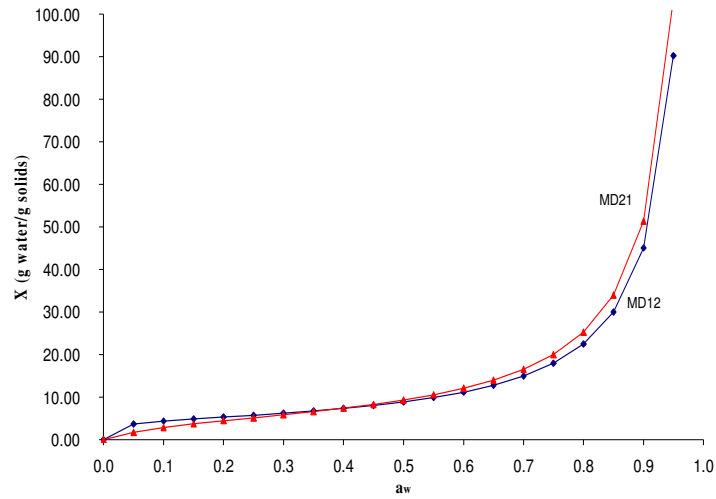
Average value for three samples was considered.

#### 3.3.2. Water activity

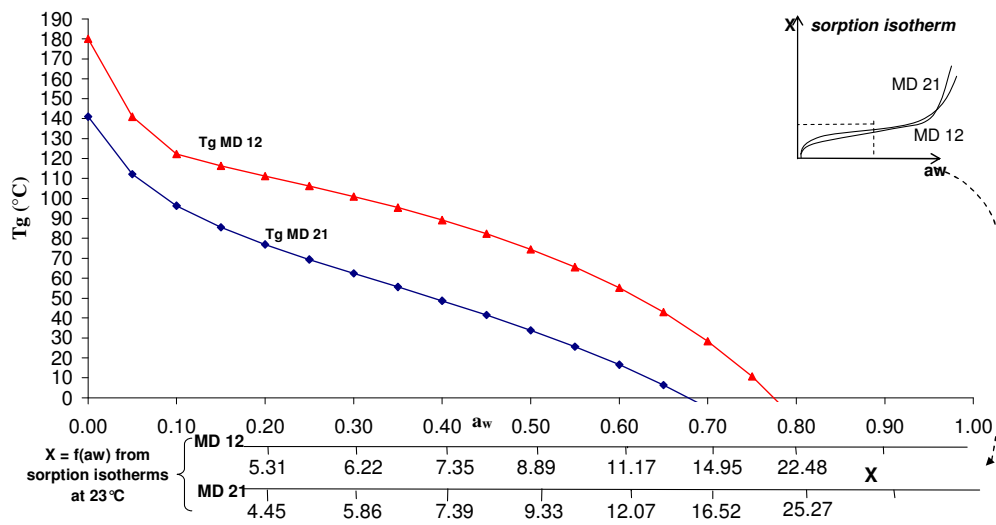
Water activity  $a_w$  of powders was measured with  $a_w$ -meter (TH2, Novasina, Switzerland) at 20°C. About 2 g of powder were placed in a sample holder in a small cell in which equilibrium was reached between powder and the above air layer. Relative humidity of air was continuously measured by a conductimeter probe, and at equilibrium its value corresponded to the water activity of the sample.

#### 3.3.3. Powder size distribution

Particle size and size distribution was measured by laser granulometry using dry mode (Mastersizer 2000, Malvern, France; range 0.02 – 2000  $\mu\text{m}$ ; accuracy  $\pm 1\%$ ). Powder sample was put on a vibrating plate and then conveyed to the laser beam by compressed air. Compressed air pressure was set to 0.5 bar, the lowest possible value to avoid breakage of particles during transport.



(a)



(b)

**Figure 2.7.** Sorption isotherms at 23°C (a) and glass transition temperatures of maltodextrin DE12 and DE21 (b).

From the laser diffraction spectrum, the volumetric fraction of particle in each size class was calculated: the smallest particles have bigger diffraction angles than the biggest particles. From volume size distribution, several diameters could be calculated:

- $d_{50}$ : Median diameter; 50% of particles have a smaller diameter
- $d_{10}$ ,  $d_{90}$ : 10 and 90% respectively of the particles have a smaller diameter
- $d_{3,2}$ : Volume-surface mean diameter (Sauter). The Sauter diameter is the diameter of a sphere having the same surface-to-volume ratio that the entire powder sample (assuming spherical particles)
- $d_{4,3}$ : Volume mean diameter.

### 3.3.4. Sorption isotherms and glass transition temperatures

Sorption isotherms of maltodextrin powders were determined by equilibrating during three months powder samples (2-3 g) at 23°C in different RH-controlled atmospheres (saturated salt solutions of LiCl (11% RH), CH<sub>3</sub>COOK (23% RH), MgCl<sub>2</sub> (33% RH), K<sub>2</sub>CO<sub>3</sub> (43% RH), Mg(NO<sub>3</sub>)<sub>2</sub> (53% RH), NH<sub>4</sub>NO<sub>3</sub> (62% RH) and NaCl (75% RH)). Water content of powder at equilibrium was then determined (weighting and oven drying). The Brunauer-Emmett-Teller (BET) equation was used to model sorption isotherms (Fig. 2.7a). Fitting parameters  $C_{BET}$  and  $x_m$  were found to be respectively 64.2 and 4.51 for MD12 and 35.18 and 4.85 for MD21 at 23°C (equation 1.3). Sorption isotherms for both maltodextrins are very close. For low  $a_w$  we can observe that MD21 is above MD12, and the contrary for high  $a_w$ .

Glass transition temperatures ( $T_g$ ) of equilibrated powders were determined by Differential Scanning Calorimetry (DSC Q100, Texas instrument, USA);  $T_g$  was determined after the second heating (heating rate 5°C.min<sup>-1</sup>) as the midpoint temperature. Gordon-Taylor equation  $T_g = f(a_w)$  was used to model glass transition curves (Fig. 2.7b). Fitting parameter K was found to be 6.93 for MD12 and 6.8 for MD21 (eq. 1.14).

Data for protein hydrolysate powders were provided by Nestlé.

### 3.3.5. Wettability

Wettability of powders was evaluated at ambient temperature. 10 g of powder were placed in a funnel (d 90 mm (superior) and 40 mm(inferior)) closed with a plug, 10 cm above a beaker (d 70mm; h 135 mm) containing 100 ml of water. The plug was then removed and powder fell on water surface. A chronometer was used to measure time necessary for all the powder to be wetted by water. Wettability was taken as the time for which the last particle of powder sample penetrated into water. Average of three measurements was considered.

### 3.3.6. Bulk and tapped density

Bulk density  $\rho_{bulk}$  (kg.m<sup>-3</sup>) was measured by weighing 100 ml of powder in a graduated cylinder. Tapped density  $\rho_{tap}$  was determined by reading the volume of 50 g of powder in a tapping machine after 10, 100 and 500 tappings (value of  $\rho_{tap}$  was considered good if no variation was observed between 100 and 500 tappings).

### 3.3.7. SEM microscopy

Powder particles were observed by Scanning Electron Microscopy (JSN - 5200, Jeol, Japan). In SEM microscopy a succession of lenses produces a finely focused electron spot on the specimen, resulting in an electron emission signal which is collected and amplified. Thanks to a cathode ray tube, images are generated. Before observation, the powder sample (some mg) is covered under vacuum with a small gold layer to increase sample conductivity (340 s, 10 mA).

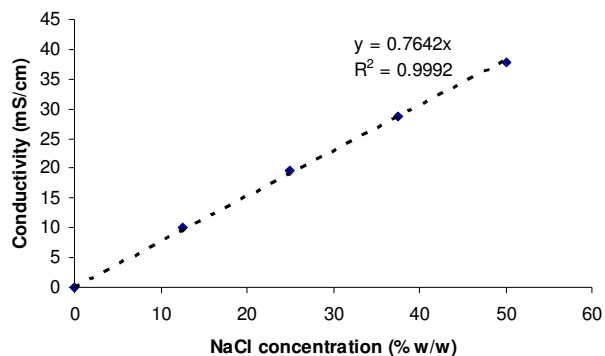


**Figure 2.8.** Conductivity of aqueous solutions of maltodextrin and NaCl as a function of salt concentration in total solids.

**Table 2.6.** Operating parameters tested for spray drying of water in NIRO Minor.

Air $T_{IN}$ (°C)	Air flow rate $\dot{m}_{air}$ (kg.h <sup>-1</sup> )	Water flow rate $\dot{m}_w$ (kg.h <sup>-1</sup> )	Rotary atomizer speed (rpm)
144	110	1.08 – 2.16 – 3.24	30000
144 – 174 – 200	110	2.16	25000
200	80 – 110	2.16	25000
200	110	1.08 – 2.16 – 3.24	25000
200	110	2.16	20000 – 25000 – 30000

**Table 2.7.** Operating parameters tested for spray drying of aqueous solutions (40% w/w) of maltodextrin in NIRO Minor.

Air T (°C)	Air flow rate (kg.h <sup>-1</sup> )	Liquid flow rate (kg.h <sup>-1</sup> )	Corresponding water flow rate (kg.h <sup>-1</sup> )	Rotary atomizer speed (rpm)	Maltodextrin (DE)
144	110	1.8 – 3.6 – 5.4	1.08 – 2.16 – 3.24	30000	12 -21
144 – 174 – 200	110	3.6	2.16	30000	12
200	80 – 110	3.6	2.16	25000	12
200	110	1.8 – 3.6 – 5.4	1.08 – 2.16 – 3.24	25000	12
200	110	3.6	2.16	20000 – 25000 – 30000	12

### 3.3.8. Conductivity of solutions for DTS measurements

To measure the salt (NaCl) concentration in spray dried powders collected along DTS experiments, samples were redissolved in water. Conductivity measurements were performed with a conductimeter (LF 197, WTW, Germany) equipped with a TetraCon 325 probe (range:  $1 \mu\text{S}\cdot\text{cm}^{-1} - 2 \text{S}\cdot\text{cm}^{-1}$ ).

2 g of powder were dissolved in 40 g of water, and the conductimeter probe was placed in the solution at ambient temperature. The calibration curve built for salt concentration corresponding to 0 and 50% of total solids is given in Fig. 2.8.

### 3.3.9. Colour

A colorimeter (CR-200, Minolta, Fr) was used to measure colour of maltodextrin powder samples containing eosine collected during residence time distribution trials. The sample holder was filled with powder, and the colorimeter measured the three chromatic coordinates L, a and b of the sample. L expresses the luminance and it could vary between 0 (dark) and 100 (white). a and b represent the chromaticity of the sample, varying from -60 to +60 (switch from green to red for a, from blue to green for b). From these measurements, the colour saturation index C (chroma) was calculated as:

$$C = \sqrt{a^2 + b^2} \quad \text{eq. 2.4}$$

## 4. Conditions of spray drying trials

### 4.1. Trials in NIRO Minor

Three sets of spray drying trials were performed; with water and with the two aqueous solutions of maltodextrin DE12 and DE21 (40% w/w).

Studied parameters (Table 2.6 and 2.7) included inlet air temperature  $T_{\text{IN}}$  (144 – 174 – 200 °C), air flow rate (80 – 110  $\text{kg}\cdot\text{h}^{-1}$ ), rotary atomizer rotation velocity (22500 – 25000 – 30000 rpm, corresponding to a pressure of 4 – 5 – 6 bar) and sprayed liquid flow rate (from 1.08 to 3.24  $\text{kg}\cdot\text{h}^{-1}$  for water trials and from 1.8 to 5.4  $\text{kg}\cdot\text{h}^{-1}$  for 40% w/w aqueous maltodextrin solutions trials). The liquid flow rates for maltodextrin trials were chosen in order to have the same amount of water to evaporate as for water drying trials. Each condition was repeated three times to verify reproducibility of the results.

The procedure for a complete spray drying trial was the following:

1. The day before the trial, liquid solution was prepared and all parts of pilot were assembled. Thermocouples and thermohygrometer were installed inside the chamber and connected to PC for data recording.
2. Inlet air was heated up to the imposed temperature  $T_{\text{IN}}$  (~30 min); 2h were waited to heat up the chamber before starting the liquid atomization.
3. Water was sprayed until reaching steady state for air temperatures and humidity measured inside the chamber (~1 h).
4. Maltodextrin solution was spray dried with a flow rate for which the total amount of water to evaporate was the same as the previously sprayed water flow rate.
5. Powder was collected during all the trial (~ 1 h), changing the glass jar every 5 to 15 minutes depending on the feed flow rate. Once the steady state for air temperatures was reached (~ 30/40 min) powder samples were used for analysis.
6. At steady state, thermohygrometer was moved to measure air humidity in different positions.



**Table 2.8.** Operating parameters tested for spray drying of protein hydrolysate solutions in NIRO FSD 4.0.

<b>Sprayed liquid</b>	<b>T<sub>IN</sub> (°C)</b>	<b>Fluid bed</b>	<b>Fines return</b>	<b>T<sub>OUT</sub> (°C)</b>
Water	180	No	Bottom	65 – 75
Protein hydrolysate solution	160	No	Top	70-75
		Yes		
	180	No	Top	75-80-88
			Bottom	80-88
		Yes	top	65-75
			Bottom	75-85
	200	No	Top	88
			Bottom	97
		Yes	Top	80-88

7. If a different operating condition had to be tested in the same spray drying session, desired parameters were changed and water was spray dried intermediately until no more powder was collected (~30 min) before spraying again the maltodextrin solution.
8. At the end of the trial, air heating was stopped and water was sprayed to cool down the chamber more quickly before shutdown. The spray dryer was then dismantled and cleaned (~2 h).

## 4.2. Trials in NIRO FSD 4.0

Studied parameters (Table 2.8) for protein hydrolysate solutions drying included inlet air temperature  $T_{IN}$  (160 – 180 – 200°C), exit air temperature  $T_{OUT}$  (65 to 90°C, corresponding to a liquid flow rate from 12 to 20 kg.h<sup>-1</sup>), use of internal fluid bed and position of fines return (top-bottom).

The initial solution (or water) was heated up to 70°C. The sprayed liquid flow rate was controlled to obtain the desired outlet air temperature: the higher the exit air temperature, the lower the sprayed liquid flow rate. For safety reasons, the exit air temperature should not be higher than 90°C.

The following procedure was followed:

1. Heating up of inlet air (for drying and fluid bed if necessary) until desired drying air temperature, then 20 minutes of running without liquid atomization.
2. Spray drying of water during 20 minutes.
3. Spray drying of liquid solution. Once the steady state (stable exit air temperature) was reached (~10 min), powder was collected during about 30 minutes. Samples for analyses were taken from the total collected powder (except powder recovered during the first 10 minutes not used for analysis).
4. If a drying parameter had to be changed during a trial, pure water was sprayed in between to “clean” the chamber until no more powder exit from the chamber and no more fines recirculation was observed (~15 min).
5. Shutdown of pilot and cleaning in place (~1 h).

## 4.3. Residence time distribution measurements in NIRO Minor

Trials were performed by spraying first a 40% w/w aqueous solution of maltodextrin DE12 coloured with eosine. Then, a 40% w/w aqueous solution with 50% maltodextrin DE12 and 50% NaCl in total solids was sprayed. The high salt concentration was chosen for analytical reasons and also to test the drying behavior of a maltodextrin solution having a salt content similar to the one in the protein hydrolysate solution. Inlet air temperature  $T_{IN}$  was set to 200 °C, to have fast drying avoiding sticking on walls (product losses) and liquid solution flow rate was chosen as 3.6 kg.h<sup>-1</sup> to have powder flow rate high enough to regularly collect powder (~24 g.min<sup>-1</sup> of dry matter). The operating procedure was the following:

1. Heating-up of drying air and of the chamber.
2. Spraying of water (2.16 kg.h<sup>-1</sup>) until reaching steady state (constant air temperatures inside the chamber).
3. Spraying of the 40% w/w MD12 coloured solution (3.6 kg.h<sup>-1</sup>) collecting regularly powder samples until reaching steady state (constant air temperatures).
4. Spraying of the 40% w/w MD12 solution containing NaCl (50%) to have an “output step” for colour and an “input step” for salt concentration. Initial time  $t = 0$  was taken once the non coloured solution arrived at the atomizer entrance. Powder samples were



*Part II – Materials and methods*

- collected every minute during the first 5 minutes, then every 2 minutes (7, 9 and 11 minutes) and then after 15, 20, 25, 35, 45 minutes.
5. After 55 minutes of running with the solution containing salt, an output step for salt concentration was performed by switching back to the 40% w/w MD12 coloured solution. This led simultaneously to an input step for color (t = 0 was taken when colored solution arrived at the atomizer entrance). During the first 3 minutes, powder samples were collected every 30 seconds, then after 4, 5, 7, 10, 16 and 25 minutes.
  6. Spraying of water and stop of air heating to shut down the pilot.

Responses to salt and colour steps were obtained respectively by conductivity and colorimetry measurements on sampled powders.



**PART III**  
**RESULTS AND DISCUSSION**



The objective of the first part of the study was to characterize the pilot spray dryer NIRO Minor and to choose the operating conditions that will be used for investigation of spray drying behavior of liquid solutions: process parameters, air properties measurement positions.

In the second part air properties measurements were used to investigate the effect of process parameters on drying behavior of water and maltodextrin solutions: inlet air temperature and flow rate, liquid feed flow rate, rotary atomizer wheel speed. Particles average water content evolution along drying was calculated from water mass balances on air between inlet and different positions in the chamber. Then the particle properties (average water content, temperature) and the glass transition temperatures of the considered material were used to define possible operating conditions and positions for which particles could exhibit a sticky behavior favorable for agglomeration inside the chamber.

In the third part a computational fluid dynamics CFD model was developed to calculate air and drops/particles properties evolution during drying and to predict sticky conditions for particles inside the chamber.

In the fourth part the determined sticky conditions were tested by inserting powder inside the chamber, to obtain agglomeration and to study the influence of powder insertion position on size enlargement.

Finally the experimental approach to study product drying behavior from air properties measurement was extended to a semi-industrial spray dryer NIRO FSD 4.0 for drying of a protein hydrolysate solution.



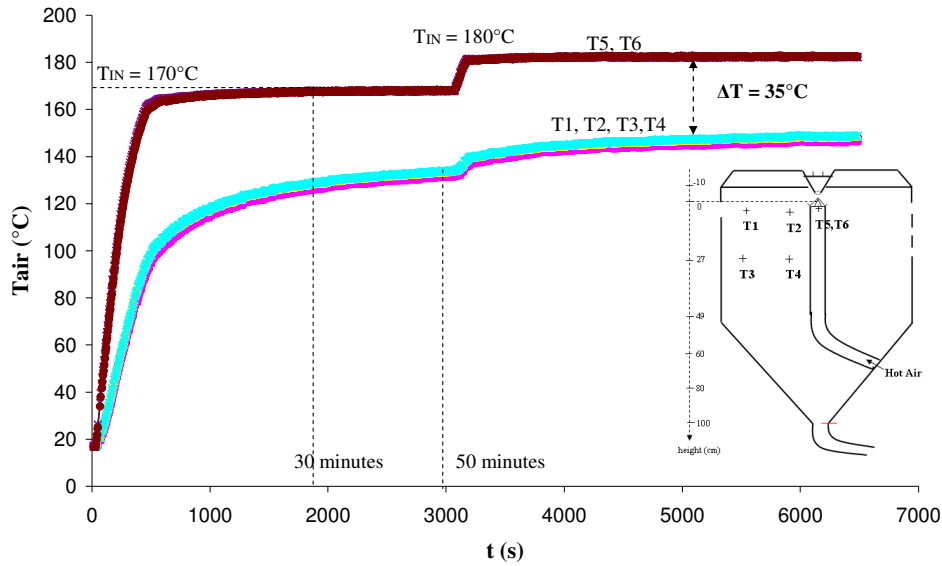


**Figure 3.1.1.** Time to reach steady state from air temperature measurements inside the NIRO Minor (no liquid atomization,  $T_{IN}$  : 170 – 180 °C, air flow rate: 110 kg.h<sup>-1</sup>).

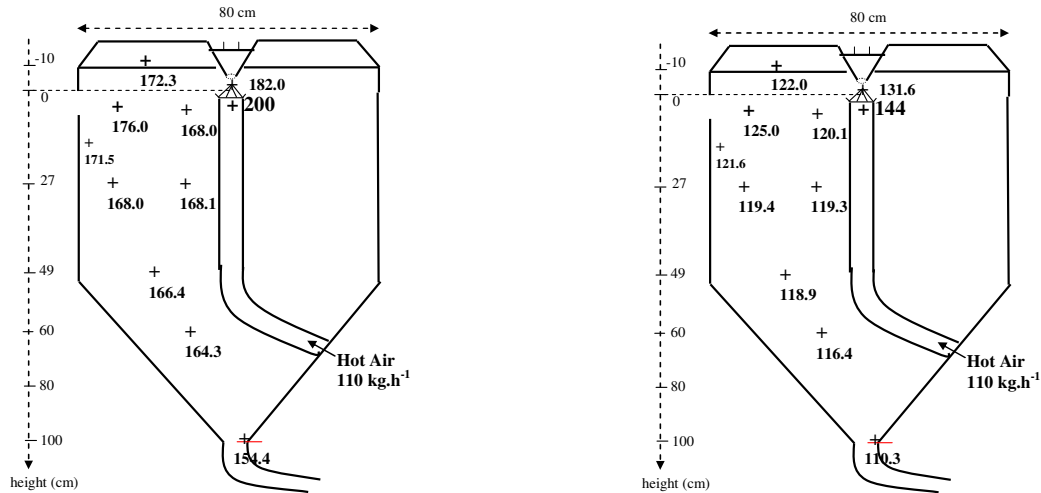


**Figure 3.1.2.** Air temperatures inside the NIRO Minor at steady state (no liquid atomization; hot air 144 and 200°C, total air flow rate 110 kg.h<sup>-1</sup>).

**Table 3.1.1.** Calculation of heat losses  $\dot{Q}_{losses}$  and global heat exchange coefficient  $h$  without liquid atomization (air  $T_{IN}$  144 and 200°C,  $\dot{m}_{air}$  110 kg.h<sup>-1</sup>,  $T_{amb}$  18°C;  $S$  3.37m<sup>2</sup>,  $C_{p,air}$  = cste = 1 kJ.kg<sup>-1</sup>).

$T_{IN}$ (°C)	$T_{wall}$ (°C)	$T_{OUT}$ (°C)	$\dot{Q}_{losses}$ (W)	$h$ (W.m <sup>-2</sup> .K <sup>-1</sup> )
144	122	110	1039	2.96
200	172	154	1405	2.71

## 1. Definition of process operating conditions

Before studying the spray drying behavior of maltodextrin solutions, the feasibility of air properties measurements (temperature T, relative humidity RH) had to be tested.

Measurements on air without liquid atomization were performed in order to estimate the time necessary to heat up the chamber and to evaluate heat losses due to heat exchanges through the chamber walls.

Then, water spray drying trials were performed in order to determine time necessary to reach steady state inside the chamber (stable T and RH) and to choose positions for air properties measurements (T, RH) in order to get representative data for the studied process.

The process operating parameters (inlet air temperature and flow rate, rotary atomizer speed, water flow rate) were chosen for further use in solution drying trials.

Then maltodextrin solutions were dried in order to choose the liquid flow rates for comparison with water drying trials and to determine the time necessary for collecting dry powder samples.

### 1.1. Measurements on air without liquid atomization

#### 1.1.1. Heating of the chamber

Time necessary to reach steady state (constant air temperature) inside the chamber was first evaluated without liquid atomization with four temperature measurements in the upper part of the chamber (Fig. 3.1.1). Two thermocouples ( $T_5$  and  $T_6$ ) were also placed inside the inlet air pipe, to verify the imposed air inlet temperature  $T_{IN}$  and to determine time necessary to heat up air at the beginning of a trial.

About 30 minutes were necessary for air temperature at the entrance of the chamber to reach the imposed value of 170°C and to be stable. After 55 minutes of running (without liquid atomization) the steady state for air temperatures in the upper part of the chamber (thermocouples  $T_1$  to  $T_4$ ) was not yet reached. Temperature of inlet air was then increased to 180°C, and after more than one hour air temperatures inside the chamber were stable at about 145°C. This put in evidence the long initial time to heat up the pilot spray dryer due to thermal inertia and possible heat losses.

#### 1.1.2. Determination of heat losses

In order to calculate heat losses due to exchanges between hot air inside the chamber and surrounding ambient air through the chamber walls, trials without liquid atomization were performed for two inlet air temperatures  $T_{IN}$  that will be used in spray drying trials, 144°C and 200°C.

Measured air temperatures inside the chamber at steady state are shown in Fig. 3.1.2. Temperatures inside the chamber were 30 to 40°C lower than inlet air temperature  $T_{IN}$ . As no liquid was dried, this temperature difference should be due to heat losses by walls.

The ambient air had a low water content  $Y_{IN}$  of  $\sim 0.005$  kg water.kg<sup>-1</sup> dry air, so that the water vapour enthalpy in air may be neglected. Assuming that air specific heat  $C_{P,air}$  is constant, the heat losses and the heat transfer coefficient through the walls can be calculated as:

$$\dot{Q}_{losses} = \dot{m}_{air} \cdot C_{P,air} \cdot (T_{IN} - T_{OUT}) \quad \text{eq. 3.1.1}$$

$$\dot{Q}_{losses} = h \cdot S \cdot (T_{wall} - T_{amb}) \Rightarrow h = \frac{\dot{Q}_{losses}}{S \cdot (T_{wall} - T_{amb})} \quad \text{eq. 3.1.2}$$

S surface of dryer chamber (3.37m<sup>2</sup>).  $T_{wall}$  internal wall temperature in chamber (°C)

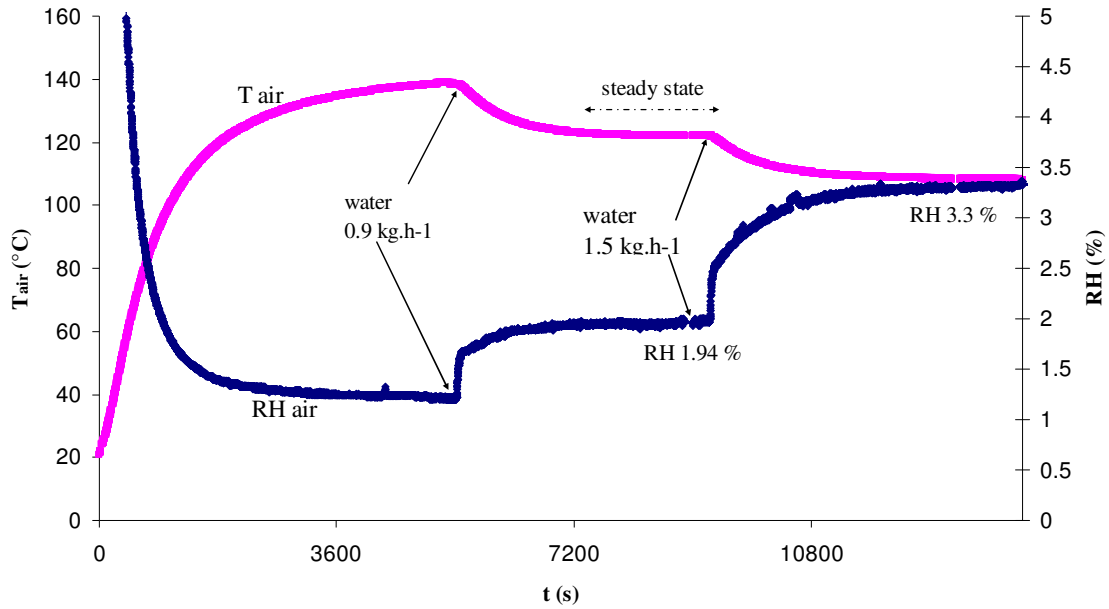


**Figure 3.1.3.** Time necessary to reach steady state from air temperature and relative humidity measurements at point A during spray drying of water when changing the sprayed liquid flow rate: 0.9 and 1.5 kg.h<sup>-1</sup> of water ( $T_{IN}$  180 °C, air flow rate 110 kg.h<sup>-1</sup>).

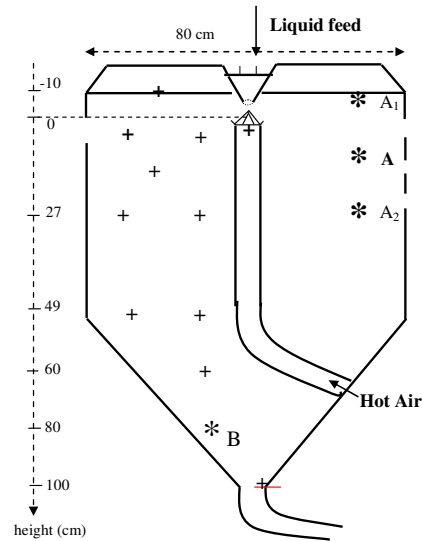


**Figure 3.1.4.** Position of K-type thermocouples (+) and positions for air relative humidity measurements (\*).

From the trials performed, the heat transfer coefficient through the walls  $h$  was calculated as  $3 \text{ W.m}^{-2}.\text{K}^{-1}$  (Table 3.1.1).

## 1.2. Water spray drying

### 1.2.1. Time to reach steady state inside the chamber

Water spray drying was performed in order to evaluate the time necessary to reach stable air temperatures and relative humidity inside the chamber.

Drying was performed at  $144^\circ\text{C}$ , and water flow rate was increased from  $0.9 \text{ kg.h}^{-1}$  ( $15 \text{ ml.min}^{-1}$ ) to  $1.5 \text{ kg.h}^{-1}$  ( $25 \text{ ml.min}^{-1}$ ). Measured air temperatures and relative humidity in the upper part of the chamber are shown on Figure 3.1.3.

More than 30 minutes were necessary to reach steady state when changing liquid flow rate.

From these results we decided the usual running up of a spray drying trial: air heating of the chamber for two hours; spraying of water during one hour before measurements and/or spraying the solution to dry; and intermediate spray of water during 30 minutes when changing the operating conditions.

### 1.2.2. Positions for air properties measurements

Trials with an inlet air temperature  $T_{\text{IN}}$  of  $150^\circ\text{C}$  were performed for different water flow rates  $\dot{m}_w$  of 1.08, 2.16 and  $3.24 \text{ kg.h}^{-1}$  in order to verify the feasibility of air properties measurements and to choose the positions for probes (Fig. 3.1.4).

Up to 12 thermocouples were placed inside the chamber to measure air temperatures. In the upper cylindrical part of the chamber, two thermocouples were placed on the same radius to measure possible differences in radial temperatures.

From temperature measurements during water spray drying, the chamber could be divided in two zones (Fig. 3.1.5). A first zone was in the upper part of the chamber surrounding the atomizer, where a high temperature decrease ( $\Delta T = 50^\circ\text{C}$  to  $100^\circ\text{C}$ ) was observed (*Zone I*). A second zone was represented by the rest of the chamber, with low temperature decrease ( $\Delta T = 4$  to  $5^\circ\text{C}$ ) from top to bottom (*Zone II*). This is in agreement with observations made by several authors (King et al., 1984; Zbicinski et al., 2002; Frydman, 1998).

No radial difference in air temperatures was observed, so that one thermocouple for each different height should be sufficient for further trials.

Air relative humidities RH (capacitive hygrometer) were measured at several points (A,  $A_1$ ,  $A_2$ , B). Values measured at points A,  $A_1$  and  $A_2$  (*top of Zone II*) were similar, so that the air water content in these three points was the same (similar temperatures). At point B higher RH were measured corresponding to higher air water content (Fig. 3.1.5).

For further spray drying trials we chose the two positions A and B to perform RH measurements. Position A was chosen as representative of the upper part of the chamber around the atomizer (limit of *Zone I*), and position B was in the bottom of the chamber, representative of the limit of *Zone II* and of air leaving the dryer chamber. During spray drying, the thermohygrometer was moved from position A to B once the steady state was reached. Response time was evaluated, and it took up to 10 minutes to measure a stable value of air RH when moving the probe.

Part III – Results and discussion

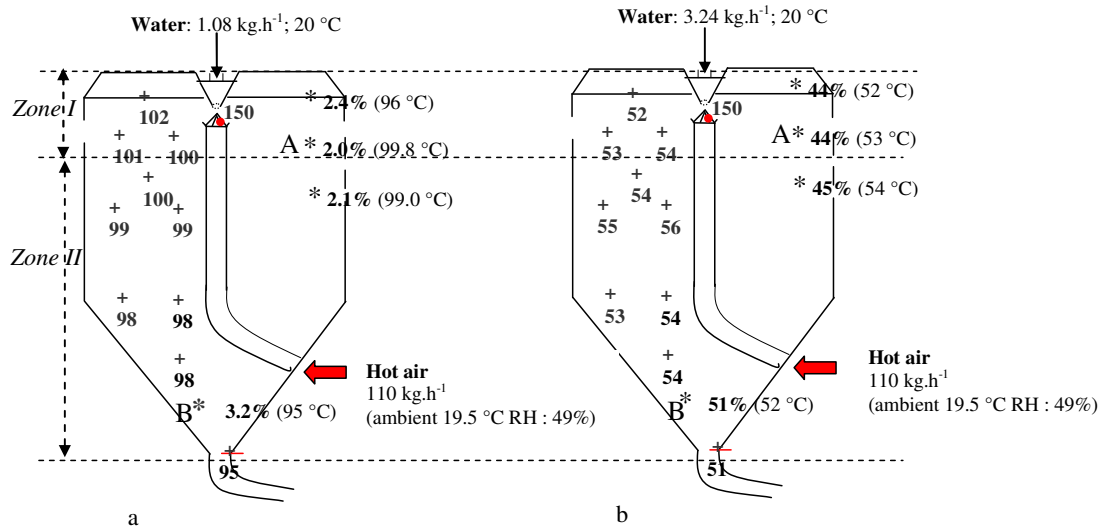


**Figure 3.1.5.** Air temperature and relative humidity at steady state during spray drying of water ( $T_{IN}$  150°C, air flow rate 110 kg.h<sup>-1</sup>; water flow rate 1.08 kg.h<sup>-1</sup> (a) and 3.24 kg.h<sup>-1</sup> (b)).

**Table 3.1.2.** Water spray drying: measured air temperatures, relative humidity and water content at point A and B at steady state.

		Water									
$T_{IN}$ (°C)		200					174	144			
$\dot{m}_{air}$ (kg.h <sup>-1</sup> )		110					80	110	110		
$v_{wheel}$ (rpm x 10 <sup>3</sup> )		22.5	25			30	25	25	25		
$\dot{m}_{liquid}$ (kg.h <sup>-1</sup> )		3.24	1.08	2.16	3.24	2.16	2.16	2.16	1.08	2.16	3.24
$T_{air}$ (°C)	A	110	124	110	85	110	98	91	92	70	52
	B	104	117	104	81	104	92	86	88	68	50
	OUT	104	117	104	81	104	92	86	88	67	50
RH air (%)	IN	0.1	0.1	0.1	0.1	0.1	0.1	0.2	0.4	0.4	0.4
	A	3.6	1.1	3.5	12.9	3.7	6.7	7.3	4.0	16.9	58.9
$Y_{air}$ (g water/kg dry air)	B	4.1	1.2	4.1	13.7	4.1	7.7	8.6	4.5	17.6	61.1
	IN	12	10	10	11	12	12	10	10	10	11
$Y_{air}$ (g water/kg dry air)	A	30	29	30	41	30	32	31	20	30	41
	B	30	19	30	41	30	32	31	20	30	41

### 1.2.3. Choice of operating parameters

Water drying trials were used to verify the feasibility of air measurements in chosen conditions and to choose the operating parameters that will be tested for solution drying. Measured air properties (T, RH) will be also used to compare drying behavior of water with maltodextrin solutions.

Process conditions should allow getting dry powders from solutions drying, in closed relation with air temperature and relative humidity variations between inlet and outlet. Tested parameters and measured air temperatures and relative humidity at points A and B are reported on Table 3.1.2.

Water flow rate  $\dot{m}_w$  was limited by the evaporative capacity of the spray dryer, thus it should be lower than  $4 \text{ kg}\cdot\text{h}^{-1}$ . We chose a maximum of  $3.24 \text{ kg}\cdot\text{h}^{-1}$ , considering that increasing the water flow rate could lead to very low values of exit air temperature  $T_{\text{OUT}}$  and high relative humidity RH, and so to possible sticking problems when drying a product solution due to a final powder with high water content.

The minimal flow rate of  $1.08 \text{ kg}\cdot\text{h}^{-1}$  was chosen considering that a lower flow rate could lead to a too low powder flow rate when drying product solutions.

According to the chosen liquid flow rates, a minimal inlet air temperature  $T_{\text{IN}}$  of  $144^\circ\text{C}$  was used so that drying could be completed inside the chamber. For the highest water flow rate of  $3.24 \text{ kg}\cdot\text{h}^{-1}$ , a high air relative humidity of 61% and low air temperature of  $50^\circ\text{C}$  were measured in the bottom of the chamber. We considered these conditions as a limit for drying of product solutions. An inlet air temperature  $T_{\text{IN}}$  of  $200^\circ\text{C}$  led for any tested conditions to low relative humidities inside the chamber (inferior to 14% for the highest water flow rate, and inferior to 5% for most of the tested parameters), so that drying of product solutions should be easy. For this reason, we chose  $200^\circ\text{C}$  as maximal inlet air temperature.

Air flow rate  $\dot{m}_{\text{air}}$  was fixed by the fan frequency, which could be varied from 25 to 45 Hz. Most of trials were performed with the maximal fan frequency (45 Hz) leading to an air flow rate  $\dot{m}_{\text{air}} = 110 \text{ kg}\cdot\text{h}^{-1}$ . In that case, for a liquid flow rate of  $2.16 \text{ kg}\cdot\text{h}^{-1}$ , the air relative humidity at point B varied from 17.6 ( $144^\circ\text{C}$ ) to 8.6 ( $174^\circ\text{C}$ ) and 4.1 ( $200^\circ\text{C}$ ). For a lower air flow rate  $80 \text{ kg}\cdot\text{h}^{-1}$  (35 Hz), it was 7.7 at  $200^\circ\text{C}$ . For low inlet air temperature  $T_{\text{IN}}$ , a low air flow rate might lead to insufficient drying at the exit of chamber.

Finally, the rotary wheel velocity  $v_{\text{wheel}}$  was varied by changing the compressed air pressure from 6 to 5 and 4 bar (30000, 25000 and 22500 rpm). This should affect the initial droplet size and thus the exchange surface with air and the final powder size.

The effect of process parameters on drying behavior will be discussed in chapter 2, together with maltodextrin solution drying.

### 1.2.4. Mass and heat balances on drying air

From measured air temperature T and relative humidity RH inside the chamber, air water content Y at different positions was determined (Mollier diagram). And it was used to calculate the evaporated water flow rate at each position from a mass balance on water in air between the entrance of the dryer and any point (\*) inside the chamber:

$$\dot{m}_{\text{ew}} = \dot{m}_{\text{air}} \cdot (Y^* - Y_{\text{IN}}) \quad \text{eq. 3.1.3}$$

**Table 3.1.3.** Calculation of heat losses  $\dot{Q}_{\text{losses}}$  and global heat transfer coefficient  $h$  with water atomization. (air  $T_{\text{IN}}$  144, 200°C,  $\dot{m}_{\text{air}}$  110 kg.h<sup>-1</sup>,  $T_{\text{amb}}$  = 18°C; S: 3.37m<sup>2</sup>,  $C_{p,\text{air}}$  = cste = 1000 J.kg<sup>-1</sup>;  $\Delta H_v$  (40°C) = cste = 2400.10<sup>3</sup> J.kg<sup>-1</sup>; all water evaporated)

$T_{\text{IN}}$ (°C)	$\dot{m}_w$ (kg.h <sup>-1</sup> )	$T_{\text{wall}}$ (°C)	$T_{\text{OUT}}$ (°C)	$\dot{Q}_{\text{losses}}$ (W)	$h$ (W.m <sup>-2</sup> .K <sup>-1</sup> )
144	1.08	90	88	991	4.08
144	2.16	70	67	913	5.21
144	3.24	52	50	712	6.22
200	1.08	124	117	1816	4.82
200	2.16	108	104	1493	5.09
200	3.24	85	81	1476	6.54

### Part III – Results and discussion

For the tested conditions (Table 3.1.2) during water spray drying, air water content did not vary from position A to B, and from the mass balance we could calculate that 100% of water was already evaporated at point A in the upper part of the chamber. Drying was then completed, and further temperature decrease from top to bottom was due to heat losses.

Assuming that the temperature decrease for air between the chamber inlet and the exit corresponds to water evaporation and heat losses, the heat balance on air allows calculating heat losses:

$$\dot{Q}_{\text{losses}} = \dot{m}_{\text{air}} \cdot C_{p,\text{air}} \cdot (T_{\text{IN}} - T_{\text{OUT}}) - \Delta H_v \cdot \dot{m}_{\text{ew}} \quad \text{eq. 3.1.4}$$

Water evaporation was assumed to occur at the air wet bulb temperature  $T_{\text{wb}}$  (in the range 40 - 45°C for air temperatures between 140 and 200°C). And air specific heat  $C_{p,\text{air}}$  and water latent heat of vaporization  $\Delta H_v(T_{\text{wb}})$  can be considered as constant.

Knowing that all the sprayed water was evaporated inside the chamber:

$$\dot{m}_{\text{ew}} = \dot{m}_{\text{air}} \cdot (Y_{\text{OUT}} - Y_{\text{IN}}) = \dot{m}_w \quad \text{eq. 3.1.5}$$

As we could expect, heat losses lowered when increasing the water flow rate because this led to lower air temperature inside the chamber and thus to a lower temperature difference between ambient air and air inside the chamber. And, for the same water flow rate, heat losses were higher for higher air inlet temperature, leading to higher temperature difference between chamber and ambient (Table 3.1.3)

However, values of the global heat exchange coefficient  $h$  obtained (eq. 3.1.2) from the heat losses calculated during water spray drying (between 4 and 6.54  $\text{W}\cdot\text{m}^{-2}\cdot\text{K}^{-1}$ ) were not in agreement with the value of 3  $\text{W}\cdot\text{m}^{-2}\cdot\text{K}^{-1}$  determined from measurements on air without atomization. And, whilst  $h$  was expected to be almost insensitive to the atomized liquid flow rate the values obtained increased with the liquid flow rate. This could suggest that a part of the air temperature decrease was due to some secondary ambient air entrance (remember that dryer is under depression), resulting in air mixing leading to lower temperatures inside the chamber. This part of temperature decrease would be independent from the liquid flow rate.

However a secondary ambient air entrance would not modify mass balance on air if the total air flow rate  $\dot{m}_{\text{air}}$  taken into account is effectively the sum of both hot inlet air (ambient air heated up to  $T_{\text{IN}}$ ) and secondary ambient air flow rates, as both airs have the same water content  $Y_{\text{IN}}$ . This requires to measure the total air flow rate at the exit of the chamber.

As heat losses, a secondary ambient air entrance would result in a non-isenthalpic drying.

#### 1.2.5. Estimation of possible secondary ambient air flow rate

In order to confirm the hypothesis of secondary ambient air entrance and to quantify its flow rate, a theoretical value for  $h$  was estimated from the nature and thickness of the dryer chamber wall :



**Table 3.1.4.** Calculation of the secondary ambient air entrance flow rate  $\dot{m}_{AMBair}$  and of the air mixture temperature  $T_{mix}$  ( $T_{IN}$  144 and 200°C,  $\dot{m}_{air}$  110 kg.h<sup>-1</sup>,  $T_{amb}$  = 18°C,  $h$  =2 W.m<sup>-2</sup>.K<sup>-1</sup>).

$T_{IN}$ (°C)	$\dot{m}_w$ (kg.h <sup>-1</sup> )	$\dot{m}_{HOTair}$ (kg.h <sup>-1</sup> )	$\dot{m}_{AMBair}$ (kg.h <sup>-1</sup> )	% secondary air	$T_{mix}$ (°C)
144	0	98.03	11.97	10.88	130.29
144	1.08	97.29	12.71	11.55	129.45
144	2.16	96.55	13.45	12.22	128.60
144	3.24	95.81	14.19	12.90	127.75
200	0	94.43	15.57	14.16	174.23
200	1.08	93.18	16.82	15.29	172.17
200	2.16	94.88	15.12	13.75	174.98
200	3.24	95.10	14.90	13.54	175.35

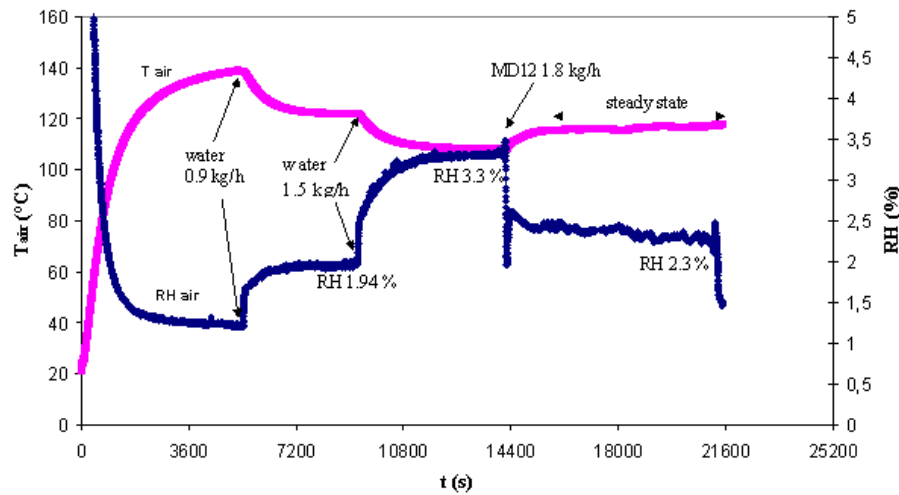
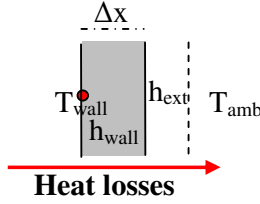


**Figure 3.1.6.** Comparison of air temperature and RH measured at point A for water and maltodextrin DE12 solution drying (liquid flow rates: 15 and 25 ml.min<sup>-1</sup> corresponding to 0.9 and 1.5 kg.h<sup>-1</sup> for water; 25 ml.min<sup>-1</sup> corresponding to 1.8 kg.h<sup>-1</sup> for maltodextrin solution ;  $T_{IN}$  180°C; air flow rate 110 kg.h<sup>-1</sup>).

Part III – Results and discussion



$$\frac{1}{h} = \frac{1}{h_{ext}} + \frac{1}{h_{wall}} = \frac{1}{h_{ext}} + \frac{\Delta x}{\lambda} \quad \text{eq. 3.1.6}$$

$\Delta x$  wall thickness (m);  $\lambda$  wall thermal conductivity ( $\text{W} \cdot \text{m}^{-1} \cdot \text{K}^{-1}$ );  $T_{wall} \sim T_{air}$  inside the chamber

Heat exchanges between ambient air and external wall are due to natural convection, for which a typical value is  $h_{ext} = 10 \text{ W} \cdot \text{m}^{-2} \cdot \text{K}^{-1}$ .

Thermal conductivity of chamber wall (inox + insulant) was assumed to be  $\sim 0.040 \text{ W} \cdot \text{m}^{-1} \cdot \text{K}^{-1}$  (data from Niro), and wall thickness  $\Delta x$  was about 1.8 cm so that  $h_{wall} = 2.2 \text{ W} \cdot \text{m}^{-2} \cdot \text{K}^{-1}$ .

The theoretical value obtained for  $h$  was about  $2 \text{ W} \cdot \text{m}^{-2} \cdot \text{K}^{-1}$ . This value is lower than the one calculated from air heat losses, confirming that the temperature decrease in the chamber is probably not only due to heat exchanges through the chamber walls.

In order to take into account a secondary air entrance, the heat balance on air (eq. 3.1.4) must be modified considering that:

$$\dot{m}_{air} = \dot{m}_{HOTair} + \dot{m}_{AMBair} = \text{total dry air flow rate} \quad \text{eq. 3.1.7}$$

$\dot{m}_{air}$  total dry air flow rate leaving the dryer ( $\text{kg} \cdot \text{s}^{-1}$ );  $\dot{m}_{HOTair}$  hot dry air flow rate, secondary ambient dry air flow rate ( $\text{kg} \cdot \text{s}^{-1}$ )

Assuming that  $T_{wall} = T_{OUT}$ , and that the quantity of water in inlet air can be neglected, the simplified heat balance on air between chamber inlet and exit at steady state becomes:

$$\dot{m}_{HOTair} C_{P,air} \cdot T_{IN} + \dot{m}_{AMBair} C_{P,air} \cdot T_{amb} = \dot{m}_{air} \cdot C_{P,air} \cdot T_{OUT} + \Delta H_v \cdot \dot{m}_{ew} + h \cdot S \cdot (T_{OUT} - T_{amb}) \quad \text{eq. 3.1.8}$$

from which

$$\dot{m}_{HOTair} = \frac{\dot{m}_{air} C_{P,air} \cdot (T_{OUT} - T_{amb}) + \Delta H_v \cdot \dot{m}_{ew} + h \cdot S \cdot (T_{OUT} - T_{amb})}{C_{P,air} \cdot (T_{IN} - T_{amb})} \quad \text{eq. 3.1.9}$$

Equations and 3.1.7 allow the calculation of the amount of hot and secondary air (Table 3.1.4). An average of 12-13% of total air flow rate appeared to be due to secondary air entrance. Assuming that this secondary ambient air enters in the chamber from the roof close to atomizer and is immediately mixed with hot air entering in the chamber, temperature of the mixture  $T_{mix}$  can be calculated as:

$$T_{mix} = \frac{\dot{m}_{HOTair}}{\dot{m}_{air}} T_{IN} + \frac{\dot{m}_{AMBair}}{\dot{m}_{air}} T_{amb} \quad \text{eq. 3.1.10}$$

This suggests that due to the secondary ambient air entrance, the temperature of the drying air entering in contact with sprayed drops could be  $T_{mix}$  instead of  $T_{IN}$ . The calculated  $T_{mix}$  without liquid atomization was in agreement with the temperature measured close to the atomizer between air disperser and rotary wheel (Fig. 3.1.2). When  $T_{IN}$  was  $144^\circ\text{C}$ , we measured  $132^\circ\text{C}$  and for  $T_{IN}$   $200^\circ\text{C}$  we measured  $182^\circ\text{C}$ .

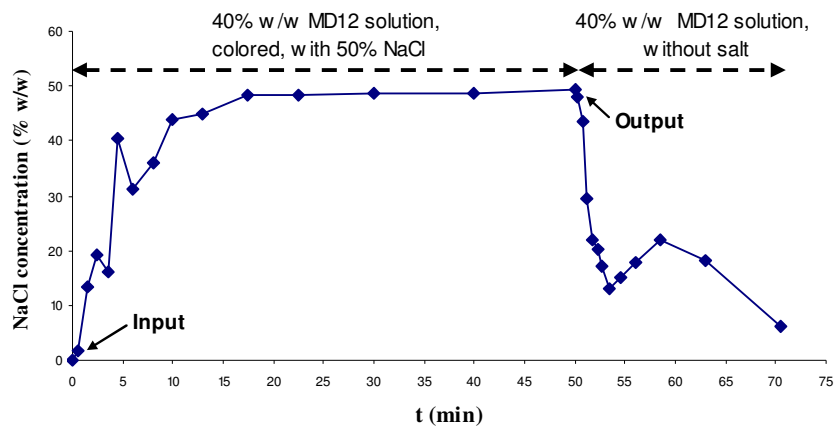


**Figure 3.1.7.** Evolution of salt concentration in collected powder as a function of time (Input step: 40% w/w MD12 solution containing 50% of NaCl in dry matter; Output step: 40% w/w MD12 aqueous solution without salt;  $T_{IN}$  200°C, air flow rate 110 kg.h<sup>-1</sup>, liquid flow rate 3.6 kg.h<sup>-1</sup>).

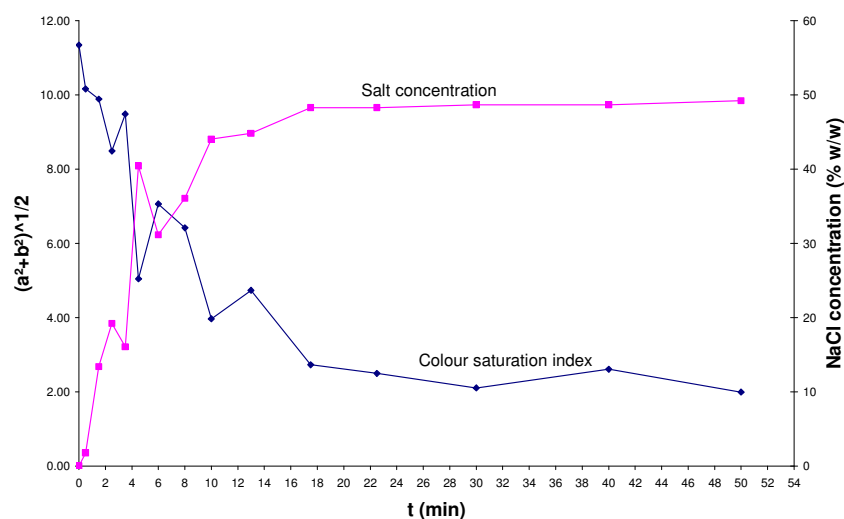


**Figure 3.1.8.** Evolution of salt concentration and of color saturation index in collected powder as a function of time during the input step (40% w/w MD12 solution containing 50% of NaCl in dry matter, colored with pink colouring;  $T_{IN}$  200°C, air flow rate 110 kg.h<sup>-1</sup>, liquid flow rate 3.6 kg.h<sup>-1</sup>).

However, it was not possible to put in evidence experimentally some secondary air entry inside the chamber. The lower air temperature measured close to atomizer could then also be due to some air recirculation inside the chamber. Air pattern was investigated by numerical simulation of the process (III.3).

### 1.3. Operating conditions for maltodextrin solutions drying

#### 1.3.1. Choice of maltodextrin solution flow rates

In order to compare water drying behavior to that of maltodextrin solutions, the feed flow rates had to be defined.

First trials were performed with the same total volumetric flow rate ( $25 \text{ ml}\cdot\text{min}^{-1}$ ) for water and maltodextrin DE12 40% w/w solution (corresponding to  $1.5 \text{ kg}\cdot\text{h}^{-1}$  for water and  $1.8 \text{ kg}\cdot\text{h}^{-1}$  for MD12 solutions). When switching from water drying to MD12 solution drying, air temperature increased and relative humidity decreased (Fig. 3.1.6). This could be due to a different drying behavior between free water and maltodextrin solutions, and to the fact that for the same volumetric flow rate the amount of water to evaporate was different:  $1.5 \text{ kg}\cdot\text{h}^{-1}$  in the case of water drying, and only  $1.08 \text{ kg}\cdot\text{h}^{-1}$  in  $1.8 \text{ kg}\cdot\text{h}^{-1}$  of 40% w/w MD12 solution.

Therefore, we decided for further trials to work with flow rates for MD solutions and water corresponding to the same amount of water to evaporate. This led to three solution flow rates of  $1.8$ ,  $3.6$  and  $5.4 \text{ kg}\cdot\text{h}^{-1}$ , corresponding to the three chosen water flow rates of  $1.08$ ,  $2.16$  and  $3.24 \text{ kg}\cdot\text{h}^{-1}$ .

#### 1.3.2. Residence time distribution inside Niro Minor

Residence time distribution of particles in the dryer was estimated to determine time necessary between two drying conditions to collect a representative powder sample and to verify if powder recirculation could occur inside the spray dryer chamber.

Particles residence time distribution (RTD) was evaluated by studying the response curve to a step input and output of solution (40% w/w) containing 50% maltodextrin and 50% NaCl as tracer. Powder samples were collected regularly along the trial at the powder outlet (after cyclone). Conductivity measurements on collected samples allowed evaluating salt concentration evolution with time (Fig. 3.1.7). For the output step, also colour of collected sample was measured. The two measurements were in agreement (Fig. 3.1.8).

The concentration of salt tracer  $C(t)$  at the outlet was normalized to the initial tracer concentration  $C_0$  to obtain the non-dimensional response  $F(t)$  (varying from 0 to 1) (Fig. 3.1.9):

$$F(t) = \frac{C(t)}{C_0}$$

Some observations could be done:

- The shape of the  $F(t) = f(t)$  curve was similar for both input and output steps. After a fast increase a decrease in salt concentration was observed after about 6-8 minutes before increasing again more slowly. This decrease could be due to detachment of powder stuck on walls, to powder recirculations inside the chamber or in the cyclone, or to some experimental error.
- 50% of the sprayed solution salt concentration  $C_0$  was reached after 2-3 minutes of running. This average powder residence time can be compared to the average air residence time calculated assuming plug flow inside the chamber, in the exit pipes and in the cyclone:

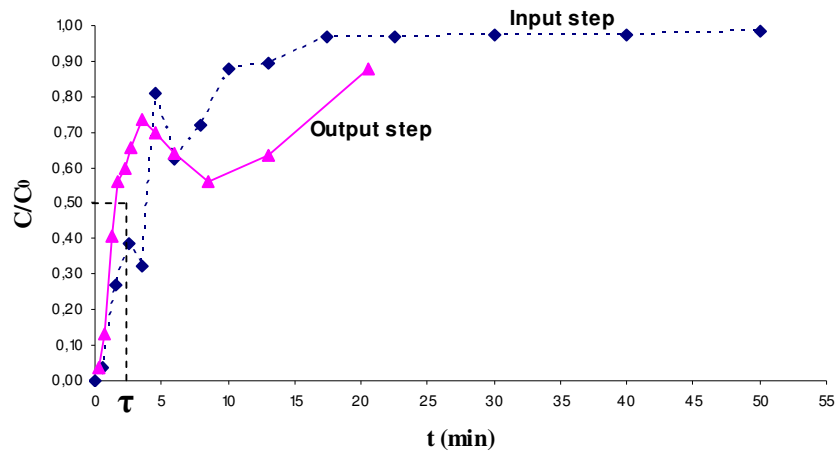


**Figure 3.1.9.** RTD response curve to input and output steps; (Input step: 40% w/w MD12 solution containing 50% of NaCl in dry matter; Output step: 40% w/w MD12 solution without salt;  $T_{IN}$  200°C, air flow rate 110  $\text{kg}\cdot\text{h}^{-1}$ , liquid flow rate 3.6  $\text{kg}\cdot\text{h}^{-1}$ ).

$$\tau_{\text{air}} = \frac{V_{\text{chamber}} + V_{\text{pipes}} + V_{\text{cyclone}}}{\dot{V}_{\text{air}}} = \frac{0.49 \text{ m}^3}{105 \text{ m}^3 \cdot \text{h}^{-1}} = 16.8\text{s} \quad \text{eq. 3.1.11}$$

$\dot{V}_{\text{air}}$  air volumetric flow rate (exit air T: 60°C; mass flow rate: 110 kg.h<sup>-1</sup>;  $\rho_{\text{air}}(60^\circ\text{C})$ : 1.05 kg.m<sup>-3</sup>)

Mean particles residence time was superior to average air residence time, as observed by Kieviet and Kerkhof (1995). This could suggest either that air flow pattern was not plug flow inside the chamber (cf. III.3) or that powder particles did not follow air during drying because of their inertia; some powder recirculations are likely to occur. Also possible collisions with chamber walls could increase the measured particle residence time.

- More than 20 minutes were necessary to reach the sprayed solution salt concentration ( $C_0$ ) in collected powder. This means that when drying parameters are changed during a trial, at least 20 minutes are necessary to collect a powder representative of the new drying conditions. For this reason, in further trials, when operating conditions must be changed, samples will be collected after 30 minutes.

A possible modelling of residence time distribution is reported in Annex I, noting that more experiments are necessary for a complete interpretation.

## Conclusion

Measurements on air temperature inside the Niro Minor pilot without liquid atomization put in evidence the long time (> 1h) necessary to heat up the chamber and the presence of heat losses, due to exchange between hot air and ambient air through chamber walls.

Water spray drying trials confirmed that drying was not isenthalpic. The heat and mass balance on water in air between entrance and exit put in evidence that the measured temperature decrease was due not only to losses by walls but probably also to some secondary ambient air entrance. However, mass balance on air to estimate the evaporated water flow rate may be used with total air flow rate measured at the exit of the equipment.

Air temperature and relative humidity can be measured inside the chamber during water or solutions spray drying. With water drying, we could determine that more than 40 minutes were necessary to reach stable values (steady state) when starting atomization. At steady state, temperatures evolved along chamber height, with no radial variations. Two positions were chosen for air relative humidity measurements: one (A) in the upper part of the chamber (limit of Zone I) and one (B) in the conical part representative of air leaving the dryer chamber.

Process operating parameters for liquid solution drying were chosen taking into account the dryer evaporative capacity and the expected effect on drying behaviour. In order to compare drying behaviour of water with drying behaviour of maltodextrin solutions, we chose to compare trials for which the water to evaporate flow rate was the same.

Injection of a coloured saline solution permitted to calculate a particle average residence time of 2 minutes, and indicated that more than 20 minutes have to be waited at steady state before collecting the powder representative of one drying condition. The wide residence time distribution may suggest that some particles are recirculating inside the chamber and/or stay, at some moment, stuck on walls.

Part III – Results and discussion

**Table 3.2.1.** Effect of liquid flow rate and rotary atomizer velocity on calculated Sauter diameter of water and maltodextrin DE12 (40 % w/w) drops ( $A_{TOT}$ : total spray exchange surface).

Liquid feed	Liquid flow rate		$\dot{m}_l$ ( $\dot{m}_w$ ) (kg.h <sup>-1</sup> )	$v_{wheel}$ (rpm)	$d_{3,2}$ ( $\mu\text{m}$ )	$A_{TOT}$ (m <sup>2</sup> .s <sup>-1</sup> )
	(ml.min <sup>-1</sup> )	(L.h <sup>-1</sup> )				
Water	36	2.16	2.16	25000	14	0.248
MD12	50	3	3.6 (2.16)	25000	34	0.147
Water	36	2.16	2.16	<b>30000</b>	13	0.277
MD12	50	3	3.6 (2.16)	<b>30000</b>	30	0.166
MD12	25	1.5	<b>1.8 (1.08)</b>	25000	30	0.084
MD12	50	3	<b>3.6 (2.16)</b>	25000	34	0.147
MD12	75	4.5	<b>5.4 (3.24)</b>	25000	37	0.204
Water	18	1.08	1.08	25000	13	0.143
Water	36	2.16	2.16	25000	14	0.248
Water	54	3.24	3.24	25000	16	0.344

**Table 3.2.2.** Example of temperature and water vapour pressure differences ( $\Delta T$ ,  $\Delta P$ ) between air and drop surface of water and maltodextrin solution at the beginning of drying (Period I) and at the beginning of the falling rate drying period for maltodextrin (Period II) ( $T_{IN}$  144°C, 2.16 kg.h<sup>-1</sup> of water and 3.6 kg.h<sup>-1</sup> MD).

Period	Air properties				Drop properties				$\Delta P$ (mbar)	$\Delta T$ (°C)
	T (°C)	RH <sub>air</sub> (%)	$P_w^{sat}(T)$ (mbar)	$P_v^{air}(T)$ (mbar)	$T_s$ (°C)	$a_w$	$P_w^{sat}(T_s)$ (mbar)	$P_v^{drop}(T_s)$ (mbar)		
I (t=0)	144	0.1	430	4.3	40	1	73.8	73.8	69.5	104
II (water)	68	14	312	44	40	1	73.8	73.8	29.8	30
II (MD)	75	14	350	44	50	0.5	120	60.0	60.0	20

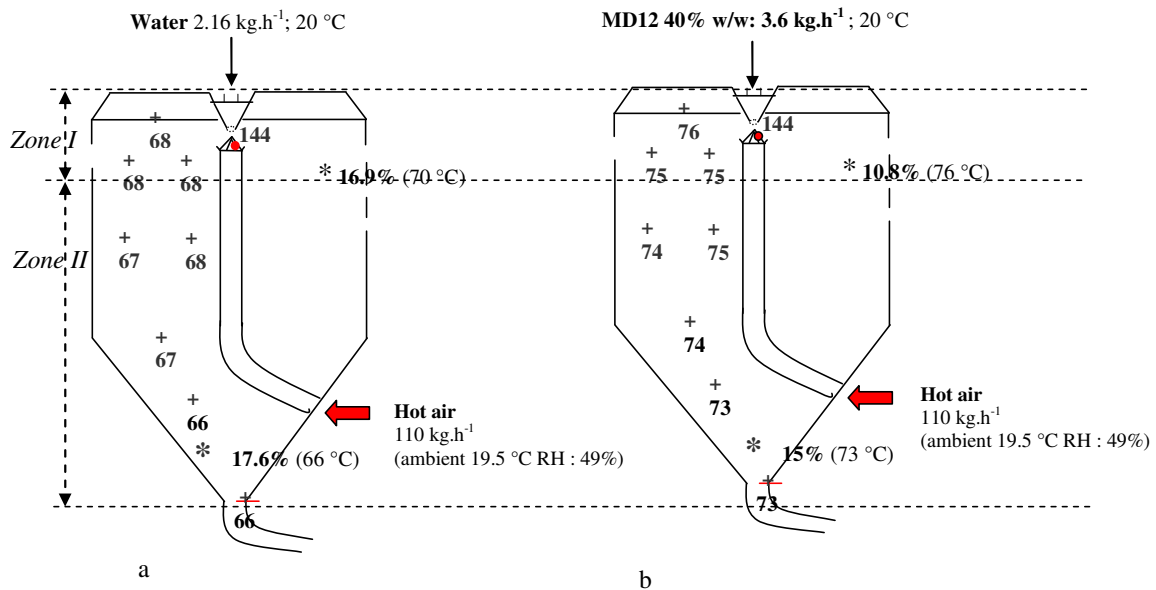


**Figure 3.2.1.** Air temperature and relative humidity measured at steady state for (a) water and (b) solution of maltodextrin DE12 with the same amount of water to evaporate ( $T_{IN}$ : 144°C, air flow rate: 110 kg.h<sup>-1</sup>, liquid flow rate: 2.16 kg.h<sup>-1</sup> (a) and 3.6 kg.h<sup>-1</sup> (b)).

## 2. Drying behavior and stickiness development for maltodextrin solutions

The objective was to link the evolution of air properties (temperature, relative humidity) inside the dryer chamber to the drying behavior of water and maltodextrin DE12 and DE21 aqueous solutions that will be compared.

For maltodextrin solutions, the effect of several process parameters on the evolution of water content of drying drops and on final powder properties (water content, water activity, size) was investigated: inlet air temperature, flow rate, liquid flow rate and rotary atomizer speed.

Maltodextrins chosen as model products are able to exhibit a sticky behavior along drying. From knowledge on the evolution of product properties and from glass transition temperatures, possible conditions and positions for which particles could be sticky inside the chamber were determined.

### 2.1. Drying of maltodextrin DE12 solutions and comparison with water

To compare drying behavior for maltodextrin solution and water, we choose to operate with the same flow rate of water to evaporate which means different volumetric liquid flow rates in relation with the density of the liquid sprayed ( $1200 \text{ kg.m}^{-3}$  to  $1000 \text{ kg.m}^{-3}$  for water) (Table 3.2.1).

#### 2.1.1. Considerations on drying behavior of water and of maltodextrin solutions

Compared to water, the maltodextrin solutions have higher viscosity and surface tension, and the total sprayed flow rate was higher (to have the same amount of water to evaporate). That leads to a higher calculated Sauter diameter (eq. 1.4) of maltodextrin drops, for the same wheel velocity (Table 3.2.1).

Assuming no size distribution in the spray, total exchange surface of the spray can be calculated as:

$$A_{\text{TOT}} = N_{\text{drops}} \cdot A_{\text{drop}} = \frac{V_{\text{TOT}}}{V_{\text{drop}}} A_{\text{drop}} = \frac{6 \dot{m}_1}{\rho_1 (\pi d_{\text{drop}}^3)} \cdot \pi d_{\text{drop}}^2 = \frac{6 \dot{m}_1}{\rho_1 d_{\text{drop}}} \quad \text{eq. 3.2.1}$$

Then, with drops diameter between 30 and 37  $\mu\text{m}$  compared to 13 and 16  $\mu\text{m}$  for water (wheel velocity 25000 rpm), with the same water flow rate, the total exchange surface for maltodextrin spray should be 60% of the exchange surface in a water spray (Table 3.2.1). This should lead to an initial evaporation rate (atomizer exit) lower when drying maltodextrin solutions.

Furthermore, water activity of water drops is equal to 1 during the whole drying process, and  $P_v(T_s) = P_w^{\text{sat}}(T_s)$ . The drops surface temperature  $T_s$  is equal to the air wet bulb temperature  $T_{\text{wb}}$  varying in the range 40 to 45°C for air inlet temperature varying between 140 and 200°C. For maltodextrin drops, surface water activity is equal to 1 only in the first period of drying (free water). But quickly the drop surface is no more saturated, and drying is controlled by water diffusion from particle core to surface (2<sup>nd</sup> period of drying) with a surface water activity inferior to 1 and a reduced vapour pressure at the drop surface:

$$P_v^{\text{drop}}(T_s) = a_w P_w^{\text{sat}}(T_s) \quad \text{and} \quad P_v^{\text{air}} = \text{RH} \cdot P_w^{\text{sat}}(T) \quad \text{eq. 3.2.2}$$



**Table 3.2.3.** Water spray drying: air temperatures, relative humidity and water content at point A and B at steady state.

		Water									
$T_{IN}$ (°C)		200						174	144		
$\dot{m}_{air}$ (kg.h <sup>-1</sup> )		110					80	110	110		
$v_{wheel}$ (rpm x 10 <sup>3</sup> )		22.5	25			30	25	25	25		
$\dot{m}_{liquid}$ (kg.h <sup>-1</sup> )		3.24	1.08	2.16	3.24	2.16	2.16	2.16	1.08	2.16	3.24
$T_{air}$ (°C)	A	110	124	110	85	110	98	91	92	70	52
	B	104	117	104	81	104	92	86	88	68	50
	OUT	104	117	104	81	104	92	86	88	67	50
RH air (%)	IN	0.1	0.1	0.1	0.1	0.1	0.1	0.2	0.4	0.4	0.4
	A	3.6	1.1	3.5	12.9	3.7	6.7	7.3	4.0	16.9	58.9
	B	4.1	1.2	4.1	13.7	4.1	7.7	8.6	4.5	17.6	61.1
$Y_{air}$ (g water/kg dry air)	IN	12	10	10	11	12	12	10	10	10	11
	A	30	29	30	41	30	32	31	20	30	41
	B	30	19	30	41	30	32	31	20	30	41

**Table 3.2.4.** Spray drying of 40% w/w maltodextrin DE12 solutions: air temperatures, relative humidity and water content at point A and B at steady state; final powder properties and calculated water content in A and B.

Maltodextrin		DE12									
$T_{IN}$ (°C)		200						174	144		
$\dot{m}_{air}$ (kg.h <sup>-1</sup> )		110					80	110	110		
$v_{wheel}$ (rpm x 10 <sup>3</sup> )		22.5	25			30	25	25	25		
$\dot{m}_{liquid}$ (kg.h <sup>-1</sup> )		3.6	1.8	3.6	5.4	3.6	3.6	<b>3.6</b>	1.8	<b>3.6</b>	5.4
$T_{air}$ (°C)	A	118	139	117	95	116	103	<b>101</b>	94	<b>76</b>	58
	B	110	130	110	91	110	97	<b>97</b>	90	<b>72</b>	55
	OUT	110	130	110	91	110	97	<b>97</b>	90	<b>72</b>	55
RH air (%)	IN	<0.5	<0.5	<0.5	<0.5	<0.5	<0.5	<b>&lt;0.5</b>	<0.5	<0.5	<0.5
	A	2.3	0.9	2.8	6.7	2.4	4.9	<b>6.1</b>	3.3	<b>10.8</b>	33.5
	B	3.0	1.1	3.1	8.2	3.3	5.7	<b>7.1</b>	4.3	<b>13.2</b>	39.0
$Y_{air}$ (g water/kg dry air)	IN	12	10	10	11	12	12	<b>10</b>	10	<b>10</b>	11
	A	26	19	29	37	27	32	<b>27</b>	17	<b>28</b>	38
	B	26	19	29	39	27	32	<b>28</b>	19.5	<b>29</b>	40
X A calculated		//	//	//	//	//	//	//	10.0	<b>11.5</b>	12.5
X B calculated		//	//	//	//	//	//	//	4.8	<b>4.8</b>	8.0
X (g water/100g solids)		1.6	1.2	1.6	3.4	1.8	2.7	<b>3.6</b>	2.9	<b>4.8</b>	8.8
$a_w$		0.05	0.05	0.05	0.12	0.05	0.10	<b>0.13</b>	0.10	<b>0.18</b>	0.39
$d_{50}$ (µm)		25	26	26	30	21	25	<b>24</b>	22	<b>23</b>	26
$d_{3,2}$ (µm)		20	17	20	20	16	19	<b>17</b>	16	<b>16</b>	16
$d_{4,3}$ (µm)		36	28	36	43	28	35	<b>28</b>	32	<b>28</b>	38
$d_{0,1}$ (µm)		13	12	13	12	11	12	<b>12</b>	10	<b>11</b>	11
$d_{0,9}$ (µm)		52	49	53	50	43	53	<b>50</b>	50	<b>46</b>	62

The surface temperature will increase, reducing temperature difference between air and drop. The driving force (water vapor pressure difference) for mass transfer is then lower than when drying water. Example is given in Table 3.2.2 for  $a_w$  decreasing to 0.5. That leads to lower evaporation rates when drying maltodextrin solutions and so to higher air temperatures and lower air water content inside the chamber compared to water drying.

These considerations were verified during experiments on water and maltodextrin DE12 solutions, using the following operating parameters: inlet air temperature  $T_{IN}$  144 – 174 – 200°C, air flow rate  $\dot{m}_{air}$  80 – 110 kg.h<sup>-1</sup>, rotary atomizer velocity  $v_{wheel}$  22500 – 25000 – 30000 rpm, liquid flow rate  $\dot{m}_l$  1.8 – 3.6 – 5.4 kg.h<sup>-1</sup> with 1.08 – 2.16 – 3.24 kg.h<sup>-1</sup> of water to evaporate.

The measured air temperatures (up to 12 points) and RH (points A and B) (Table 3.2.3, 3.2.4) gave cartographies at steady state. An example is given in Figure 3.2.1 for drying of water and maltodextrin DE12 solution at 144°C. Some observations can be made :

- For the same water flow rate to evaporate, temperatures inside the chamber when drying maltodextrin solutions were superior to temperatures measured during water drying; RH were lower, with a lower air water content Y (calculated from T and RH values) at any point of the chamber.
- A big decrease of air temperature was observed in the upper part of the chamber close to atomizer (Zone I). In this zone, temperature decrease varied from 50 to 100°C depending on process parameters. Below this zone just a slight temperature decrease (~4 to 7°C) was observed between point A and the exit of the chamber (point B).
- Air water content Y, increased strongly from inlet to point A, and then small (or no) variations were observed from A to B.

This means that most of drying occurred in the upper part of the chamber around the atomizer exit (Zone I). However, for maltodextrin, drying was not completed in all cases in Zone I, as it was for water drying.

### 2.1.2. Effect of process parameters on spray drying behavior of maltodextrin solutions

Measured air and product properties for the tested conditions are reported in Table 3.2.4. In the co-current spray dryer used, we assumed that drying particles follow the air flow pattern in the chamber and that the dry air flow rate is the total dry air flow rate measured at the exit.

Drying particles average water content  $X^*$  inside the chamber was then calculated from water balances on product and air, between entrance and any point (\*) inside the chamber.

The air water content  $Y^*$  was deduced from  $T_{air}$  and RH (Mollier diagramme) and the average water content  $X^*$  of the particles during drying was calculated as :

$$X^* = \frac{\dot{m}_w - \dot{m}_{ew}^*}{\dot{m}_s} = \frac{\dot{m}_w - (\dot{m}_{air} \cdot (Y^* - Y_{IN}))}{\dot{m}_s} \quad \text{eq. 3.2.3}$$

$X^*$  particle water content (g water.g<sup>-1</sup> total solids);  $\dot{m}_w$  water flow rate in liquid feed (kg.s<sup>-1</sup>);  $\dot{m}_{ew}^*$  amount of evaporated water at considered point (kg.s<sup>-1</sup>);  $\dot{m}_s$  solids flow rate in liquid feed (constant, kg.s<sup>-1</sup>)

Part III – Results and discussion

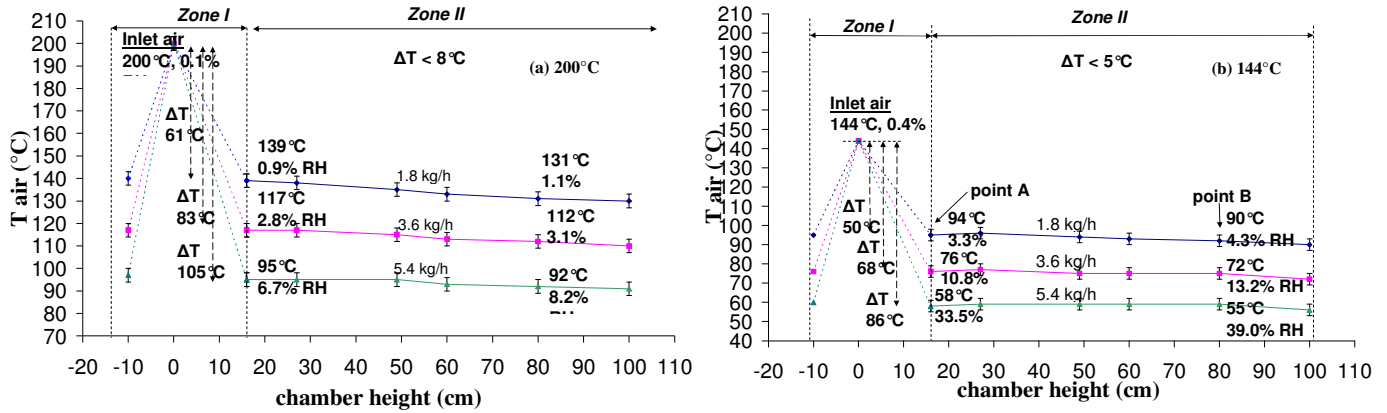


**Figure 3.2.2.** Effect of feed flow rate on measured air temperatures and relative humidities at steady state inside the NIRO Minor as a function of chamber height for maltodextrin DE12 solutions (40% w/w) ((a) T<sub>IN</sub> 200°C (b) T<sub>IN</sub>: 144°C ; air flow rate 110 kg.h<sup>-1</sup>; liquid flow rate 1.8 – 3.6 – 5.4 kg.h<sup>-1</sup>; rotary atomizer velocity: 25000 rpm).

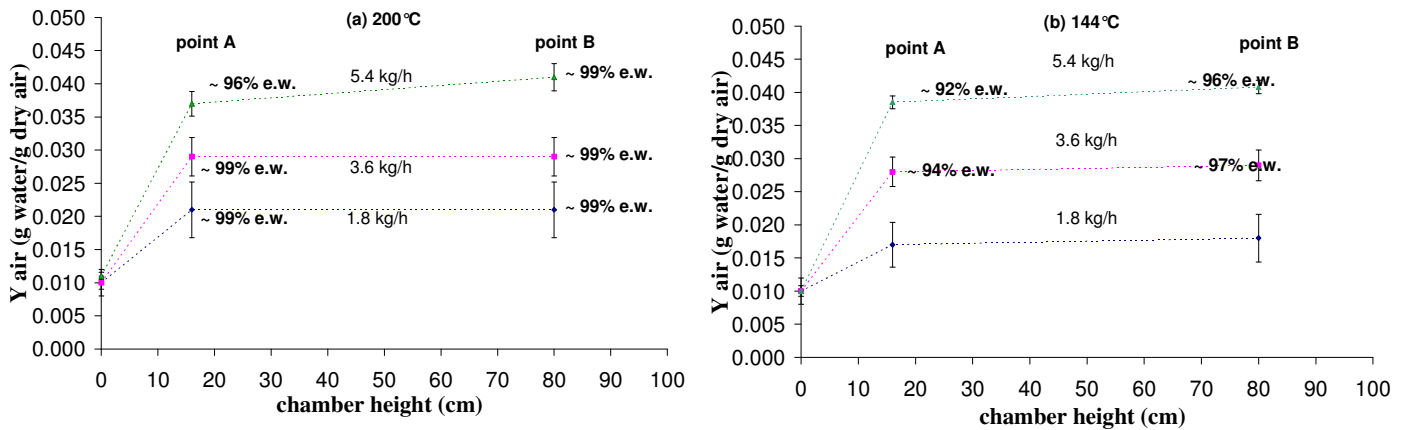


**Figure 3.2.3.** Effect of feed flow rate on air water content Y and percent of evaporated water at point A and B at steady state for solution of maltodextrin DE12 40% w/w. ((a) T<sub>IN</sub> 200 °C; (b) T<sub>IN</sub> 144 °C; air flow rate 110 kg.h<sup>-1</sup>; liquid flow rate 1.8 – 3.6 – 5.4 kg.h<sup>-1</sup>; rotary atomizer velocity: 25000 rpm).

### ***Effect of liquid flow rate***

When increasing the atomized liquid flow rate from 1.8 to 3.6 and 5.4 kg.h<sup>-1</sup>, lower air temperatures and higher air relative and absolute humidities  $Y$  were observed inside the chamber at any level for the same air inlet temperature (Fig.3.2.2 and Fig. 3.2.3).

Higher temperature decrease in *Zone I* can be explained by the fact that when increasing the liquid flow rate a bigger number of larger drops was formed by atomization, leading to a larger exchange surface at the beginning of drying (Table 3.2.1). From the initial moment, heat exchange was enhanced and a larger amount of water was evaporated leading to higher water contents and lower temperatures everywhere inside the chamber.

For trials at **200°C**, air temperatures decreased in *Zone I* from 200°C to 139, 117 and 95°C for respectively 1.8 3.6 and 5.4 kg.h<sup>-1</sup> of total liquid flow rate. Air relative humidity inside the chamber was lower than 3% for 1.8 and 3.6 kg.h<sup>-1</sup> and inferior to 10% even for the highest liquid flow rate of 5.4 kg.h<sup>-1</sup> (8.2% at point B).

Due to the accuracy of the RH measurements ( $\pm 1\%$ ), it was not possible to solve the mass balance on water in air to calculate average particle water content inside the chamber. At low relative humidity, 1% of error in RH measurement could lead to more than 20% error in determination of air water content and so in the solution of the mass balance on water in air. But in any case we could observe that air water content did not vary from position A to B (Fig. 3.2.3a), so that we could assume that for an inlet air temperature of 200°C drying was already completed in *Zone I*; only for the highest tested liquid flow rate of 5.4 kg.h<sup>-1</sup> drying air water content increased slightly from A to B (from 38 to 39 g.kg<sup>-1</sup>), meaning that drying still continued below *Zone I*. Further decrease in air temperatures (3 to 8°C) was due to heat losses; the lower the liquid flow rate, the higher the temperatures inside the chamber and so the heat losses, leading to a more important air temperature decrease from the top to the bottom of the chamber.

According to the very fast drying and the high temperatures inside the chamber, final powder water content was low. For 1.8 and 3.6 kg.h<sup>-1</sup> it was inferior to 2%, and for 5.4 kg.h<sup>-1</sup> it was of 3.5%. Water activity was never higher than 0.12, in agreement with MD12 sorption isotherms and inferior to the air relative humidity at the exit of the chamber.

Final powder size increased with liquid flow rate, in agreement with the bigger size of initial atomized drops (Table 3.2.1). The biggest differences could be seen for the average volumetric diameter  $d_{4,3}$  that increased from 28 to 36 and 43  $\mu\text{m}$  for respectively 1.8, 3.6 and 5.4 kg.h<sup>-1</sup>. The mean and the Sauter diameters  $d_{50}$  and  $d_{3,2}$  increased slightly with the flow rate (from 26 to 30  $\mu\text{m}$  for  $d_{50}$  and from 17 to 20  $\mu\text{m}$  for  $d_{3,2}$ ). In any case 90% of the final powder was smaller than 53  $\mu\text{m}$  (Table 3.2.4.).

For an inlet air temperature of **144 °C** (Fig. 3.2.2b and 3.2.3b), the effect of liquid flow rate on air properties and final powder characteristics was more important. For the lowest liquid flow rate of 1.8 kg.h<sup>-1</sup>, air temperature decrease in *Zone I* was of 50°C, with a relative humidity at point A of 3.3%. Increasing the liquid flow rate to 3.6 and 5.4 kg.h<sup>-1</sup>, air temperature decrease in *Zone I* increased to 73 and 86°C respectively, with relative humidities increasing to 10.8 and 33.5%. For any liquid flow rate, air water content increased from point A to B, meaning that drying still continued in *Zone II*. From mass balances we calculated that powder average moisture content at point A was still higher than 10%, while final recovered powder had a moisture content varying from 2.9 to 8.8 % (Table 3.2.4.).

The highest liquid flow rate of 5.4 kg.h<sup>-1</sup> appeared to be a drying limit for trials at 144°C. In this situation, air in *Zone II* was cold (<60°C) and humid (34-39 % RH) so that drying rate was low and a still humid final powder ( $X = 8.8\%$ ) was obtained. In this case, an important

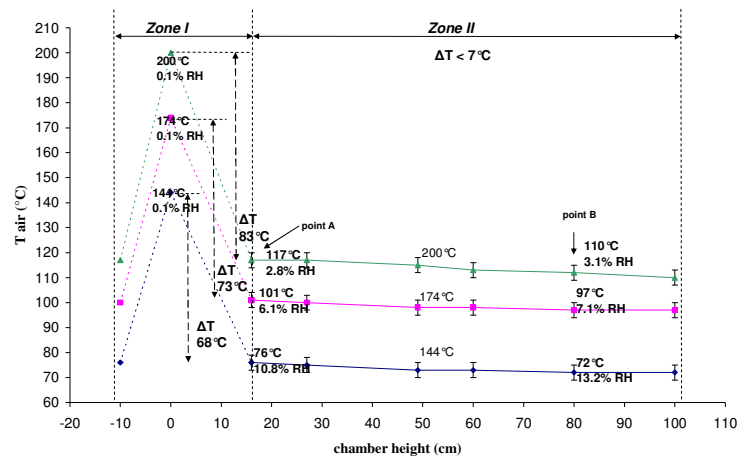


**Figure 3.2.4.** Effect of inlet air temperature on measured air temperatures and relative humidities at steady state inside NIRO Minor as a function of chamber height for maltodextrin DE12 solutions 40% w/w. ( $T_{IN}$ : 144 – 174 – 200°C; air flow rate: 110 kg.h<sup>-1</sup>; liquid flow rate: 3.6 kg.h<sup>-1</sup>; rotary atomizer velocity: 25000 rpm).

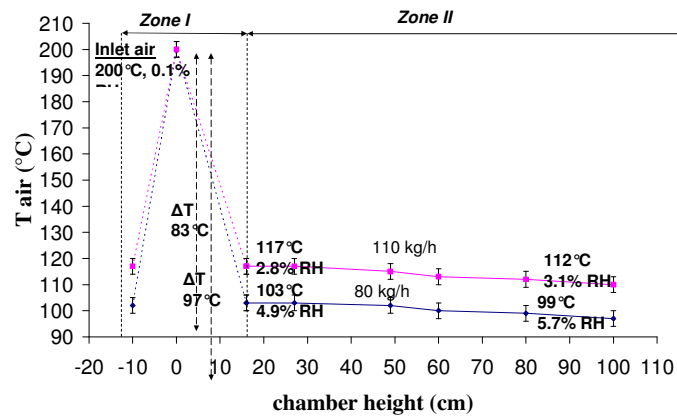


**Figure 3.2.5.** Effect of drying air flow rate on measured air temperatures and relative humidities at steady state as a function of chamber height for maltodextrin DE12 solutions ( $T_{IN}$  200°C; air flow rate 80 – 110 kg.h<sup>-1</sup>; liquid flow rate 3.6 kg.h<sup>-1</sup>; rotary atomizer velocity 25000 rpm).

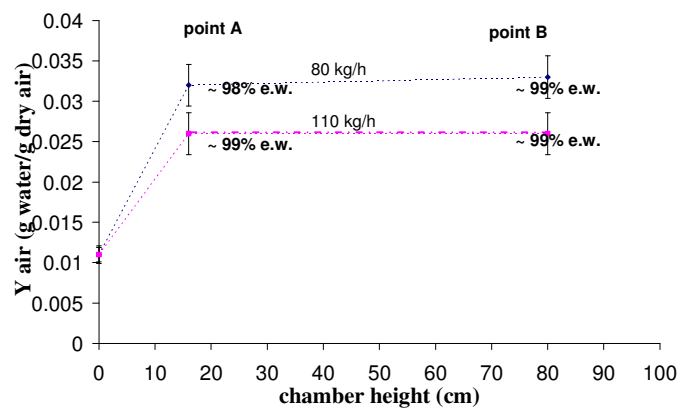


**Figure 3.2.6.** Effect of drying air flow rate on calculated air water content Y and percent of evaporated water at point A and B at steady state for solution of maltodextrin DE12 40% w/w ( $T_{IN}$  144 °C; air flow rate 110 kg.h<sup>-1</sup>; liquid flow rate 1.8 – 3.6 – 5.4 kg.h<sup>-1</sup>; rotary atomizer velocity 25000 rpm).

### Part III – Results and discussion

part of product (~50%) was found stuck on the chamber walls. Collected powder water activity was of 0.39, equal to the air relative humidity at the exit of the chamber.

As for trials at 200°C, final powder moisture content increased with the liquid flow rate (Table 3.2.4) and powder size slightly increased. Differences could be better observed on  $d_{4,3}$  that increased from 28 to 32 and 38  $\mu\text{m}$ , while Sauter diameter was in any case about 16 $\mu\text{m}$  and median diameter  $d_{50}$  varied from 22 to 26  $\mu\text{m}$ ; 90% of powder was smaller than 62  $\mu\text{m}$ .

#### ***Effect of inlet air temperature***

Inlet air temperature determined the initial temperature difference  $\Delta T$  between air and drops surface and so the initial evaporation rate. For the same liquid flow rate of 3.6  $\text{kg}\cdot\text{h}^{-1}$  of MD12 solution, increasing the inlet air temperature from 144°C to 174°C and 200°C led to a faster evaporation rate, resulting in a bigger air temperature decrease in *Zone I*. It was of 86°C for  $T_{\text{IN}} = 200^\circ\text{C}$  compared to 73°C and 50°C for respectively 174°C and 144°C (Fig. 3.2.4).

In *Zone II*, between point A and the bottom of the chamber ( $T_{\text{OUT}}$ ), a small decrease in air temperature was measured: respectively 4 and 7°C for inlet air temperature of 144 and 200°C. For trials at 200°C, this variation was essentially due to heat losses since air water content was constant between A and B showing that drying was completed in zone I. For inlet air temperature of 144°C and 174°C, air water content increased slightly from 28 (A) to 29 (B)  $\text{g}\cdot\text{kg}^{-1}$ , (Table 3.2.4) showing that drying continued in *Zone II*.

Final powder water content depended on inlet air temperature. It varied from 1.6% for inlet air temperature of 200°C to 3.6 and 4.8% for 174 and 144°C, for the same feed flow rate.

#### ***Effect of rotary atomizer velocity***

A higher rotary atomizer speed should lead to the formation of a larger number of smaller liquid drops for the same liquid flow rate (Table 3.2.1).

For a liquid flow rate of 3.6  $\text{kg}\cdot\text{h}^{-1}$ , final powder size was almost insensitive to an increase of velocity from 22500 to 25000 rpm. But, when increasing velocity to 30000 rpm,  $d_{4,3}$  of collected powder decreased from 36  $\mu\text{m}$  to 28  $\mu\text{m}$ ,  $d_{50}$  from 26 to 21  $\mu\text{m}$  and  $d_{3,2}$  from 20 to 16  $\mu\text{m}$ . Due to the increased total exchange surface of the spray a better drying should be expected, but no difference in air temperatures and water content could be observed with an inlet air temperature of 200°C, as evaporation was in any case so fast that drying was already completed in zone I. Powders with the same moisture content ( $1.6 \pm 0.2\%$ ) were obtained for the tested rotary wheel velocities.

#### ***Effect of air flow rate***

Two different air flow rates were tested (80 and 110  $\text{kg}\cdot\text{h}^{-1}$ ) at 200°C, with a maltodextrin solution flow rate of 3.6  $\text{kg}\cdot\text{h}^{-1}$ . For a given inlet air temperature and liquid flow rate, the initial evaporation rate ( $t = 0$ ) was the same in both cases (same temperature difference between air and drops, and same spray exchange surface).

Depending on air flow rate, we observed different air water content and air temperature decrease (Fig. 3.2.5 and 3.2.6). The lower the air flow rate, the higher the air temperature decrease as:

$$\Delta T_{\text{air}} = \frac{\dot{m}_{\text{ew}} \cdot \Delta H_v}{c_p \cdot \dot{m}_{\text{air}}} \quad \text{eq. 3.2.4}$$

The air water content (and thus relative humidity) for the same amount of evaporated water is higher for lower air flow rates, according to the mass balance of water in air:

$$\dot{m}_{\text{air}} Y_{\text{IN}} + \dot{m}_{\text{ew}} = \dot{m}_{\text{air}} Y^* \Rightarrow Y^* = Y_{\text{IN}} + \frac{\dot{m}_{\text{ew}}}{\dot{m}_{\text{air}}} \quad \text{eq. 3.2.5}$$

**Table 3.2.5.** Comparison between spray drying of solutions of maltodextrin DE12 and DE21. Air temperatures, relative humidity and water content at point A and B inside the chamber at steady state; measured final powder properties and calculated water content in A and B.

Maltodextrin	DE21			DE12			
$T_{IN}$ (°C)	144			144			
$\dot{m}_{air}$ (kg.h <sup>-1</sup> )	110			110			
$v_{wheel}$ (rpm)	25000			25000			
$\dot{m}_{liquid}$ (kg.h <sup>-1</sup> )	1.8	3.6	5.4	1.8	3.6	5.4	
$T_{air}$ (°C)	A	93	72	//	94	76	58
	B	88	70	//	90	72	55
	OUT	88	70	//	90	72	55
RH air (%)	IN	<0.5	<0.5	//	<0.5	<0.5	<0.5
	A	3.4	11.5	//	3.3	10.8	33.5
	B	3.9	13.1	//	4.3	13.2	39.0
$Y_{air}$ (g water/ kg dry air)	IN	7	7	//	10	10	11
	A	16	25	//	17	28	38
	B	16.5	26	//	19.5	29	40
X A calculated	9	11.5	//	10.0	12.0	12.5	
X B calculated	5.0	5.5	//	4.8	4.8	8.0	
X (g water/100g solids)	3.5	5.5	//	2.9	4.8	8.8	
$a_w$	0.10	0.23	//	0.10	0.18	0.39	
$d_{50}$ (µm)	23	23	//	22	23	26	
$d_{3,2}$ (µm)	16	16	//	16	16	16	
$d_{4,3}$ (µm)	29	30	//	32	28	38	
$d_{0,1}$ (µm)	11	11	//	10	11	11	
$d_{0,9}$ (µm)	47	48	//	50	46	62	

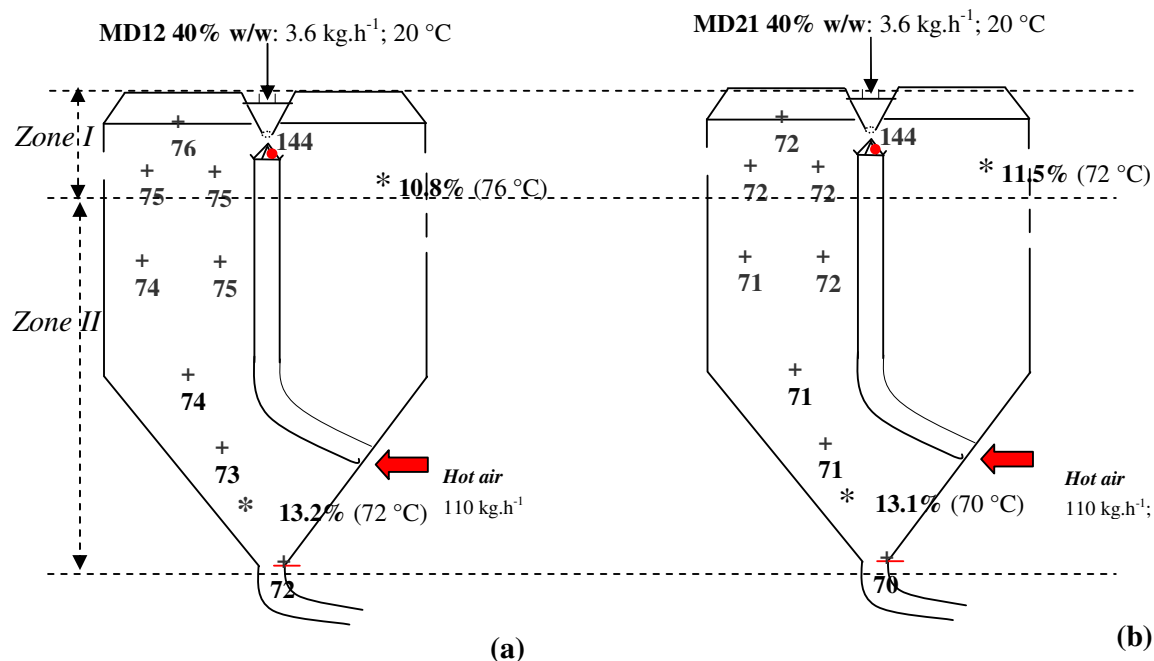


**Figure 3.2.7.** Air temperature and relative humidity at steady state for solution of (a) maltodextrin DE12 and (b) DE21 ( $T_{IN}$  144 °C; air flow rate 110 kg.h<sup>-1</sup>; liquid flow rate 3.6 kg.h<sup>-1</sup>; rotary atomizer velocity 30000 rpm).

For this reason, drying behavior was different. With an air flow rate of  $80 \text{ kg}\cdot\text{h}^{-1}$ , water content at point A was  $32 \text{ g}\cdot\text{kg}^{-1}$  and temperature decrease was  $97^\circ\text{C}$ , with a relative humidity of 4.9%. When the air flow rate was increased from 80 to  $110 \text{ kg}\cdot\text{h}^{-1}$ , the air water content calculated at point A was  $29 \text{ g}\cdot\text{kg}^{-1}$  and the air temperature decrease in *Zone I* was  $82^\circ\text{C}$ , with a relative humidity in A of 2.9%.

Due to a lower air temperature and a higher RH, drying in zone II was slower with the lower air flow rate, leading to a more humid final powder (2.7% instead of 1.6%).

### ***Conclusion on the effect of operating parameters***

Air properties evolution (T, RH) could be measured for maltodextrin solution spray drying, and allowed estimating the drying behavior and average water content of particles inside the chamber.

We put in evidence how drying appeared to be very fast, and most of drying was performed just after drops were formed. This result is in agreement with literature (King, 1984) For high inlet air temperature and/or low liquid flow rate, we can assume that drying is completed in the upper part of the chamber and no more variation of product water content occurs in the bottom part.

Air relative humidity at the exit of the chamber (position B) was a good indicator of final powder water activity as observed by Schuck (2008) but it was usually slightly higher than final powder water activity, meaning that equilibrium between exit air and powder is not totally reached.

Size of final powder was just slightly dependent on tested operating conditions. In all trials the powder  $d_{50}$  was between 16 and  $20 \mu\text{m}$ , with 90% of the powder smaller than  $50 \mu\text{m}$ .

## **2.2. Comparison between MD21 and MD12 and water drying behavior**

The influence of the nature of the dried product was studied by comparing spray drying of solutions of maltodextrin DE12 and DE21. The chemical structure of glucose chains in these two maltodextrins led to a different affinity for water, with consequences on drying and sticking properties.

Drying of maltodextrin DE 21 solutions (40% w/w) was done with the same liquid flow rates as for MD12 solutions. The inlet air temperature was fixed at  $144^\circ\text{C}$ , the temperature for which the drying of MD12 solution lead to variations of air properties (RH, Y) in the chamber when changing flow rate.

For the same atomized liquid flow rate, measurements of air properties inside the chamber suggested that the drying behavior of MD21 and MD12 solutions was different (Table 3.2.5 and Fig. 3.2.7). For liquid flow rates of 1.8 and  $3.6 \text{ kg}\cdot\text{h}^{-1}$ , measured values for temperatures, relative humidities and air water content during drying of MD21 were between the ones measured during water and during MD12 drying. The initial evaporation of water from drops of MD21 solution was easier than for MD12 solution in *Zone I*. From water mass balance at point A we calculated an average MD21 particle water content of 11.5%, and 12% for MD12. In the second part of the chamber the lower air temperatures for MD21 drying led to a reduced evaporation rate, so that final powder moisture content (and water activity) of MD21 powder was slightly higher than the one of MD12 powder (3.5 compared to 2.9% for  $1.8 \text{ kg}\cdot\text{h}^{-1}$  and 5.5% compared to 4.8% for  $3.6 \text{ kg}\cdot\text{h}^{-1}$ ).

When increasing the total flow rate of solution to  $5.4 \text{ kg}\cdot\text{h}^{-1}$ , no more powder could be recovered for MD21 (semi-liquid product was stuck on chamber walls), while MD12 powder could still be obtained.



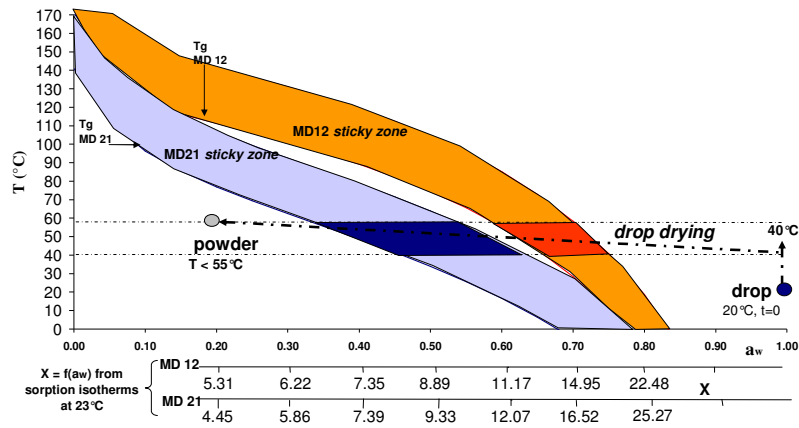


Figure 3.2.8. Sticky zones for maltodextrin DE12 and DE21.

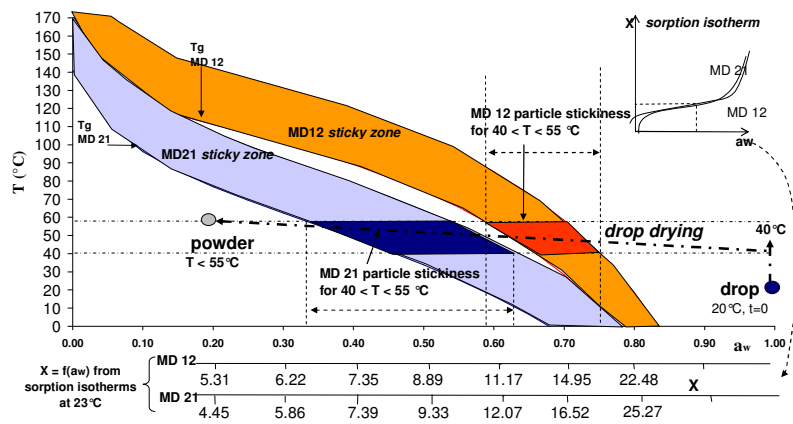


Figure 3.2.9. Evolution of drops properties during spray drying of maltodextrin DE12 and DE21 solutions ( $X = f(a_w)$  sorption isotherms at 23°C,  $T_{sticky} = T_g + 30^\circ\text{C}$ ).

Table 3.2.6. Possible stickiness of particles at point A during drying of solutions of maltodextrin DE12 and DE21 (40 % w/w) inside NIRO Minor (air inlet 144 °C, 110 kg.h<sup>-1</sup>).

	Liquid (water) flow rate (kg.h <sup>-1</sup> )	T powder (°C)	T <sub>wb</sub> (°C)	ΔY <sub>A-IN</sub> (g.kg <sup>-1</sup> )	X <sub>A</sub> (%)	T <sub>g A</sub> (°C)	Sticky in A
MD12	1.8 (1.08)	55	40	0.007	10 ± 5	65-95	Too low accuracy
MD12	3.6 (2.16)	50	40	0.018	12.0 ± 0.5	53-83	NO
MD12	5.4 (3.24)	41	40	0.027	12.5 ± 0.5	43-73	NO
MD21	1.8 (1.08)	55	40	0.009	9 ± 5	30-60	Too low accuracy
MD21	3.6 (2.16)	47	40	0.018	12.0 ± 0.5	10-40	YES
MD21	5.4 (3.24)	//	//	//	//	//	BLOCKAGE

Differences between drying behavior of the two maltodextrins can be explained by considering their properties.

A first difference is the viscosity of the liquid solutions (Fig. 2.4). At 20°C the MD21 solution (40% w/w) has a viscosity more than 50% lower than MD12 (0.028 Pa.s compared to 0.065 Pa.s). This can lead to a higher diffusivity of water in MD 21 drops and therefore faster drying.

MD21 has smaller chains than MD12, with lower molecular weight. This leads to lower glass transition temperatures  $T_g$  for MD21 compared to MD12 (140°C instead of 180°C for dry powders). And for humid powder (or particle during drying), for water activity inferior to 0.8,  $T_g$  of MD21 are always lower (~ -40°C) than MD12 ones, depending on the water activity (linked to water content by sorption isotherms) (Fig. 3.2.8.).

As far as the particle is in conditions of temperature and water activity (water content) above the glass transition line, it could be considered as liquid or sticky (see bibliography). Due to their lower glass transition temperatures, particles of MD21 will exhibit a sticky/liquid behavior during drying till water activity (water content) values lower than for MD12 particles.

When drying 5.4 kg.h<sup>-1</sup> of maltodextrin DE12 solution at 144°C, a powder with a final water content of 8.8% was recovered. This value for a powder temperature of ~ 40°C (wet bulb temperature of drying air) was already below glass transition of MD12 so that powder could still be collected. But for MD21 the drying and exit conditions would be above or close to glass transition temperatures (Fig. 3.2.8), and this could explain why a liquid flow rate of 5.4 kg.h<sup>-1</sup> of maltodextrin 21 solution at 144°C could not be dried and resulted in semi-liquid feed stuck on walls.

### 2.3. Stickiness of maltodextrin DE12 and DE21 particles along spray drying

The objectives were to find and control operating conditions for which drying particles may exhibit a sticky behaviour in the chamber. These conditions could then be used for dry powder insertion and collisions with the sticky drying particles, leading to adhesion and formation of solid bridges to build agglomerates.

A particle becomes *sticky* when its surface reaches a critical viscosity value of  $10^6 - 10^8$  Pa.s. in relation with the glass transition temperatures  $T_g$  of the considered material. This value is obtained for a domain of temperatures ( $T = f(a_w)$ ; sticky region) between  $T_g$  and a sticky temperature  $T_{sticky}$  10 to 30 degrees higher than  $T_g$ . For maltodextrins  $T_{sticky}$  is about 30°C higher than  $T_g$  (Palzer, 2005b). Above  $T_{sticky}$ , particles can still be considered as liquid while below  $T_g$ , particles surface is no more sticky and the powder is considered as stable.

Knowing the initial and final temperature and water content of the drop/particle, it is possible to represent the drying pattern of a liquid solution droplet on the T- $a_w$  diagram with sticky regions (Fig. 3.2.8 and 3.2.9). At the beginning of drying ( $t = 0$ ), liquid drops are formed with a water activity close to 1 (free water) and an initial temperature equal to the liquid solution temperature (~ 20°C). Almost instantaneously, the surface temperature will rise up to the wet



bulb temperature of the drying air. For inlet air used in spray drying trials ( $T_{air}$  between 144 and 200°C with  $Y$  between 0.007 and 0.012 g.kg<sup>-1</sup>), air wet bulb temperature was between 40 and 45°C.

Once the water activity of drop surface is inferior to 1 (fast initial evaporation), the surface temperature increases until reaching final powder temperature. For most of the tested conditions, final maltodextrin powder (DE12 and 21) was in the stable zone below glass transition temperatures: powder temperature varying between 40 and 55°C for water content varying between 8.5 and 1.6%.

During the drying process, during a short period of time, inside the chamber, the drop/particle surface should cross the *sticky region*. For MD12 particles the sticky region is crossed for values of water activity between 0.60 and 0.75, corresponding to water content between 11 and 20% (sorption isotherms); and for MD21 particles for a larger range of water activity between 0.35 and 0.65, corresponding to a water content between 6 and 13 %.

For maltodextrin DE12 drying, for inlet air 200°C, drying was completed in the upper part of the chamber. Particles in *Zone I* were very close to their final water content so too dry to present a sticky behaviour below the atomization zone.

For a lower inlet air temperature of 144°C, from mass balance of water in air, at point A, the estimated average maltodextrin particles water content varied from 10 to 13% depending on the liquid flow rate (Table 3.2.6). But these particles properties ( $X$ ,  $T$ ) also correspond to a state below the glass transition.

Considering that surface water content was probably lower than the average one (humid core), we concluded that MD12 particle at point A was too dry to exhibit a sticky behaviour. Except for the high liquid flow rate of 5.4 kg.h<sup>-1</sup>, particles with an estimated average water content of 12.5%, were close to the glass transition temperature curve and could possibly be sticky in *Zone I*; however these drying conditions corresponded to the limit evaporative capacity of the dryer so that they were not considered in the following study of powder insertion.

For MD21 average calculated water content at point A was slightly lower than the one calculated for MD12 solutions drying in the same conditions. However due to the lower glass transition temperatures, when drying 3.6 kg.h<sup>-1</sup> of MD21 solution, particles at point A should still be above or inside the sticky zone (water content 11.5%). In these drying conditions MD21 particles could have a sticky behaviour all along drying in the chamber (*Zone I and II*).

## Conclusion

Air temperatures and relative humidities were measured inside the NIRO spray dryer during drying of water and maltodextrin DE12 and DE21 solutions.

Air properties evolution inside the chamber was found to be representative of drying process and allowed estimating liquid drops drying behaviour for different process parameters. In particular, the average particle water content evolution along drying could be calculated from a water mass balance in air. In any situation, water evaporation from drop was very fast as soon as in contact with hot air, in the upper part of the chamber, close to the atomizer.

A high percentage of water was removed in the upper part, but for the highest flow rates and lowest drying air temperatures, drying continued at a lower rate in the rest of the chamber.

Drying behaviour of water and maltodextrin solutions was compared for the same amount of water to evaporate. From the different measured air temperatures and relative humidities it was concluded that evaporation of water bound with dry matter in solution was more difficult

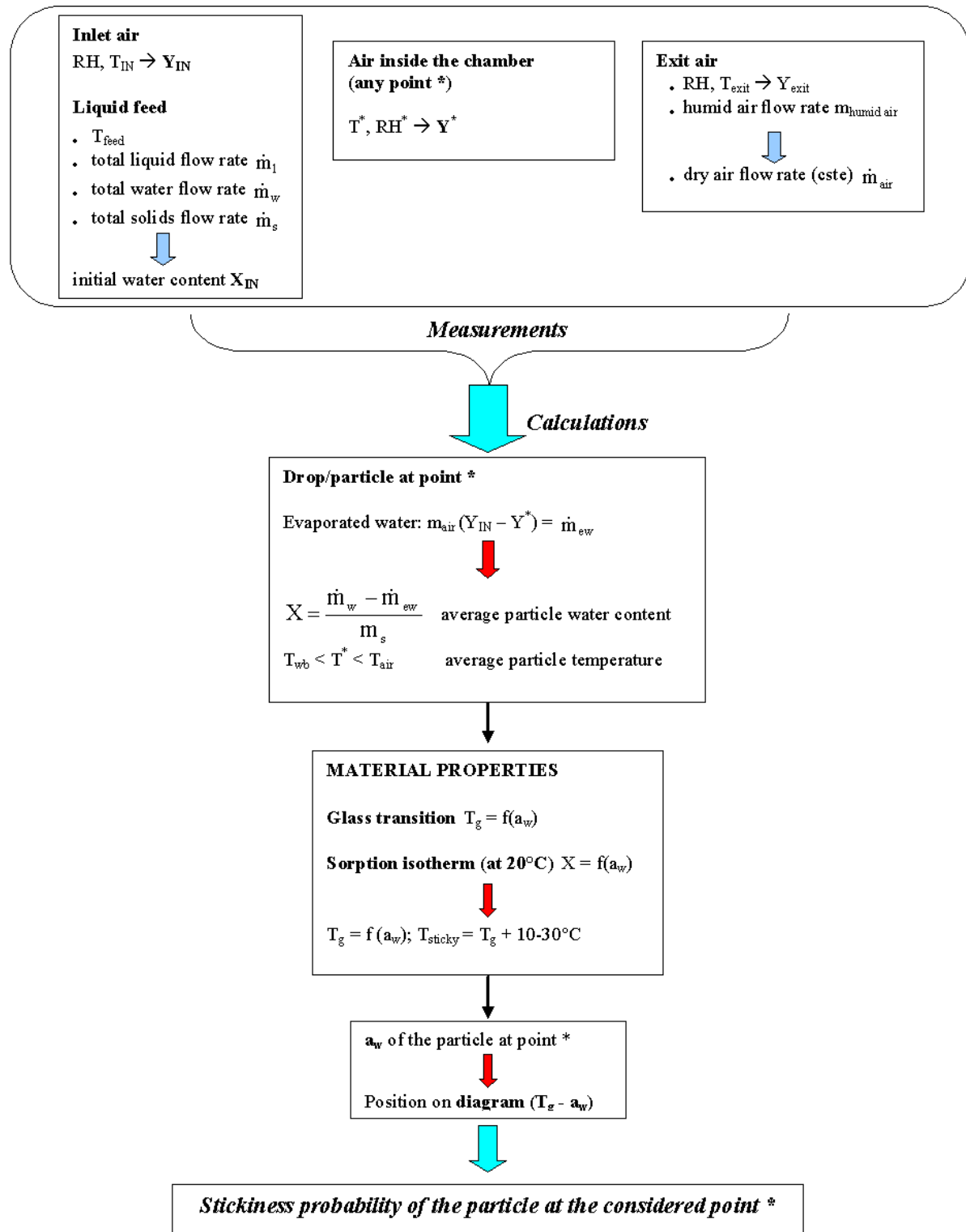


**Figure 3.2.10.** Scheme of data, measurements and calculations used to investigate particle stickiness in spray drying.

than evaporation of free water, for which drying was already completed in the first zone close to atomizer.

Final powder water activity was inferior to the air relative humidity measured at the exit of the chamber, indicating that in our experiments, equilibrium between air and product was not reached at the exit of the chamber.

From knowledge of glass transition temperatures and sorption isotherms of dried material, it was possible to estimate the domain of water content and water activity ( $T$ ,  $a_w$ ,  $X$ ) for which particle could be sticky along their drying inside the chamber. Coupling this information with calculated particle average water content inside the chamber (from air properties), possible conditions and positions can be determined to have maltodextrin in a sticky state.

MD12 was very quickly dried below its glass transition temperature in any tested condition, and thus could exhibit a sticky behaviour only close to atomizer (drops formation).

MD21 drying was found to be easier than drying of MD12 in the upper part of the chamber, but due to the lower glass transition temperatures MD21 particles might be sticky all along drying inside the chamber (liquid flow rate  $3.6 \text{ kg}\cdot\text{h}^{-1}$ ; inlet air temperature  $144^\circ\text{C}$ ).

The approach proposed to investigate particle stickiness development is based on air properties measurements ( $T$ ,  $\text{RH}$ ) and product characteristics ( $T_g = f(a_w)$ ; sorption isotherms) (Fig.3.2.10). It can be applied for different products and dryers, but some comments must be added:

-The air flow rate at the different positions where air properties are measured, must be known, which is not easy because of possible air recirculations, mixing with additional air (fines return)...

-The use of sorption isotherms at  $23^\circ\text{C}$  is representative of equilibrium at a fixed temperature. We also assumed that they represent desorption (drying) at temperatures between  $20$  to  $50^\circ\text{C}$ : for the two maltodextrins these curves are very close.

-The conditions for stickiness of particle surface were deduced from an average water content for particle (with humid core), which could be considered because of the small size of drops/particles.



### 3. Spray drying CFD simulation

The objective of the numerical simulation was to calculate the evolution of air and drops properties inside the Niro spray dryer. The evolution of drop temperature and water content during drying as a function of their position (time) could be used to identify “sticky regions”. To simulate the spray drying process, Computational Fluid Dynamics (CFD) was used with the software Fluent 6.3 (Ansys, USA).

Modelling is a simplified representation of the real process complexity. Simulation of spray drying required the choice of model equations, definition of geometry, of material properties and of boundary conditions before numerical solution (Fig. 3.3.1). Some parameters of the process were unknown and some simplifying hypotheses were used to reduce complexity trying to remain close to reality.

Measurements of air temperature and humidity inside the chamber were used for identification of model parameters and for model validation.

#### 3.1. The model

The model considered two phases: a continuous phase (drying air) and a discrete phase (liquid drops). Besides mass and heat balances equations, CFD allowed solving the Navier-Stokes equations for turbulent flows, using the Reynolds-Averaged Navier-Stokes equations (RANS) with a closure model (Fluent user guide, 1998).

##### 3.1.1. Equations for the continuous phase: air

The mass conservation (continuity equation) and the momentum conservation equations were solved to calculate air flow rate (vector intensity and direction) at any point in the chamber. Energy equation was solved to calculate heat exchanges. Equations were solved in an Eulerian reference frame (fixed  $r$ ,  $z$ ,  $\theta$  coordinates). Axi-symmetry was assumed (**Hypothesis 1**) ( $dx/d\theta = 0$  whatever the variable  $x$ ) and only steady state was simulated (**Hypothesis 2**).

- **Continuity equation**

The general form of the total mass conservation equation, valid for incompressible as well as compressible flows is:

$$\frac{\partial \rho_{\text{air}}}{\partial t} + \vec{\nabla} \cdot (\rho_{\text{air}} \vec{u}) = S_m \quad \text{eq. 3.3.1}$$

$\rho_{\text{air}}$  gas density ( $\text{kg.m}^{-3}$ );  $u$  fluid velocity ( $\text{m.s}^{-1}$ );  $S_m$  mass source term ( $\text{kg.m}^{-3}.\text{s}^{-1}$ ).

The mass source term corresponds to the mass flow rate per unit volume added to the continuous phase from the dispersed phase (e.g. evaporated water).

At steady state we have:

$$\frac{\partial \rho_{\text{air}}}{\partial t} = 0 \Rightarrow \vec{\nabla} \cdot (\rho_{\text{air}} \vec{u}) = S_m \quad \text{eq. 3.3.2}$$

- **Momentum conservation equations**

Conservation of momentum in an inertial (non-accelerating) reference frame is written as:



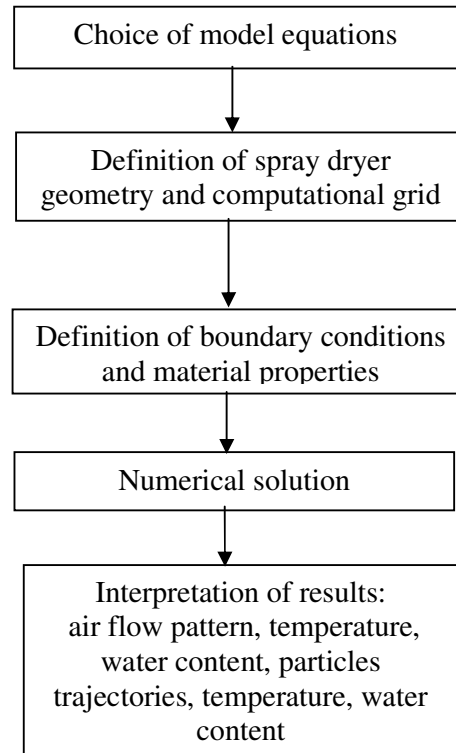


**Figure 3.3.1.** Steps for implementing a CFD model of spray drying.

$$\frac{\partial \rho_{\text{air}} \bar{\mathbf{u}}}{\partial t} + \bar{\nabla} \cdot \rho_{\text{air}} \bar{\mathbf{u}} \bar{\mathbf{u}} = -\bar{\nabla} P + \bar{\nabla} \cdot \bar{\boldsymbol{\tau}} + \rho_{\text{air}} \bar{\mathbf{g}} + \bar{\mathbf{F}} \quad \text{eq. 3.3.3}$$

P static air pressure (Pa);  $\bar{\boldsymbol{\tau}}$  stress tensor;  $\rho_{\text{air}} \bar{\mathbf{g}}$  gravitational force;  $\bar{\mathbf{F}}$  external forces (e.g. from interaction with dispersed phase).

At steady state, the accumulation term  $\frac{\partial}{\partial t}(\rho_{\text{air}} \bar{\mathbf{u}})$  was zero.

The stress tensor  $\bar{\boldsymbol{\tau}}$  is given by :

$$\bar{\boldsymbol{\tau}} = \mu_{\text{eff}} (\bar{\nabla} \bar{\mathbf{u}} + {}^t \bar{\nabla} \bar{\mathbf{u}}) - \frac{2}{3} \mu \bar{\nabla} \cdot \bar{\mathbf{u}} \bar{\mathbf{I}} \quad \text{eq. 3.3.4}$$

$\mu_{\text{eff}}$ : gas effective viscosity (Pa.s) (depending on turbulence model being used), and the second term is the effect of volume dilatation;  $\mu$  viscosity (Pa.s);  $\bar{\mathbf{I}}$  identity matrix.

### • Energy equation

The energy equation has the following form:

$$\frac{\partial}{\partial t}(\rho_{\text{air}} E) + \bar{\nabla} \cdot (\bar{\mathbf{u}} (\rho_{\text{air}} E + P)) = \bar{\nabla} \cdot (\lambda_{\text{eff}} \bar{\nabla} T - \sum_j H_j \bar{\mathbf{j}}_j + \bar{\mathbf{u}} (\bar{\boldsymbol{\tau}})_{\text{eff}}) + S_h \quad \text{eq. 3.3.5}$$

with 
$$E = H - \frac{P}{\rho} + \frac{\mathbf{u}^2}{2}$$

$\lambda_{\text{eff}}$  gas effective thermal conductivity ( $\text{J.s}^{-1}.\text{m}^{-1}.\text{K}^{-1}$ );  $\bar{\mathbf{j}}_j$  diffusion flux of species  $j$  ( $\text{kg}.\text{m}^{-2}.\text{s}^{-1}$ ); H gas specific enthalpy ( $\text{J}.\text{kg}^{-1}$ ); T air temperature (K);  $S_h$  heat source term ( $\text{W}.\text{m}^{-3}$ ).

The first three terms on the right side represent energy transfer due to conduction, species diffusion and viscous dissipation, respectively. The heat source term  $S_h$  includes all the volumetric heat sources (e.g. from drops heating and vaporization).

### • Turbulence modelling

To take into account turbulent flow inside the spray dryer chamber, a standard k-epsilon model has been used (Launder and Spalding, 1974) (**Hypothesis 3**). This is a semi-empirical model based on model transport equations for the turbulent kinetic energy  $k$  ( $\text{m}^2.\text{s}^{-2}$ ) and its dissipation rate  $\epsilon$  ( $\text{m}^2.\text{s}^{-3}$ ):

$$\frac{\partial}{\partial t}(\rho_{\text{air}} k) + \bar{\nabla} \cdot (\rho_{\text{air}} k \bar{\mathbf{u}}) = \bar{\nabla} \cdot \left[ \left( \mu + \frac{\mu_t}{\sigma_k} \right) \bar{\nabla} k \right] + G_k - \rho_{\text{air}} \epsilon - Y_M \quad \text{eq. 3.3.6}$$

$$\frac{\partial}{\partial t}(\rho_{\text{air}} \epsilon) + \bar{\nabla} \cdot (\rho_{\text{air}} \epsilon \bar{\mathbf{u}}) = \bar{\nabla} \cdot \left[ \left( \mu + \frac{\mu_t}{\sigma_\epsilon} \right) \bar{\nabla} \epsilon \right] + C_1 \frac{\epsilon}{\kappa} G_k - C_2 \rho_{\text{air}} \frac{\epsilon^2}{k} \quad \text{eq. 3.3.7}$$

$C_1 = \text{cste} = 1.44$ ;  $C_2 = \text{cste} = 1.92$ ;  $\sigma_k =$  turbulent Prandtl number for  $k = 1.0$ ;  $\sigma_\epsilon = \sigma_k =$  turbulent Prandtl number for  $\epsilon = 1.3$ ;  $\mu_t$  gas turbulent viscosity (Pa.s)

$G_k$  represents the generation of turbulent kinetic energy due to the mean velocity gradients, and  $Y_M$  represents the contribution of the fluctuating dilatation in compressible turbulence to the overall dissipation rate.

By combining  $k$  and  $\epsilon$ , a turbulent (or « eddy ») viscosity is calculated:

$$\mu_t = \rho_{\text{air}} C_\mu \frac{k^2}{\epsilon} \quad \text{where } C_\mu = \text{constant} = 0.09 \quad \text{eq. 3.3.8}$$

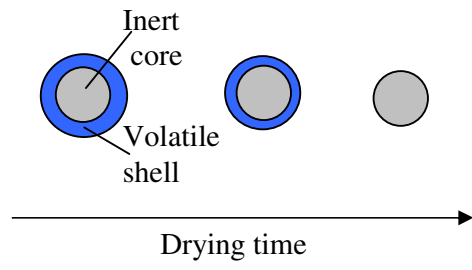


**Figure 3.3.2.** Scheme of liquid drops drying in CFD simulation.

This turbulent viscosity is added to the fluid molecular viscosity to give an effective viscosity  $\mu_{\text{eff}} = \mu + \mu_t$  that is used in the turbulent momentum conservation equations.

### 3.1.2. Equations for the discrete phase: drops/particles

Liquid drops were considered as perfect spheres (**Hypothesis 4**) composed by an inert core surrounded by a volatile component (water) without interaction (no diffusion) between them (**Hypothesis 5**) (Fig. 3.3.2).

#### • Trajectory calculation

Trajectory of a particle (or drop) was predicted by integrating the forces balance on the particle, which is written in a Lagrangian reference frame (moving along particle trajectories). The particle inertia is equal to the sum of forces acting on the particle (drag forces, gravitational forces...):

$$\frac{d\vec{u}_p}{dt} = F_D \cdot (\vec{u} - \vec{u}_p) + \vec{g}(\rho_p - \rho_{\text{air}})/\rho_p + \vec{F} \quad \text{eq. 3.3.9}$$

$\vec{u}$  air velocity ( $\text{m}\cdot\text{s}^{-1}$ );  $\vec{u}_p$  particle velocity ( $\text{m}\cdot\text{s}^{-1}$ );  $\rho_{\text{air}}$ ,  $\rho_p$  air and particle density ( $\text{kg}\cdot\text{m}^{-3}$ );  $\vec{g}$  gravity acceleration ( $\text{m}\cdot\text{s}^{-2}$ );  $\vec{F}$  other forces (specific situations, like Coriolis force).

$F_D \cdot (\vec{u} - \vec{u}_p)$  is the drag force per unit particle:

$$F_D = \frac{18\mu}{\rho_p \cdot d_p^2} \cdot \frac{C_D \text{Re}}{24} \quad \text{eq. 3.3.10}$$

$d_p$  particle diameter (m), Re Reynolds number,  $C_D$  drag coefficient

For laminar flow  $\text{Re} < 0.2$ ,  $C_D = 24/\text{Re}$  (Stokes law)

For semi-turbulent flow  $0.2 < \text{Re} < 1000$ ,  $C_D = 0.4 + 40/\text{Re}$

For turbulent flow  $\text{Re} > 1000$ ,  $C_D = 0.44$

#### • Heat and mass transfers

Without considering radiation (**Hypothesis 6**), particle temperature was calculated according to a heat balance that relates the sensible heat change in the drop to the convective and latent heat transfer between the drop and the continuous phase:

$$m_p \cdot C_{p,\text{drop}} \cdot \frac{dT_p}{dt} = h_c \cdot A_{\text{drop}} (T_{\text{air}} - T_p) - \dot{m}_{\text{ew}} \cdot \Delta H_v \quad \text{eq. 3.3.11}$$

$m_p$  particle total mass (kg);  $C_{p,\text{drop}}$  drop (water) specific heat ( $\text{J}\cdot\text{kg}^{-1}\cdot\text{K}^{-1}$ );  $A_{\text{drop}}$  drop surface ( $\text{m}^2$ ),  $h_c$  convective heat transfer coefficient ( $\text{J}\cdot\text{s}^{-1}\cdot\text{K}^{-1}\cdot\text{m}^2$ ),  $\Delta H_v$  water latent heat of vaporization ( $\text{J}\cdot\text{kg}^{-1}$ ),  $\dot{m}_{\text{ew}}$  evaporation rate ( $\text{kg}\cdot\text{s}^{-1}$ );  $T_p$  drop temperature (assumed to be homogeneous between core and surface –  $T_p = T_s$  (**Hypothesis 7**)) ( $^{\circ}\text{C}$ ).

The evaporation rate during drying was calculated as:

$$\dot{m}_{\text{ew}} = k_c \cdot A_{\text{drop}} \cdot (C_{w,s} - C_{w,b}) \cdot M_w \quad \text{eq. 3.3.12}$$

$k_c$  mass transfer coefficient ( $\text{m}\cdot\text{s}^{-1}$ );  $C_{w,s}$  water vapour concentration at the surface of the drop ( $\text{mol}\cdot\text{m}^{-3}$ );  $C_{w,b}$  bulk air vapour concentration ( $\text{mol}\cdot\text{m}^{-3}$ );  $M_w$  water molecular weight ( $\text{kg}\cdot\text{mol}^{-1}$ )

The convective heat transfer coefficient  $h$  and mass transfer coefficient  $k_c$  are calculated from Ranz-Marshall correlations valid for  $1 < \text{Re} < 450$ ,  $\text{Pr} < 250$ ,  $\text{Sc} < 250$ :

$$\text{Nu} = h \cdot d_p / k_{\infty} = 2 + 0.6 \text{Re}^{1/2} \cdot \text{Pr}^{1/3}$$

$$\text{Sh} = k_c \cdot d_p / D_w = 2 + 0.6 \text{Re}^{1/2} \cdot \text{Sc}^{1/3}$$

Nu Nusselt number,  $k_{\infty}$  thermal conductivity of continuous phase ( $\text{W}\cdot\text{m}^{-1}\cdot\text{K}^{-1}$ ), Sh Sherwood number  $D_w$  water vapour diffusion coefficient in air ( $\text{m}^2\cdot\text{s}^{-1}$ ), Pr Prandtl number ( $C_p \cdot \mu_{\text{air}} / k_{\infty}$ ), Sc Schmidt number ( $\mu_{\text{air}} / (D_w \cdot \rho_{\text{air}})$ )

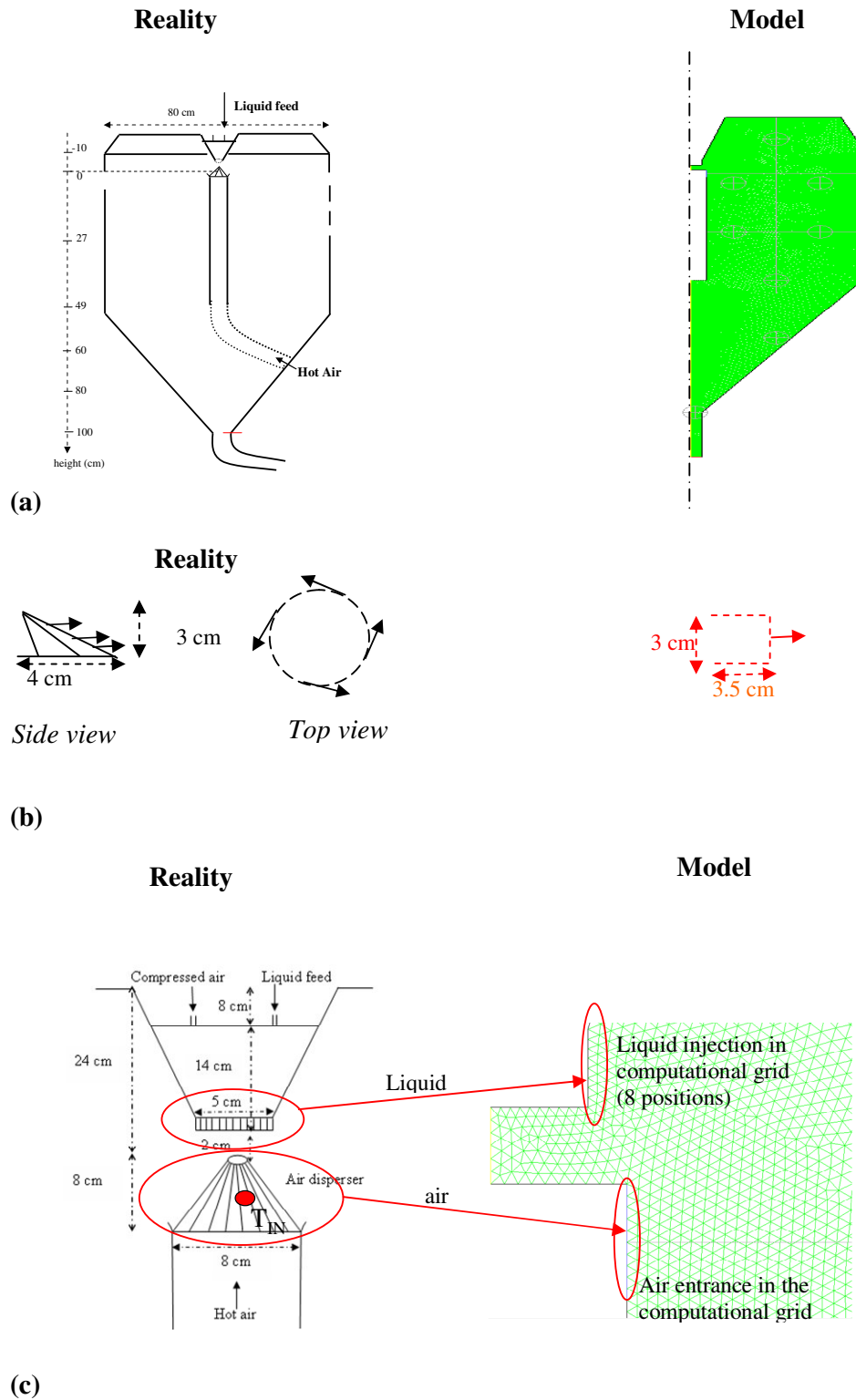


**Figure 3.3.3.** Simplified geometry for (a) spray dryer chamber; (b) air disperser; (c) air and liquid entrance inside the computational grid.

### Part III – Results and discussion

Considering water vapour as an ideal gas (**Hypothesis 8**) and uniform drop temperature so that  $T_s = T_p$  (**Hypothesis 6**) the surface vapour concentration is calculated as:

$$C_{w,s} = \frac{P_v^{\text{drop}}(T_p)}{RT_p} \quad \text{eq. 3.3.13}$$

By default the vapour pressure  $P_v^{\text{drop}}$  at the drop surface is the water saturated pressure  $P_w^{\text{sat}}$  at particle temperature  $T_p$ . That corresponds to a situation in which liquid shell is composed by free water, with no interaction with the solid core.

To simulate the drying of maltodextrin solutions, we must consider the fact that water is bound with solids and that diffusion from core to surface appears, reducing the evaporation rate. Thus, the vapour pressure  $P_v^{\text{drop}}$  at the drop surface will be reduced by multiplying  $P_w^{\text{sat}}$  by a **coefficient x** lower than 1, considered as constant (**Hypothesis 9**):

$$P_v^{\text{drop}}(T_p) = x \cdot P_w^{\text{sat}}(T_p) \quad 0 < x < 1; \quad x = \text{constant} \quad \text{eq. 3.3.14}$$

This approach is similar to the definition of a coefficient  $f = \dot{m}_{\text{ew},l} / \dot{m}_{\text{ew}}$  used by several authors (Langrish and Kockel, 2001) for the “Characteristic Drying Curve” Model (see Bibliography 6.2.3)

This coefficient will be identified using experiments with the specific dried solution (see 3.2.4).

#### 3.1.3. Definition of the dryer geometry

Geometry of the drying chamber has been designed with the software GAMBIT, also used for building the computational grid exported to Fluent. Some simplifications have been adopted:

- A 2D axisymmetric geometry has been considered to reduce the complexity of the system and computational time (Fig. 3.3.3a). (**Hypothesis 1**)
- Geometry of inlet air disperser has been simplified adopting an equivalent cylindrical section (Fig. 3.3.3b) without considering blades. (**Hypothesis 10**)
- Liquid drops inlet has been considered as a cylindrical section in which every grid segment of the section corresponded to a liquid injection to simulate liquid spray by rotary wheel (Fig. 3.3.3c). (**Hypothesis 11**)

Two computational grids made of triangular cells were then built; a coarse grid with 11000 cells and a fine grid with 44000 cells.

#### 3.1.4. Boundary conditions

According to the chosen equations and geometry of the chamber, boundary conditions had to be defined to start simulation (Table 3.3.1). Product properties used in simulation are listed in Annex II.

##### **Boundary conditions for air**

Inlet air velocity was defined from the condition “mass flow inlet” of Fluent, in which initial air mass flow (usually  $110 \text{ kg.h}^{-1}$ ) and velocity vector direction have to be defined. The chosen model allows considering also swirl velocity of air (2D axisymmetric swirling flow). Considering the angle formed by air disperser blades, we estimated that the inlet swirl component of air velocity was five times bigger than the radial component ( $v_t = 5.v_r$ ), and that axial component was neglectable ( $v_x = 0$ ) (Fig. 3.3.4). So we defined (**Hypothesis 12**)

$$\dot{m}_{\text{air}} = 110 \text{ kg.h}^{-1} \text{ with } v_x = 0 \text{ and } v_t/v_r = 5$$

**Table 3.3.1.** Boundary conditions to be defined for CFD spray drying simulation.

<u><b>Air</b></u>	
<u><b>Inlet</b></u>	
	<ul style="list-style-type: none"> <li>• Temperature <math>T_{IN}</math> (K)</li> <li>• Water content <math>Y_{IN}</math> (kg water.kg<sup>-1</sup> dry air)</li> <li>• Velocity → Flow rate <math>\dot{m}_{air}</math> (kg.s<sup>-1</sup>) + direction of velocity</li> <li>• Turbulence parameters (turbulence <b>intensity</b> (%) and hydraulic diameter <math>d_{hyd}</math> of entrance sections(m))</li> </ul>
<u><b>Walls</b></u>	
	<ul style="list-style-type: none"> <li>• Heat transfer coefficient <math>h</math> (W.(m<sup>2</sup>.K)<sup>-1</sup>)</li> <li>• External temperature <math>T_{amb}</math> (K)</li> <li>• <math>v_{air} = 0</math></li> </ul>
<u><b>Exit of chamber</b></u>	
	<ul style="list-style-type: none"> <li>• Imposed pressure <math>P_{out}</math> (Pa) (no diffusive flux perpendicular to exit section)</li> </ul>
<u><b>Liquid drops</b></u>	
<u><b>Inlet</b></u>	
	<ul style="list-style-type: none"> <li>• Liquid flow rate <math>\dot{m}_l</math> (kg.s<sup>-1</sup>)</li> <li>• Radial velocity <math>v_r</math> and swirl velocity <math>v_t</math> (m.s<sup>-1</sup>)</li> <li>• Size (mean diameter <math>d_p</math> (m)) and size distribution</li> <li>• Initial water content <math>X_{IN}</math> (kg water.kg<sup>-1</sup> solution)</li> <li>• Initial temperature <math>T_p</math> (K)</li> <li>• <math>P_v^{drop}(T_p)</math></li> </ul>
<u><b>Wall</b></u>	
	<ul style="list-style-type: none"> <li>• “Reflect” or “trap” of simulated particles colliding with chamber walls.</li> </ul>
<u><b>Exit</b></u>	
	<ul style="list-style-type: none"> <li>• Escape (particles leave the chamber)</li> </ul>

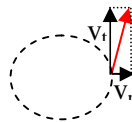


**Figure 3.3.4.** Inlet air velocity direction.

### Part III – Results and discussion

As inlet air turbulence parameters we defined turbulence intensity and hydraulic diameter of entrance air.

The turbulence intensity expresses velocity fluctuations with respect to air average velocity. An initial value of 50% was chosen, assuming that air disperser caused a strong turbulence at the entrance of the chamber. A sensibility study to verify the effect of different values of this parameter on simulation results has been done (see 3.2.1).

The hydraulic diameter (for initial Reynolds number calculation) of the flat air conduct formed by air disperser vanes blade is equal to two times the gap between two blades, so that we have  $d_{\text{hyd}} = 2 \times 2 \text{ mm} = 4 \text{ mm}$ .

To consider the fact that air is sucked by a fan (depression), a negative pressure at air outlet (-100Pa) was imposed (in the same order of magnitude than the measured value (-250Pa)).

The spray dryer chamber was not perfectly insulated, so that thermal losses due to heat exchange with ambient air had to be considered. For this purpose, a global heat transfer coefficient  $h$  was defined, as the sum of the thermal resistance of the wall (including insulation) and the thermal resistance of the external boundary layer (see 1.1.2).

According to experimental results in chapter 1.1.2., the heat transfer coefficient was taken equal to  $2 \text{ W}\cdot\text{m}^{-2}\cdot\text{K}^{-1}$ , and a secondary entrance of ambient air equal to 12% of total air flow rate was considered (**Hypothesis 13**). We assumed that secondary air entrance occurred close to the atomizer, and we took it into account by proportionally lowering air inlet temperature  $T_{\text{IN}}$  with :  $T_{\text{IN}} = 0.88T_{\text{hot air}} + 0.12T_{\text{amb}}$

For  $T_{\text{amb}} = 18^\circ\text{C}$  and  $T_{\text{hot air}} = 144^\circ\text{C}$  and  $200^\circ\text{C}$ ,  $T_{\text{IN}}$  was  $129^\circ\text{C}$  and  $188^\circ\text{C}$  respectively.

#### **Boundary conditions for liquid drops**

Liquid drops were injected into the computational domain from every cell of the liquid entrance. Liquid entrance was a “moving wall” having the same velocity than rotary wheel (30000 rpm).

Swirl ( $v_t$ ) and radial ( $v_r$ ) velocity for inlet drops were calculated with the equations (Masters, 1985):

$$v_t = \pi \cdot d \cdot v_{\text{wheel}} \quad \text{eq. 3.3.15}$$

$$v_r = 0.024 \cdot \sqrt[3]{\frac{\rho_l \cdot \pi^2 \cdot v_{\text{wheel}}^2 \cdot d_{\text{wheel}} \cdot \dot{V}^2}{\mu \cdot h^2 \cdot n^2}} \quad \text{eq. 3.3.16}$$

$d_{\text{wheel}}$  rotary wheel diameter (0.05m);  $N$  rotary wheel velocity (500rps);  $\rho_l$  liquid density ( $\text{kg}\cdot\text{m}^{-3}$ );  $\dot{V}$  volumetric feed rate ( $\text{m}^3\cdot\text{h}^{-1}$ );  $\mu$  liquid viscosity (water = 1 cP at  $20^\circ\text{C}$ , MD12 40% = 28 cP at  $20^\circ\text{C}$ , MD21 40% = 65 cP at  $20^\circ\text{C}$ );  $n$  number of rotary wheel vanes (24);  $h$  height of vanes (0.006 m).

$v_t$  was about  $78.5 \text{ m}\cdot\text{s}^{-1}$  and  $v_r$  varied from 0.70 to  $1.5 \text{ m}\cdot\text{s}^{-1}$  depending on liquid flow rate.

The mean initial size of drops was deduced from final powder distribution, considering that there was no size variation between initial drop and final powder (**Hypothesis 14**). Drops of uniform diameter (**Hypothesis 15**) were considered ( $27 \mu\text{m}$ , median diameter measured for maltodextrin powders). For water drying simulation, a smaller diameter of  $14\mu\text{m}$  was considered, according to empirical correlations to calculate initial diameter of water drops. Some simulations were also performed by considering a Rosin-Rammler size distribution for initial liquid spray.



**Table 3.3.2.** Hypothesis used in CFD simulation of spray drying model.

1. 2D Axy-symmetric geometry.
2. Simulation at steady state.
3. k-epsilon model for turbulence
4. Liquid drop considered as perfect sphere.
5. No interaction (diffusion) between solid core and liquid shell of the particle.
6. No radiation.
7. Uniform drop temperature.
8. Air and water vapor considered as ideal gas.
9. Constant coefficient  $x$ , to lower vapour pressure at drop surface when feed is aqueous solution instead of water.
10. Simplified inlet air disperser geometry (equivalent cylindrical section without blades).
11. Simplified liquid drops inlet (8 injection points).
12. Inlet air direction estimated as  $v_i = 5 \cdot v_r$ , with no initial axial component ( $v_x = 0$ ).
13. Secondary ambient air entrance equal to 12% of total air flow rate, considered close to the atomizer.
14. Initial liquid solution drop size was taken from final powder size distribution, assuming neglectable shrinking.
15. Uniform diameter of sprayed drops.

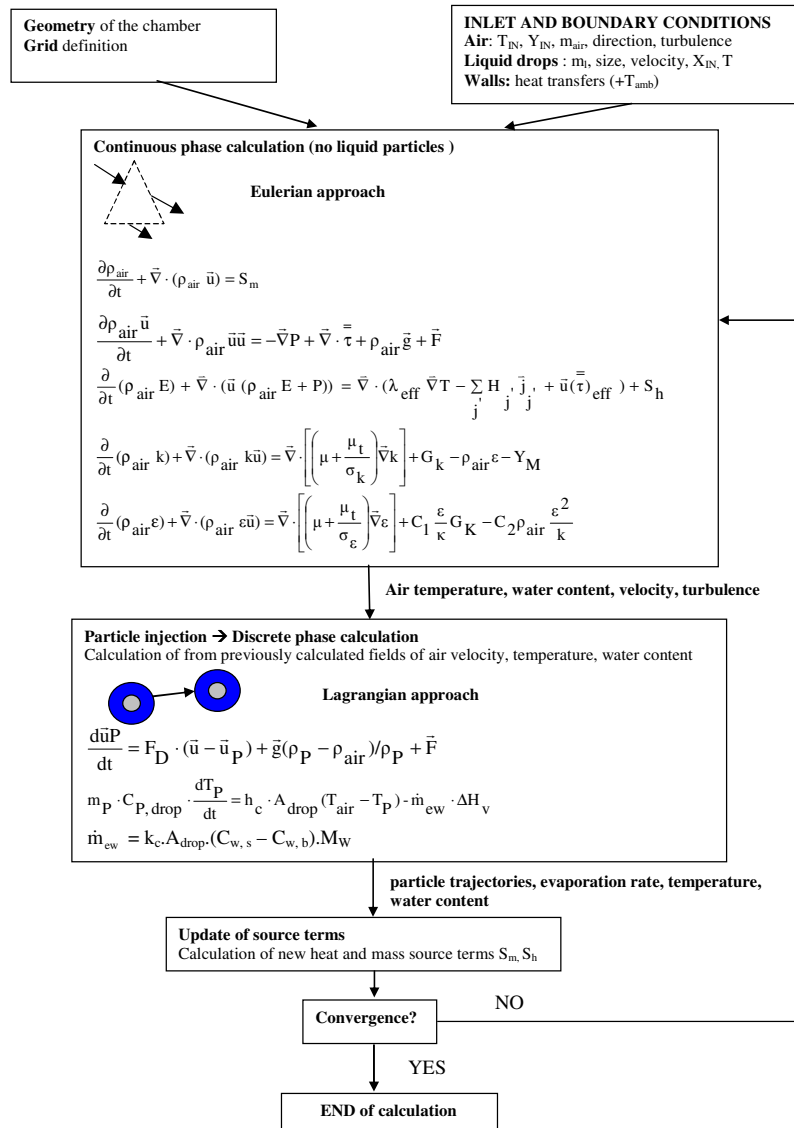


**Figure 3.3.5.** Algorithm used for CFD simulation at steady state.

For water drying simulation, particle reaching the walls were considered as “trapped”; in this case evaporation continued while the particle remains in the collision position. For liquid solution simulation, a “reflect” condition was preferred, in which particles rebound inside the chamber after collision against wall.

The coefficient “x” to lower vapour pressure at drop surface was taken as constant and equal to 1 for water simulation and determined from experimental data for maltodextrin solutions (section 3.2.4).

### **3.1.5. Numerical solution**

With the considered hypothesis (Table 3.3.2), the chosen geometry and boundary conditions, the model equations were solved at steady state to calculate air and particles properties evolution (Fig. 3.3.5)

The different equations (for continuity, momentum, turbulence k- $\epsilon$ , heat and mass transfers) were solved for the continuous phase with the finite elements method. Equations were integrated on a grid divided in triangular cells (2D), which represents the modelled region. In the Eulerian approach, every finite volume cell was crossed by fluid (air). To check that simulation results were independent from the computational grid, a sensibility analysis was performed by varying the number of grid cells (11000 and 44000). The finer the grid, the more accurate the results; but computational time is strongly dependent on grid size, so that optimum must be found between results accuracy and computational time.

After solving the continuous phase equations, discrete phase equations were solved with a Lagrangian approach: particles were followed along their trajectory during time with implicit-Eulerian scheme. A significant number of particles was simulated so that turbulent dispersion and size distribution could be taken into account.

The source terms coming from the interactions between the two phases were then updated and calculation was iterated until convergence, when residuals between variables calculated in two iterations were lower than  $10^{-3}$ .

**Table 3.3.3.** Initial conditions for CFD simulations to determine simulation parameters (RR=Rosin- Rammler size distribution).

	Parameter to test				
	Grid size	Inlet air turbulence intensity	h	d <sub>p</sub>	Correction coefficient x
<b>Inlet air</b>					
T <sub>IN</sub> (°C)	129	129	<b>129</b>	129	129
Y <sub>IN</sub> (kgH <sub>2</sub> O/kg dry air)	0.005	0.005	0.005	0.005	0.005
$\dot{m}_{air}$ (kg.h <sup>-1</sup> )	110	110	110	110	110
Turbulence intensity (%)	50	<b>10-30-50</b>	50	50	50
Hydraulic diameter (m)	0.04	0.04	0.04	0.04	0.04
<b>Liquid feed</b>					
$\dot{m}_{liquid}$ (kg.h <sup>-1</sup> )	//	//	0.00-1.08-2.16-3.24	2.16-3.6	0.00-1.08-2.16-3.24
Concentration (%water)	//	//	100	100-60	100
N° liquid injection	//	//	8	8	8
d <sub>p</sub> (µm)	//	//	13.5	<b>13.5-27-34-50-29.5 (RR)</b>	13.5
T <sub>p</sub> (K)	//	//	18	18	18
P <sub>v</sub> = x P <sub>w</sub> <sup>sat</sup>	//	//	1 (Pv=Psat)	1	<b>From 0.05 to 1</b>
<b>Boundary conditions</b>					
T <sub>amb</sub> (K)	18	18	18	18	18
h (W/(m <sup>2</sup> .K))	2	2	<b>2</b>	2	2
v <sub>wheel</sub> (rpm)	30000	30000	30000	30000	30000
<b>Geometry</b>					
Cells (n°)	<b>11000 44000</b>	44000	44000	44000	44000
<b>Numerical resolution</b>					
Order	2 <sup>nd</sup>	2 <sup>nd</sup>	2 <sup>nd</sup>	2 <sup>nd</sup>	2 <sup>nd</sup>
Iterations	100	1000	1000	1000	1000

**Table 3.3.4.** Simulated (NUM) and experimental (EXP) air T<sub>OUT</sub> for different water flow rates with h = 2 W.m<sup>2</sup>.K<sup>-1</sup> and air T<sub>IN</sub> = 129°C (experimental: air T<sub>IN</sub> 144°C).

Water flow rate (kg.h <sup>-1</sup> )	T <sub>OUT</sub> EXP (T <sub>IN</sub> 144°C) (°C)	T <sub>OUT</sub> NUM (T <sub>IN</sub> 129°C) (°C)
0	112	112.2
1.08	88	89.6
2.16	66	67.7
3.24	47	46.4

## 3.2. Determination of simulation parameters

First simulations were performed to determine or validate the choice of parameters as grid size, inlet air turbulence intensity, global heat transfer coefficient  $h$ , inlet air  $T_{IN}$ , inlet drop diameter  $d_p$ , coefficient  $x$ . Simulation conditions are reported in Table 3.3.3.

### 3.2.1. Validation of the global heat transfer coefficient $h$ and $T_{IN}$ with water drying

Simulation of water drying for different liquid flow rates were performed to validate the chosen global heat exchange coefficient  $h = 2 \text{ W.m}^{-2}.\text{K}^{-1}$ . The inlet air temperature  $T_{IN}$  corresponds to air temperature at the entrance of the chamber after mixing with secondary ambient air.

Calculated exit air temperature  $T_{OUT}$  in simulation of water drying at different flow rates with inlet air  $T_{IN} = 129^\circ\text{C}$  and  $h = 2 \text{ W.m}^{-2}.\text{K}^{-1}$  was in agreement with experimental results (Table 3.3.4). These operating conditions were then applied for further simulations.

### 3.2.2. Sensibility to inlet air turbulence intensity and grid size effect

A simulation was performed for hot air without liquid atomization to test sensibility of results of calculated air temperature and velocity to grid size and air turbulence intensity. Two grid sizes were tested (11000 and 44000 cells) and three turbulence intensities (10 – 30 – 50%).

The simulation performed with a four times finer grid (44000 cells), resulted in an increased computational time (45 min for 500 iterations, compared to 5min with the first grid).

Whatever the grid size, simulation results were close to experimental values ( $\pm 1.5^\circ\text{C}$ ) (Fig. 3.3.6). From temperature and velocity values on a radial line at 25 cm from the top of chamber, some slight differences between the two simulations (Fig. 3.3.7) were observed leading to choose, as a security, the finest grid (44000 cells) with a still reasonable calculation time.

The turbulence intensity was varied from 50 to 30 and 10%. Comparing results for calculated air temperatures and velocity on a radial line 25 cm below the top chamber, we can see that simulations results were independent from turbulence intensity (Fig. 3.3.8).

Turbulence intensity seems to have no effect on simulation results, so we choose a value of 50%, as the air disperser geometry was more likely to produce a big turbulence (24 blades with narrow space between them).

### 3.2.3. Sensibility to initial drop diameter

Effect of initial liquid droplet size on simulation was tested during simulation of water drying ( $P_v^{\text{drop}} = P_w^{\text{sat}}$ ). Initial liquid drop diameters were chosen from empirical correlations and/or from particle size distribution of the final maltodextrin powders.

A first simulation was performed as a reference for water drying (water flow rate  $2.16 \text{ kg.h}^{-1}$ ;  $T_{IN}$ :  $144^\circ\text{C}$  ( $\rightarrow 129^\circ\text{C}$ ); air flow rate:  $110 \text{ kg.h}^{-1}$ ), considering three different initial drop diameters  $d_p$ :

$d_p = \text{cst} = 13.5 \mu\text{m}$  as  $d_{3,2}$  of water drops (empirical correlation, Masters, 1985)

$d_p = \text{cst} = 27 \mu\text{m}$  as  $d_{50}$  of final powder obtained for maltodextrin drying

$d_p = \text{cst} = 50 \mu\text{m}$  as maximal particle diameter of maltodextrin powder

Higher drop diameter lead to higher air temperatures due to lower exchange surface between air and drops. Anyway, differences in calculated air temperatures inside the chamber (Fig. 3.3.9a) between the three simulated cases were never higher than  $1.5^\circ\text{C}$ , except for values at points 1 and 3 for an initial diameter of  $50 \mu\text{m}$ . However, such a big diameter is unlikely to be representative of water spray (only a small fraction of maltodextrin powder (1-4%) was bigger than  $50 \mu\text{m}$ ).

Part III – Results and discussion

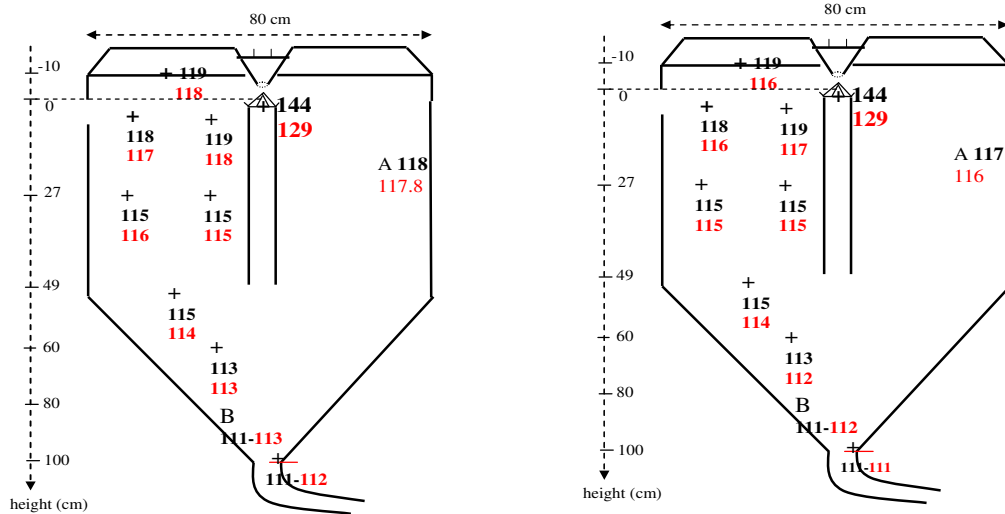


**Figure 3.3.6.** Air temperatures inside the chamber; comparison between calculated (red) and experimental values (black). (a) grid size 11000 cells (b) grid size 44000 cells ( $T_{IN}$ : 129 °C, air flow rate: 110 kg.h<sup>-1</sup>, no liquid atomization, 50% turbulence intensity).

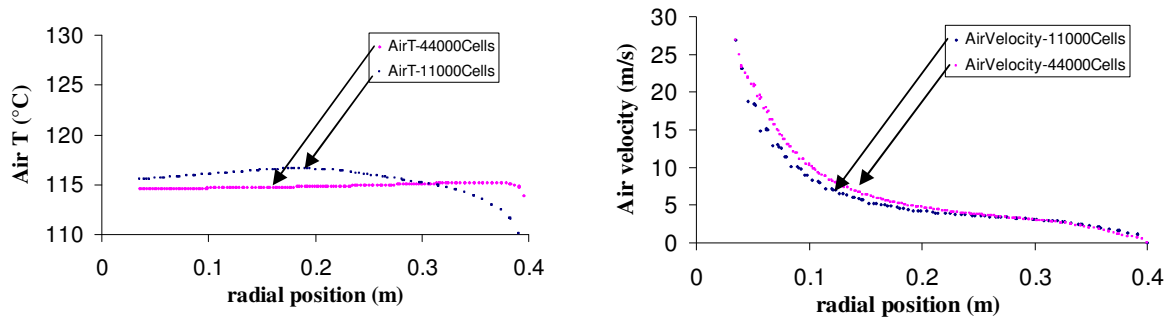


**Figure 3.3.7.** Effect of grid size on calculated air temperature (a) and velocity (b) on a radial lines 25 cm below top of chamber ( $T_{IN}$ : 129 °C, air flow rate: 110 kg.h<sup>-1</sup>, no liquid atomization, 11000-44000 cells, 50% turbulence intensity).

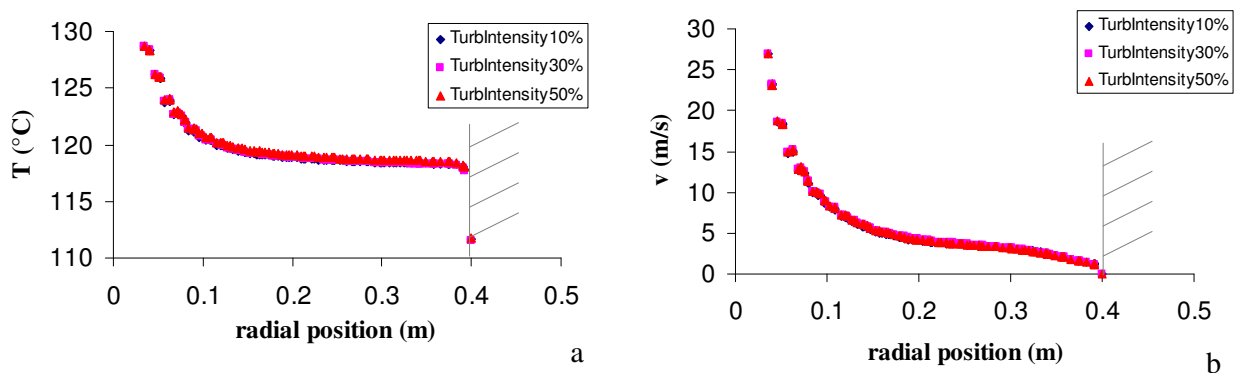


**Figure 3.3.8.** Effect of turbulence intensity on calculated air temperature (a) and velocity (b) on a radial line 14 cm below top of chamber ( $T_{IN}$ : 129 °C, air flow rate: 110 kg.h<sup>-1</sup>, no liquid atomization, 44000 cells, 10-30-50% turbulence intensity).

According to the empirical correlations, an initial constant drop diameter of 13.5  $\mu\text{m}$  was chosen for simulation of water spray drying.

A second sensibility study was then done simulating a liquid flow rate of 3.6  $\text{kg}\cdot\text{h}^{-1}$  with 60% water, as in maltodextrin solution drying. A Rosin-Rammler distribution for initial liquid spray was chosen from final powder distribution ( $d_{\text{RR}}$ : 29.5  $\mu\text{m}$ ,  $n$ : 1.39, 10 size classes). The results of calculated air temperatures were compared to results of simulations done with constant drop diameters:

$$d = \text{cste} = 27 \mu\text{m} = d_{50} \text{ final powder}$$

$$d = \text{cste} = 34 \mu\text{m} = d_{4,3} \text{ final powder (calculated from empirical correlations in 3.2.2)}$$

Simulated air temperatures (Fig. 3.3.9b) for an initial constant drop diameter of 34  $\mu\text{m}$  were about 3°C higher than those obtained with 27  $\mu\text{m}$ , which were closer to the values calculated for Rosin-Rammler distribution ( $\pm 0.5^\circ\text{C}$ ). For this reason, the constant diameter 27  $\mu\text{m}$  was chosen for MD drying simulations.

#### 3.2.4. Effect of drop vapour pressure $P_v$

The coefficient  $x$  was chosen to lower the drop vapour pressure for MD solutions, to take into account the reduced evaporation rate of water in solution compared to free water.  $x$  was chosen as constant during drying, even if in a rigorous way  $P_v$  should vary along drying as does surface water activity.

Simulation was performed for a liquid flow rate of 3.6  $\text{kg}\cdot\text{h}^{-1}$  (2.16  $\text{kg}\cdot\text{h}^{-1}$  of water to evaporate) ( $T_{\text{IN}}$ : 144°C ( $\rightarrow$  129°C); air flow rate: 110  $\text{kg}\cdot\text{h}^{-1}$ ), considering several values of the coefficient: 1; 0.5; 0.2; 0.15; 0.1; 0.05.

It was necessary to lower  $x$  till 0.15 to observe a variation of calculated air temperatures. When lowering  $P_v$  below  $0.15P_{\text{sat}}$ , results of simulation became very sensitive to small variations of the coefficient (Fig. 3.3.9c)

The values for correction coefficient  $x$  to be used in simulation of MD12 and MD21 solution drying were determined to get an agreement between experimental and simulated values of air temperature, air absolute humidity and particle water content inside the chamber for a reference case (3.6  $\text{kg}\cdot\text{h}^{-1}$  liquid flow rate,  $T_{\text{IN}}$  144°C ( $\rightarrow$  129°C), air flow rate 110  $\text{kg}\cdot\text{h}^{-1}$ ) (Fig. 3.3.10). It was found to be of 0.12 for MD21 solution simulation and 0.09 for MD12 solution simulation.

Part III – Results and discussion

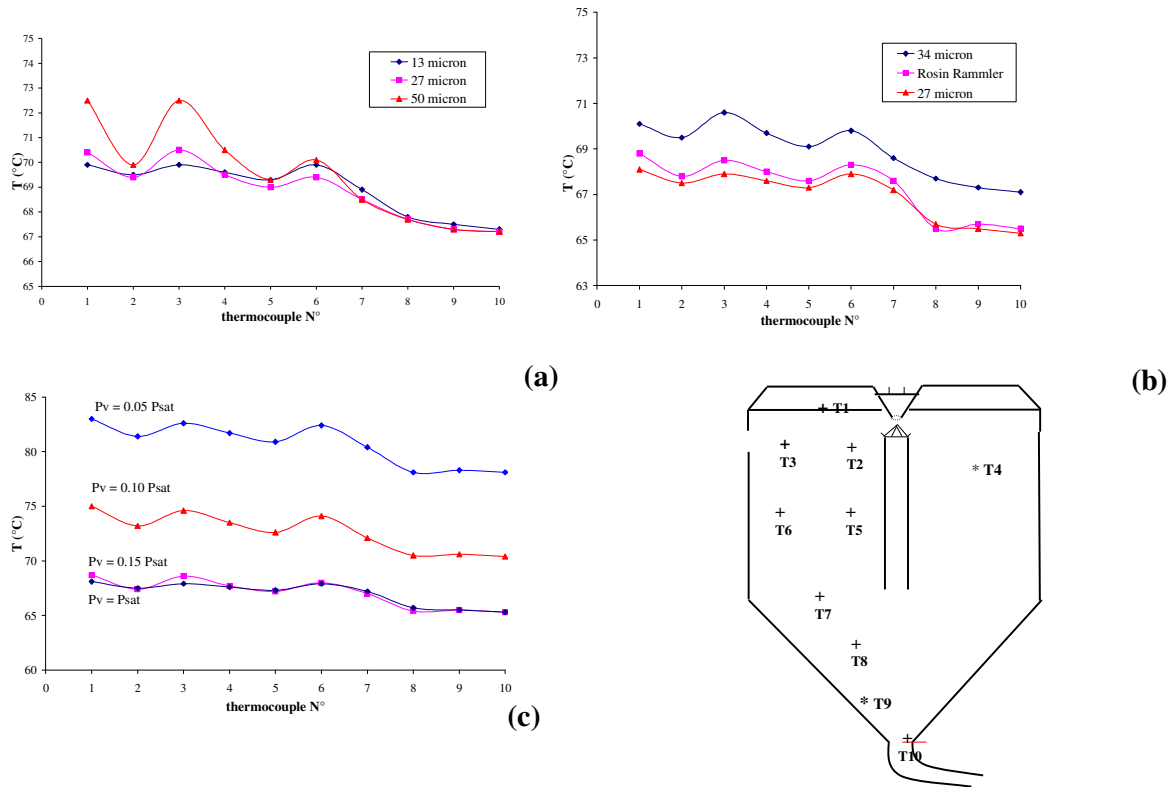


**Figure 3.3.9.** Effect on simulated air temperatures inside the chamber of (a) initial water drops diameter; (b) initial 40% w/w solutions drops diameter; (c) surface vapour pressure for correction coefficient of 0.15 – 0.1 – 0.05 ( $T_{IN}$  129°C, air flow rate 110 kg.h<sup>-1</sup>; liquid flow rate 3.6 kg.h<sup>-1</sup> (2.16 kg.h<sup>-1</sup> of water)). ( $T_{IN}$  129°C, air flow rate 110 kg.h<sup>-1</sup>; water flow rate 2.16 kg.h<sup>-1</sup>).

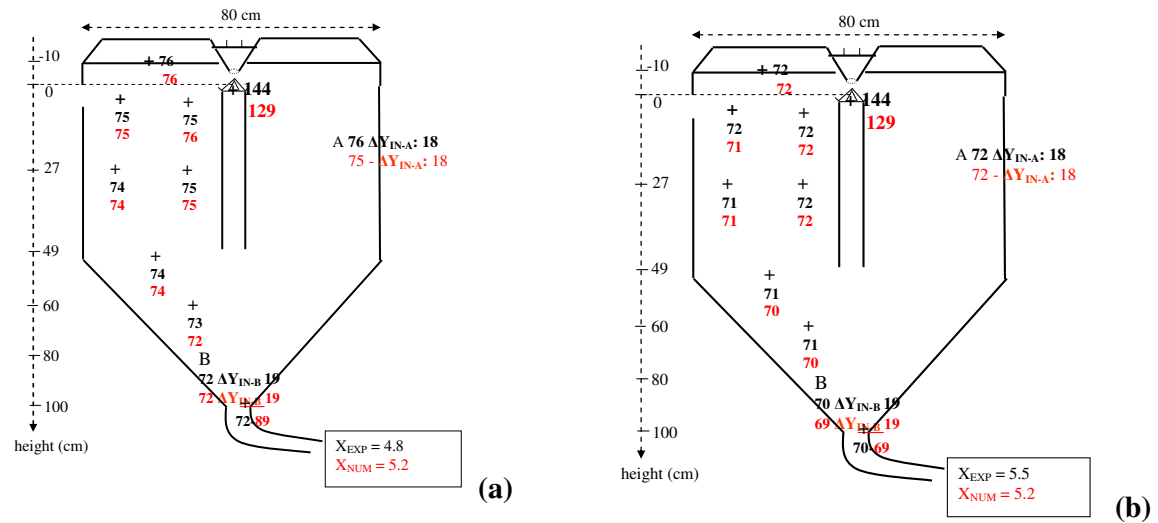


**Figure 3.3.10.** Comparison between calculated (red) and experimental values (black) of air temperatures and air water content inside the chamber and of final powder water content. (a) MD12 (b) MD21 ( $T_{IN}$  129°C, air flow rate 110 kg.h<sup>-1</sup>, 3.6 kg.h<sup>-1</sup>, correction coefficient 0.12 for MD21 and 0.09 for MD12).

### 3.3. Application of simulation

The parameters defined in the last section were used to validate the model for other conditions tested experimentally. And simulations were used to get information about the behaviour of air (continuous phase) and drying particles (dispersed phase).

#### 3.3.1. Model validation

Chosen conditions for model validation were drying of a liquid flow rate of  $1.8 \text{ kg.h}^{-1}$  with  $T_{\text{IN}} 129^\circ\text{C}$  for MD12 and MD21, and of  $3.6 \text{ kg.h}^{-1}$  with  $T_{\text{IN}} 188^\circ\text{C}$  for MD12 (to compare with  $3.6 \text{ kg.h}^{-1}$  and  $129^\circ\text{C}$  for reference) (Table 3.3.5). Validation was done by comparing the simulated air temperatures and water contents inside the chamber and final powder water content, with the experimental values. Results of simulations and experimental measured values are shown in Fig. 3.3.11.

The model correctly predicted air temperature and water content inside the chamber, for the chosen flow rates and for a higher inlet air temperature.

#### 3.3.2. Continuous phase at steady state: air

Simulation allowed obtaining the air flow pattern inside the chamber, as well as the evolution of air properties as temperature and water content along the chamber at steady state.

##### *Air flow inside the chamber at steady state*

The air flow pattern inside the chamber was the same for all the simulated cases. From air path lines (Fig. 3.3.12.1) we could see that two main recirculation zones appear above and below atomization. Hot air is ejected from air entrance with a high radial velocity ( $\approx 13 \text{ m.s}^{-1}$ , Fig. 3.3.12.2). When the air jet arrives close to the chamber wall it is split in two parts resulting in air recirculations. In these zones radial and axial velocities become negative (Fig. 3.3.12.2 and 3.3.12.3b).

A third small recirculation zone could be observed close to chamber wall at the beginning of the conical part. In this zone air recirculation in the central part of the chamber caused a deviation of air resulting in a localized “sucking effect” that put in rotation air generating this small recirculation.

Swirl velocity decreased with radial position from center to wall (Fig. 3.3.12.3a) putting in evidence the centrifugal effect on air. Without friction, the air kinetic moment is constant inside the chamber, so that when radius increased swirl velocity should decrease.

Absolute velocity magnitude inside the chamber was in the order of  $2 \text{ m.s}^{-1}$ .

The air turbulence intensity (Fig. 3.3.12.4a) compared the velocity fluctuations to the absolute velocity. Inside the chamber, turbulence intensity was quite small. The highest intensity was observed close to the air entrance (we imposed 50% as initial value) where we had the most of turbulence kinetic energy (k) production. Production of k is related to appearance of shear stress; zones of k production are concentrated close to the border between fast inlet air jet and slow surrounding air. In the core of inlet air jet there was no production of k as velocity was homogeneous. Another zone of production of k was located close to the rotary atomizer (high shear stress); turbulence was then transported to the inlet air jet zone (Fig. 3.3.12.4b,c).

As a consequence turbulent kinetic energy was high in the upper part of the chamber close to atomization. High turbulence results in better heat and mass transfers according to Ranz and Marshall, so that evaporation rate will be increased in this part of the chamber.



**Table 3.3.5.** Parameters used in CFD simulations of maltodextrin DE12 and DE21 solutions drying.

	MD21	MD12	MD12
<b>Inlet air</b>			
$T_{IN}$ (°C)	129	129	<b>188</b>
$Y_{IN}$ (kgH <sub>2</sub> O/kg dry air)	0.006	0.006	0.006
$\dot{m}_{air}$ (kg.h <sup>-1</sup> )	110	110	110
Turbulence intensity (%)	50	50	50
Hydraulic diameter (m)	0.04	0.04	0.04
<b>Liquid feed</b>			
$\dot{m}_{liquid}$ (kg.h <sup>-1</sup> )	<b>1.8-3.6- 4.23-5.4</b>	<b>1.8-3.6</b>	<b>1.8-3.6</b>
Concentration (%water)	60	60	60
N° liquid injection	8	8	8
$d_p$ (µm)	27.0	27.0	27.0
$T_{liquid}$ (°C)	18	18	18
$P_v^{drop} = x \cdot P_w^{sat}$	0.09 $P_w^{sat}$	0.12 $P_w^{sat}$	0.12 $P_w^{sat}$
<b>Boundary conditions</b>			
$T_{amb}$ (°C)	18	18	18
$h$ (W/(m <sup>2</sup> .K))	2	2	2
$v_{wheel}$ (rpm)	30000	30000	30000
<b>Geometry</b>			
Cells (n°)	44000	44000	44000
<b>Numerical resolution</b>			
Order	2 <sup>nd</sup>	2 <sup>nd</sup>	2 <sup>nd</sup>
Iterations	500	500	500

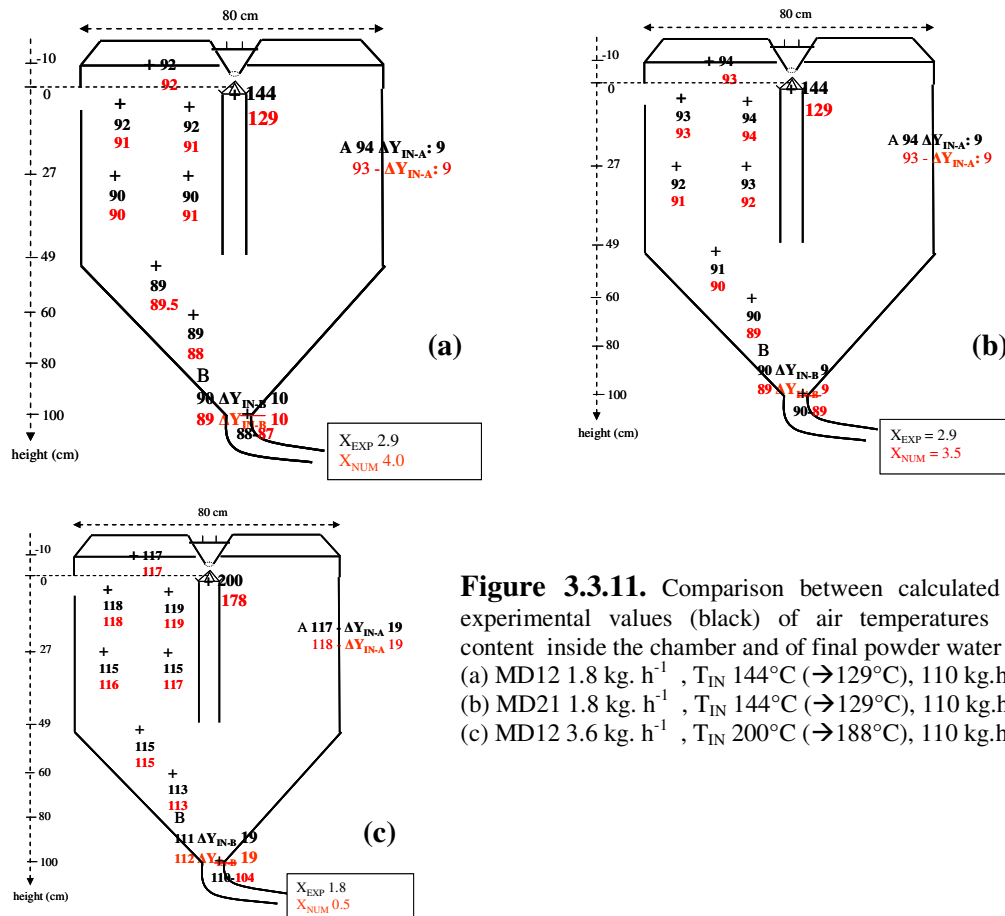


**Figure 3.3.11.** Comparison between calculated (red) and experimental values (black) of air temperatures and water content inside the chamber and of final powder water content.

(a) MD12 1.8 kg. h<sup>-1</sup>,  $T_{IN}$  144°C (→129°C), 110 kg.h<sup>-1</sup>;  
 (b) MD21 1.8 kg. h<sup>-1</sup>,  $T_{IN}$  144°C (→129°C), 110 kg.h<sup>-1</sup>;  
 (c) MD12 3.6 kg. h<sup>-1</sup>,  $T_{IN}$  200°C (→188°C), 110 kg.h<sup>-1</sup>

### ***Evolution of air properties inside the chamber***

Air temperatures and water contents evolution inside the chamber were in agreement with experimental measured values (Fig. 3.3.12.5 and 3.3.12.6).

In any condition air water content increased strongly and temperatures decreased in the upper part of the chamber due to high evaporation rate observed in this zone (Fig. 3.3.13). Just a slight evolution of air temperatures and water content was observed in the cylindrical part of the chamber, because air recirculations helped in homogenizing values. In the conical part, air water content and temperatures were constant, showing that no more evaporation occurred.

In the upper part of the chamber, close to atomizer, evolutions of evaporation rate were similar for MD21 and MD12 solutions whilst for pure water evaporation rate was higher close to the atomizer. The evaporation of free water is easier than the water from solutions (see chapter 3.2).

Enthalpy of the inlet air was high when entering the chamber (high air temperature). Then due to mixing with returning air, enthalpy decreased (humid air) and remained constant in the evaporation zone (Fig. 3.3.14). Close to chamber walls, enthalpy decreased due to heat losses, and then air returned backwards to the atomization zone. Due to the air recirculation in the upper part of the chamber, some air mixing occurred even without liquid atomization (Fig. 3.3.15) so that temperatures close to the atomizer at steady state were lower than the inlet hot air temperature  $T_{IN}$ .

### ***3.3.3. Discrete phase at steady state: drying particles***

80 particles (10 for each liquid injection point) representative of the total liquid flow rate were simulated. For each particle, trajectory, velocity, evolution of mass and of temperature were calculated.

Atomized particles were sucked by the inlet air jet and followed air trajectories in the upper part of the chamber (Fig. 3.3.16). Each particle coming from the same injection point had a different trajectory due to the dispersion caused by air turbulence. Particles mass evolution in the upper part of the chamber showed that most of drying was completed close to the air entrance before arriving to the chamber wall. Particle residence time in this part of the chamber was very short. In less than 0.5s, particles arrived close to chamber walls and could be recirculated with air.

Residence time of particles inside the chamber varied between 20 and 55 s. These values are lower than the average particle residence time of 2 minutes measured experimentally (residence time distribution trial – III.1.). This could be due to the fact that in simulation we applied the “rebound” conditions for particles that hit the chamber walls, while in reality particles could remain stuck on chamber walls and detach later, by this increasing their residence time. Furthermore, in simulation we did not take into account exit pipes and cyclone.

Particle concentration inside the chamber was high close to the atomizer due to particle injection and to recirculations in the upper part of the chamber (Fig. 3.3.17). A high particle concentration could also be observed in the conical part due to the decrease of chamber section and to air recirculation (close to the walls).

For each particle, the evolution of temperature and water content could be represented as a function of drying time (Fig. 3.3.18).

Particles were injected at 18°C and were theoretically almost immediately (<0.05 s) heated up to the wet bulb temperature of drying air. In the simulation of maltodextrin solutions drying, drops temperature during drying was found to be 73°C for MD12 ( $P_v = 0.09P_w^{sat}$ ) and 70°C for MD21 ( $0.12P_w^{sat}$ ) with air at 129°C. These temperatures are different from the real air wet bulb temperature (40°C).

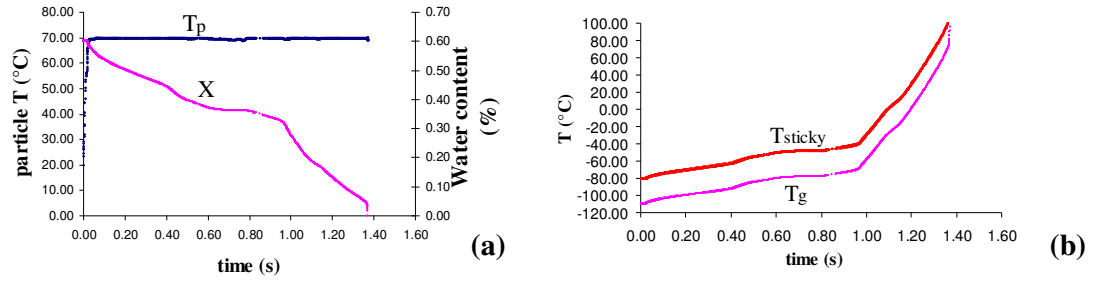


**Figure 3.3.18.** (a) Calculated evolution of a MD21 particle temperature and water content during drying and (b) evolution of its  $T_g$  and  $T_{\text{sticky}}$ .

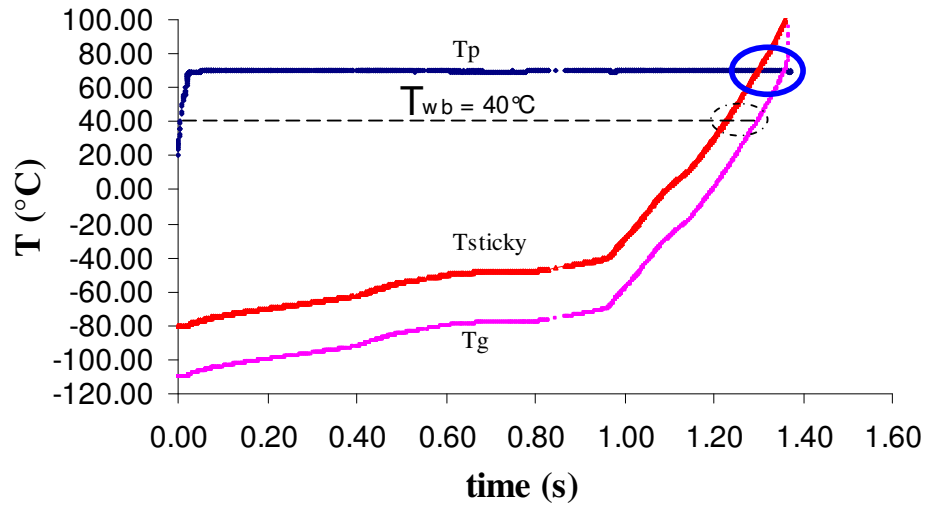


**Figure 3.3.19.** Determination of time gap for which a MD21 simulated particle temperature is sticky inside the chamber.

As we assumed that the particle surface was covered by pure water until end of drying, simulated temperature remained constant since drops are not completely dry when they reach the chamber exit. The calculated powder water content was 4% ( $X_{OUT} = 4\%$ ) in agreement with experimental results.

The water evaporation rate was correctly predicted. However, the simulated drop temperature was too high (70°C) since the temperature measured on final powders was never higher than 55°C whatever the drying conditions. Thus, surface properties of the particle during drying are not totally well predicted by the model.

### 3.4. Determination of powder stickiness inside the chamber

From the knowledge of particle water content evolution during drying, the evolution with time of their glass transition temperature  $T_g$  and sticky temperature  $T_{sticky}$  (related to  $a_w$ ) could be represented (Fig 3.3.18). And the time gap for which a drying particle should be in a sticky state ( $(T, a_w)$  in the sticky zone  $(T_g, T_{sticky}, a_w)$ ) could be determined for each particle (Fig. 3.3.19).

In this context, an overestimation of particle temperature during drying should mean that the particle should be considered as “liquid” for a longer time. As a consequence for the calculated particle temperature of 70°C instead of 40-50°C, the moment when the liquid drop should cross the sticky zone (before becoming no more sticky) should be delayed.

In the example on Fig.3.3.19, with the simulated particle  $T$  of 70°C stickiness occurred for  $1.30 < t < 1.40$  s, while considering a drop temperature of 40°C stickiness would occur for  $1.20 < t < 1.30$  s.

From trajectories calculations, we represented positions inside the chamber for which particles MD21 were liquid, sticky and no more sticky (Fig. 3.3.20). In Figure 3.3.21 the sticky positions inside the dryer chamber are represented for drying of 3.6 and 1.8 kg.h<sup>-1</sup> at 129°C of MD12 and MD21.

MD12 particles exhibit a sticky behavior only in a small region inside the chamber located in the upper part. Below they were too dry to be sticky, and close to atomizer particles were still in a liquid state. Considering the delay in reaching the sticky state in simulation due to overestimation of particle temperature, the sticky state should be reached close to the atomizer if we consider a particle temperature of 40°C.

For MD21 with the highest flow rate (3.6 kg.h<sup>-1</sup>), a sticky behavior of particles is expected in a wider region extending in the whole cylindrical part of the chamber. These results were in agreement with the determined possible sticky zones inside the chamber in chapter 2.4.

These drying conditions could then be suitable for testing agglomeration feasibility by powder insertion trials.

For both maltodextrins DE12 and DE21, some of the particles arrived at the chamber walls while being still in the “liquid” state, which was in agreement with some powder found stuck on chamber walls during spray drying experiments.

#### 3.4.1. Effect of liquid feed flow rate on particle stickiness for MD12 and MD21

The liquid feed flow rate has been changed for a given inlet air temperature  $T_{IN}$  of 129°C to evaluate the effect of this parameter on the possible sticky zones.

For a low liquid flow rate of 1.8 kg.h<sup>-1</sup>, the evaporation rate was high close to atomizer and product was almost completely dried in the upper part of the chamber. Considering that real



drops temperature should be of about 40°C, for both maltodextrin solutions stickiness was likely to appear only close to atomizer (Fig. 3.3.21c,d).

For a high liquid flow rate of 5.4 kg.h<sup>-1</sup> particles always remain above the sticky zone in the liquid state (Fig. 3.3.22). This was in agreement with MD21 experiments when no powder could be produced. For MD12, some powder could still be collected, but with very high final moisture content (> 8%) and with a big part of the powder lost due to sticking on walls.

An intermediate liquid flow rate of 4.32 kg.h<sup>-1</sup> was then simulated for MD21 drying. In this case the possible sticky zone was larger than with a flow rate of 3.6 kg.h<sup>-1</sup>. Stickiness seemed possible also in the conical part of the chamber (Fig. 3.3.23a). These conditions will be used in powder insertion trials to validate the stickiness prediction.

#### ***3.4.2. Effect of inlet air temperature***

Experimental conditions for drying of MD12 at 200°C were also simulated to verify the effect of inlet air temperature  $T_{IN}$  on stickiness prediction.  $T_{IN}$  in simulation was lowered to 188°C to take into account the secondary ambient air entrance. As expected, in this case particles exhibit a sticky behavior only close to atomizer (Fig. 3.3.23b).

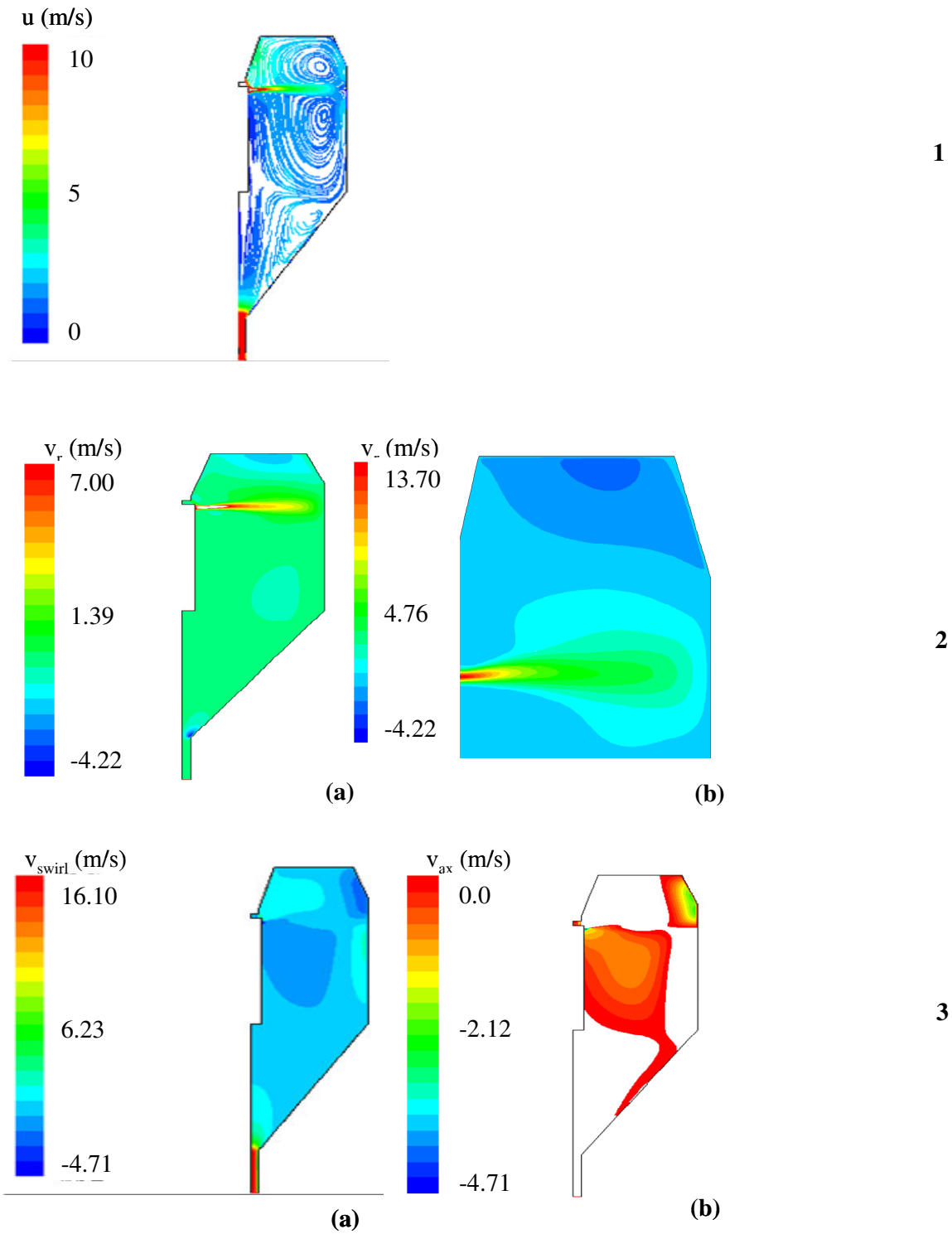


**Figure 3.3.12a.** Air properties simulation when drying MD21 40% w/w solution (liquid feed:  $3.6 \text{ kg}\cdot\text{h}^{-1}$ , air:  $129^\circ\text{C}$ ,  $110 \text{ kg}\cdot\text{h}^{-1}$ ). **1.** Air pathlines inside the spray dryer chamber colored by velocity magnitude ( $\text{m}\cdot\text{s}^{-1}$ ); **2.** (a) Air radial velocity inside the chamber and (b) in the upper part of the chamber; **3.** (a) Air swirl velocity inside the chamber and (b) zones where axial velocity is negative (*to be continued on next page*)

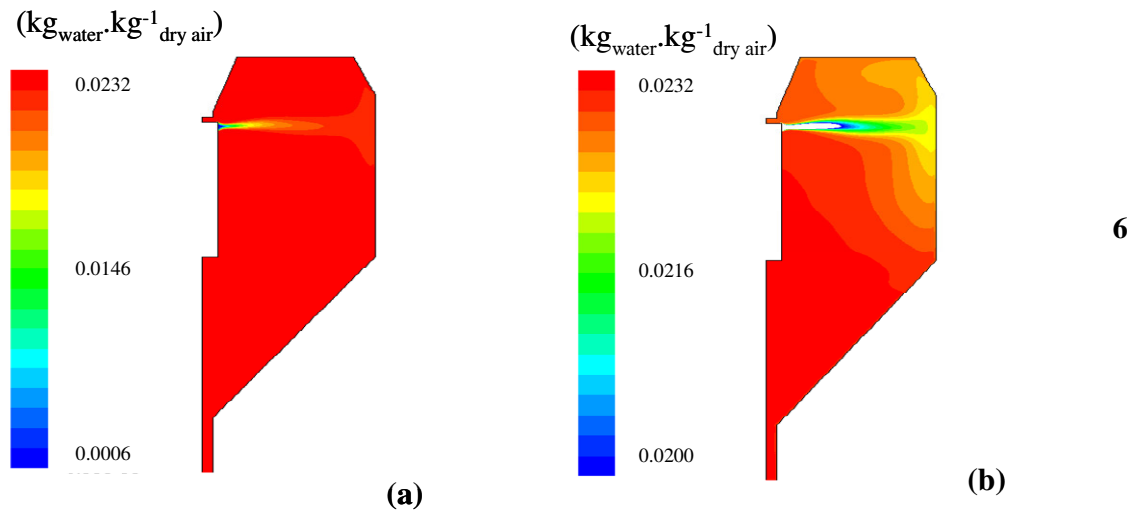
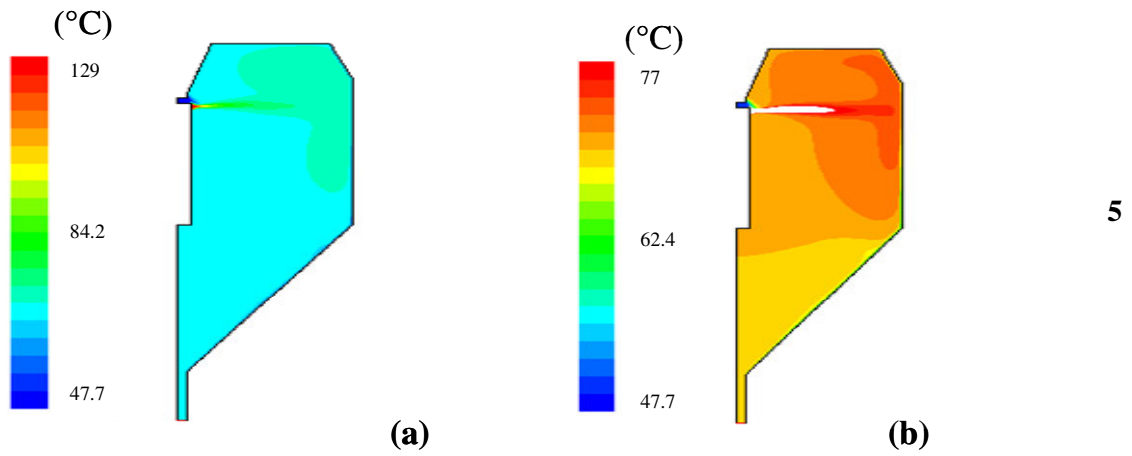
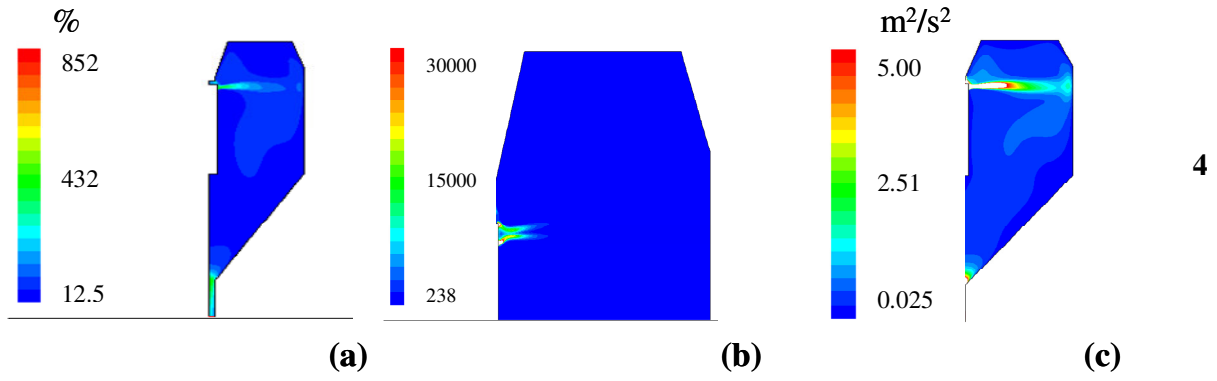


**Figure 3.3.12b.** Air properties simulation when drying MD21 40% w/w solution (liquid feed:  $3.6 \text{ kg}\cdot\text{h}^{-1}$ , air:  $129^\circ\text{C}$ ,  $110 \text{ kg}\cdot\text{h}^{-1}$ ). **4.** (a) Air turbulence intensity; (b) production of turbulent kinetic energy  $k$  and (c) turbulent kinetic energy; **5.** Air temperature inside the chamber (a) whole temperature range (b) temperatures between  $47$  and  $77^\circ\text{C}$ ; **6.** Air water content inside the chamber (a) whole range (b) water content between  $20$  and  $23 \text{ g water}\cdot\text{kg}^{-1}$  dry air.



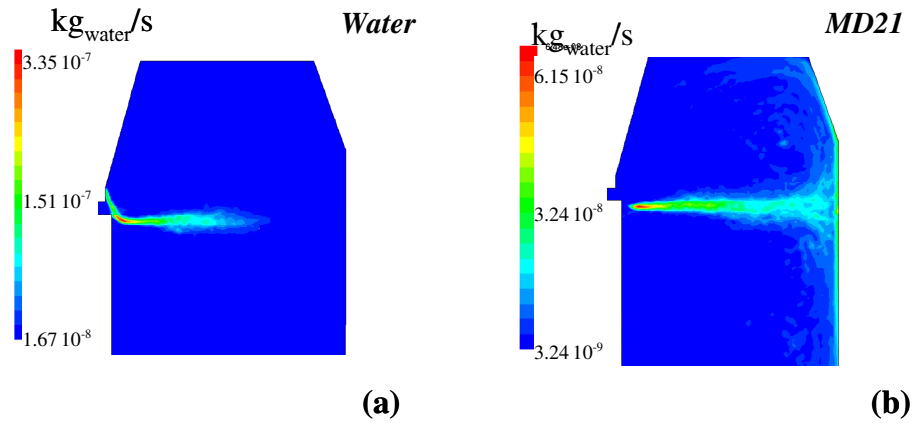


**Figure 3.3.13.** Water evaporation rate ( $\text{kg}\cdot\text{s}^{-1}$ ) during simulation of (a) spray drying of water, (b) of maltodextrin DE21 40% w/w solution (water feed:  $2.16 \text{ kg}\cdot\text{h}^{-1}$  liquid feed:  $3.6 \text{ kg}\cdot\text{h}^{-1}$ , air:  $129^\circ\text{C}$ ,  $110 \text{ kg}\cdot\text{h}^{-1}$ ).

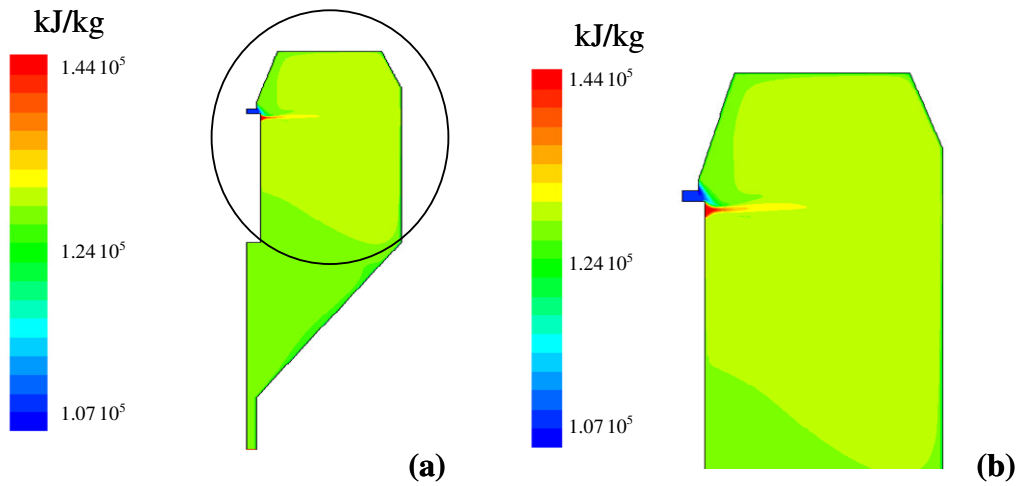


**Figure 3.3.14.** Humid air enthalpy inside the chamber at steady state calculated during drying of MD21 40% w/w solution. (liquid feed:  $3.6 \text{ kg}\cdot\text{h}^{-1}$ , air:  $129^\circ\text{C}$ ,  $110 \text{ kg}\cdot\text{h}^{-1}$ ). (a) whole chamber, (b) upper part of chamber.

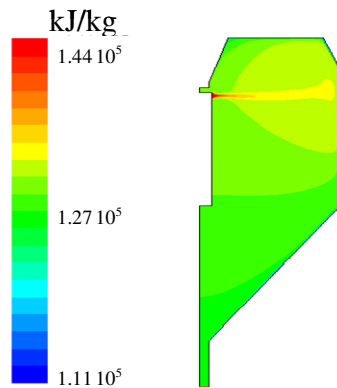


**Figure 3.3.15.** Humid air enthalpy inside the chamber at steady state calculated without liquid atomization. (air:  $129^\circ\text{C}$ ,  $110 \text{ kg}\cdot\text{h}^{-1}$ )

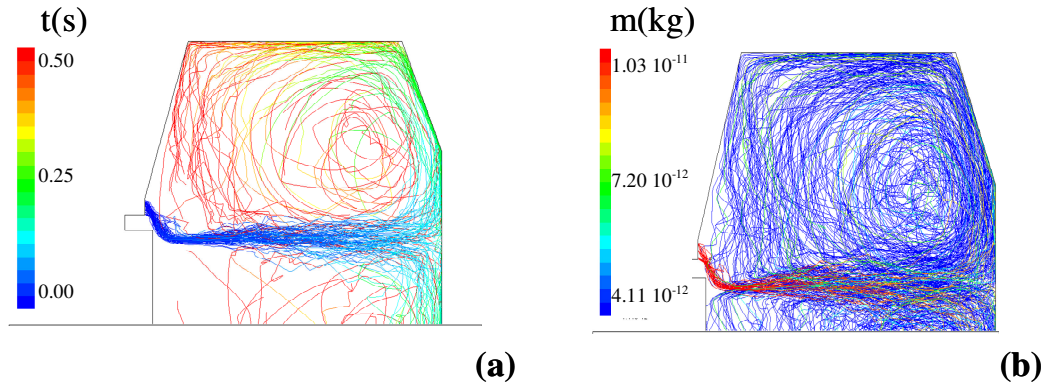


**Figure 3.3.16.** Simulated MD21 particles trajectories colored by (a) particle residence time and (b) mass.

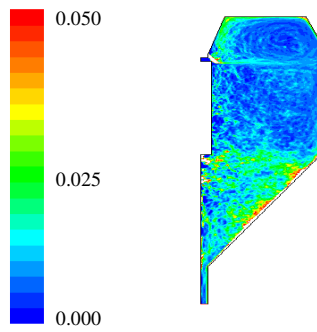


**Figure 3.3.17.** Simulated MD21 particles concentration inside the spray dryer chamber.

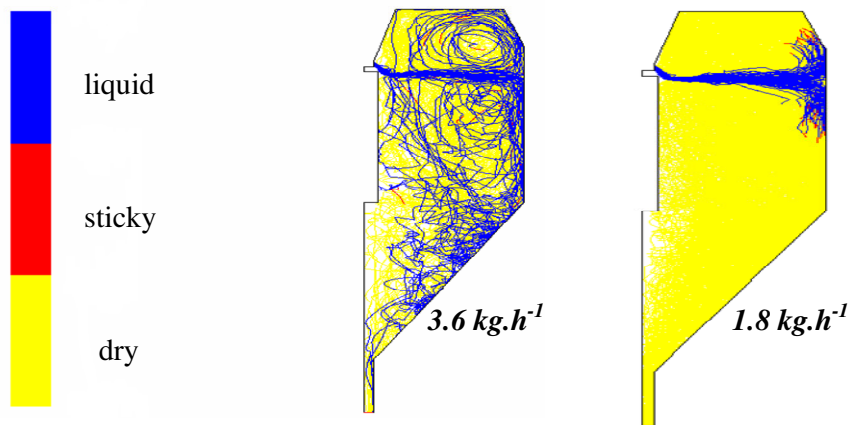


**Figure 3.3.20.** Calculated particle sticky behavior inside the chamber from simulation of spray drying of maltodextrin DE21 solution. (liquid feed: (a)  $3.6 \text{ kg.h}^{-1}$  and (b)  $1.8 \text{ kg.h}^{-1}$ ; air:  $129^\circ\text{C}$ ,  $110 \text{ kg.h}^{-1}$ ).

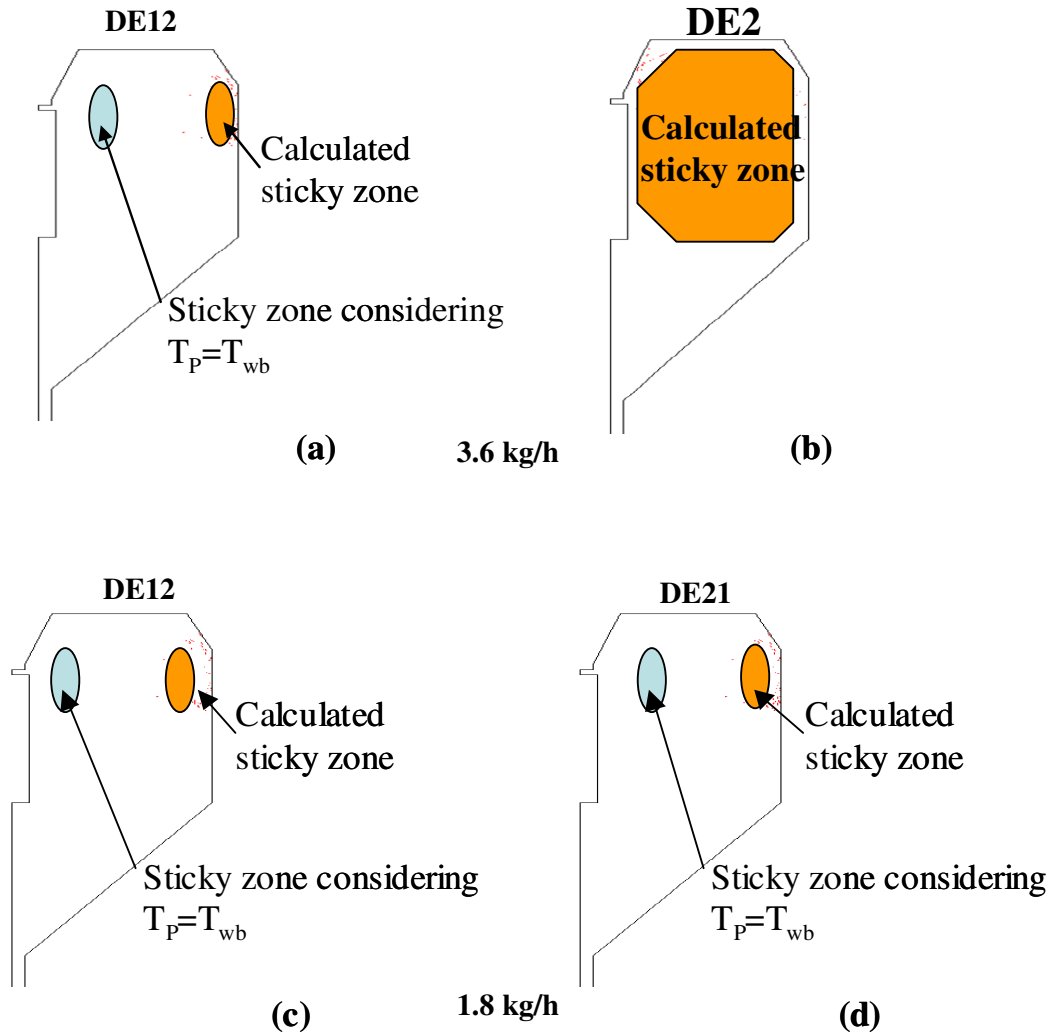


**Figure 3.3.21.** Calculated sticky zones inside the chamber from simulation of spray drying of (a) maltodextrin DE12 solution ; (b) maltodextrin DE21 solution (liquid feed:  $3.6 \text{ kg}\cdot\text{h}^{-1}$ ); (c) maltodextrin DE12 solution; (d) maltodextrin DE21 solution. (liquid feed:  $1.8 \text{ kg}\cdot\text{h}^{-1}$ ; air:  $129^\circ\text{C}$ ,  $110 \text{ kg}\cdot\text{h}^{-1}$ ).

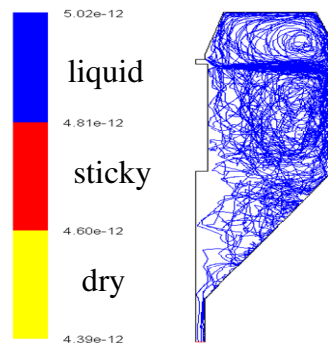


**Figure 3.3.22.** Calculated particle sticky behavior inside the spray dryer chamber from simulation of spray drying of maltodextrin DE21 40% w/w solution. (liquid feed:  $5.4 \text{ kg}\cdot\text{h}^{-1}$ ; air:  $129^\circ\text{C}$ ,  $110 \text{ kg}\cdot\text{h}^{-1}$ ).

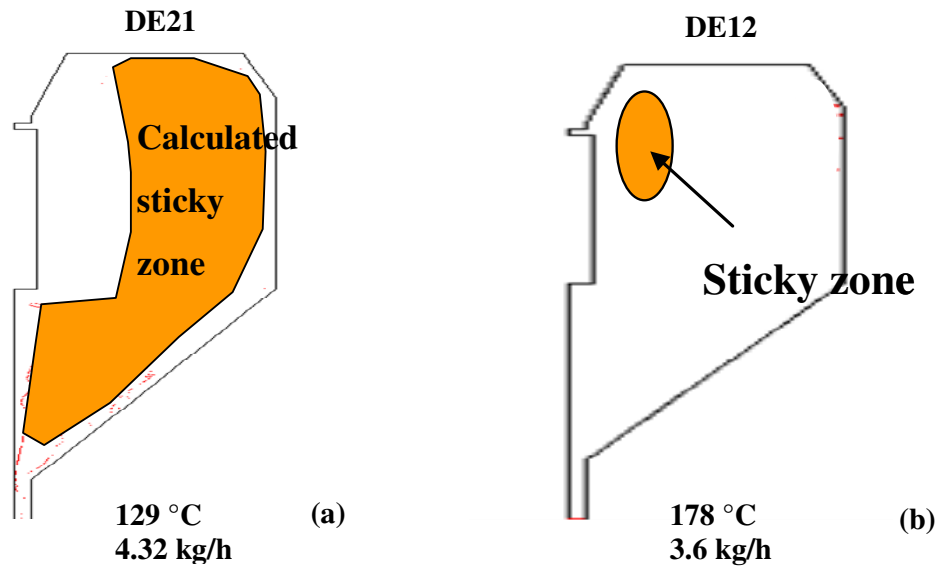


**Figure 3.3.23.** Calculated sticky zones inside the chamber from simulation of spray drying of (a) maltodextrin DE21 solution. (liquid feed:  $4.32 \text{ kg}\cdot\text{h}^{-1}$ ; air:  $129^\circ\text{C}$ ,  $110 \text{ kg}\cdot\text{h}^{-1}$ ) (b) of maltodextrin DE12 solution. (liquid feed:  $3.6 \text{ kg}\cdot\text{h}^{-1}$ ; air:  $178^\circ\text{C}$ ,  $110 \text{ kg}\cdot\text{h}^{-1}$ ).



## **Conclusion**

A numerical CFD simulation of the spray drying of maltodextrin DE12 and DE21 aqueous solutions in the NIRO spray dryer was performed at steady state.

Several hypotheses were made on the geometry of the chamber and on air and product properties. In particular water diffusion from particle core to its surface was not taken into account when drying solutions. But, to simulate the lower drying rate in this case compared to free water, the drop water vapour pressure was decreased by multiplying the saturating water vapour pressure by a coefficient  $x$ . This coefficient was determined in order to adjust calculated air temperatures values to experimental values in a reference situation.

The model was validated on different drying conditions (air inlet temperature and liquid flow rate), and results of simulation were in agreement with experimental values for air temperatures and relative humidity and for final powder water content.

Simulation allowed obtaining further information not acquired by direct measurements, especially on air flow pattern and drying particles properties evolution. Air recirculations zones were put in evidence, mainly above the atomization zone. These recirculations helped to understand the homogenization of air temperatures.

Particle water content evolution could be followed inside the chamber, and from these results the evolution of particle glass transition and sticky temperatures could be calculated. The time gap and the positions for which each particle had a temperature between glass transition and sticky temperature were determined, leading to the identification of possible sticky zones inside the spray dryer.

It appeared that MD12 was quickly dried below glass transition in the upper part of the chamber, while MD21 could exhibit a sticky behaviour in a wider part of the chamber depending on the liquid flow rate. These results were in agreement with the experimental prediction of possible sticky zones. They will be tested during powder insertion trials in the next part.

However, particle temperature was over-estimated, probably due to the choice of the low drop water vapour pressure. In simulation the evaporation occurred at a constant high temperature superior to the drying air wet bulb temperature and to the measured temperature of final powders. As a consequence, drying particles could be considered in the prediction as liquid or sticky for a longer time compared to reality.

Furthermore we did not take into consideration the fact that liquid or sticky particles could remain stuck on chamber walls.

In conclusion, the simplified CFD simulation approach allowed a correct calculation of air properties evolution which could help to predict possible stickiness during drying of an aqueous solution. Some experimental data are necessary especially for adjusting the coefficient for vapour pressure, which is specific of the considered drying material.



## 4. Powder insertion inside NIRO Minor to perform agglomeration

The objectives were to verify predicted sticky conditions during maltodextrin DE12 and DE21 solutions drying and to use them to obtain particles agglomeration inside the spray dryer chamber. Agglomeration could modify some end-use properties of produced powder, and in particular it could improve flowability and wettability.

Experiments required developing a specific powder insertion system allowing inserting powder at different positions inside the chamber.

### 4.1. Theoretical considerations: factors affecting agglomeration inside spray dryer

We consider as agglomerate a structure formed by several particles bound together, in which the single particles could still be identified.

Agglomeration inside the spray dryer chamber requires collisions between two or more particles followed by adhesion between their surfaces. In this way, stable solid bridges between particles are created, leading to formation of a new bigger structure (agglomerate).

Collisions between particles are forced by inserting particles inside the chamber to impact the drying drops/particles.

The extent of agglomeration and the structure of obtained agglomerates depend on several factors as:

- **Stickiness of colliding particles:** at least one of the colliding particles should have a sticky surface to have adhesion.
- **Collision probability:** it depends on possible collision area between inserted particles and drying drops, and on particle/drop density in this area.
- **Force of the impact:** it could affect the final structure of the agglomerates (more or less compact) or lead to a result different from agglomeration as coalescence (one final particle) or rebound.

The operating conditions, the powder insertion position and the nature of drying and inserted particles will determine the collision efficiency and the result of collisions.

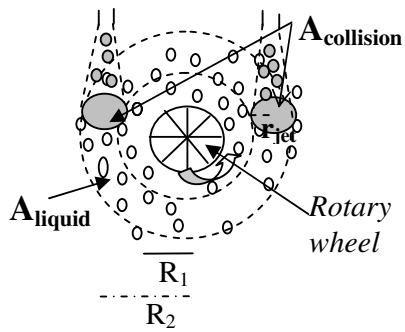
#### 4.1.1. Stickiness of colliding particles

Agglomeration requires collisions between a sticky particle and another dry or sticky particle. A particle is considered as sticky if its surface is in the domain defined by  $a_w$ ,  $T_g$ ,  $T_{sticky}$  (Fig. 3.2.9). Above  $T_{sticky}$ , the particle can still be considered as liquid, while below  $T_g$  it is considered as dry and no more sticky.

In our study, the sticky particles needed for agglomeration are the particles that are drying inside the chamber, with insertion of dry (non-sticky) particles. Another possibility should be to heat up and/or humidify the inserted particles (e.g. by use of steam) so that they could become sticky inside the chamber.

During experimental study and CFD simulation, possible sticky conditions for maltodextrin DE12 and DE21 solutions along drying were proposed. Maltodextrin DE12 was found to be sticky only close to the atomizer, while maltodextrin DE21 could exhibit a sticky behaviour in *Zone I* (upper part of the chamber, between atomizer and point A) or below for specific drying conditions (air 144°C; liquid flow rate 3.6 (experiments) - 4.32 kg.h<sup>-1</sup>(simulation)).





Surface crossed by sprayed drops ( $A_{liquid}$ )

$$A_{liquid} = \pi(R_2^2 - R_1^2)$$

Surface crossed by inserted powder jet ( $A_{collision}$ )

$$A_{collision} = n^0 \text{ powder insertion} \times (\pi r_{jet}^2)$$

Fraction of spray in collision area

$$\text{Collision area \%} = (A_{collision}/A_{liquid}) * 100$$

**Figure 3.4.1.** Possible collision area between drying particles and inserted particles.

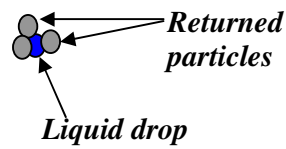


**Figure 3.4.2.** Possible collisions between a drying drop and several returned particles when ratio between inserted powder and drying particles is high in possible collision zone.

We should note that if the liquid spray has a large size distribution, the smallest droplets could be dried faster than the bigger ones, so that a fraction of the drying particles could already be too dry to be sticky at the moment of collision. In this case, collisions between dry particles would result in rebound without agglomeration.

On the other side, some particles could still be in the liquid state. Collisions between a liquid particle and another liquid particle or a dry particle would result respectively more in coalescence or covering than in agglomeration.

#### **4.1.2. Collision probability between drying particles and inserted particles**

The extent of possible agglomeration inside the spray dryer is limited by the collision probability between the inserted particles and the drying particles. In fact, only a part of the particles inside the chamber can be reached by the inserted particles depending on insertion device (local or symmetrical), on position and on drops/particle density.

Considering two vertical powder jet injections above the liquid spray (ejected horizontally from rotary wheel), the possible collision area between inserted particles and drying drops could be represented as on Figure 3.4.1.

The closer the particle injection to the rotary wheel, the bigger would be the fraction of liquid spray that could come in contact with the inserted particles.

Collision probability depends also on particles/drops number density in the possible collision area. Increasing the liquid feed and/or the inserted powder flow rate would result in a higher particle number density in the collision zone, leading to a higher collision probability.

The higher the ratio between inserted particle flow rate and drying drops flow rate, the higher is also the probability that an atomized particle could be reached by several (returned) particles, so that a “grape” structure could be formed (one particle surrounded by more than two other particles, Fig. 3.4.2).

Drying drops density is maximal close to atomizer, where all the liquid drops are concentrated in a small volume fraction. Fines particles should then be inserted immediately close to the atomizer to maximize collision probability (like usually done in industrial practice), together with the fact that drying drops are not yet too dry to be sticky.

Agglomeration probability would also be increased by returning the same particles several times, until reaching a critical size for which it can be considered as agglomerate. In this case, some sieving/classification of produced powder should be necessary.

#### **4.1.3. Force of the impact between particles**

The force of the impact may also affect the strength of the link created between particles, and so the kind of structure formed.

Depending on powder insertion position, collision energy could be different. Inserted particles have a kinetic energy  $E_K$  that depends on their mass and their velocity. In pneumatic conveying particle velocity can be assumed as equal to the velocity of the transport compressed air  $v_{\text{transportAir}}$ , and independent from the insertion position inside the chamber:

$$E_k = \frac{1}{2} m v^2 = \frac{1}{2} m (v_{\text{transportAir}})^2$$

But the kinetic energy of drying particles inside the chamber would depend on position inside the chamber. Their velocity would vary between a maximum value corresponding to the rotary wheel peripheral velocity ( $\sim 70 \text{ m.s}^{-1}$  for a rotary speed of 30000 rpm) immediately close to atomizer where drops are formed and a minimum value corresponding to the minimal velocity of the particles assumed to be equal to air speed inside the chamber ( $\sim 1 \text{ m.s}^{-1}$ , in NIRO Minor). So kinetic energy of drying particles will vary between

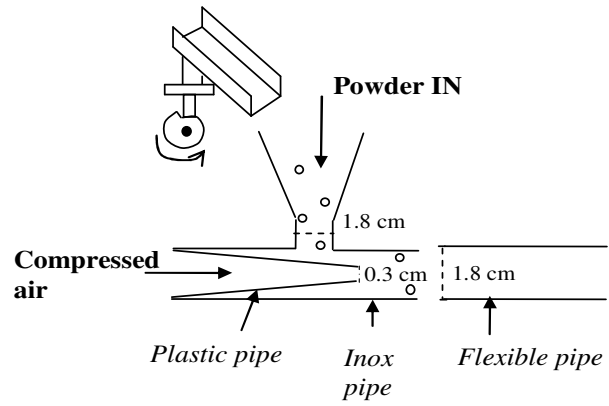


**Figure 3.4.3.** Powder insertion device.

### Part III – Results and discussion

$$\begin{aligned} E_{k,\max} &= \frac{1}{2} m (70)^2 && \text{immediately close to atomizer} \\ E_{k,\min} &= \frac{1}{2} m (1)^2 && \text{inside the chamber} \end{aligned}$$

So that  $E_{k,\max} = 4900 E_{k,\min}$

The collisions with drying particles of high kinetic energy (e.g. close to atomizer) could more likely lead to coalescence between particles. If coalescence (or covering) occurs, the resulting size enlargement would be small. Considering a median diameter for liquid drops of 25  $\mu\text{m}$  ( $\rightarrow V_{\text{drop}} = 8.18 \cdot 10^{-15} \text{ m}^3$ ), coalescence between two liquid drops should give a final diameter of 31.5  $\mu\text{m}$ :

$$\begin{aligned} V_{\text{tot}} &= V_1 + V_2 = 8.18 \cdot 10^{-15} + 8.18 \cdot 10^{-15} = 16.36 \cdot 10^{-15} \text{ m}^3 \\ d_{\text{drop}} &= ((6 V_{\text{tot}})/\pi)^{1/3} = 31.5 \mu\text{m} \end{aligned}$$

If the new formed particles were returned again inside the chamber with coalescence with another liquid drop (25  $\mu\text{m}$ ) and so on, 75 collisions would be necessary to reach a final diameter of 100  $\mu\text{m}$ .

So coalescence of a fraction of the spray would result in a small variation of final powder size distribution. Also instant properties would not change significantly, as powder smaller than 50  $\mu\text{m}$  is usually considered as “fine”, with poor instant properties.

## 4.2. Powder insertion system

Taking into account the described factors affecting agglomeration, powder insertion trials performed in NIRO Minor required:

- The **development of a specific powder insertion device**, to introduce powder inside the chamber in a controlled way.
- The **choice of the insertion positions inside the chamber**, depending on drying particles stickiness and affecting contact efficiency.
- The **choice of operating conditions**, as drying parameters and inserted powder kind and flow rate. They determine possible drying drops stickiness and particles/drops number density (collision probability).

### 4.2.1. Design of powder insertion device

A specific powder insertion device was designed in order to introduce a desired amount of powder in a continuous flow, inside the spray dryer chamber (Fig. 3.4.3).

Powder was manually inserted on a vibrating plate to be continuously introduced into a funnel at the bottom of which it was transported by compressed air inside the chamber (Venturi effect). With this system, a regular powder flow rate could be sent into the chamber. Pipes diameter was chosen as small as possible in order to guarantee a high air velocity (better sucking effect) but not too small in order to avoid blockage of the system by powder. Some ambient air was introduced with powder, and the total air (cold compressed air and ambient air) entering with powder could modify the drying behaviour of liquid drops inside the chamber. This was taken into account by increasing inlet hot air temperature. This secondary air (ambient + compressed) flow rate was measured and fixed between 7-10  $\text{kg}\cdot\text{h}^{-1}$ , the minimal amount to guarantee good powder flowing.

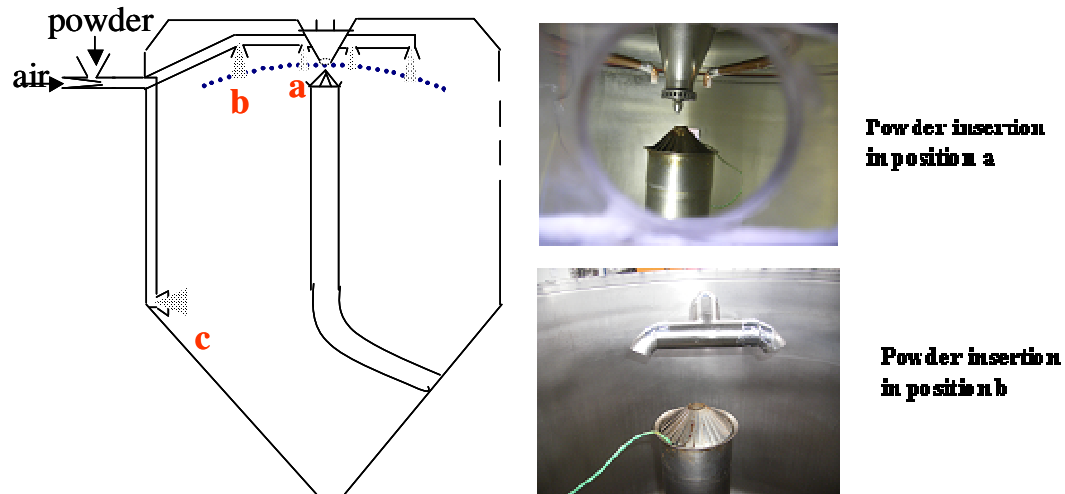


**Figure 3.4.4.** Powder insertion positions inside the chamber of NIRO Minor  
a: above spray close to atomizer in two symmetrical points;  
b: above spray far from atomizer (*Zone I*) in two symmetrical points;  
c: in the middle of the chamber in one point.

#### 4.2.2. Choice of insertion positions and powder jet shape

Pipes for powder insertion entered into the chamber by the side window, and powder was inserted in the chamber in three different positions (3 different experiments) (Fig. 3.4.4): above the liquid spray close to atomizer (position a), in the upper part of the chamber (*Zone I*) (position b), and in the middle of the chamber (position c). These choices were done in order to test the effect of insertion position on final powder properties.

In position (a) drop density is high leading to a high collision probability. Atomized drops should still be in a liquid state, and their velocity is close to the rotary wheel peripheral speed, leading to high impact energy. In this position coalescence or covering of the inserted particle was more likely to occur than agglomeration.

In position (b) impact energy and drying particle density would be lower. Drying particles of maltodextrin DE21 should be in the sticky state, so that this position should be favorable for agglomeration. Maltodextrin DE12 particles should be already too dry to be sticky, so that no agglomeration (or small fraction) was expected.

In position (c) no agglomeration was expected when drying maltodextrin DE12, whilst maltodextrin DE21 particles might still be sticky (high liquid flow rate).

Powder was inserted as a “cloud” obtained with a cylindrical pipe exit (cloud observed outside the chamber). Two different diameters for insertion pipes were tested (1 and 3cm), as the shape of powder cloud could also affect the efficiency of contact modifying the possible contact area between inserted particle and particle inside the chamber. The smallest pipes led to a more narrow jet of powder, with higher particle number density at the exit but with smaller powder dispersion inside the chamber.

In positions **a** and **b**, powder was inserted in two symmetrical points to increase collision probability. In preliminary trials we also tried to insert the powder close to the atomizer (position **a** in Fig. 3.4.4), but below the rotary wheel. In this case it was more difficult to install the powder insertion pipe inside the chamber, with a lower accuracy in determining the powder insertion position; furthermore with this system insertion was done just in one point. For these reasons insertion in position **a** below the wheel was not used in following trials.

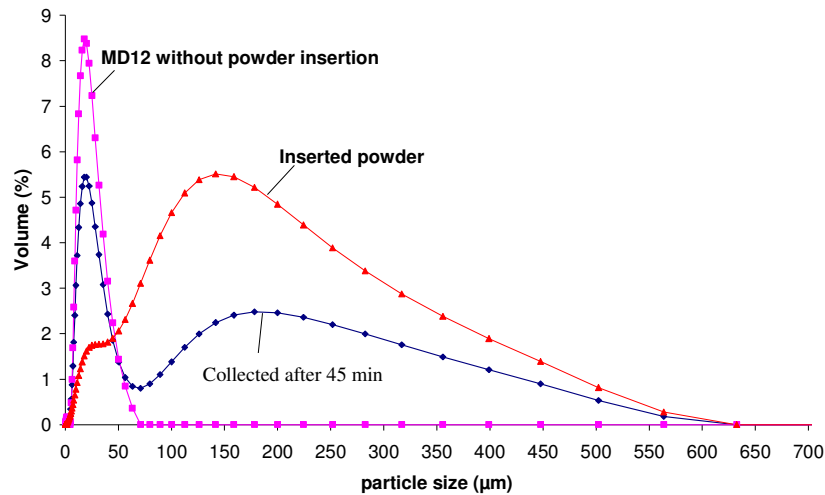
#### 4.2.3. Choice of operating conditions

Powder insertion trials were performed during drying of maltodextrin solutions in conditions where particles were found to have a sticky behaviour inside the chamber. Spray drying operating parameters were:

- Liquid feed: maltodextrin DE12 and DE21 solution (40% w/w), 3.6-4.23 kg.h<sup>-1</sup> (24-28.8 g.min<sup>-1</sup> of solids).
- Drying air: 110 kg.h<sup>-1</sup>, 149°C

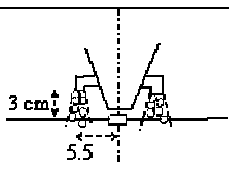
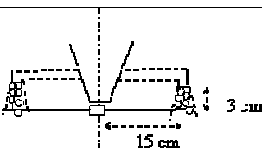
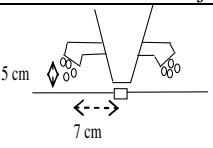
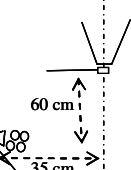
Air temperature was raised up to 149°C (compared to usual 144°C) to compensate the effect of the insertion of cold air (ambient + compressed) with inserted powder. In this way air temperatures measured inside the chamber were the same that temperatures measured during trials without fines return (similar drying behavior).

In these drying conditions we determined that maltodextrin DE12 was sticky only immediately close to atomizer (position **a**), while maltodextrin DE21 should be sticky in a wider part of the chamber.



**Figure 3.4.5.** Evolution of particle size distribution due to powder insertion in spray dryer: MD12 before powder insertion, MD12 powder inserted (position **b**) and powder collected after 45 min of powder insertion.

**Table 3.4.1.** Conditions for powder insertion trials with maltodextrin 40 % w/w solutions (Inlet air: 149°C, 110 kg.h<sup>-1</sup>; secondary air: 23°C, 7 kg.h<sup>-1</sup>; liquid feed: 3.6 and 4.23 kg.h<sup>-1</sup>; insertion ≈ 50% of collected powder).

<i>Insertion position</i>	<i>Powder insertion</i>	<i>Comments</i>
<p><b>a</b> Close to atomizer</p>	 <p>-) Cylindrical pipe (d=1cm) exit, vertical insertion → Narrow jet.</p>	<p>Two points for insertion</p> <p>High drop density</p> <p>High impact energy</p> <p>Small insertion pipes → small collision area</p> <p>Atomized drop still liquid</p>
<p><b>b<sub>1</sub></b> Zone I</p>	 <p>-) Cylindrical pipe (d=1cm) exit, vertical insertion → Narrow jet.</p>	<p>Two points for insertion</p> <p>Stickiness expected for MD21; MD12 already too dry</p> <p>Small insertion pipes → small collision area</p>
<p><b>b<sub>2</sub></b> Zone I</p>	 <p>-) Cylindrical pipe (d=3cm) exit, 45° inclination → wide “cloud”.</p>	<p>Two points for insertion</p> <p>Stickiness expected for MD21; MD12 already too dry</p> <p>Large insertion pipes → wide collision area</p>
<p><b>c</b> Middle of chamber</p>	 <p>-) Oriented horizontally.</p> <p>-) Cylindrical pipe exit (d=3cm) → wide “cloud”</p>	<p>Single point for insertion</p> <p>Low particles number density</p> <p>Particles already too dry to be sticky?</p>

### ***Choice of powder to insert***

During drying of maltodextrin DE12, insertion of a powder of the same nature that drying solution (maltodextrin DE12) but with a different size distribution (bigger particles) was initially performed. The resulting powder had a size distribution in between the size distribution of inserted powder and the size distribution of powder dried without powder introduction. It was not possible to determine if differences in measured particle size distribution were due to agglomeration or just to powder mixing (Fig. 3.4.5).

For this reason in further trials, inserted powder was the powder produced during the drying trial (powder recycling).

Powder was regularly collected once the collecting jar was full (usually each 5 to 10 minutes, depending on liquid and powder flow rate), and half of the collected powder was then reinserted inside the chamber during the next 5 to 10 minutes; the other half was used for powder analysis. This way of operating was chosen in order to simulate continuous recycling and led to an increasing returned powder flow rate.

### ***Procedure for powder insertion***

Usual development of a powder insertion trial was the following:

- Steady state for air temperatures inside the chamber was reached with spray drying of water and then maltodextrin solution without powder insertion but with the introduction of compressed air of insertion device.
- Powder samples were collected once the collecting jar was full (about 5 min), and half of each sample was returned inside the chamber during the next 5 minutes.
- Powder insertion was performed during 60 to 90 minutes.
- If drying conditions had to be changed, powder insertion was stopped and at least 30 minutes of running were performed with the new operating parameters before starting again powder insertion.

The four tested conditions for powder insertion trials in NIRO Minor are summarized in Table 3.4.1. with some comments for each case.

## **4.3. Results of powder insertion trials**

### ***4.3.1. Size enlargement observations***

Increasing the inlet air temperature to 149°C when returning powder, instead of 144°C without powder return, led to similar measured air temperatures inside the chamber (Fig. 3.4.6), thus it seems to allow keeping the same drying behaviour despite the cold secondary air entrance.

As expected, when drying maltodextrin DE12 no size enlargement could be observed in any tested condition. For maltodextrin DE21 some agglomeration could be obtained and results are given in Table 3.4.2.

Size enlargement became observable after 15-20 minutes of powder recycling. Mean diameter  $d_{4,3}$  increased until reaching a maximum stable value after 45-50 minutes of running.

For trials without powder insertion, a maximum of 3% of final powder was bigger than 100  $\mu\text{m}$ , probably due to recover of powder stuck on chamber walls or to spontaneous agglomeration due to collisions caused by air turbulence. Powder recycling led to an average particle size increase, with a larger fraction of powder having a diameter bigger than 100  $\mu\text{m}$ .

The agglomerated fraction (eg. particles > 100  $\mu\text{m}$ ) depended on insertion position and liquid/powder flow rate, and it varied from 3% up to 16% of total powder volume. It was maximal when recycling powder in *Zone I* using large pipes ( $b_2$ ), or in the middle of the chamber with the highest atomized liquid flow rate.



**Table 3.4.2.** Size of collected powder for spray drying of MD21 solutions (40% w/w) without and with powder insertion ( $T_{IN}$  149°C, air flow rate 110 kg.h<sup>-1</sup>, final sample).

<i>Position of powder insertion</i>	$\dot{m}_1$ (kg.h <sup>-1</sup> )	<i>Fraction &gt; 100µm</i>	$d_{10}$ (µm)	$d_{50}$ (µm)	$d_{90}$ (µm)	$d_{4,3}$ (µm)	$d_{3,2}$ (µm)
No insertion	3.60	2-3%	10	24	56	34	16
No insertion	4.23	2-3%	10	21	58	33	15
<b>a</b> Close to atomizer	3.60	3%	11	23	54	34	16
	4.23	8%	12	25	89	42	22
<b>b<sub>1</sub></b> Zone I	3.60	5%	11	22	50	34	16
	4.23	8%	11	24	85	42	17
<b>b<sub>2</sub></b> Zone I (big pipes)	3.60	8%	11	25	82	42	18
	4.23	16%	11	25	120	47	17
<b>c</b> Middle of the chamber	3.60	9%	11	26	94	43	17
	4.23	15%	12	29	133	55	20

**Table 3.4.3.** Properties of collected powder and of the fraction bigger than 100µm (MD21 solutions (40% w/w),  $T_{IN}$  149°C, air flow rate 110 kg.h<sup>-1</sup>, solution flow rate 3.60 kg.h<sup>-1</sup>, final sample).

<i>Insertion position</i>	<b>X</b> (g water.100g <sup>-1</sup> solids)		<b>a<sub>w</sub></b>		<b>Wettability</b> (s)	
	total powder	fraction >100 µm	total powder	fraction >100 µm	total powder	fraction >100 µm
No powder insertion	6.11	-	0.31	-	400	-
<b>a</b> Close to atomizer	6.06	6.08	0.30	0.29	380	instant
<b>b<sub>1</sub></b> Zone I	5.65	5.55	0.29	0.29	315	instant
<b>b<sub>2</sub></b> Zone I (big pipes)	6.05	6.10	0.31	0.30	420	instant
<b>c</b> Middle of the chamber	6.12	5.53	0.33	0.29	450	instant

Due to the limited amount of agglomerated fraction in final powder, the properties of the whole collected powder (water content, water activity, density, wettability) were similar to the properties of powder obtained from trials without powder return (Table 3.4.3.).

After sieving, the final fraction of particles superior to 100  $\mu\text{m}$  was analyzed, showing a very good wettability ( $<1$  s) and flowability, so that we considered this part of the powder as “agglomerated fraction”. Non agglomerated powder had a wetting time superior to 5 minutes. On the photos of collected powder by electron scanning microscopy (SEM), particles bigger than 100  $\mu\text{m}$  appeared to be made of several small particles forming a “grape” structure (Fig. 3.4.8).

#### **4.3.2. Discussion on agglomeration**

Produced powder was continuously reinserted inside the chamber, but size enlargement for maltodextrin DE21 began after more than 15 minutes. This long time meant that part of collected powder had been reinserted several times inside the chamber, increasing the probability of collisions with sticky particles, with progressive enlargement. But previous particle residence time distribution trials (without powder insertion) showed that more than 20 minutes were necessary to see all the powder coming from previous drying conditions leaving the chamber.

The inserted maltodextrin DE21 powder had a water content inferior to 6.5% and a temperature of  $\sim 40^\circ\text{C}$  which represent conditions below glass transition and thus was not sticky (Fig. 3.2.9). The formation of an agglomerated fraction was then possible thanks to the stickiness of drying drops surface. The observed size enlargement confirmed the predicted stickiness of MD21 particles inside the chamber in the tested spray drying conditions. These powder insertion trials could be seen as a specific stickiness test.

Agglomeration was not possible during drying of maltodextrin DE12, as particles were already dried below glass transition close to the atomizer. In this case one possibility for agglomeration should be to introduce sticky particles, for example by using steam to heat up and humidify returned particles when entering inside the chamber.

The agglomerated fraction was in any case lower than 17% of the collected powder. A first reason could be that a fraction of the collected powder has never been returned inside the chamber. Furthermore powder insertion was localized in one or two points, which was limiting for the possible collision area between inserted powder and sticky drying particles.

In trials with powder insertion in positions a and b above the rotary wheel, the shape of the liquid spray could also limit the possible collision area. Actually, at the end of the trial some liquid solution was stuck on the transport pipes, suggesting that liquid spray was not only horizontally ejected from the rotary atomizer, but that it could have a wider shape with some drops going upward and therefore not entering the collision area. This could also be due to some dispersion caused by the drying air, which comes from below the wheel and can push upward the liquid drops.

Increasing the liquid feed from 3.6 to 4.23  $\text{kg}\cdot\text{h}^{-1}$  and consequently the returned powder flow rate, resulted in obtaining a bigger fraction of agglomerated powder for any insertion position (Table 3.4.2.), according to the higher particle density.

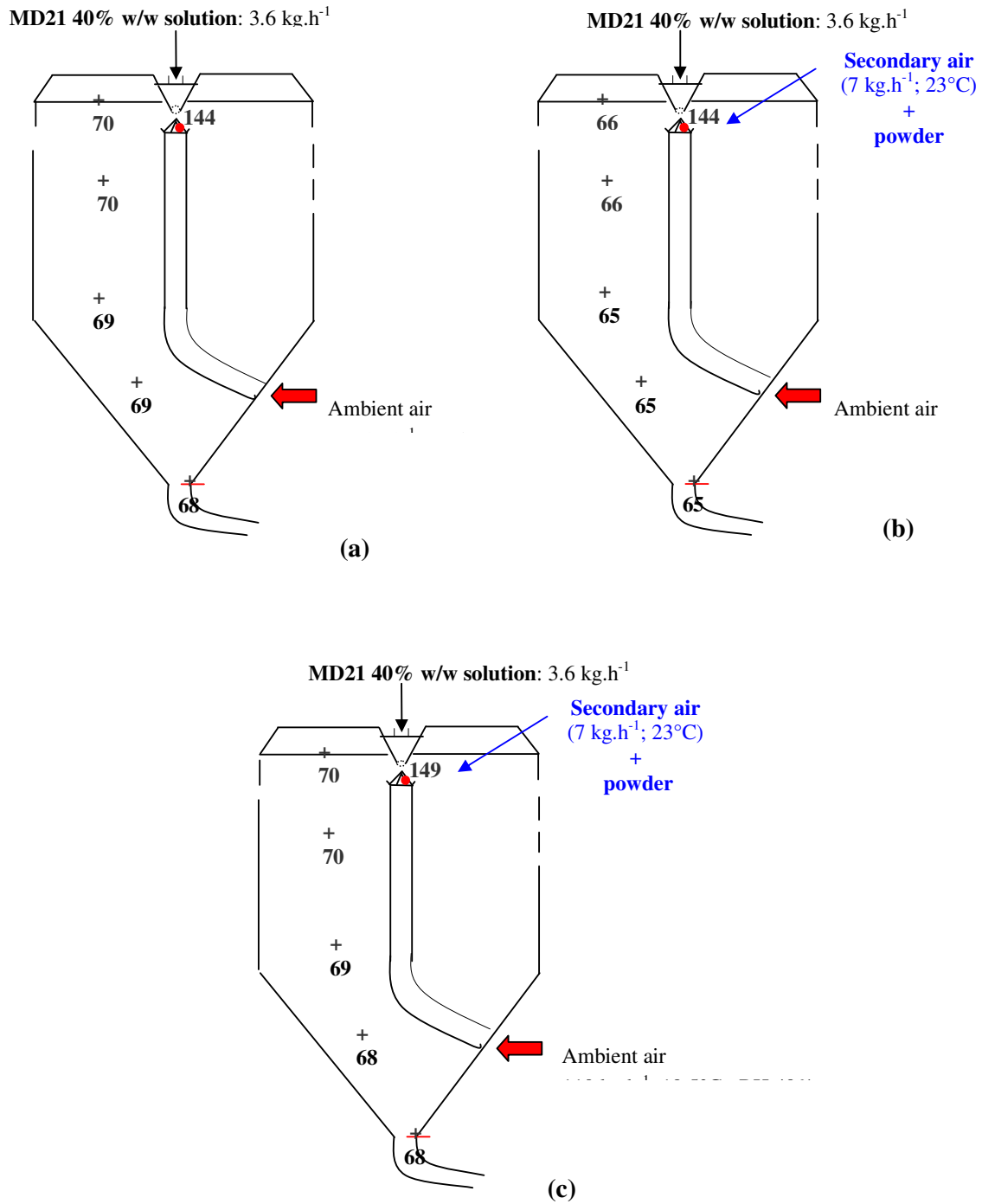


**Figure 3.4.6.** Comparison between measured air temperatures at steady state during drying of MD21 solution; (a) without or (b) with powder insertion and  $T_{IN}$  144°C; (c) with powder insertion and  $T_{IN}$  149°C (air flow rate 110 kg.h<sup>-1</sup>; liquid flow rate 3.6 kg.h<sup>-1</sup>; secondary air flow rate 7 kg.h<sup>-1</sup>).

The powder insertion position determined the contact probability between drying particles and inserted powder (collision area and particle number density) and the possible adhesion of colliding particles to form stable agglomerates (particle stickiness and impact energy).

When recycling close to the atomizer (position **a**), no powder enlargement was observed for a liquid flow rate of  $3.6 \text{ kg.h}^{-1}$ . Some size enlargement appeared only when increasing the liquid flow rate up to  $4.23 \text{ kg.h}^{-1}$  (8% of powder with  $d > 100 \mu\text{m}$ ). In this insertion position, contact probability was high (high drops density). But atomized drops were still liquid, and kinetic energy at the impact was high so that coalescence between returned powder particles and drops was more likely to occur with formation of a single particle with a similar diameter as the initial drop.

When recycling in *Zone I* far from atomizer (position **b**), a bigger size enlargement was observed: 5 to 16% of powder had a diameter higher than  $100 \mu\text{m}$ , depending on liquid flow rate and powder insertion pipes diameter (shape of powder jet, area of contact). In this case powder was returned in the upper part of the chamber, where drops surface could still be sticky but where drops are no more completely liquid. As a consequence, solid bridges could be formed at the surface of colliding particles, leading to agglomeration.

A bigger amount of agglomerated powder was obtained by using pipes with the bigger diameter of 3 cm. This caused a wider powder cloud, so that a bigger fraction of drying particles could be reached by the inserted powder.

When returning powder in the middle of the chamber (position **c**), a fraction of large particles varying between 9 and 15% was obtained. This showed that stickiness of maltodextrin DE21 was still possible in this position in the tested drying conditions. In this case, the amount of agglomerated powder was limited by the lower particle number density and by the fact that powder insertion was performed only in one point. Some recirculations inside the chamber could also help collisions with sticky drops in the upper part of the chamber. It should have been interesting to compare the mechanical resistance of the agglomerates obtained in different conditions.

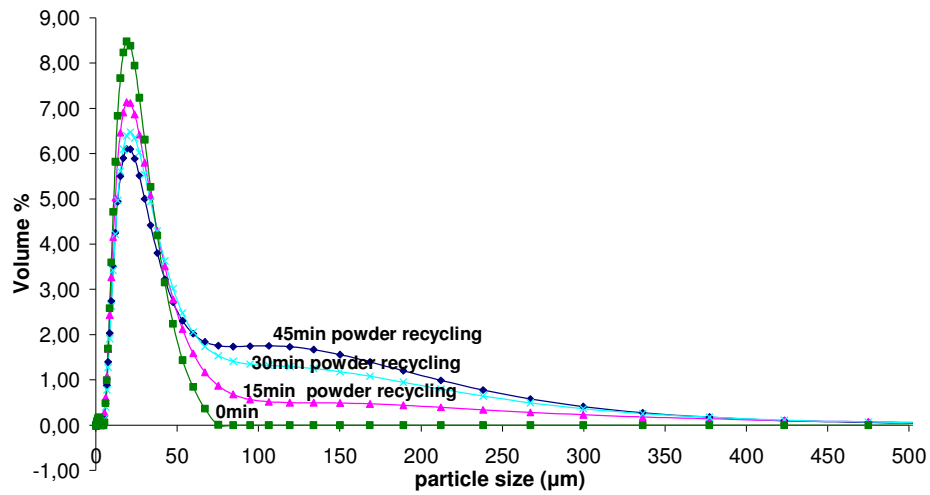


**Figure 3.4.7.** Particle size distribution of MD21 powder collected after 15, 30 and 45 minutes of powder insertion inside the chamber of NIRO Minor (return position  $b_1$ : Zone I; Solution flow rate  $4.23 \text{ kg}\cdot\text{h}^{-1}$ ).

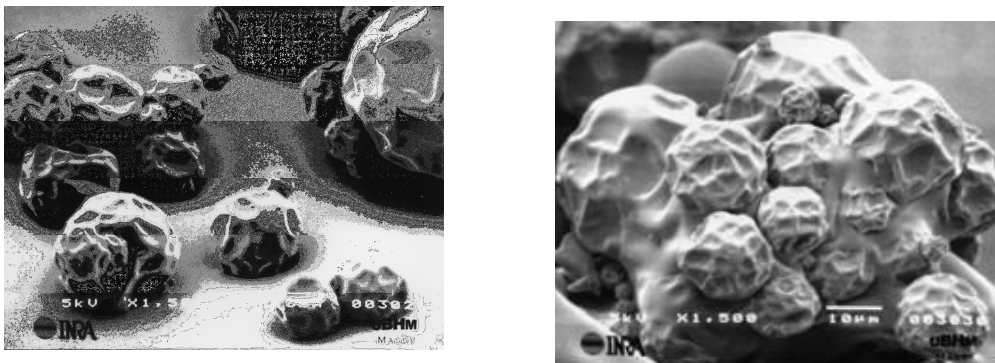


**Figure 3.4.8.** SEM photos of MD21 non agglomerated and agglomerated ( $> 100 \mu\text{m}$ ) particles.

## **Conclusion**

When drying maltodextrin DE12, no size increase was observed when inserting powder. This is in agreement with the predicted almost instant drying of MD12 solution below the sticky region.

When drying maltodextrin DE21, reinsertion of powder led to some agglomeration. The properties of the whole powder (water content, water activity, wettability) were not different from the properties of powder collected during trials without powder insertion. But a fraction up to 17% of final powder bigger than 100  $\mu\text{m}$  could be obtained, with good flowability and instant properties. In practice that means that in our case, particles may be reinserted several times until reaching a final desired size, but this increases the residence time with possible product degradation.

These results confirmed the predicted particle stickiness at given positions during drying of maltodextrin DE21 aqueous solutions inside the chamber, for the tested operating parameters. In industrial practice fines are usually inserted close to the liquid entrance, where the drops density is maximal. But we showed that this position was not the best for inserting powder with the objective of size increase, because the sprayed drops could still be in the liquid state. In this case collisions are more likely to give coalescence or particle covering, with small size enlargement.

The extent of size enlargement limited to 17% (particles bigger than 100  $\mu\text{m}$ ) was mainly due to the designed insertion device, limiting the collision probability between drying drops and returned particles. Furthermore according to the insertion position some liquid particles could already be too dry and/or some impact could result in coalescence.

Agglomeration could be certainly improved by modifying powder insertion so that a higher fraction of the liquid spray/drying particles could be reached by returned particles. A symmetrical regular insertion below (or above) atomizer wheel could be used. Final powder could also be sieved in order to recycle only the not agglomerated fraction, as sometimes done for fines return in industry.

**Table 3.5.1.** Fixed parameters during spray drying of protein hydrolysate solution in NIRO FSD 4.0.

Parameter	Value
Inlet drying air flow rate $\dot{m}_{air}$ (kg.h <sup>-1</sup> )	350
Total fluid bed air flow rate $\dot{m}_{air,fb}$ (kg.h <sup>-1</sup> )	100
Primary fluid bed inlet air temperature $T_{fb,1}$ (°C)	55
Secondary fluid bed inlet air temperature $T_{fb,2}$ (°C)	45
Nozzle compressed air pressure $P_{nozzle}$ (bar)	2.5
Pneumatic fines return transport air pressure $P_{finesRet}$ (bar)	2.5
Liquid feed temperature $T_1$ (°C)	70

**Table 3.5.2.** Studied parameters during spray drying of protein hydrolysate solution in NIRO FSD 4.0.

Sprayed liquid	$T_{IN}$ (°C)	Fluid bed	Fines return	$T_{OUT}$ (°C)
Water	180	No	Bottom	65 – 75
Protein hydrolysate solution	160	No	Top	70-75
		Yes		
	180	No	Top	75-80-88
			Bottom	80-88
		Yes	top	65-75
			Bottom	75-85
	200	No	Top	88
			Bottom	97
Yes		Top	80-88	

## 5. Industrial application: spray drying of protein hydrolysate

The objectives were to investigate the spray drying feasibility of a protein hydrolysate solution by varying several process parameters, observing the powder characteristics. The industrial requirement was to obtain powders with final water content  $X$  inferior to 5g water per 100g total solids and with good flowability.

To understand the drying behaviour of this new product we wanted to apply the previously described approach: measurements (T, RH) on drying air in the chamber and relation with product properties ( $X$ ,  $a_w$ ,  $T_g$ ) that are different from maltodextrin properties.

The two spray dryers (NIRO FSD 4.0 and NIRO Minor) are co-current dryers but they are different for several aspects:

- Evaporative capacity multiplied by 5 (up to 20 kg.h<sup>-1</sup>).
- Bi-fluid nozzle atomizer (instead of rotary), with vertical spray jet.
- Hot air inlet from the top of the chamber.
- Fines permanently returned, with pneumatic conveying (additional compressed air).
- Possible use of internal fluid bed (additional hot air flow rate).
- Total air exit from the top, resulting from the addition of inlet hot air, fluid bed air, compressed air (fines return, nozzle and nozzle cooling (Fig.2.2b)).

### 5.1. General conditions of trials

Studied parameters included drying air inlet temperature, liquid flow rate, use of internal fluid bed, and position of fines return in the chamber (top or bottom of chamber).

The sprayed liquid flow rate was controlled by imposing the outlet air temperature: for safety reasons, the exit air temperature should not be higher than 90°C. The higher the exit air temperature, the lower the sprayed liquid flow rate.

The fixed and variable parameters are given in Tables 3.5.1. and 3.5.2.

Measurements of air properties (temperature, relative humidity) were performed in the chamber, assumed to be representative of liquid drop drying.

### 5.2. Water drying without fluid bed: drying behavior and measurements feasibility

Two drying conditions with water were performed (without use of bottom fluid bed) to test the feasibility of air properties measurements (T, RH) in the chamber and as a reference for the drying conditions that will be used for solution drying.

Two liquid flow rates, 12 and 15 kg.h<sup>-1</sup>, were tested, corresponding respectively to air exit temperatures ( $T_{OUT}$ ) of 65 and 75°C for a drying air inlet ( $T_{IN}$ ) temperature of 180°C (Fig. 3.5.1a).

At point 4 (close to spray), the measured air temperature was of 69°C and 59°C for a water flow rate of respectively 12 and 15 kg.h<sup>-1</sup>. Further in the chamber (points 2 and 3), air temperatures were 3°C lower, and at point 5 they were respectively 8°C and 13°C lower. In the top of the chamber, close to the air exit (point 5), temperature was higher (74°C and 65°C respectively for the two water flow rates).

The high difference between 180°C ( $T_{IN}$ ) and the mean temperature inside the chamber (69°C and 59°C for 12 and 15 kg.h<sup>-1</sup>) was due to the quick drying when the hot air contacts the sprayed drops (point 4). The low temperature in the bottom of the chamber could also be due to the introduction of cold compressed air for fines return that could not be stopped (unknown



Part III – Results and discussion

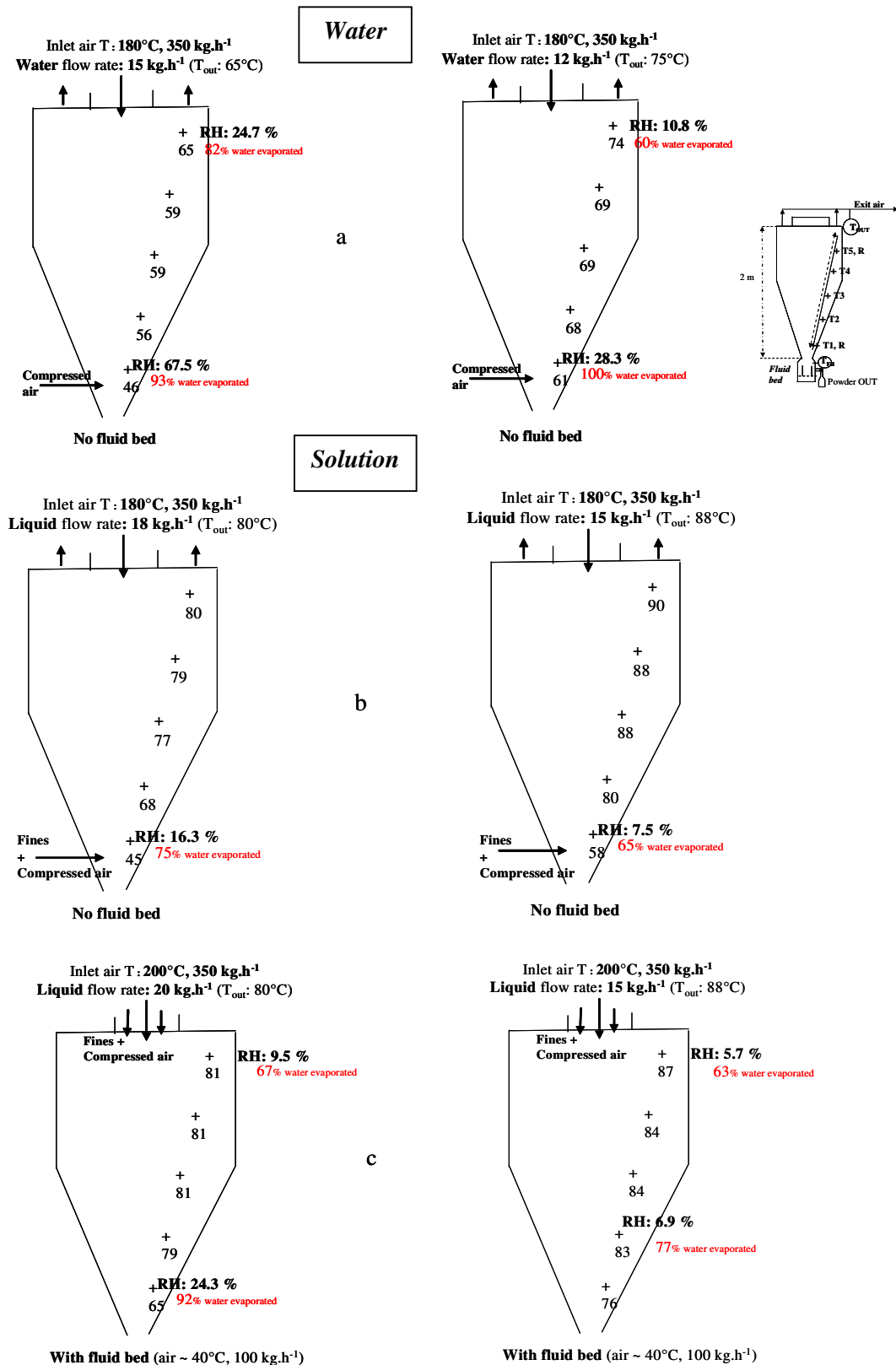


**Figure 3.5.1.** Air cartographies at steady state during water and protein hydrolysate solution drying  
 (a) Inlet air temperature 180°C; water flow rate 12 – 15 kg.h<sup>-1</sup>; no fluid bed;  
 (b) Inlet air temperature 180°C; liquid flow rate 15 – 18 kg.h<sup>-1</sup>; no fluid bed; bottom fines return;  
 (c) Inlet air temperature 200°C; solution 40% w/w; liquid flow rate 15–20 kg.h<sup>-1</sup>; + fluid bed; top fines return.  
 flow rate, but small).

The high temperature in the top, close to air exit, may be due to mixing of inlet hot air with cold humid air coming upwards (Fig 2.2.c).

Air relative humidity was measured at points 1 and 5. As expected, an increase of the water flow rate (12 to 15 kg.h<sup>-1</sup>) resulted in an increase of evaporated water and therefore of the air relative humidity: 10.8 to 24.7% for point 5 and 28.3 to 67.5% for point 1. A mass balance on water in air showed that 93% to 100% of water was evaporated in the bottom of the chamber. However, this calculation was done with the inlet air flow rate of 350 kg.h<sup>-1</sup> (measured at the entrance) not taking into account the effect of fines recycling compressed air and cooling air of nozzle entries. Values at point 5 should be considered carefully due to mixing with inlet hot “dry” air that could decrease the exit air total water content.

From water spray drying trial we could determine that measurements of air temperature and relative humidity inside the chamber were possible, but positions for measurements should be chosen carefully, taking into account air flow pattern inside the chamber that could lead to mixing of air. Furthermore the total air flow rate should be measured at the exit of the chamber in order to perform more accurate mass balances on water in air.

More generally, operating conditions for which we observed in the chamber low air temperature and high relative humidity could lead locally to drying problems when a real solution will be sprayed: sticking on walls, final powder too humid.

### 5.3. Protein hydrolysate solution drying trials feasibility

Operating conditions for all the spray drying trials of protein hydrolysate solution are reported in Table 3.5.3, together with the properties of the collected powder (when they could be measured).

#### 5.3.1. Drying trials for $T_{IN} 180^{\circ}C$

The main part of the study was performed for an inlet air temperature of 180°C, as suggested by a preliminary feasibility study made in Nestlé PTC for the considered product. For safety reasons, exit air temperature could not be higher than 90°C, corresponding to minimal liquid flow rate of 15 kg.h<sup>-1</sup> (corresponding to 9.5 kg.h<sup>-1</sup> of water to evaporate) at this inlet air temperature. Trials were performed with and without use of fluid bed, recycling fines at the top or at the bottom of the chamber. The exit air temperatures were between 65 and 88°C, for liquid flow rates between 23 and 15 kg.h<sup>-1</sup>.

Trials without fluid bed were performed in order to characterize the powder entering the possible fluid bed and to better understand the role of this fluid bed.

The solution flow rate was decreased from 20 to 15 kg.h<sup>-1</sup> corresponding respectively to 12.5 and 9.5 kg.h<sup>-1</sup> of water to evaporate and to exit air temperatures between 75 and 88°C. The highest liquid flow rate of 20 kg.h<sup>-1</sup> led to a “pasty” product which blocked the exit of the chamber. Desired specifications for powder moisture content could never be reached. Even for the lowest liquid flow rate of 15 kg.h<sup>-1</sup> powder moisture content was about 6 g water/100 g total solids. Use of fluid bed was then compulsory for reaching specifications.

Position of fines return affected the average size of recovered powder. Returning fines at the bottom of the chamber instead of top, led to particles with lower median diameters: 60 – 40 µm, compared to 90 – 70 µm when fines were introduced at the top (Table 3.5.3).

When using the fluid bed, powders ( $X < 8$  g water.100 g<sup>-1</sup> total solids) were obtained only when returning fines particles at the top of the chamber. Recycling fines at the bottom of the chamber led to a blockage of the fluid bed whatever the solution flow rate between 20 and

**Table 3.5.3.** Powder properties for protein hydrolysate solution spray drying in NIRO FSD 4.0

T <sub>IN</sub> (°C)	Fluid Bed	Fines return	T <sub>OUT</sub> (°C)	Liquid flow rate (kg.h <sup>-1</sup> )	X (gH <sub>2</sub> O/100gTS)	a <sub>w</sub>	d <sub>0,5</sub> (µm)	ρ <sub>bulk</sub> (g.ml <sup>-1</sup> )	ρ <sub>tap</sub> (g.ml <sup>-1</sup> )
180	No	Top	75	20.0 (12.5 water)	9.97 (“paste”)	//	//	//	//
			80	18.0 (12.0 water)	8.6	0.36	89	0.46	0.53
		88	15.0 (9.5 water)	6.2	//	74	0.58	0.64	
		Bottom	80	18.0 (12.0 water)	7.6	//	58	0.54	0.59
			88	15.0 (9.5 water)	6.5	0.27	41	//	//
	Yes	Top	65	23.0 (15.0 water)	8.03	0.28		0.40	0.44
			75	20.0 (12.5 water)	<u>5.7</u>	0.19	126	0.52	0.58
		Bottom	75	20.0 (12.5 water)	Fluid bed blocked	//	//	//	//
			85	16.0	Fluid bed blocked	//	//	//	//
	160	No	Top	70	16.2	Fluid bed Blocked	//	//	//
Top			75	14.8	6.8	0.29	67	0.58	0.64
Yes		Top	70	16.2	6.3	0.18	93	0.53	0.59
		<b>Top</b>	<b>75</b>	<b>14.8</b>	<b>5.15</b>	<b>0.19</b>	<b>96</b>	<b>0.51</b>	<b>0.57</b>
200	Yes	Top	88	15.0 (9.5 water)	4.6	0.20	99	0.54	0.58
		<b>Top</b>	<b>80</b>	<b>20.0 (12.5 water)</b>	<b>5.1</b>	<b>0.21</b>	<b>198</b>	<b>0.47</b>	<b>0.57</b>
	No	Top	88	15.0 (9.5 water)	Fluid bed blocked	//	//	//	//
		Bottom	97(too high)	//	//	//	//	//	//

16 kg.h<sup>-1</sup>. When compared with trials performed without fluid bed in the same conditions (solution flow rate 20 kg.h<sup>-1</sup>, exit air temperature 75°C, top fines return), the use of the fluid bed allowed decreasing the powder water content from 9.97 (“paste”) without fluid bed to 5.7 g water/100 g total solids (Fig. 3.5.2). And, without fluid bed the median particle size was inferior to 90µm whilst with the fluid bed it increased up to 126 µm. This indicates that size enlargement occurred with the use of the fluid bed, and SEM observations showed that particles were agglomerated (Fig. 3.5.3)

As a conclusion, with an inlet air T<sub>IN</sub> of 180°C, the required specification for final product moisture content (5%) could never be reached. Other inlet air temperatures (higher) and/or solution flow rates have to be tested, or lower flow rates should be used at 180°C.

The use of fluid bed associated with top recycling of fines seemed to help decreasing final moisture content of powders, and increasing final powder size.

Another comment is that the mean water content X and water activity a<sub>w</sub> of the “best” powders correspond to a position above the equilibrium sorption isotherm (Fig. 3.5.4a). Drying is a desorption process, leading to some hysteresis (curve above) compared to adsorption.

This isotherm was measured at 23°C for a product of the same type (composition may slightly vary). The shape of the sorption isotherm curve could suggest that some crystallization can occur (but unknown composition) when equilibrating the powder for measuring sorption isotherms, resulting in a lower water content for a given water activity.

Based on sorption isotherm, an average water content of 5% should correspond to a water activity of 0.5 and to a product above glass transition at ambient temperature (Fig. 3.5.4b), which thus should not be stable. However, the powders obtained with a measured water activity of 0.19 and water content of 5.7% were stored at ambient temperature during several months (T<sub>g</sub> ~ T<sub>amb</sub>) without observing any caking. This could be due to a different surface composition of particles with formation of a “crust” preventing particles from caking.

All these last comments on this complex product need some further verification/confirmation with other trials and measurements.

### 5.3.2. Effect of inlet air temperature (160°C and 200°C)

Use of drying air with higher inlet temperature (e.g. 200°C) should lead to lower water content for powder. As an important part of the cost of the spray drying process is due to the heating of air, it was interesting to test a lower inlet air temperature T<sub>IN</sub> of 160°C, and check the powder properties.

Trials with inlet air temperature of 160°C and 200°C were performed with fines return on top (that gave the best results during drying at 180°C), with and without the fluid bed.

For inlet air at 160°C, without using the fluid bed, even with the minimum tested liquid flow rate (14.8 kg.h<sup>-1</sup>, corresponding to an outlet temperature of 75°C), the collected powder was too humid (X = 6.8 g water.100 g<sup>-1</sup> dry matter) and increasing the atomized liquid flow rate to 16.2 kg.h<sup>-1</sup> resulted in the blockage of installation (powder caking at the exit of the chamber) (Table 3.5.3).

The use of the integrated fluid bed allowed reducing final powder moisture content almost until specification (5.1% for 14.8 kg.h<sup>-1</sup>). The use of fluid bed also led to higher average particle size (from 67 to 97 µm) as already observed for air at 180°C. However the powder median diameter was inferior to 100 µm (it was of 126 µm for 180°C with a 20 kg.h<sup>-1</sup> solution flow rate for the same exit air temperature (75°C)).

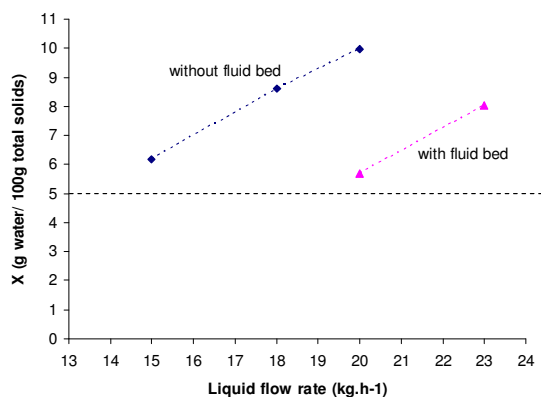


**Figure 3.5.2.** Final powder moisture content of protein hydrolysate powder as a function of liquid flow rate and effect of use of fluid bed (Inlet air temperature 180°C, top fines return).

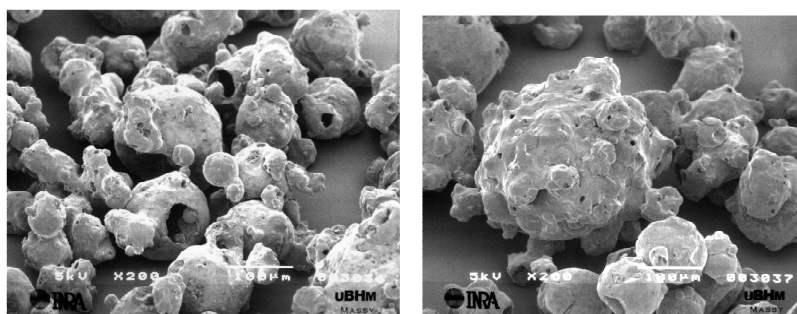


**Figure 3.5.3.** SEM photos of protein hydrolysate powder.

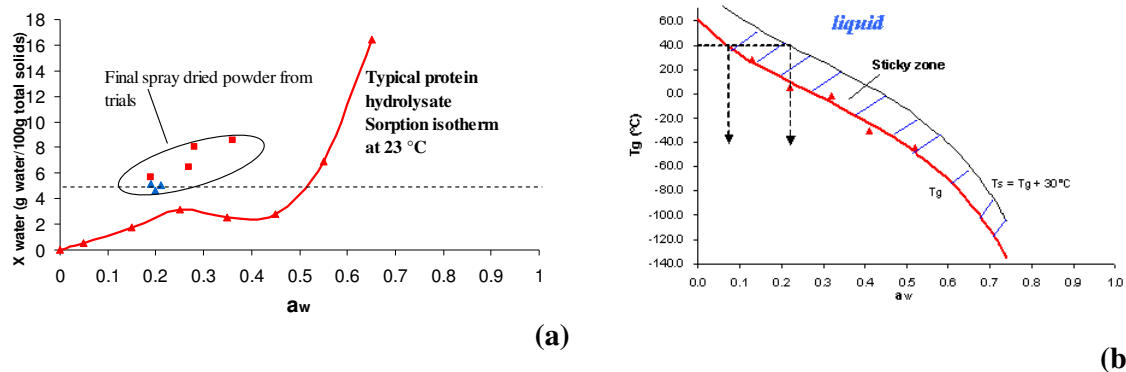


**Figure 3.5.4.** Typical sorption isotherm at 23°C and measured  $X, a_w$  on obtained powder (a); glass transition temperatures of protein hydrolysate powder as a function of water activity (b).

As a conclusion, with an inlet air temperature of 160°C, it was possible to obtain a dry powder almost within required specification by limiting the solution flow rate (<15 kg.h<sup>-1</sup>). Even in this case, use of fluid bed was compulsory to achieve specifications (as for 180°C). The average diameter of the powder was inferior to 100 µm (lower than for drying at 180°C).

For inlet air T<sub>IN</sub> 200°C, without fluid bed partial or complete blocking of the installation occurred due to strong adhesion of the powder on the walls of the outlet cone. To obtain a dry product within the required specification, the use of fluid bed was therefore necessary. In these conditions, solution flow rates up to 20 kg.h<sup>-1</sup> allowed getting powders with water content close to the specification of 5 g water.100 g<sup>-1</sup> dry matter. Higher liquid flow rates led to larger median particles diameters up to 200 µm for 20 kg.h<sup>-1</sup>.

## 5.4. Discussion about the drying behavior, the role of fines return and fluid bed during protein hydrolysate solution spray drying

### 5.4.1. Spray drying behavior: air properties evolution inside the chamber

Air cartographies (T, RH) at steady state (after 20 minutes of drying – T<sub>IN</sub> 180°C) without fluid bed for solution flow rates of 15 and 18 kg.h<sup>-1</sup> are given in Figure 3.5.1b.

Most of the observations made for water drying trials are still valid (big air temperature decrease of about 100°C due to fast water evaporation, then homogeneous temperatures (ΔT ~ 15°C between top and bottom) with possible air mixing inside the chamber and temperature decrease at point 1 due to fines return compressed air inlet).

Comparing the cartographies obtained when spraying water with those for the protein hydrolysate solution with the same water flow rate to evaporate (18 kg.h<sup>-1</sup> liquid solution and 12 kg.h<sup>-1</sup> of water), we can observe that the drying behavior was different (Fig. 3.5.1a and 3.5.1b). Even if the amount of water to evaporate was the same (12 kg.h<sup>-1</sup>), temperatures inside the tower were almost 10°C higher (points 3-4) in the case of protein hydrolysate solution drying, indicating that drying was slower. For hydrolysate solutions drying, only 75% of water was evaporated in the lower part of the chamber, compared to 100% for water drying (water mass balance on air). So the drying kinetics of hydrolysate solution were slower, due to water bound with dry matter inside the liquid droplets.

Cartographies for inlet air temperature T<sub>IN</sub> 200°C were obtained while using also the fluid bed (Fig. 3.5.1c). This results in an additional flow rate of 100 kg.h<sup>-1</sup> of hot dry air (T = 55°C and 45°C) that entered in the chamber from the bottom. As a consequence, measured air temperature and relative humidity inside the chamber resulted from a mixing of hot drying air, fluid bed drying air and secondary compressed air for fines return, nozzle air and cooling (unknown flow rate and temperature). This means that balances on evaporated water inside the chamber should be considered carefully, as calculated air water content comes from this mixing of air streams (not all known).

Due to the higher air temperatures inside the chamber (compared to trials with inlet air at 160°C and 180°C), drying particles could have a higher temperature at the chamber exit. The liquid was initially sprayed at 70°C, and it was then cooled down due to evaporation. In the first drying phase (free water evaporation, surface water activity equal to 1) surface temperature will be equal to the air wet bulb temperature (40-45°C for air at 160-200°C). After constant evaporation rate phase, the particle will be heated until possibly reaching the surrounding air temperature (upper limit). Assuming thermal equilibrium in the bottom of the chamber between air and particle, when drying at 200°C, particles should enter the fluid bed with a temperature of 65-75°C (compared to 45-60°C when drying at 180°C).

This different temperature could affect particle behaviour (stickiness) inside the fluid bed.

**Table 3.5.4.** Powder properties at the exit of fluid bed for different inlet drying air temperatures.

<i>Inlet air <math>T_{IN}</math></i> (°C)	<i>Fines return</i>	<i>Exit air <math>T_{OUT}</math></i> (°C)	<i>Liquid flow rate</i> ( $\text{kg}\cdot\text{h}^{-1}$ )	<i>X</i> (g/100g solids)	<i>a<sub>w</sub></i>	<i>d<sub>50</sub></i> ( $\mu\text{m}$ )
160	Top	75	14.8	5.15	0.19	96
180	Top	75	20.0	5.7	0.19	126
200	Top	80	20.0	5.1	0.21	198

#### 5.4.2. Position of fines return (top and bottom)

When no fluid bed was used, the position for fines introduction slightly influenced the powder water content, and in any case drying inside the chamber was insufficient.

When the fluid bed was used it caused important changes in the drying behavior (Table 3.5.3). Actually, when the fines particles were inserted in the upper part of the chamber, next to the atomization device, dry powder was recovered (5.7 – 8.03 g water/ 100 g dry matter), even with high liquid flow rates (23 kg.h<sup>-1</sup>) and low exit air temperatures (65°C).

When fines were introduced at the bottom of the chamber, no powder was recovered even for low liquid flow rates (16 kg.h<sup>-1</sup>) and high exit air temperatures (85°C). Dry fines collided with less humid drops and collisions were not efficient. Since in this last case no coalescence had occurred at the top, the moisture content of drying drops was still high and caused blocking of the fluid bed.

From these results, it can be assumed that if dry fines are introduced at the top of the chamber, they collide with liquid drops leading to coalescence and decreasing the total water content of the new formed structure, helping in drying and allowing achieving lower final moisture content. This helps avoiding sticking on walls in the bottom of the chamber.

#### 5.4.3. Role of the fluid bed (with top fines return)

Use of fluid bed was important **to improve drying** until reaching required specifications and **to increase particle size**.

The Niro FSD 4.0. was designed so that the use of fluid bed is compulsory for good drying. Chamber height is limited (2 m) and drops are fast vertically ejected from the nozzle to the bottom of the chamber, so that they do not have enough time to be completely dried inside the chamber considering limitations in drying air temperature.

Insertion of additional drying air for the fluid bed (100 kg.h<sup>-1</sup>, 45-55°C) lead to a further particle drying inside the fluid bed, and also to a different drying behavior inside the chamber as this air entered into the chamber and was mixed with primary drying air. However, some data are missing to completely explain the role of fluid bed:

- geometry of the fluid bed is not completely defined;
- air/particles trajectories are unknown;
- air temperature measurement inside the fluid bed (about 40°C in our trials) was not in complete agreement with temperatures of fluid bed drying air (45-55°C) and of air coming from the chamber (45-60°C) that could also enter in the fluid bed (quite unlikely). Position of this thermocouple was not well known.

It can be assumed that the initial size of the sprayed droplets was similar for all the tested conditions (same nozzle, air pressure, liquid feed composition and temperature, liquid flow rate between 14.8 and 20 kg.h<sup>-1</sup>). But powders with different median particle size were obtained: between 41 and 200 µm depending on the liquid flow rate, the inlet air temperature, the use of the fluid bed and the fines return at the top or bottom of the chamber. Therefore, in some cases, size enlargement occurred inside the drying chamber and/or in the fluid bed.

This may be due to collisions between two or more particles that can be:

- A liquid drop and a fine particle recycled at the top of the chamber. The sprayed solution was heated up to 70°C before spraying (low viscosity), and collision with a dry fine particle (median diameter 25 µm) will more likely lead to coalescence and partial drying of the drop (small size enlargement; e.g. two particles of 25 µm should lead to a particle of 31 µm ( $d_{tot} = d_{drop} \cdot (2)^{1/3}$ )).
- Particles with sticky surface due to water content, temperature, surface composition leading to agglomerates (larger particles).





This second situation could occur when fluid bed was used, either inside the fluid bed or in the lower part of the chamber by contact between drying drops/particles and fines particles coming upwards from the fluid bed inside the chamber.

Assuming thermal equilibrium between particles and air inside the fluid bed, particles will reach a temperature of about 40°C (measured in the top part of fluid bed). From glass transition data (Fig. 3.5.4b), particles with a temperature of about 40°C could be sticky when their surface water activity is between 0.1 and 0.25.

This is in agreement with the obtained results on final powder. For all the trials performed with the fluid bed (whatever the inlet air temperature), powders with a water activity about 0.2 (0.18 – 0.21) had median diameters larger than 93 µm (93 – 198 µm) whilst without fluid bed (and therefore agglomeration) particles diameters were inferior to 90 µm (46 – 89 µm).

However, for a similar average final powder water activity, median diameter was bigger in trials with a higher inlet drying air temperature (Table 3.5.4) (96 µm for 160°C; 126 µm for 180°C; 198 µm for 200°C).

This could also be explained by the fact that particle surface could be less humid than the average value of the particle, and so a higher surface temperature would be needed to have a sticky behavior: for example, if surface water activity is 0.1, to be inside the sticky zone surface temperature should be of ~50°C.

When inlet air temperature is higher, particles temperatures in the chamber are also higher with a lower surface viscosity. Thus they could exhibit a more sticky behavior when entering in the fluid bed, leading to a wider size enlargement.

## **Conclusion**

The solution of protein hydrolysate was successfully dried within required specifications for final moisture content ( $\approx$  5% powder water content).

The approach of air properties measurement inside spray dryer chamber was successfully applied to a different equipment to help interpretation of drying behavior of a protein hydrolysate solution.

Comparison between air temperatures and relative humidity measured during water and solution drying showed a different drying behavior. Air measurements inside the chamber were then confirmed to be possible good indicators of drying behavior, but for further study the complex air flow pattern should be determined in order to choose good positions for probes (possible air mixing inside the chamber). Total air flow rate should be measured at the exit, to take into account all the secondary unknown air flow rates.

The use of fluid bed (with additional hot air) and fines return on top of chamber were necessary conditions to obtain a dry product within specification. It was assumed that there was coalescence between sprayed drops and recycled fines close to the atomizer, participating in decreasing drop/particle water content into the chamber; then inside or close to the fluid bed sticking between particles was possible, as their surface reached appropriate conditions of water activity and temperature to be in a rubbery sticky state. The inlet air temperature and liquid flow rate determine moisture content and surface temperature of the powder entering the fluid bed. A higher inlet air temperature led to a wider size enlargement inside the fluid bed.

And the use of the bottom fluid bed could also help agglomeration by moving back upwards the smallest particles inside the chamber, where they could collide with drying drops.



## **CONCLUSION**



## Conclusion

This study had the objective to better understand the evolution of particle properties along spray drying in relation with measurements on air inside the chamber of a single-stage cocurrent pilot spray dryer equipped with rotary atomizer.

Air temperature and relative humidity were successfully measured during drying of water and maltodextrin DE12 and DE21 solutions, using thermocouples and a capacitive hygrometer. These measurements were used for a mass balance on water in air between the entrance and different points inside the chamber. With the assumption that particles and air were circulating together, exchanging heat and water, it was possible to deduce the evolution of the average particle water content along the chamber.

The effect of several process parameters (inlet air temperature, air flow rate, liquid flow rate, rotary atomizer speed) on drops drying behavior was studied. In any conditions, most of drying occurred very fast, close to the atomizer because of high temperature and water pressure gradients. We must note that the tested air humidity sensor was resistant to high temperatures but not well adapted for low air relative humidity in these conditions. At high temperature it led to a big error in determination of low air water content and thus for the mass balance on water in air. But that situation corresponded to high inlet air temperature and/or low liquid flow rate, for which drying was very fast and considered as already completed close to the atomizer. Particles already reached their final water content in the upper part of the chamber.

For all other operating conditions (low air temperature, high liquid flow rate) for which drying continued further inside the chamber, it was possible to follow air properties corresponding to increase of water contents and decrease of temperatures.

Air relative humidity at the exit of the chamber was found to be an indicator of final powder water activity and water content, although equilibrium between air and product was never reached.

The process was studied by drying water as a reference and solutions of two maltodextrins DE12 and DE21. These two products differ in ability to dry and lead to possible sticking conditions interesting for the final objective of agglomeration.

For the same amount of water to evaporate and for the same operating conditions, air temperatures inside the spray dryer chamber were lower and relative humidity higher when drying water. It was possible to show that the evaporation of free water was easier compared to the evaporation of water bound to solute in solution. The difference in measured air properties for the two maltodextrins solutions showed a drying behavior for MD21 closer to water compared to MD12. It was in relation with their different domains ( $T$ ,  $a_w$ ) of glass transition and viscous state not favorable to easy drying.

For maltodextrin solutions drying, the average particle water content was calculated from air water content evolution, at different positions in the chamber. In combination with glass transition temperatures and equilibrium sorption isotherms it was possible to determine operating conditions and positions inside the dryer for which particles could be considered as sticky.

Due to its higher glass transition temperatures (function of  $a_w$  and  $X$ ), maltodextrin DE12 was, in the tested conditions, quickly “dried” until values of water content and water activity for which the particle is below the sticky zone. Stickiness was then envisaged only close to the atomizer.



Maltodextrin DE21 had lower glass transition temperatures, with a sticky zone corresponding to lower values of water content and water activity, so that particles should be sticky in a wider part of the chamber, depending on operating conditions.

Spray drying simulation was also investigated to predict stickiness. A simplified Computational Fluid Dynamics (CFD) model was used to obtain further information on air flow pattern, to put in evidence possible air recirculations zones and follow the evolution of temperatures and water content of particles.

To take into account the reduced evaporation rate when drying liquid solutions compared to free water (used in classical model), particle drying was simulated by considering a reduced drop water vapour pressure. A different coefficient ( $<1$ ) for the two maltodextrins was used with a value for maltodextrin DE21 intermediate between water (1) and maltodextrin DE12. Evolution of particle average water content could be correctly described. The main advantage of this approach is that it is easily applicable to different dryer geometry and products (coefficient to determine), as composition and diffusion are not directly considered. On the other side, differences between core and surface were not taken into account and particle surface properties are not accurately predicted especially temperature.

Calculated possible sticky zones for MD12 and MD21 were in agreement with the experimental determined ones, showing that CFD could be used for a qualitative estimation of the effect of operating parameters on particle stickiness.

The predicted sticky regions were tested by performing agglomeration of particles of maltodextrins DE12 and DE21, inside the dryer. A special device was designed to reinsert regularly part of the produced powder, at different positions inside the chamber. Collisions between returned particles and drying sticky particles led to the production of a fraction of big particles with improved flowability and wettability. This size enlargement confirmed the predicted stickiness in a wide part of the chamber for maltodextrin DE21, whilst, as expected, no agglomeration was obtained when drying MD12.

It was possible to put in evidence that the biggest agglomerated fraction was obtained when inserting powder not immediately close to the atomizer, as usual in industrial practice for fines return. This position is usually chosen because of the high liquid drops density, leading to a big collision probability. But collisions in this position are more likely to give particle covering or coalescence, with small size enlargement. As a consequence, particles should be returned several times to increase size, and this could lead to product degradation.

Local insertion in the top part at a distance of the atomizer, or in the middle of the chamber, led to a maximum of 16 % of agglomerated particles with a size superior to 100  $\mu\text{m}$ . So the estimation of particle stickiness from measurements on air and product characteristics could allow optimizing the choice of powder insertion position depending on the desired product properties. But powder insertion has to be improved and optimised for a regular symmetrical insertion, to return only the fines, and with possibility to insert different particles, not only the ones produced.

The developed experimental approach was applied to a semi-industrial spray dryer equipped with nozzle atomizer, fines return and internal fluid bed, using air measurements to better understand the drying of a particular product, with some constraints, either for the product or for the equipment. Properties as glass transition temperature diagram and sorption isotherms for the studied product were used to interpret results.

This application put in evidence some limitations to take into account. First, exact determination of air flow rate including some air entrances (e.g. air for fines return, fluid bed, nozzle) is crucial for solving mass balances. In industrial dryers air flow rate is often





measured just at the entrance of the chamber, while a measure at the exit could be useful to determine the total air flow rate inside the dryer. Furthermore, some air recirculations occur, especially in relation with the geometry of the chamber. This means that air flow pattern should be known in order to choose positions for air properties measurements that could be representative of the drying particles properties. This flow pattern has to be estimated as in this study (temperature measurements) or measured (velocity measurements) or predicted by simulation.

The study with the semi-industrial spray dryer with fines return, confirmed that fines insertion close to the atomizer had as main function to improve drying by decreasing particles water content at the beginning of drying, while size enlargement occurred mainly inside the integrated fluid bed. This return of fines means a high residence time for some particles which can have a bad effect on quality, depending on their heat sensitivity. Inside or close to the fluid bed using controlled heated air, the particles could reach equilibrium with air due to their residence time. Controlling air temperature and relative humidity is a way to control powder characteristics and possible stickiness, before final powder exit. In that case if no fines were produced during this final step in fluid bed, some other particles could be introduced close to the atomizer to participate and complete the composition of drops and to improve their drying and agglomeration.



## List of symbols

<i>Symbol</i>	<i>description</i>	<i>Units</i>
A	Total exchange surface of liquid spray	m <sup>2</sup>
A <sub>drop</sub> , A <sub>tot</sub>	Drop surface, surface of N <sub>drops</sub>	m <sup>2</sup>
A <sub>pipe</sub>	Pipe section	m <sup>2</sup>
a <sub>w</sub>	Water activity	
b	Height of rotary wheel vanes	m
C, C <sub>GAB</sub>	BET and GAB parameters	
C <sub>D</sub>	Drag coefficient	
C <sub>p</sub>	Specific heat	J.kg <sup>-1</sup> .K <sup>-1</sup>
C <sub>w,b</sub>	Water vapour concentration in bulk air	mol.m <sup>3</sup>
C <sub>w,s</sub>	Water vapour concentration at drop surface	mol.m <sup>3</sup>
D	BET parameter	
d <sub>3,2</sub>	Sauter diameter	m
d <sub>drop</sub>	Drop diameter	m
d <sub>or</sub>	Nozzle orifice diameter	m
d <sub>p</sub>	Particle diameter	m
D <sub>w</sub>	Water vapour diffusion coefficient in air	m <sup>2</sup> .s <sup>-1</sup>
E <sub>k</sub>	Kinetic energy	Kg.m <sup>2</sup> .s <sup>-2</sup>
f	Fan frequency	Hz
F <sub>D</sub>	Drag force	N
g	Gravity acceleration	m.s <sup>-2</sup>
H	Air mass enthalpy	kJ.kg <sup>-1</sup>
h	Global heat exchange coefficient	W.m <sup>-2</sup> .K <sup>-1</sup>
h <sub>c</sub>	Convective heat transfer coefficient between air and drops	W.m <sup>-2</sup> .K <sup>-1</sup>
J	Mass diffusion flux	kg.m <sup>2</sup> .s <sup>-1</sup>
k	Turbulent kinetic energy	m <sup>2</sup> .s <sup>-2</sup>
k <sub>c</sub>	Mass transfer coefficient	s.m <sup>-1</sup>
k <sub>eff</sub>	Gas effective thermal conductivity	J.s <sup>-1</sup> .m <sup>-1</sup> .K <sup>-1</sup>
$\dot{m}$	Mass flow rate	kg.s <sup>-1</sup>
M	Molecular weight	g.mol <sup>-1</sup>
$\dot{m}_{ew}, \frac{dm}{dt}$	Evaporated water mass flow rate	kg.s <sup>-1</sup>
N <sub>drops</sub>	Number of drops	
N	Rotation speed	rpm
P	Static air pressure	Pa
P <sub>finerReturn</sub>	Pressure of compressed air for fines return	Pa
P <sub>nozzle</sub>	Pressure of compressed air for bifluid nozzle	Pa
P <sub>v,air</sub> , P <sub>v</sub>	Water vapour pressure of air, of product	Pa
P <sub>v,drop</sub>	Water vapour pressure at drop surface	Pa
P <sub>w</sub> <sup>sat</sup>	Saturated water vapour pressure of pure water	Pa
$\dot{Q}_{losses}$	Heat losses flow rate	kJ.s <sup>-1</sup>
RH	Air relative humidity	
S	Surface of spray dryer chamber walls	m <sup>2</sup>
S <sub>m</sub>	Mass source term	kg.m <sup>-3</sup> .s <sup>-1</sup>
S <sub>h</sub>	Heat source term	W.m <sup>-3</sup>
T	Temperature	°C
T <sub>dp</sub>	Air dew point temperature	°C
T <sub>exit</sub>	Air temperature at the exit of spray dryer	°C
T <sub>fb,1</sub>	Primary fluid bed air temperature	°C
T <sub>fb,2</sub>	Secondary fluid bed air temperature	°C
T <sub>g</sub>	Glass transition temperature	°C
T <sub>s</sub>	Drop surface temperature	°C
T <sub>sticky</sub>	Sticky temperature	°C
T <sub>wall</sub>	Chamber wall temperature	°C
T <sub>wb</sub>	Air wet bulb temperature	°C

$u$	Fluid velocity	$m.s^{-1}$
$u_p$	Particle velocity	$m.s^{-1}$
$\dot{V}_{air}$	Volumetric air flow rate	$m^3.s^{-1}$
$v$	Velocity	$m.s^{-1}$
$v_{wheel}$	Rotary wheel velocity	rps
$w$	Mass fraction	
$X$	Powder water content (dry basis)	$kg\ water.kg^{-1}\ total\ solids$
$X_c$	Critical water content	$kg\ water.kg^{-1}\ total\ solids$
$X_{eq}$	Product water content at equilibrium	$kg\ water.kg^{-1}\ total\ solids$
$X_{wet}$	Powder water content (wet basis)	$kg\ water.kg^{-1}\ powder$
$Y$	air water content	$kg\ water.kg^{-1}\ dry\ air$
$\gamma_c$	Shear velocity gradient	$s^{-1}$
$\Delta H_v$	Specific heat of vaporization	$J.kg^{-1}$
$\varepsilon$	Turbulent kinetic energy dissipation rate	$m^2.s^{-3}$
$\eta_{thermal}$	Process thermal efficiency	
$\lambda$	Thermal conductivity	$W.m^{-1}.K^{-1}$
$\mu, \mu_g$	Viscosity, at glass transition temperature	Pa.s
$\mu_{eff}$	Gas effective viscosity	Pa.s
$\mu_t$	Turbulent air viscosity	Pa.s
$\rho$	Density	$kg.m^{-3}$
$\rho_{bulk}, \rho_{tap}$	Bulk, tapped density	$kg.m^{-3}$
$\sigma$	Surface tension	$N.m^{-1}$
$\sigma_k, \sigma_e$	Turbulent Prandtl number	
$\tau$	Mean residence time	s

#### Subscripts

air	Dry air
amb	At ambient temperature
ax	Axial
IN	At air inlet
l	Liquid
OUT	At the chamber outlet
p	Particle/drying drop
s	Solid
vapour	Water vapour
w	Water

## REFERENCES

- Adhikari B., Howes T., Bhandari B.R., Truong V., 2001.** Stickiness in foods: a review of mechanisms and test methods. *International Journal of Food Properties*, 4(1), 1-33.
- Adhikari B., Howes T., Bhandari B., 2003.** Surface stickiness of drops of carbohydrate and organic acid solutions during convective drying: experiments and modeling. *Drying Technology*, 21(5), 839-873.
- Adhikari B., Howes T., Bhandari B.R., Truong V., 2004.** Effect of addition of maltodextrin on drying kinetics and stickiness of sugar and acid-rich foods during convective drying: experiments and modelling. *Journal of Food Engineering*, 62(1), 53-68.
- Adhikari B., Howes T., Lecomte D., Bhandari B.R., 2005.** A glass transition temperature approach for the prediction of the surface stickiness of a drying droplet during spray drying. *Powder Technology*, 149, 168-179.
- Adhikari B., Howes T., Shrestha A., Bhandari B.R., 2007.** Effect of surface tension and viscosity on the surface stickiness of carbohydrate and protein solutions. *Journal of Food Engineering*, 79(4), 1136-1143.
- Aguilera J.M., Lilford P.J., 2008.** Food materials science – principles and practice. Springer, New York, 620 pp.
- Alamilla-Beltrán L., Chanona-Pérez J.J., Jimenez-Aparicio A.R., Gutierrez-Lopez G.F., 2005.** Description of morphological changes of particles along spray drying. *Journal of Food Engineering*, 67, 179-184.
- Albrecht H.E., 2003.** Laser Doppler and Phase Doppler Measurements Techniques. Berlin, Heidelberg, New York, Springer-Verlag, 738pp.
- Bhandari B.R., 1992.** Etude du procédé de séchage par pulvérisation Leafflash pour les produits alimentaires. Thèse ENSIA, 161p.
- Bhandari B.R., Howes T., 1999.** Implication of glass transition for the drying and stability of dried foods. *Journal of Food Engineering*, 40, 71-79.
- Bhandari B.R., Hartel R.W., 2005.** Phase transitions during food powder production and powder stability. In: Encapsulated and Powdered foods. Ed. C.Onwulata, Taylor & Francis, New York, 261-292.
- Bhandari B.R., 2008.** Stickiness and caking in food preservation. In: Handbook of food preservation. Ed. M.S. Rahman, CRC Press, Taylor & Francis, New York, 17, 387-401.
- Bimbenet J.J., Dumoulin E., 1999.** Séchage des solutions sucrées par atomisation: théorie, procédés industriels, exemples d'application. In: Eau, sucre et poudres alimentaires. VIII Colloque Cedus, Paris, 31-39.
- Bimbenet J.J., Duquenoy A., Trystram G., 2002.** Génie des procédés alimentaires. Dunod, Paris, 554 pp.
- Birchal V.S., Huang L.X., Mujumdar A.S., Passos M.L., 2006.** Spray dryers: modelling and simulation. *Drying Technology*, 24, 359-371.
- Boonyai P., Bhandari B., Howes T., 2004.** Stickiness measurement techniques for food powders: a review. *Powder Technology*, 145, 34-46.
- Boonyai P., Howes T., Bhandari B., 2006.** Applications of the cyclone stickiness test for characterization of stickiness in food powders. *Drying Technology*, 24(6), 703-709.
- Boonyai P., Howes T., Bhandari B., 2007.** Instrumentation and testing of a thermal mechanical compression test for glass-rubber transition analysis of food powders. *Journal of Food Engineering*, 78(4), 1333-1342.
- Buffo R.A., Probst K., Zehentbauer G., Luo Z., Reineccius G.A., 2002.** Effects of agglomeration on the properties of spray dried encapsulated flavours. *Flavour and Fragrance Journal*, 17, 292-299.
- Chen X.D., 2002.** Heat-mass transport and microstructural aspects of the drying of single

- droplets containing food solids/solute- Recent development. *Drying'2002, Proceedings 13<sup>th</sup> IDS*, (A) 88-95.
- Chuy L.E., Labuza T.P., 1994.** Caking and stickiness of dairy-based food powders as related to glass transition. *Journal of Food Science*, 59(1), 43-46.
- Dodge L.G., 1987.** Comparison of performance of drop-sizing instruments. *Applied Optics*, 26, 1328-1341.
- Downtown G.E., Flores-Luna J.L., King C.J., 1982.** Mechanism of stickiness in hygroscopic, amorphous powders. *Industry Engineering and Chemistry Fundamentals*, 21, 447 – 451.
- Ducept F., Sionneau M., Vasseur J., 2002.** Superheated steam dryer: simulations and experiments on product drying. *Chemical Engineering Journal*, 86, 75-83.
- Fang Y., Selomulya C., Chen X.D., 2008.** On measurement of food powder reconstitution properties. *Drying Technology*, 26(1-3), 3-14.
- Filkova I., Mujumdar A.S., 1995.** Industrial spray drying systems. In: Handbook of industrial drying. Ed. A.S. Mujumdar, Marcel Dekker, New York, 9, 263-307.
- Fitzpatrick J.J., Iqbal T., Delaney C., Twomey T., Keogh M.K., 2004.** Effect of powder properties and storage conditions on the flowability of milk powders with different fat contents. *Journal of Food Engineering*, 64, 435-444.
- Fluent, 1998.** Fluent 5 User's guide, Vol. 1 to 4.
- Frias J.M., Oliveira J.C., Schittkowski K., 2001.** Modeling and parameters identification of a maltodextrin DE12 drying process in a convection oven. *Applied Mathematical Modelling*, 25, 449-462.
- Frydman A., 1998.** Caractérisation expérimentale et modélisation d'un procédé de séchage par pulvérisation dans la vapeur d'eau surchauffée. Thèse ENSIA, 185p.
- Gong Z., Zhang M., Mujumdar A.S., Sun J., 2008.** Spray drying and agglomeration of instant bayberry powder. *Drying Technology*, 26(1-3), 116-121.
- Goula A.M., Adamopoulos K.G., 2008.** Effect of maltodextrin addition during spray drying of tomato pulp in dehumidified air. I. Drying kinetics and product recovery. *Drying Technology*, 26 (4-6), 714-725.
- Graham B.A., 1997.** Recent advances in agglomeration during spray drying. *Food Australia*, April, 184-185.
- Guo B., Fletcher D.F., Langrish T.A.G., 2004.** Simulation of the agglomeration in a spray using Lagrangian particle tracking. *Applied Mathematical Modelling*, 28(3), 273-290.
- Hecht J.P., King C.J., 2000.** Spray drying: influence of developing drop morphology on drying rates and retention of volatile substances. Part 1&2. *Ind. Eng. Chem. Res.*, 39, 1756-1774.
- Heinrich S., Peglow M., Ihlow M., Henneberg M., Mörl L., 2002.** Analysis of the start-up process in continuous fluidized bed spray granulation by population balance modelling. *Chemical Engineering Science*, 57, 4369-4390.
- Hennigs C., Kockel T.K., Langrish T.A.G., 2001.** New measurements of the sticky behavior of skim milk powder. *Drying Technology*, 19(3-4), 471-484.
- Hogg R., 1992.** Agglomeration models for process design and control. *Powder Technology*, 69, 69-76.
- Horvat A., Kaucic V., Masters K., Golob J., 2002.** Influence of atomisation system on sodium disilicate characteristics. *Drying'2002, Proceedings 13<sup>th</sup> IDS*, (A), 696-703.
- Huang L., Kumar K., Mujumdar A.S., 2004.** Simulation of a spray dryer fitted with a rotary disk atomizer using a three-dimensional computational fluid dynamic model. *Drying Technology*, 22(6), 1489-1515.
- Huang L.X., Kumar K., Mujumdar A.S., 2006.** A comparative study of a spray dryer with rotary disc atomizer and pressure nozzle using computational fluid dynamic simulations. *Chemical Engineering and Processing*, 45, 461-470.

- Huntington D.H., 2004.** The influence of the spray drying process on product properties. *Drying Technology*, 22(6), 1261-1287.
- Jeanet R., Ducept F., Dolivet A., Méjean S., Schuck P., 2008.** Residence time distribution: a tool to improve spray-drying control. *Dairy Science & Technology*, 88(1), 31-43.
- Jimenez Munguia M.T., 2007.** Agglomération de particules par voie humide en lit fluidisé. Thèse ENSIA, 134p.
- Karel M., Anglea S., Buera P., Karmas R., Levi G. Roos Y., 1994.** Stability-related transitions of amorphous foods. *Thermochimica Acta*, 246(2), 249-269.
- Kemp I.C., Oakley D.E., 2002.** Modeling of particulate drying in theory and practice. *Drying Technology*, 20(9), 1699-1750.
- Kerkhof P.J.A.M., 1994.** The role of theoretical and mathematical modelling in scale-up. *Drying Technology*, 12(1-2), 1-46.
- Kieviet F.G., Kerkhof P.J.A.M., 1995.** Measurements of particle residence time distributions in a co-current spray dryer. *Drying Technology*, 13(5-7), 1241-1248.
- Kieviet F.G., Kerkhof P.J.A.M., 1996.** Using computational fluid dynamics to model product quality in spray drying: air flow, temperature and humidity patterns. *Drying '96*, 10<sup>th</sup> Int. Drying Symposium, (A), 259-266.
- Kieviet F.G., Van Raaij J., Kerkhof P.J.A.M., 1997.** A device for measuring temperature and humidity in a spray dryer chamber. *Trans. IChemE*, 75(A), 329-333.
- Kim K.Y., Marshall J.R., 1971.** Drop-size distributions from pneumatic atomizers. *AIChE Journal*, 17(3), 575-584.
- King C.J., Kieckbusch T.G., Greenwald C.G., 1984.** Food-quality factors in spray drying. In: *Advances in drying*. Ed. A.S. Mujumdar, Hemisphere, New York, Vol. 1, 71-120.
- Knight P.C., 2001.** Structuring agglomerated products for improved performance. *Powder Technology*, 119, 14-25.
- Kudra T., 2002.** Sticky region in drying - Definition and identification. The International Conference on Energy-Saving Technologies for Drying and Hygrothermal Processing, Moscow.
- Langrish T., Fletcher D.F., 2001.** Spray drying of food ingredients and applications of CFD in spray drying. *Chemical Engineering and Processing*, 40, 345-354.
- Langrish T., Kockel T.K., 2001.** The assessment of a characteristic drying curve for milk powder for use in computational fluid dynamics modelling. *Chemical Engineering Journal*, 84, 69-74.
- Lazar M.E., Brown A.H., Smith G.S., Wong F.F., Lindquist F.E., 1956.** Experimental production of tomato powder by spray drying. *Food Technology*, 10, 129-134.
- Lefebvre A.H., 1989.** Atomization and sprays. Hemisphere, New York, 421p.
- Lloyd R.J., Chen X.D., Hargreaves J.B., 1996.** Glass transition and caking of spray-dried lactose. *International Journal of Food Science and Technology*, 31(4), 305-311.
- Lockemann C.A., 1999.** A New Laboratory Method to Characterize the Sticking Property of Free Flowing Solids. *Chemical Engineering Process*, 38, 301-306.
- Masters K., 1985.** *Spray Drying*. Fourth edition, Longman Scientific and Technical, J. Wiley & Sons, New York, 696 p.
- Mathlouthi M., Rogé B., 2003.** Water vapour sorption isotherms and the caking of food powders. *Food Chemistry*, 82, 61-71.
- Melcion J.P., Ilari J.L., 2003.** Technologie des pulvérulents dans les IAA. Lavoisier, Paris, 814 pp.
- Mounir S., Allaf K., 2008.** Three-stage spray drying: new process involving instant controlled pressure drop. *Drying Technology*, 26(4-6), 452-463.
- Mujumdar A.S., 1995.** *Handbook of industrial drying*. Marcel Dekker, New York, 1423pp.
- Nath S., Satpathy G.R., 1998.** A systematic approach for investigation of spray drying processes. *Drying Technology*, 16(6), 1173-1193.



- Nijdam J.J., Guo B., Fletcher D.F., Langrish T.A.G., 2004.** Challenges of simulating droplet coalescence within a spray. *Drying Technology*, 22(6), 1463-1488.
- Oakley D.E., 1994.** Scale-up of spray dryers with the aid of computational fluid dynamics. *Drying Technology*, 12(1-2), 217-233.
- Oakley D.E., 2004.** Spray dryer modeling in theory and practice. *Drying Technology*, 22(6), 1371-1402.
- Ortega-Rivas E., 2005.** Handling and Processing of food powders and particulates. In: Encapsulated and Powdered foods. Ed. C. Onwulata, Taylor & Francis, New York, 75-144.
- Ozkan N., Walisinghe N., Chen X.D., 2002.** Characterization of stickiness and cake formation in whole and skim milk powders. *Journal of Food Engineering* 55, 293-303.
- Ozmen L., Langrish T.A.G., 2002.** Comparison of glass transition temperature and sticky point temperature for skim milk powder. *Drying Technology*, 20(6), 1177-1192.
- Palzer S., 2005a.** Contrôle de l'agglomération de polymères de dextrose par l'application du concept de la transition vitreuse. *Industries Alimentaires et Agricoles*, 122(12), 20-27.
- Palzer S., 2005b.** The effect of glass transition on the desired and undesired agglomeration of amorphous food powders. *Chemical Engineering Science*, 60, 3959-3968.
- Petersen M., Gude K.F., 1973.** Improvements in and relating to spray drying devices for the production of powder, e.g. milk powder. Patent GB 1 329 791.
- Pietsch W., 1991.** Size enlargement and agglomeration. Wiley, Chichester, 532p.
- Písecký J., Hansen S.P., 1990.** Process and spray drying apparatus for producing stable particle agglomerates. Patent EP 0 378 498.
- Písecký J., 1997.** Handbook of Milk Powder Manufacture. Niro A/S, Copenhagen, 261 p.
- Räederer M., 2001.** Drying of viscous, shrinking products: modelling and experimental validation. PhD Thesis, TUM Freising (Germany), 124 pp.
- Räederer M., Besson A., Sommer K., 2002.** A thin film dryer approach for the determination of water diffusion coefficients in viscous products. *Chemical Engineering Journal*, 86, 185-191.
- Roos Y.H., Karel M., 1991a.** Applying state diagrams to food processing and development. *Food Technology*, 45, 66-70.
- Roos Y.H., Karel M., 1991b.** Phase transition of amorphous sucrose and frozen sucrose solution. *Journal of Food Science*, 56(1), 266-267.
- Roos Y.H., Karel M., 1991c.** Plasticizing effect of water on thermal behavior and crystallization of amorphous food models. *Journal of Food Science*, 56(1), 38-43.
- Roos Y.H., 1995.** Glass transition-related physicochemical changes in foods. *Food Technology*, 10, 97-102.
- Roos Y.H., 2002.** Importance of glass transition and water activity to spray drying and stability of dairy powders. *Le Lait*, 82, 475-484.
- Roustapour O.R., Hosseinalipour M., Ghobadian B., 2006.** An experimental investigation of lime juice drying in a pilot plant spray dryer. *Drying Technology*, 24, 181-188.
- Ruan R., Long Z., Chen P., Huang V., Almaer S., Taub I., 1999.** Pulse NMR study of glass transition in maltodextrin. *Journal of Food Science*, 64(1), 6-9.
- Schubert H., 1993.** Instantization of powdered food products. *International Chemical Engineering*, 33(1), 28-45.
- Schuck P., Roignant M., Brulé G., Méjean S., Bimbenet J.J., 1998.** Caractérisation énergétique d'une tour de séchage par atomisation multiple effet. *Ind. Alim. Agr.*, 115, 9-14.
- Schuck P., 2002.** Spray drying of dairy products: state of the art. *Le Lait*, 82, 375-382.
- Schuck P., Mejean S., Dolivet A., Jeantet R., 2005a.** Thermohygrometric sensor: a tool for optimizing the spray drying process. *Innovative Food Science and Emerging Technologies*, 6(1), 45-50.

- Schuck P., Blanchard E., Dolivet A., Méjean S., Onillon E., Jeantet R., 2005b.** Water activity and glass transition in dairy ingredients. *Le Lait*, 85(4-5), 295-304.
- Schuck P., Dolivet A., Méjean S., Jeantet R., 2008.** Relative humidity of outlet air: the key parameter to optimize moisture content and water activity of dairy powders. *Dairy Science & Technology*, 88(1), 45-52.
- Schulz M.E., 1966.** Verfahren zum Zerstäubungstrocknen und Instantisieren von Gut. Patent DE 1 228 567.
- Sears J.T., Ray S., 1980.** Acoustic spray drying of particle suspensions. *Drying A*, Hemisphere, New York, 332-338.
- Senoussi A., 1994.** Séchage par pulvérisation de liquides alimentaires contenant des substances labiles. Thèse ENSIA, 139p.
- Shrestha A.K., Howes T., Adhikari B.P., 2007a.** Effect of protein concentration on the surface composition, water sorption and glass transition temperature of spray-dried skim milk powders. *Food Chemistry*, 104(4), 1436-1444.
- Shrestha A.K., Howes T., Adhikari B.P., 2007b.** Water sorption and glass transition properties of spray dried lactose hydrolysed skim milk powder. *LWT - Food Science and Technology*, 40(9), 1593-1600.
- Shrestha A.K., Ua-Arak T., Adhikari B.P., 2007c.** Glass transition behavior of spray dried orange juice powder measured by differential scanning calorimetry (DSC) and thermal mechanical compression test (TMCT). *International Journal of Food Properties*, 10(3), 661-673.
- Shrestha A.K., Howes T., Adhikari B.P., Bhandari B.R., 2008.** Spray drying of skim milk mixed with milk permeate: effect on drying behavior, physicochemical properties, and storage stability of powder. *Drying Technology*, 26(1-3), 239-247.
- Sommerfeld M., 2001.** Validation of a stochastic Lagrangian modelling approach for inter-particle collision in homogeneous isotropic turbulence. *Int. J. Multiph. Flow*, 27, 1829-1858.
- Straatsma J., Van Houwelingen G., Steenbergen A.E., De Jong P., 1999a.** Spray drying of food products: 1. Simulation model. *Journal of Food Engineering*, 42, 67-72.
- Straatsma J., Van Houwelingen G., Steenbergen A.E., De Jong P., 1999b.** Spray drying of food products: 2. Prediction of insolubility index. *Journal of Food Engineering*, 42, 73-77.
- Teunou E., Fitzpatrick J.J., Synnott E.C., 1999.** Characterisation of food powder flowability. *Journal of Food Engineering*, 39, 31-37.
- Truong V., Bhandari B.R., Howes T., 2005a.** Optimization of co-current spray drying process of sugar-rich foods. Part I. Moisture and glass transition temperature profile during drying. *Journal of Food Engineering*, 71(1), 55-65.
- Truong V., Bhandari B.R., Howes T., 2005b.** Optimization of co-current spray drying process for sugar-rich foods. Part II. Optimization of spray drying process based on glass transition concept. *Journal of Food Engineering*, 71(1), 66-72.
- Tsourouflis S., Flink J.M., Karel M., 1976.** Loss of Structure in freeze Dried Carbohydrate Solutions. Effect of Temperature, Moisture Contents and Compositions. *Journal of the Science of Food and Agriculture*, 27(6), 509-519.
- Turchiuli C., Eloualia Z., El Mansouri N., Dumoulin E., 2005.** Fluidised bed agglomeration: agglomerates shape and end-use properties. *Powder Technology*, 157, 168-175.
- Upadhyaya R.L., 1982.** Some progress in atomization. *Drying'82*, 2<sup>nd</sup> Int. Drying Symposium, 171-177.
- Verdurmen R.E.M., Menn P., Ritzert J., Blei S., Nhumai G.C.S., Sorensen T.S., Gunging M., Straatsma J., Verschueren M., Sibeijn M., Schulte G., Fritsching U., Bauckhage K., Tropea C., Sommerfeld M., Watkins A.P., Yule A., Schonfeldt H.,**

- 2004.** Simulation of agglomeration in spray drying installations: the EDECAD project. *Drying Technology*, 22(6), 1403-1461.
- Villiermaux J., 1993.** Génie de la réaction chimique – conception et fonctionnement des réacteurs. Lavoisier, Paris 448 p.
- Vuataz G., 2002.** The phase diagram of milk: a new tool for optimizing the drying process. *Le Lait*, 82, 485-500.
- Walton D.E., Mumford C.J., 1999.** Spray dried products-Characterization of particle morphology. *Trans IChemE*, 77(A), 21-38.
- Woo M.W., Daud W.R.W., Tasirin S.M., Talib M.Z.M., 2007.** Optimization of the spray drying operating parameters - a quick trial-and-error method. *Drying Technology*, 25(10-12), 1741-1747.
- Woo M.W., Daud W.R.W., Tasirin S.M., Talib M.Z.M., 2008.** Effect of wall surface properties at different drying kinetics on the deposition problem in spray drying. *Drying Technology*, 26(1-3), 15-26.
- Wu Z., Liu X., 2002.** Drying solution atomized in pulsating flow. *Drying Technology*, 20(6), 1101-1121.
- Xiao Z., Xie X., Yuan Y., Liu X., 2008.** Influence of atomizing parameters on droplet properties in a pulse combustion spray dryer. *Drying Technology*, 26(4-6), 427-432.
- Yarin A.L., Brenn G., Kastner O., Rensink D., Tropea C., 1999.** Evaporation of acoustically levitated droplets. *Journal of Fluid Mechanics*, 399, 151-204.
- Zapsalis C, Beck R.A., 1985.** Food chemistry and nutritional biochemistry. Wiley, New York, 1219 pp.
- Zbicinski I., Strumillo C., Delag A., 2002.** Drying kinetics and particle residence time in spray drying. *Drying Technology*, 20(9), 1751-1768.

## **ANNEXES**



## ANNEX I – Modeling of residence time distribution function in NIRO Minor

For determination of Residence Time Distribution (RTD) of particles, spray drying tower with powder recirculation (e.g. fines return) was represented as several groups composed by a series of Continuously Stirred Tank Reactors (CSTR) (Jeantet et al., 2008). Ducept et al. (2002) also applied this concept to a superheated steam dryer to validate CFD simulations, varying operating parameters.

The residence time distribution (RTD) function  $E(t)$  can be obtained by deriving the cumulative frequency  $F(t)$ :

$$E(t) = \frac{dF(t)}{dt}$$

For a group  $i$  of  $n_i$  reactors where  $\tau_i$  is the mean residence time in group  $i$ ., the  $E_i(t_i)$  function is (Villiermaux, 1993):

$$E_i(t_i) = \left(\frac{n_i}{\tau_i}\right)^{n_i} \cdot \frac{t_i^{n_i-1} \cdot \exp(-n_i \cdot t_i/\tau_i)}{(n_i - 1)!}$$

Deriving the response curve  $F(t) = C(t)/C_0 = f(t)$  to injection steps in Niro Minor spray dryer, we observed 2 important peaks then two small peaks on the  $E(t)$  curve with maxima at approximately 2, 4, 9 and 15 min (Fig. I.1). Our system (without fines return) was then represented by 3 groups of CSTR reactors (Fig. II.2), each group being characterized by the number of CSTR reactors  $n_i$ , the fraction of particles  $a_i$  (%) passing through the group and an average residence time  $\tau_i$ . We assumed that all the powder passed through the first group of reactors (1) (main particle residence time), and then just a fraction passed through the other two groups of reactors (2 and 3), which expressed powder recirculations inside the chamber.

After the first two CSTR reactors (1 + 2), the RTD function is

$$E_a(t) = (1-a_2) E_1(t) + a_2 E_1(t)*E_2(t)$$

Then, adding the other CSTR reactor, the total residence time distribution curve  $E_{tot}(t)$  is:

$$E_{tot}(t) = (1-a_3) E_a(t) + a_3 E_a(t)*E_3(t)$$

where symbol \* represents the convolution product of two functions. Actually,  $E(t)$  is the response to a unit-pulse  $x(t) = \delta(t)$ . For a complex pulse  $x(t) \neq \delta(t)$ , the response curve is the sum of the contributions of all the components of  $x(t)$  expressed as the convolution product of  $x(t)$  by  $E(t)$ :

$$x(t_1) * E(t_2) = \int_0^{t_2} x(t_1)E(t_2 - t_1)dt_1$$

Parameters of the model ( $n_i$ ,  $\tau_i$ ,  $a_i$ ) were adjusted in order to get the best fit between experimental and theoretical  $E(t) = f(t)$  curves (Fig. I.1 and I.2). The number of experimental points was not sufficient to have a good adjustment.

In the studied conditions residence time of 70% of the powder inside the pilot spray dryer was of about 1.2 min, but about 30% of the powder stayed inside the pilot for an average time of about 15 min. This fraction could represent recirculation of particles and/or particles stuck on walls which detach at one moment during the experiment leading to a delay of about 15 min in powder recovery. But these results neither allow to determine where recirculation occurred, nor to evaluate the influence of the cyclone.

This part of experimental study should be repeated and improved in order to verify the proposed model.

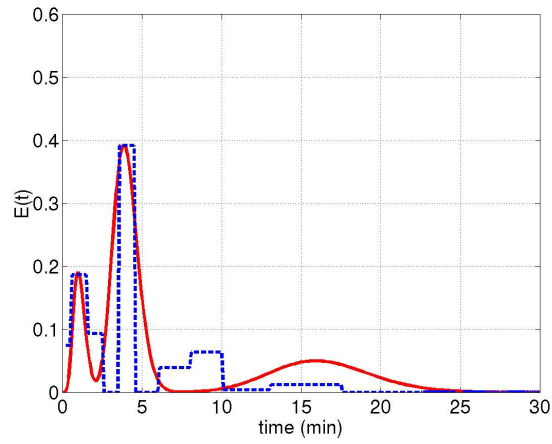


**Figure I.1.** Experimental (dashed line) and fitted (continuous line)  $E(t)$  curve in NIRO *Minor* spray dryer for an injection step.

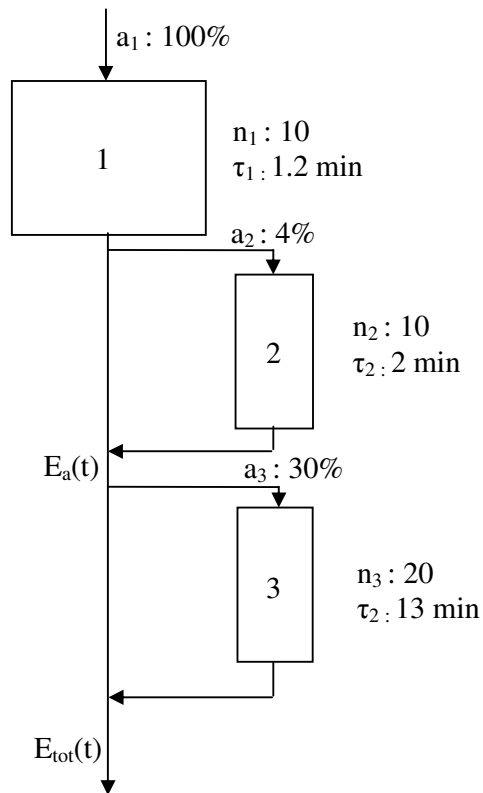


**Figure I.2.** Model of particles Residence Time Distribution in NIRO *Minor* pilot spray dryer.  
 ( $n_i$  number of CSTR reactors in group  $i$ ;  $a_i$  fraction of powder passing through group  $i$ ;  $\tau_i$  average residence time in group  $i$  (min)).

## Annex II – Air and water properties for CFD simulation

Air (continuous phase) was a mixture of air and water vapour assumed to be an ideal gas. Gas density, viscosity, thermal conductivity and specific heat were calculated from ideal gas mixing. Specific heat, thermal conductivity and viscosity of dry air and water vapour were assumed to be constant during simulation (figures are from software data base):

### Dry Air (0°C)

$C_{p,air}$ : 1006 J.kg<sup>-1</sup>.K<sup>-1</sup>  
Thermal conductivity : 0.0242 W.m<sup>-1</sup>.K<sup>-1</sup>  
Viscosity : 1.79 10<sup>-5</sup> Pa.s

### Water vapour

$C_{p,vapour}$ : 2014 J.kg<sup>-1</sup>.K<sup>-1</sup>  
Thermal conductivity: 0.0261 W.m<sup>-1</sup>.K<sup>-1</sup>  
Viscosity: 1.34 10<sup>-5</sup> Pa.s

### Discrete phase

Properties of “volatile” fraction are that of liquid water properties and assumed to be constant during simulation (20°C).

$\rho_{water}$  : 998.2 kg.m<sup>-3</sup>  
 $C_p$ : 4182 J.kg<sup>-1</sup>.K<sup>-1</sup>  
 $\Delta H_v$ : 2.5 10<sup>6</sup> J.kg<sup>-1</sup>  
 $D_{w,a}$  (diffusivity of water vapour in air): 3 10<sup>-5</sup> m<sup>2</sup>.s<sup>-1</sup> (40°C)

The saturated water vapour pressure was defined with a polynomial expression as a function of particle temperature:

$$P_w^{sat}(T) = 0.18709 T^3 - 167.29 T^2 + 50095.97 T - 5020436 \text{ (T in K)}$$





## ANNEX III - Articles, congresses, industrial visits/contacts

- **Articles and International Congresses**

Gianfrancesco A., Turchiuli C., Dumoulin E., 2008. *Powder agglomeration during the spray drying process: measurements of air properties*, Dairy Sci. Technol. 88, 53-64.

Gianfrancesco A., Turchiuli C., Palzer S., Dumoulin E., 2008. *Prediction of powder agglomeration during the spray drying process*; oral presentation in RELPOWFLOW congress, Tromso (Norway), 10-12 June.  
*Article accepted for publication in Particulate Science and Technology.*

Gianfrancesco A., Turchiuli C., Dumoulin E., 2007. *Evolution of air properties in spray drying chamber in relation with controlled powder agglomeration*; oral presentation in AFSIA (French association of drying in food industry) Congress, Biarritz (France), 24-25 May.

Gianfrancesco A., Turchiuli C., Dumoulin E., 2007. *Powder agglomeration during the spray drying process*; oral presentation in PARTEC 07, Particle Technology International Conference, Nuremberg (Germany), 27-29 March.

Gianfrancesco A., Turchiuli C., Dumoulin E., 2007. *Powder agglomeration during the spray drying process: measurements of air properties*; oral presentation in "3<sup>rd</sup> International Spray Dried Milk Conference", San Francisco (USA), 25-28 February.

- **Oral presentations in the *Biopowders* network meetings**

29 June 2006: *Controlled powder agglomeration during the spray drying process*, SIK Research Center, Gothenburg (Sweden).

10 March 2006: *Research proposal: powder agglomeration during the spray drying process*, Delft University (The Netherlands).

18 September 2008: *Powder stickiness during spray drying process in relation with agglomeration*, Final Biopowders Workshop, Agroparistech Massy (France).

- **Other presentation (invited)**

26 May 2008: *Powder stickiness during spray drying process in relation with agglomeration*. 2<sup>nd</sup> European Workshop on Food Engineering and Technology, EFFOsT, Agroparistech Massy (France).

- **Industrial visits/contacts**

<i>Company</i>	<i>Date</i>
SOFIVO INGREDIENTS	14-10-05
INRA-AGROCAMPUS RENNES	20-10-05
DIANA-NATURALS	14-11-05
ARMOR-PROTEINES	14-11-05
SOCIETE LAITIERE DE MAYENNE	15-11-05
TECHNI-PROCESS	08-12-05
CD-ADAPCO	10-01-06
DSM	07-03-06
NESTLE PTC Singen	11-04-06
NESTLE NRC Lausanne	17-12-07





## ABSTRACT

Food instant powders like milk, soups, juices, coffee, are usually produced by spray drying followed by a further step of agglomeration to get larger particles (from 50-100  $\mu\text{m}$  to 250-500  $\mu\text{m}$ ) with a narrow size distribution and modified structure (porosity) to obtain good handling and instant properties (wettability, dispersability, solubility). Agglomeration of spray dried powders is performed either outside or inside the drying chamber in a fluid bed, or by return of dry fines into the chamber.

Agglomeration of particles requires collisions and adhesion to create links between particles. Stickiness of particle surface will depend on the presence of components able to develop such property. For carbohydrates, stickiness is related to the glass transition appearing when varying water content, water activity and temperature, three parameters representative of drying.

A methodology was developed to associate the evolution of drying air properties to drops drying along the chamber. Measurements of air temperature and relative humidity allowed to calculate the drops water content at any position in the dryer, and to deduce the possible sticky conditions and positions.

Spray drying of aqueous solution of a model product able to stick (maltodextrin DE12 and DE21) was performed in a co-current pilot spray dryer equipped with a rotary atomizer. Studied process parameters included liquid feed flow rate (1 to 3.2  $\text{kg}\cdot\text{h}^{-1}$  evaporated water), inlet air temperature (144 to 200°C), air flow rate (80-110  $\text{kg}\cdot\text{h}^{-1}$ ), rotary atomizer velocity (22500 to 30000 rpm).

Maltodextrin DE12 drops were quickly dried below the glass transition temperature, and stickiness seemed possible only next to the atomizer. Maltodextrin DE21 might present a sticky behaviour in a wider part of the chamber due to conditions corresponding to lower glass transition temperatures, especially for high liquid flow rate and low inlet air temperature. Computational Fluid Dynamics was used to simulate the drying of solutions, and to predict possible sticky conditions and positions. These conditions were tested and validated by performing agglomeration trials introducing powder at different positions inside the chamber. Finally, this experimental approach using air properties measurements was applied to interpret the drying behaviour of a different product (protein hydrolyzate) in a pilot spray dryer at higher scale, equipped with fines return and internal fluid bed.

**Keywords:** spray drying, agglomeration, stickiness, glass transition, CFD modelling

## RESUME

Les poudres alimentaires instantanées (lait, soupe, jus, café) sont habituellement produites par séchage par pulvérisation, suivi d'une étape ultérieure d'agglomération pour augmenter la taille des particules (de 50-100  $\mu\text{m}$  à 250-500  $\mu\text{m}$ ) avec une distribution de taille étroite et une structure modifiée (porosité), pour améliorer la manutention et les propriétés instantanées (mouillabilité, dispersibilité, solubilité). L'agglomération est réalisée dans un lit fluidisé intérieur ou extérieur à la chambre de séchage, ou par réinsertion des fines (sèches) dans la chambre. L'agglomération de particules passe par les contacts et l'adhésion entre particules pour créer des liaisons entre elles. Les propriétés collantes de la surface d'une particule dépendent de la présence de constituants capables de développer un comportement collant. Pour les polysaccharides le collage est lié à la transition vitreuse, en relation avec la teneur en eau, l'activité de l'eau et la température, paramètres représentatifs du séchage.

Une méthode est développée pour relier l'évolution des propriétés de l'air de séchage au séchage des particules dans la chambre. Les mesures de la température de l'air et de son humidité relative ont permis de calculer l'évolution de la teneur en eau des gouttes dans la chambre, et d'en déduire des conditions opératoires et positions où les particules seraient collantes.

Des solutions aqueuses de produits modèles (collants) (maltodextrine DE12 et DE21) ont été séchées dans un séchoir pilote en co-courant, avec turbine de pulvérisation. L'effet de différents paramètres ont été étudiés : le débit liquide (1 à 3,2  $\text{kg}\cdot\text{h}^{-1}$  d'eau évaporée), la température d'entrée de l'air (144 à 200°C), le débit d'air (80 – 110  $\text{kg}\cdot\text{h}^{-1}$ ) et la vitesse de rotation de la turbine (22500 à 30000 rpm).

Les particules de maltodextrine DE12 sont rapidement séchées en dessous de la température de transition vitreuse, et le collage est envisagé seulement près de l'atomiseur. La maltodextrine DE21 montre un comportement collant dans une large partie de la chambre, dû à de plus faibles températures de transition vitreuse, en particulier pour des forts débits de liquide et des faibles températures de l'air de séchage.

La mécanique des fluides numérique (CFD) est aussi utilisée pour simuler le séchage de solutions, et pour prédire l'existence de conditions collantes. Ces conditions ont été testées et validées par des essais d'agglomération réalisés en introduisant de la poudre à différents endroits dans la chambre. Enfin, cette approche expérimentale basée sur la mesure des propriétés de l'air a été appliquée pour interpréter le comportement au séchage d'un produit différent (hydrolysat de protéines) dans un séchoir pilote à plus grande échelle, équipé d'un retour de fines et d'un lit fluidisé interne.

**Mot clés :** séchage par pulvérisation, agglomération, collage, transition vitreuse, simulation CFD